2012

Synthesis and characterization of biocompatible PEGylated poly (a-amino acid) random and block copolymers for application to solid surfaces

Tracy L. Armstrong

SYNTHESIS AND CHARACTERIZATION OF BIOCOMPATIBLE PEGylated POLY (α-AMINO ACID) RANDOM AND BLOCK COPOLYMERS FOR APPLICATION TO SOLID SURFACES

by

TRACY L. ARMSTRONG

A DISSERTATION

Submitted in partial fulfillment of the requirements

for the degree of Doctor in Philosophy

in

The Biotechnology Science and Engineering Program

to

The School of Graduate Studies

of

The University of Alabama, Huntsville

HUNTSVILLE, ALABAMA

2012

In presenting this dissertation in partial fulfillment of the requirements for a doctoral degree from The University of Alabama, Huntsville, I agree that the Library of this University shall make it freely available for inspection. I further agree that permission for extensive copying for scholarly purposes may be granted by my advisor or, in her absence, by the Chair of the Department (Director of the Program) or the Dean of the School of Graduate Studies. It is also understood that due recognition shall be given to me and to The University of Alabama, Huntsville in any scholarly use which may be made of any material in this dissertation.

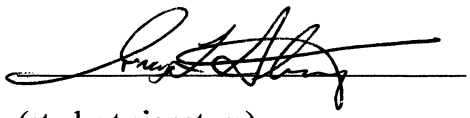

3-21-12

(student signature) (date)

DISSERTATION APPROVAL FORM

Submitted by Tracy L. Armstrong in partial fulfillment of the requirements for the degree of Doctor of Philosophy in Biotechnology and accepted on behalf of the Faculty of the School of Graduate Studies by the dissertation committee.

We, the undersigned members of the Graduate Faculty of the University of Alabama Huntsville, certify that we have advised the supervised candidate on the work described in the dissertation. We further certify that we have reviewed the dissertation manuscript and approve it in partial fulfillment for the requirements of the degree of Doctor of Philosophy in Biotechnology.

C. [signature] 3/19/12 Committee Chair

(Date)

[signature] March 16, 2012 Dr. Khursheed Anwer

[signature] 03/16/2012 Dr. Bernhard Vogler

[signature] 3/16/2012 Dr. Emanuel Waddell

[signature] 20 Mar 12 Dr. Jeffrey Weimer

[signature] 3/16/12 Department Chair

[signature] College Dean

Rhonda Kay Reed 3/28/12 Graduate Dean

ABSTRACT

School of Graduate Studies

The University of Alabama, Huntsville

Degree: Doctor of Philosophy Program: Biotechnology Science and Engineering

Name of Candidate: Tracy L. Armstrong

Title: Synthesis and Characterization of Biocompatible PEGylated Poly(α-amino acid) Random and Block Copolymers for Application to Solid Surfaces.

Poly(ethylene glycol) (PEG) has proved to be a superior biomaterial with the ability to provide a stealth character by means of PEG-coating material surfaces. In aqueous media, PEG has a large excluded volume with a low interfacial free energy in water. Therefore, approaching molecules are repelled due to an entropic effect which prevents protein adherence to the substrate. However, the effects of molecular weight on coating density are up for debate, as it is possible that steric hindrance causes large voids in the surface coating.

Poly(amino acid)s can be classified into biological and synthetic poly(amino acid)s, where biologically derived poly(amino acid)s are biosynthesized by living organisms. Two such examples are, poly(γ-L-glutamate) and poly(N^{ε}-L-lysine).

Amino acid N-carboxyanhydride (NCA) ring opening polymerization (ROP) using nucleophiles as initiators offers the greatest potential for the synthesis of high molecular weight synthetic homo poly(amino acid)s and poly(amino acid) copolymers. Sequence control of the poly(amino acid)s, however, is not achievable. Moreover, as described by Ballard and Kricheldorf, the association of growing oligopeptides via hydrogen bonds results in a phase

separation on a molecular level, that is, the formation of β-sheets between oligopeptides leading to chain termination. Therefore, the products of NCA ROPs lack molecular weight and polydispersity control. The occurrence of β-sheet secondary structures inhibits the kinetics and slows or prematurely terminates polymerization and is the main cause for a loss of control over molecular weight and polydispersity of the products.

The focus of this work is on the synthesis of poly(amino acid)s by NCA ROP that is initiated by primary amines (small molecules and macromers) in the presence of urea. Urea interrupts the formation of hydrogen bonds during the early stages of chain growth, thus suppressing the formation of the β-sheet secondary structures.

Experiments were conducted with side chain protected lysine, cysteine, and glutamate *N*-carboxyanhydrides to demonstrate that β-sheet formation is present in hexylamine initiated homo-oligomers (< 10mers). It was observed that all urea free synthesized oligomer of *N*-hexylamine-poly(cysteine) retained a β-sheet structure regardless of oligomer length. Synthesis utilizing urea caused a reduction in β-sheet formation, and an increase in disordered oligomer chains. *N*-hexylamine-poly(L-lysine) and *N*-hexylamine poly(L-glutamate) showed β-sheet secondary structure as 4mers and 5mers, respectively. The oligomers developed α-helices, as described in literature (≥ 12mers±1 for L-lysine and 9mers ±1 for L-glutamate) at longer chain lengths of 13mers and 11mers for *N*-hexylamine-poly(L-lysine) and *N*-hexylamine poly(L-glutamate) respectively .

PEGylated poly(amino acid)s (paas) were successfully synthesized in the presence of urea, yielding products that were of desired molecular weight and architecture. Random and block copolymers were initiated by α-amino-ω-methoxy poly(ethylene glycol) (M_w 5kDa) and synthesized to yield polymers with amino acid repeat units totaling between 60 and 120 repeat units. Gel permeation chromatography (GPC) and proton nuclear magnetic resonance (^{1}H NMR)

experiments showed that living polymerization was achieved and yielded polymers with polydispersity indexes (PDI) between 1.13 and 1.34. Higher PDIs were observed consistently in the random copolymers indicating that a blocky nature could have been induced due to differences in chemical reactivities. Regardless, living polymerization techniques yielded polymer products that could be useful for surface modifications in biologically implantable devices.

Since protected amino acid NCAs were used to prevent side chain reactions, it was first necessary to deprotect the side chains of the paas to expose the thiol groups for polymer application to gold surfaces. Typically, selective deprotection is desired when heteropolymers are synthesized, but a single deprotection was desired for this study. Successful removals of trifluoroacetyl, carboxybenzyl, and benzyl protective groups were achieved utilizing K_2CO_2, and H_2O, and MeOH. Removal of the protecting groups was monitored by ^1H NMR and showed that successful global deprotection could be achieved in short order.

Finally, the deprotected poly(amino acid)s were non-specifically deposited onto uniformly coated gold on silica surfaces, as well as, sputtered and nano particulate gold on silica surfaces. PEGylated random and block copolymers were observed on the surfaces utilizing atomic force microscopy (AFM), which showed that the solid gold surface was uniformly covered with PEGylated polymer that yielded characteristic lamellar formation. The gold nano-particle showed a less uniform coating, and demonstrated that PEG could bind to the silica regions in addition to the thiol-gold interactions that were seen in the gold coated surfaces. The gold coated surfaces showed PEGylated polymers were bound only to regions where gold was present. AFM images of gold sputtered silica showed interesting topography, as the PEGylated polymers appeared to yield some spiral like formation on the gold nano particle surfaces, which is commonly termed screw formation. The gold sputtered surfaces showed that cysteine NCA could

be incorporated into the copolymer to efficiently provide an anchor for the PEG chain, which could render the surface biocompatible.

This study made several important contributions to the field: first, β-sheet secondary structure formation was observed in oligomers as hypothesized in literature. Also, a one pot method was used to globally remove select protective groups from α-amino acids. Finally, the use of cysteine NCA in living ring opening polymerization with mPEG-NH_2 as the macroinitiator, yielded copolymers of specific molecular weight and low PDIs. This PEGylated poly (amino acid) s were used to coat gold on silica surfaces and gold nano particles on gold surfaces, using the thiol as an anchor point, and rendering the surface more biocompatible based on the known properties of the amino acids, PEG, and the PEGylated poly(amino acid)s on nano-particle gold.

Abstract Approval: Committee Chair C. [signature] 3/19/12

(Date)

Department Chair [signature] 3/16/12

Graduate Dean Chonda Kay Steede 3/28/12

AKNOWLEDGMENTS

I would like to thank my advisor, and mentor, Dr. Carmen Scholz, for her guidance and help with the completion of this project and dissertation. I would like to express my gratitude for your unwavering patience and instruction during my time under your direction. Your belief in me and perpetual support has meant more to me than words on paper can express.

I would also like to thank Dr. Randall Wilson for his assistance with the circular dichroism experiments, and initial data analysis. To Dr. Steve Edmondson, I express my gratitude for his help with the programming necessary for the CD analysis software that was vital to this project. Thank you to, Keerthi Prasad.Venkataramanan for our many discussions and assistance with my research. His friendship and help was invaluable to me. To Bobbi Johnson, and Brenda Wright, your friendship, time, and help through the struggles will remain a part of me for many years to come.

To my committee, I would like to express my extreme gratitude for their support, advisement, and time. To Dr. Jeffery Weimer, thank you for your advice and attention to detail. You selflessly gave me opportunities to branch out, and explore new facets of research through cooperative projects with your lab. To Dr. Bernhard Vogler, the years of instruction and guidance has made my success as a student possible. Without your knowledge this process would have been much more difficult. To Dr. Emanuel Waddell, your passion and knowledge has given me the motivation I needed to continue slugging my way through the difficult times. Your uncanny ability to put thing into perspective has helped me more than you will know. To Dr. Kursheed Anwer, from Expression Genetics, thank you for taking time from your busy schedule to help me through this life changing endeavor. Your unique perspective and words of encouragement have been an inspiration to me during the final steps of this journey.

Many thanks go to Dr. Joseph Ng, the director of the Biotechnology Science and Engineering program. From the first time we met, you believed in me. I cannot begin to express

how much your mentorship, knowledge, and words of encouragement have meant to me. Your faith kept me coming to the lab day and night, and gave me the courage and strength to continue to the end.

I would like to thank the UAH department of Chemistry and the National Institute of Health (Grant: 2-RO1-EY01-16674-04A1) for their financial support, and the UAH program of Biotechnology Science and Engineering for the opportunity to pursue an advanced degree in a field that is very dear to me.

Finally, I would like to thank my family and friends who have stood behind me through thick and thin throughout all of these years. Your support has kept me strong during the rough times, and your joy at my accomplishments has made those moments that much more special. To William and Zachary, thank you for all the times you patiently stayed at school with me, so I could finish that one last experiment before I could call it a day.

TABLE OF CONTENTS

LIST OF FIGURES

LIST OF TABLES

LIST OF SCHEMES

LIST OF TERMS

^{1}H-NMR	proton nuclear magnetic resonance
3D	three dimensional
α-pinene	(1S)-(-)-alpha-pinene
aa	amino acid
ACN	acetonitrile
AFM	atomic force microscopy
AMD	age-related macular degeneration
ATR	attenuated total reflectance
Bnl	benzyl protective group
BRIP	Boston Retinal Implant Project
Cbz	carboxybenzyl protective group
CD	circular dichroism
-COOH	carboxylic group
CONTIN	convex constraint method for CD
CONTIN/LL	Johnson's minimal basis-random selection method for CD
CP/MAS	^{13}C cross-polarization/magic angle spinning

d	distorted
De M^{-1} cm^{-1}	per residue molar absorbance units
DLC	diamond like carbon
DMF	*N*-*N*-dimethylformamide
DMSO-d_6	Dimethy sulfoxide-d_6
$\overline{DP}_n$	degree of polymerization
EtOAc	ethyl acetate
EtOH	ethanol
FTIR	Fourier transform infrared
GPC	gel permeation chromatography
HCl	hydrochloric acid
HPLC	High Pressure Liquid Chromatography
IR	Infrared
LCST	lower critical solution temperature
LROP	living ring opening polymerization
MD	macular dystrophy
MeOH	methanol
M/I	monomer/initiator ratios

mPEG	monomethyl ether of PEG
mPEG-NH_2	methoxy polyethylene glycol amine or α-methoxy-ω-amino PEG
Mw	molecular weight
NACE	nonaqueous capillary electrophoresis
NCAE-MS	nonaqueous capillary electrophoresis coupled with online mass spectroscopy
NCA	α-amino acid *N*-carboxyanhydride
-NH_2	amino group
NMR	nuclear magnetic resonance
NPLC	N-hexylamino-p(L-cysteine)
NPLG	N-hexylamino-p(L-glutamate)
NPLL	N-hexylamino-p(L-lysine)
nuc/bas	nucleophilicity/ basicity ratio
paa	poly(amino acid)
PD	polydispersity
Pd/C	palladium on carbon
PDI	polydispersity index
PEG	polyethylene glycol
PEG-paa	PEGylated poly(amino acid)

PEO	polyethyleneoxide
PI	poly (imide)
PLC	poly ($_{L}$-Cysteine)
PLL	poly ($_{L}$-Lysine)
PLG	poly ($_{L}$-Glutamic acid)
POE	polyoxylethylene
r	regular
RDS	retinal degeneration slow
ROP	ring opening polymerization
RP	retinitis pigmentosa
SAMs	self assembling monolayers
SELCON3	self consistent method for CD
TFA	triflouroacetamide protective group

CHAPTER 1

Bibliographic Study of Poly (Amino Acid)s and Living Ring Opening Polymerization

1.1. Introduction

Retinitis pigmentosa (RP) and age-related macular degeneration (AMD) are conditions that cause a gradual loss of photoreceptor cells and will lead to total blindness over time. The neural retina, however, remains largely intact and patients suffering blindness from these conditions still perceive phosphenes from electrical stimulation of the retina [2–4]. The healthy sensory retina contains 100 to 130 million photoreceptors, of which 95% are rods. This leads to a network of approximately 1.2 million ganglion cells [5]. The central portion of the retina is the macula. It measures between 1 and 2 mm in diameter, has a high concentration of rods and cones, provides the central vision, and provides the ability to view objects with a higher resolution [2], [6]. Early experiments by Tassicker (1956) demonstrated that patients could see light when the retina was stimulated by implantation of a light sensitive selenium cell [5].

Age-related macular degeneration is a disease that usually presents itself after 50 to 60 years of age [2], [7], [8]. It progressively destroys the macula, and the center of vision is impaired making it very difficult to drive, read, or perform other normal daily tasks. AMD is diagnosed in one of two forms; non-neovascular (commonly called dry form) or neovascular (commonly called wet form). Neovascular references the growth of new blood vessels in the macula where blood and fluid leakage will permanently damage the retina [7]. Non-neovascular AMD occurs when small yellow deposits, called drusen, begin to accumulate under the retinal pigmented epithelium and neurosensory retina. These deposits irreversibly damage the

photoreceptor rich region of the retina causing a gradual loss of vision [5], [7], [9]. Studies have shown that several of the most common risk factors for AMD are cigarette smoking and genetic heredity [5], [7].

Retinitis pigmentosa is a large group of inherited disorders in which abnormalities of the rod and cone photoreceptors cause a gradual loss of sight [10–13]. The onset of the disease is highly variable, and can occur in early childhood, where others remain asymptomatic until adulthood. Patients with RP initially experience defective dark adaption, or night blindness. Which later progresses to constriction of their field of vision constricts and they develop tunnel vision. Late RP exhibits a total loss of vision, even in the central field. RP may be inherited in a number of different ways: an autosomal dominant, autosomal recessive, an X-linked trait, or a mitochondrial disorder [6], [10], [13]. Currently there are more than 100 genes known to cause RP. It can occur alone or be part of a syndrome involving abnormalities outside of the retina, such as Usher syndrome and Bardet-Biedl syndrome [6], [13].

Currently there are no cures for AMD and RP; and treatments can only slow the progressive loss of sight. Recent advances, however, in technology and engineering have enabled several groups to begin work on prosthetic retinal implants that may enable mechanical restoration of sight to those suffering from AMD and RP. Essentially, retinal implants function by producing a small localized current that changes the membrane potential of adjacent retinal neurons [5].

One such device, that will address RP and AMD, is a retinal implant that is being developed by the Boston Retinal Implant Project (BRIP) research group. The device (Figure 1.1) is a wirelessly operated, minimally invasive retinal prosthesis that conforms to the outer wall of the eye and drives a poly(imide) (PI) micro-fabricated iridium oxide stimulating electrode array

[14]. This part of the implant needs to be hermetically sealed, but biocompatibility is of minimal interest at this time.

The part of the implant of interest here is the electrode stimulating array that is implanted into the sub retinal space, and must be completely biocompatible [14], [15]. The thin electrode array consists of a 10 μm thick polyimide flexible film with iridium oxide stimulating electrodes [14], which needs to be rendered hermetically sealed and biocompatible. If water is able to leak into the poly(imide) array, it will cause the electrode to short out.

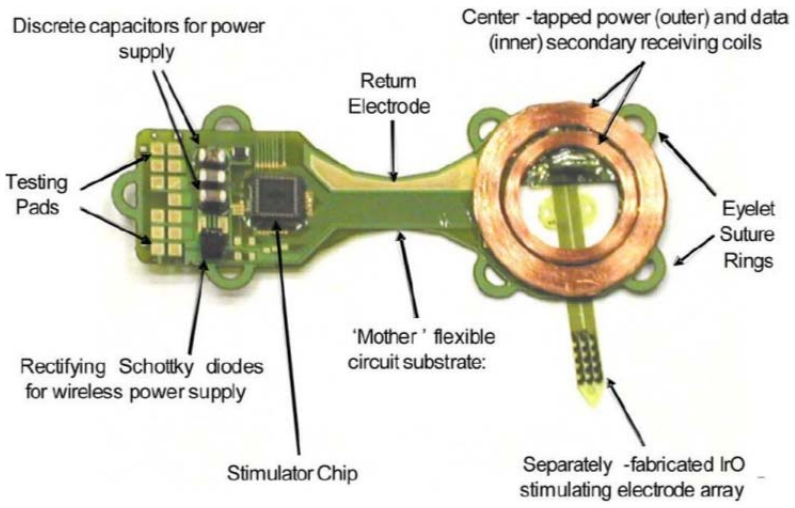

Figure 1.1. Retinal implant model engineered by the Boston Retinal Implant Project. The IrO stimulating electrode array is the region of the implant device that will require modification to render it biocompatible.

When placing any foreign objects into the body, however, one must address biocompatibility of the implanted device. This is an ever present problem with any apparatus inserted into mammalian tissues, especially those that need to be placed in the tissues for long periods of time or even for a lifetime. One of the major problems of implanted devices is the undesired interactions of the foreign materials with the immune system and biomolecules; such as

lipids, proteins, fats, and enzymes [16]. When any foreign material is placed into an organism, disturbances are created at the cell-device interface. The devices can cause a cytotoxic effect, blood coagulation, injury to the biologic membranes, tissue damage, or elicit an immune mediated response and scar tissue or glia formation [14–17]. Additionally, the implanted device itself may undergo deterioration due to chemical attack, physical deformation, and mechanical dysfunction [16], [18]. Therefore, it is necessary to develop methods and materials for rendering these implants inert upon insertion into the highly specific tissues of the body, including the eyes.

As previously mentioned, BRIP's retinal implant has a flexible electrode stimulating array that is comprised of 10 μm PI enclosed circuitry, and is the only part of the retinal implant that will be placed in the eye between the pigmented epithelium and the outer layer of the retina. The PI has a certain degree of hydrophilicity; however, this facilitates water and ion leakage into the circuitry. This may cause failure of the device. To hermetically seal the electronic array, a diamond like carbon (DLC) can be applied by laser ablation. DLC, however, is not completely biocompatible and requires an additional coating, but did exhibit minimal damage to the retinal tissue *in vivo* when compared to other types of substrates [15], [19].

The inherent issues faced with many biomedical implants may be overcome by coating their surfaces with polyethylene glycol (PEG) based copolymers. PEG has been shown to be highly biocompatible, and does not solicit any antigenic effects or generate cytotoxicity [16], [20–24]. PEG can easily be removed via biofluids and excreted from the organism, as it is water soluble [16], [25], [26]. Therefore, PEG has been widely investigated for use as drug carriers, coating medical instruments, implants, and films.

The advantages of PEGylated poly(amino acid)s has led to the development of a large interest in synthetic routes for preparation of polypeptides that mimic natural polymers, as well as completely artificial polypeptide sequences for applications in medicine, biology and

biotechnology [27]. Standard chemical polymerization methods of α-amino acids, however, have had problems with various side reactions that limit the molecular weight (Mw), architecture, and the ability to gain control over the reactions.

Recent advances in biological and chemical syntheses of α-amino acids have enabled the preparation of increasingly complex polymers of controlled Mw and sequence. Within limits, biologically functional polypeptides can be synthesized chemically by a solid phase Merrifield-type synthesis, or solution coupling methods. It should be noted for clarity, that polypeptides can be referred to as proteins only if they serve a biological function. Conversely, chemical syntheses, using α-amino acids, yield poly(amino acid)s (paa) that may contain only a limited number of monomer unit types in the polymer chain. These chemical methods typically give very broad molecular weight distributions of chain lengths and prohibit the synthesis of well-defined block copolymers. Some applications require paas, however, that has a length of less than 100 monomer units and still has a strictly controlled Mw, which will require the implementation of an alternate synthesis method.

One severe problem in the synthesis of paas is that the β-sheet formation can occur within growing oligomers. The rigid β-sheets do not continue to grow, or do so at a very slow rate [28–31]. This secondary structure formation will cause a loss in control over Mw and polydispersity [29]. Additionally, control over chain growth and architecture of block copolymers has been hindered by the complexity of the polymerizations, which can proceed through several mechanistic pathways. In general, there are two major categories of α-amino acid *N*-carboxyanhydride (NCA) polymerizations based on the type of initiator employed [28–30], [32].

α-amino NCAs have four reactive sites, including two electrophilic groups, C(O)-2 and C(O)-5, and two nucleophilic groups, the N-H and C-H, after they are deprotonated. These structural properties cause complex chemistry that makes careful selection of the proper

polymerization initiators necessary, as not all initiators facilitate true polymerization [28]. As stated by Kricheldorf, true initiators may be subdivided into two classes: protic nucleophiles and bases, and aprotic nucleophiles and bases [28]. In addition, these initiators need to be classified according to the following criteria:

1. The site on the NCA where the initiator attacks.
2. The relative reactivity of the initiator in comparison to the chain end.
3. Formation of dead chain ends upon covalent bond formation of the initiator into the peptide chain itself.

With regard to the first point, water, alcohols, and primary amines all attack the C-5 of the carbonyl group of the NCA exclusively when monomer/initiator (M/I) ratios >1 are used [28–30], [33], [34]. Regarding the second point, however, water, alcohols, and aromatic amines are less nucleophilic than amine or carbamate active end groups, and the rate of initiation will be slower than the rate of propagation. When a nucleophile is used, however, the amine mechanism will be followed as in Scheme 1.1.A. The reaction mechanism in Scheme 1.1.B illustrates the reaction when a strong base is used to initiate polymerization, and polymerization proceeds by the activated monomer mechanism [27], [28]. When considering the third point, water, alcohols, primary, and most secondary amines can form dead chain ends by the formation of covalent bonds. Therefore, control over the reaction must be gained to effectively produce a true polymerization synthesis scheme [27–30], [32–36].

A method of ring opening polymerization (ROP) of α-amino acids, therefore, has been developed and used to synthesize PEGylated (paa)s from NCAs, which takes advantage of the amine mechanism to make well-defined block copolymers. Furthermore, performing ROP under living conditions allows for the creation of block copolymers of a desired architecture. The control over molecular weight is accomplished by stoichiometric ratios where the molar monomer

concentration [M] and initiator concentration [I] ratios will determine the length of the paa molecules [27], [36].

Previous work has shown that one solution used to manage the lack of control over polydispersity, molecular weight, and polymer sequence was the use of transition metal complexes in the synthesis process developed by Deming *et al.* [28–30]. Another novel approach, by Hadjichristidis *et al.* [28], [29], [36], was the use of high vacuum techniques to purify the monomers, solvents, and initiator by. The use of metal complexes, however, requires more intricate experimental conditions as they are difficult to remove during product purification. Additionally, high vacuum techniques require highly specialized equipment and can procedurally be very time consuming.

1.2. Mechanisms of NCA Polymerization

Traditionally, NCA based polymerizations are initiated using bases and nucleophiles. The most common type of nucleophiles are primary amines, and the bases are usually alkoxide anions [37]. With this being stated, there are three possible mechanisms for NCA polymerization: normal amine mechanism, carbamate mechanism, and activated monomer mechanism. The key factor in determining which mechanism will ensue is the type of amine used in the reaction: primary, secondary or tertiary (Scheme 1.1).

Primary amines are basic and can stabilize the initially formed carbamic acid by deprotonation. This allows chain growth to proceed in two possible ways; the amine mechanism, or the carbamate mechanism [28] (scheme 1.1A). Idelson and Blout (1958), and others, determined that decarboxylation of carbamic acids, and protonation of carbamate ions are reversible reactions [28], [30], [34], [38]. The mechanism followed will largely depend on the

temperature, solvent, CO_2 pressure, and concentration of protons in the reaction flask [28], [34], [38].

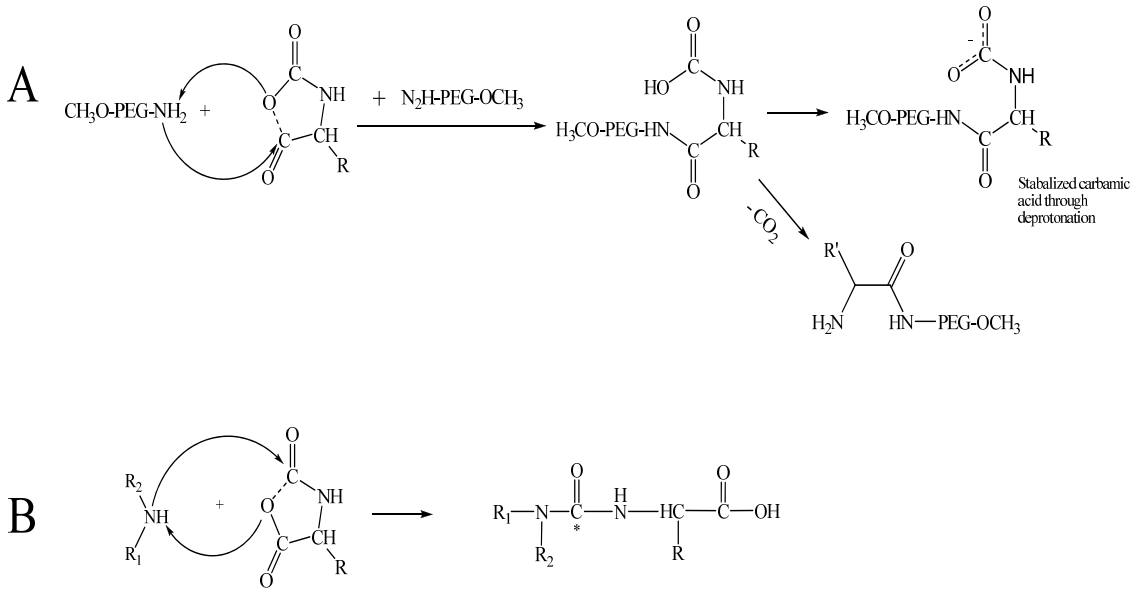

Scheme 1.1. The generalized reactions for the primary amine/ carbamate (A) and activated monomer (B) mechanisms for *N*-unsubstituted NCA compounds.

It was also shown that secondary and tertiary amines may be used to initiate polymerization, but these amines cause alternate routes of synthesis to occur and often lead to truncated, or dead polymer chains. Secondary amines can act as nucleophiles, thus attacking the C(O)-5, or can act as a strong base, attacking the *N*-proton as seen with tertiary amines [28] (Scheme 1.1B). The route followed is generally determined by the nucleophilicity/basicity (nuc/bas) ratios. This ratio is not easily determined, however, experimental results have allowed for secondary amines to be subdivided into two categories: class I and class II. Class I, which are aliphatic secondary amines, have a low nuc/bas ratio when compared to diethylamine. These amines may allow the reaction to follow the carbamate mechanism. Class II secondary amines exhibit a high nuc/bas ratio than that of diethylamine, are generally aromatic, have a low basicity [28], and will cause

the reaction to follow the activated monomer mechanism. Some secondary amines, such as diethylamine, may act as one class or the other depending on reaction conditions [28]. Tertiary amines are more basic than nucleophilic; therefore, they do not follow the amine or carbamate mechanism. Tertiary amines attack at the C(O)-5 carbon, and cause a deprotonated species to develop. The deprotonated NCA anion can then act as a nucleophile [39], as discussed below.

1.2.1. The Amine Mechanism

The amine mechanism is the most likely pathway of NCA polymerization when primary aliphatic amines are used to initiate the synthesis process. These amines are basic enough to stabilize the initially formed carbamic acid, but not so strong that deprotonation of the NCA anion occurs as with the activated monomer mechanism (see Scheme 1.4) [28], [40], [41]. The use of an aliphatic primary amine, as an initiator, facilitates the nucleophilic attack of the amine on the C(O)-2, which causes subsequent ring opening to occur under the release of CO_2 [28] (Scheme 1.2). If decarboxylation is too slow or there is steric hindrance of the amino group, the reaction will switch to the carbamate mechanism (Scheme 1.3) [27], [42]. As long as the amine mechanism dominates the reaction, true living nature of the growing polymer chains will remain intact [28].

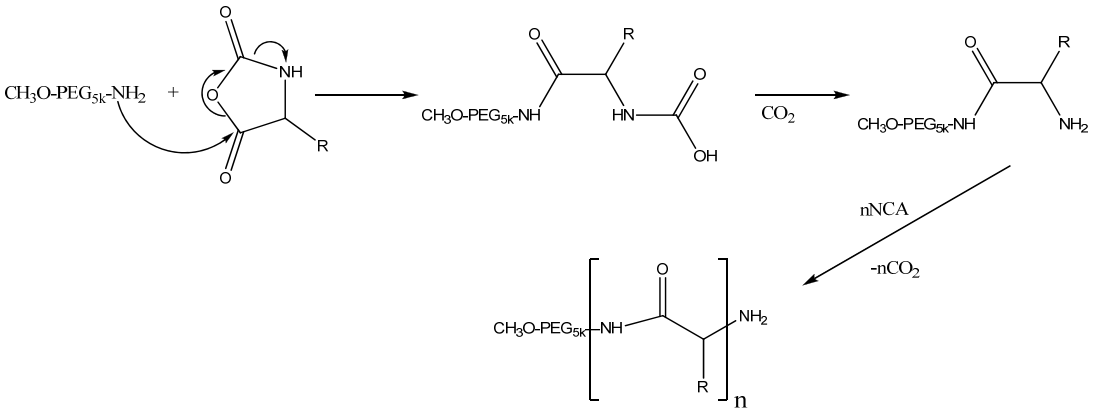

Scheme 1.2. Primary amine mechanism.

1.2.2. The Carbamate Mechanism

The formation of hydantoic acid end groups can be explained by the carbamate mechanism. It was determined that the rate of propagation, when using a primary amine, will determine if the primary amine or activated monomer mechanism will occur. If propagation is faster than decarboxylation of the intermediately formed anhydride isomerization can occur [28]. In the carbamate mechanism, there is a formation of acidic end groups, and true living character of the polymer chain is lost [28], [38]

In the carbamate mechanism, the primary amine acts as a strong enough base, that it deprotonates the intermediate carbamic acid. The intermediate forms and the nucleophilic reaction with an NCA monomer results in an intermediate anhydride, and a new peptide bond is formed after decarboxylation [38], [41]. Then, polymerization can continue as per the normal amine mechanism. It has been shown that the kinetics of the carbamate mechanism is much slower than that of the amine mechanism [28], [38], [41].

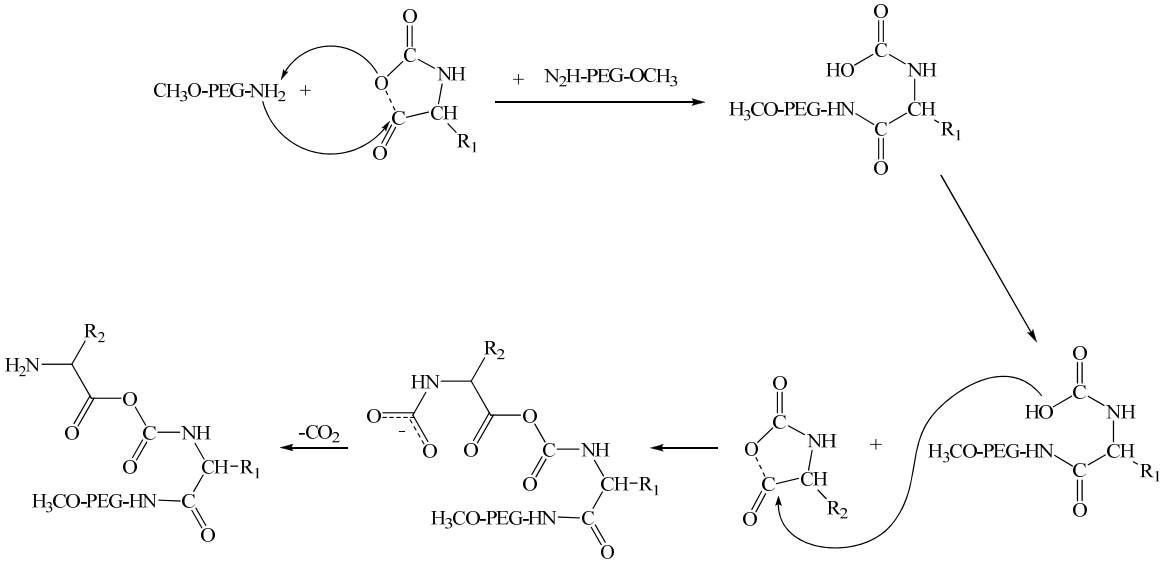

Scheme 1.3. The carbamate mechanism.

1.2.3. The Activated Monomer Mechanism

Weiland (1951) postulated that the nucleophilic attack of the tertiary amine attacks the C(O)-5 of the NCA ring [31]. When the initiator acts as a strong base, or the amino group is sterically hindered (as with trialkylamines), the deprotonated NCA anion becomes nucleophilic enough to act as the initiator [28], [38], [39]. The attack of the ionized NCA molecule on another NCA forms an amide anion, which acts as a base to, in turn, abstract an N-H proton from yet another NCA [39]. Thus, an *N*-acylated NCA and an ionized NCA are formed, and propagation of the growing chain continues [28], [39].

1.3. Research Objectives and Specific Aims

The long term objective of this research was to develop a novel coated surface, which is biomedically relevant. It was desired to synthesize a variety of PEGylated poly(amino acid)s where the paa moiety is either a block or randomized copolymer. The paas will then be grafted to the surfaces of gold-coated silica wafers, or silica wafers carrying Au-nanoparticles, which may be used as retinal implant surfaces. Furthermore, it is necessary to determine which block and/or random copolymers yield the highest density of polymer in a given area on the surfaces. This work is guided by a central hypothesis that water soluble PEGylated paa polymers, of strict molecular weights and architectures, can be synthesized with a living ring opening polymerization technique. It is required that these polymers form a coating of a high enough concentration on solid gold on silica substrate to render the surface biocompatible. The paa polymers that exhibited the best coating properties would then be applied to gold wafers, and ultimately to a gold nano particulate coated surface, as needed to support the collaborative efforts with the BRIP.

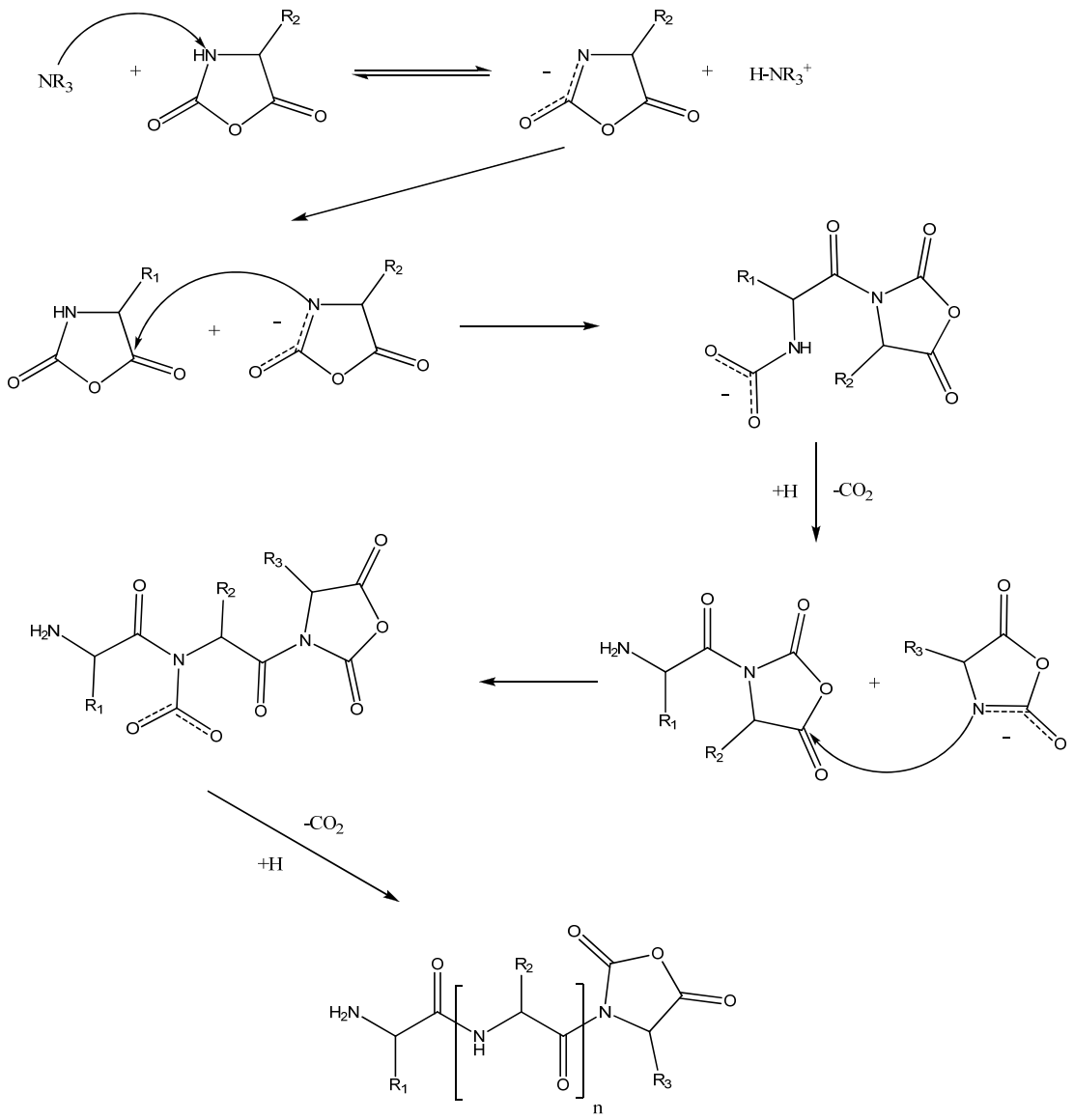

Scheme 1.4 The activated monomer mechanism.

To summarize the objectives for this work:

- Specific aims one and two are centered around developing and synthesizing water soluble PEGylated poly(amino acid)s under living conditions that are of low polydispersity,

strictly controlled molecular weight, and do not show any cross-linking or network formation.

- The third objective centers around simplifying the deprotection into a single step process when using triflouroacetyl (TFA), Benzyl (Bnl), and carboxybenzyl (Cbz) protective groups on the amino acids.
- Finally, the fourth aim focuses on deposition of the paa products onto gold covered silica surfaces to produce a dense uniform monolayer that can be utilized on a retinal implant that has been engineered by the Boston Retinal Implant Project research group.

Specific Aim 1: Confirm that the addition of urea to the reaction eliminates the formation of β-sheet secondary structure in the oligomers of the growing polymer chain, thus allowing for living polymerization conditions to promote bond formation between the paa chain end and free monomer units.

Hypothesis: A major problem with primary amine initiated LROP (Scheme 1.5), is the development of side reactions. These side reactions are a result of a retardation of reaction kinetics after initiation has taken place, which results in chain termination, truncation and a lack of living polymers [27], [28], [33], [36]. The addition of urea to the reaction will prevent β-sheet secondary structure formation during the oligomer stage of polymerization by interfering with H-bond formation.

It is suggested that control over side reactions can be maintained using urea in lieu of the use of the high vacuum technique developed by Hadjichristidis *et al.* (2000) [36]. Also, it has been shown that lowering temperatures to around 0°C has been used to slow reaction rates to inhibit the side reactions, which allows for the minimization of polymer chain truncation. Reaction times, however, can be as long as weeks or months [43], whereas the urea based method

allows reaction completion to be achieved in a matter of days. Lastly, organometallic initiators have been used by Deming to gain control over the reaction process [27], [29], [35], [36] and it is suggested that the use of urea in place of these metal complexes will achieve an equivalent effect.

Urea can be used to facilitate polymerization under living conditions at ambient temperatures, via the primary amine mechanism (Scheme 1.2), by reducing the formation of secondary structure (β sheet). The use of urea prevents intermolecular hydrogen bonding from occurring (Scheme 1.2). Therefore, suppression of *in situ* formation of secondary structure yields control over molecular weight of the resulting product and a narrow weight distribution.

Specific Aim 2: Synthesize biocompatible block and random copolymers by ring opening polymerization of α-amino acid *N*-carboxyanhydrides (NCA) of protected TFA-L-Lysine, Benzyl-L-Glutamate and S-Cbz-L-cysteine amino acids under living conditions.

A 5,000 Da α- methoxy-ω-amino Polyethylene glycol (mPEG-NH_2) will be used as a nucleophilic macroinitiator employing conditions that will allow for absolute control over molecular weight and yields of polymers of low polydispersity.

Hypothesis: PEGylated paa block and random copolymers can be synthesized by means of a living ring opening polymerization technique using urea to reduce secondary structure formation of the oligomers. This will promote pseudo second order kinetic reactions that are favorable for the chemical process to follow the primary amine mechanism as in Scheme 1.1.A. This technique allows for total control over molecular weight, architecture and polydispersity without the use of organometallic complexes or high vacuum techniques.

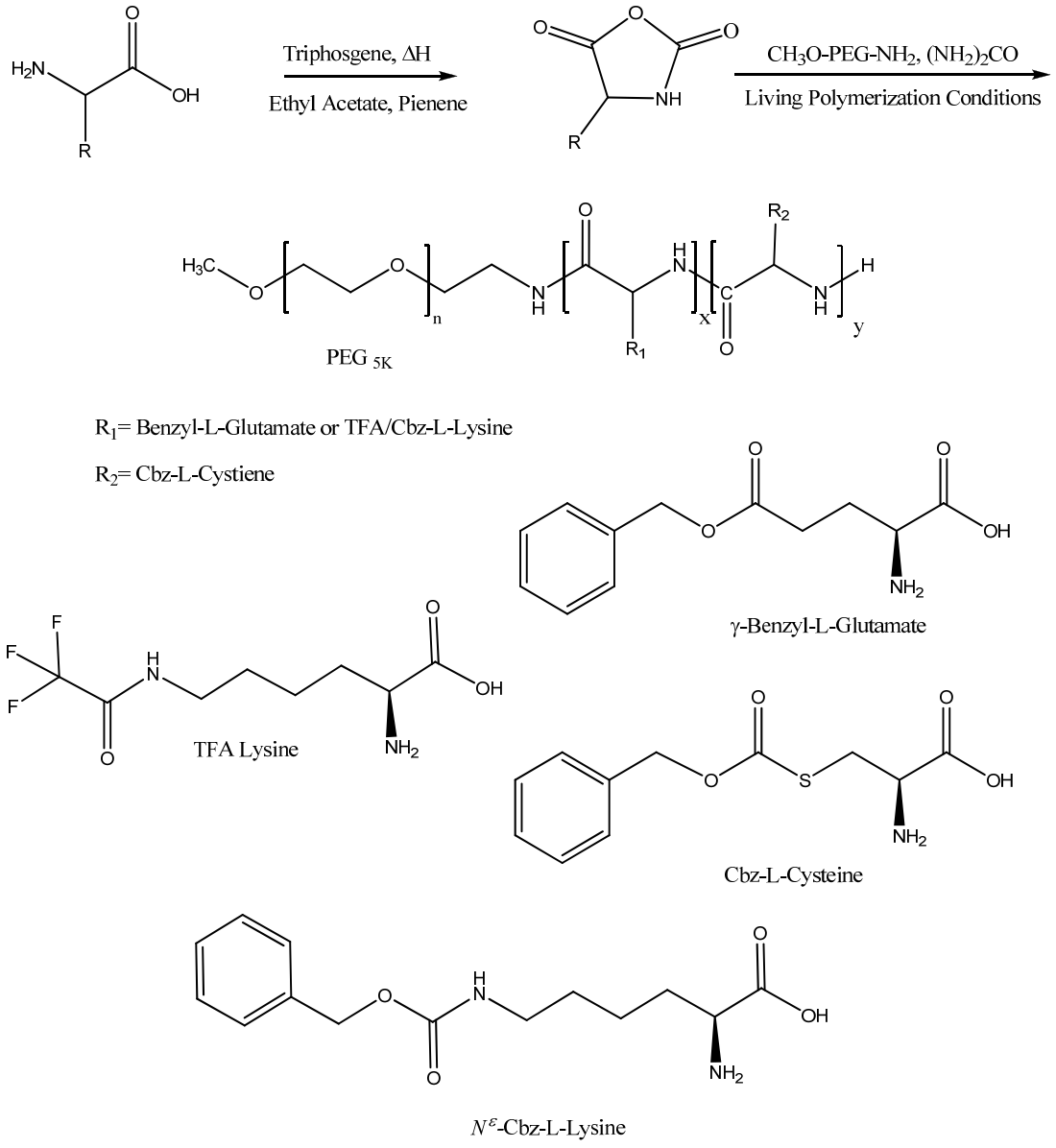

Scheme 1.5. General reaction scheme, and monomer units for the synthesis of PEG-b-p(paa) block co-polymers and PEG-b-p(paa) random copolymers.

Prior research into the synthesis of PEG-b-paa block polymers yielded significant and novel contributions to the field of NCA living ring opening polymerization (LROP) of amino acids. Previous methods of LROP did not allow for the use of macroinitiators, and commonly employed the use of metal catalysts. Reaction conditions were used that allowed for the

employment of a weak basic nucleophilic primary amine macroinitiator, or more specifically α-methoxy-ω-amino PEG, which did not require the use of metallic catalysis (Scheme 1.1, 1.2 and 1.3(1)).

It has previously been shown that the carbamate mechanism (Scheme 1.3(2)) is followed when the decarboxylation is retarded by high CO_2 levels, high pressure problems, and β-sheet formation of the oligomers, creating a dead polymer and a broad Mw distribution[28], [31], [34], [36], [40], [42], [44]. Additionally, the use of a strong base, such as a tertiary amine, causes the polymerization to follow the activated monomer mechanism [30], and causes chain truncation that does not allow living polymerization to occur (Scheme 1.3 (3)).

Specific Aim 3: To remove the protective groups of N^6- TFA-L-lysine, γ-benzyl-L-glutamate, and S-Cbz-L-cysteine are removed by a technique that allows simultaneous cleavage of the carboxybenzyl (Cbz) and the trifluoroacetyl (TFA), and Benzyl (Bnl) groups of the PEGylated poly(amino acid) polymers, to make them water soluble and expose the reactive functional groups on the side chains (Scheme 1.4). Previous methods required the use of two separate reactions to cleave the specific protective group from the associated amino acids.

Hypothesis: The typical method for the removal of the TFA protective group from an amino acid requires a hydrolytic cleavage in the presence of a methyl ester [45]. The Cbz and Benzyl protective group can be removed by catalytic hydrogenation or treatment with HBr, which yields a terminal carbamic acid and that can readily decarboxylate to give a free amine [46]. It is proposed, however, that a novel method can cleave TFA and Cbz, and benzyl protective groups from PEGylated block and copolymer products with a single chemical reaction (Scheme 1.6). The implementation of a single deprotection process will improve yields, and reduce the possibility of contamination of the polymer product.

Specific Aim 4: Demonstrate that use of deprotected cysteine residues, in the PEGylated paas block and randomized copolymers, effectively coat gold solid matrices to create a reasonably uniform monolayer across the surface. This will allow for the eventual application onto gold nano particle coated diamond like carbon (DLC) surfaces, as they are of interest for retinal implant prostheses.

Hypothesis: The biocompatibility of the retinal implant is paramount, and can theoretically be achieved by use of PEGylated paa block copolymers. Previous work has used methods that require thiolation of the polymer after synthesis for grafting onto a gold surface. Here, it is proposed that the use of L-cysteine in the block and randomized poly(amino acid) polymers will allow for the formation of coated surfaces of high enough density to be a primary candidate product for biocompatibility studies in a retinal implant.

Previous work by Scholz *et al.* (2006) with paas, used post-synthesis thiolation of the PEGylated copolymer products for application as a SAM on gold surfaces [47]. This technique, however, proved to be very difficult, as it created truncated small molecules and disulfide based network copolymers. This method had appeared promising, in theory, but was abandoned due to the aforementioned problems and the development of protected L-cysteine amino acids that could be used in LROP copolymer synthesis.

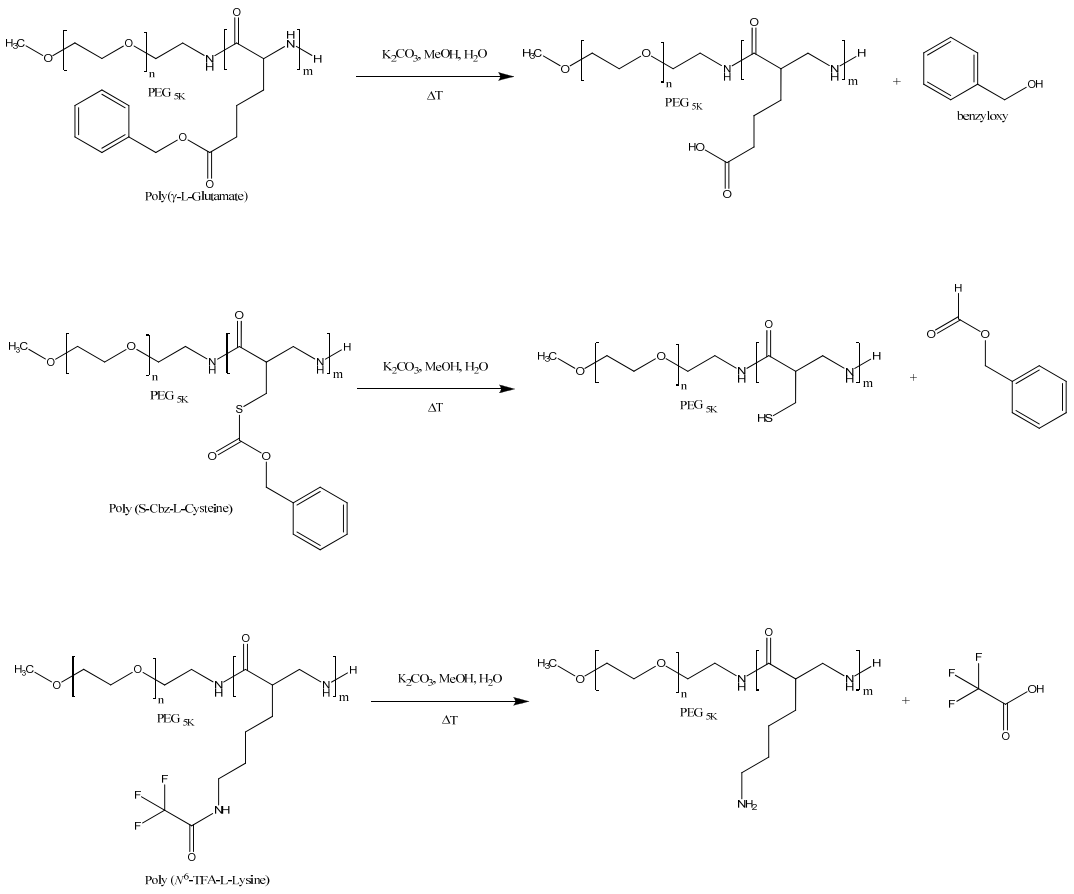

Scheme 1.6. Deprotection scheme for Trifluoroacetic acid and Carboxybenzyl functional groups.

1.4. Review of Relevant Literature

1.4.1. Brief History and Review of Mainstream Living Ring Opening Polymerization Techniques

Since the late 1940s, NCA polymerization has been one of the most widely used methods for synthesizing poly(amino acid)s on a large scale. These materials, however, do not have the sequence specificity or monodispersity of proteins. These polymers have primarily been homopolymers, or random copolymers [27], [48]. Due to these problems, these polymers had

little use with regard to biomedical applications. Further attempts to create stereo-specific polymers and block copolymers with NCAs have resulted in polymers that did not have the desired composition and contained significant homopolymer contaminants [27], [48–52]. The major limitation of NCA polymerizations has been the presence of side reactions that yield broad molecular weight distributions, restrict control over molecular weight, and inhibit the synthesis of well-defined block copolymers [27], [53].

Polypeptides are usually synthesized by the Merrifield process, and are used in a wide range of applications in medicine and drug therapy. By contrast, NCA based paas are employed to coat and modify material properties for uses in biomedical applications such as drug delivery systems, gene delivery, and coatings. There are generally two major classes of cyclo-monomers used to make polyamides: lactams and *N*-carboxyanhydride of α-amino acids (NCA). Lactams are often used to synthesize fiber forming materials and thermoplastics on a large scale, whereas, NCAs are used to synthesize polymers that resemble naturally found poly(amino acid)s, such as poly(glutamate) [42].

Deming *et al.*(2005) studied hydrogels that have shown strong implication for use in wound management and healing. These paas were block co-poly(amino acid)s that consisted of a charged, polyelectrolyte hydrophilic block of either poly-L-lysine (+) or poly-L-glutamic acid (-). It also contained a hydrophobic block that consisted of poly-L-leucine [54], [55]. These block copolymers were synthesized by a nickel (II) and cobalt (II) NCA polymerization catalyst system. It was shown by Kissel *et al.* (2002), that hydrogel formation was influenced by concentration dependence [56]. The gel formation is influenced, to a large extent, by the conformation and length of the hydrophobic blocks. In an aqueous environment, the hydrophobic blocks self assemble. The hydrophilic blocks do not have much effect on gel formation; however they do still have some effect [55].

Work by Kricheldorf, *et al.*, showed that nucleophilic ring opening polymerization could yield a controlled reaction under living conditions due to the incorporation of initiator by the amine or carbamate mechanism, as the initiation rate is higher than the propagation rate [28]. Little effort, however, has been made to confirm this hypothesis. It is hypothesized that the complexity of the polymerization, where the initiation by a primary amine is facilitated, comes from the existence of side and termination reactions [27], [28], [30], [42].

1.4.2. Poly(Ethylene Glycol)

1.4.2.a. Biocompatibility of Poly(Ethylene Glycol)

Poly(ethylene glycol) (PEG) is a polyether compound, of the general chemical structure H-(OCH_2CH_2)$_n$-OH and the general structure shown in Figure 1.2, and has many applications from industrial manufacturing to medicine. PEG is commercially available in a variety of molecular weights (Mw), ranging from 400 to 100,000 Da. The Mw of interest is usually governed by the intended use of the polymer.

Additionally, it should be noted that PEG is also known as polyoxylethylene (POE), and Polyethyleneoxide (PEO), of which all are chemically synonymous. The term PEG usually refers to molecules of a molecular weight less than 20 kDa.

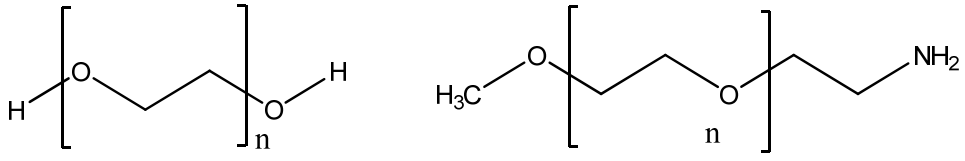

Figure 1.2. General structure of Polyethylene Glycol (A), and the functionalized derivative m-PEG-NH_2 (B).

Surfaces coated with PEG have been shown to reduce protein adsorption and cell adhesion [57]; additionally it reduces the effects of tissue damage and cytotoxic effects [16], [21], [57]. Some surfaces coated with PEG do not exhibit antigenic effects [20], [21], which are thought to lead to its ability to repel proteins [23]. Also, PEG that has been grafted onto surfaces has been shown to prevent bacterial colonization of biomaterial implanted surfaces [24], [35].

PEG is very effective in aqueous solution, where it exposes uncharged hydrophilic groups and demonstrates a very high surface mobility [20], [24], [58], [59]. There are two main contributing factors to the repulsive forces of PEG: a large excluded volume and a mixing interaction component [58]. First, the excluded volume results from a low interfacial free energy in water [60], [61]. When a protein molecule approaches the PEG coated surface, the available volume for each polymer segment is reduced and causes a loss of conformational autonomy of the PEG chains. The second factor is the osmotic interaction that occurs between the protein and the PEG segments. The protein reduces the number of PEG's available conformations by either compressing or penetrating the PEG, thus causing an osmotic repulsive force [62–64].

Chronic implantation and assimilation of biomechanical devices into higher organism's tissues can be achieved by coating these devices with a PEGylated monolayer. As previously discussed, PEG is very useful for rendering biomedical devices compatible, as well as, for use as biodegradable drug delivery vehicles and coatings [14–17].

1.4.2.b. Functionalized Poly(Ethylene Glycol) Derivatives

In order to guarantee a pre-determined chemical architecture, it is often necessary to utilize derivatives of PEG, such as monomethyl ether of PEG (mPEG). The presence of only one reactive end group reduces the possibilities of cross-linking and improves the homogeneity of the PEGylated product [25]. Figure 1.1A shows that the functional end of the PEG is a hydroxyl,

which can react to create a linear polyether. As will be addressed later, it is necessary to employ a strong enough nucleophilic mPEG derivatives that will create an amide bond during the synthesis of an amino acid based PEGylated polymer. Therefore, it has been observed that α-methoxy-ω-amino PEG (mPEG-NH_2) can be used as a nucleophilic macroinitiator in the synthesis of PEGylated paas using living ring opening polymerization (LROP) [28], [29], [42], [57], [65].

1.4.2.c. α-methoxy-ω-amino PEG as a Macroinitiator

α-methoxy-ω-amino (mPEG-NH_2) is an inert material that is a derivative of biocompatible PEG with a chemical structure of $H_3C\text{-}O\text{-}(CH_2CH_2O)_n\text{-}CH_2CH_2\text{-}NH_2$ (Figure 1.1B). The $mPEG_{5k}\text{-}NH_2$ is an excellent macroinitiator, as the amine end's unshared electron pairs enable the molecule to act as a nucleophile and a base. This promotes ring opening polymerization of NCAs under living conditions via the amine mechanism [28], [29], [42], [57].

1.4.3. Amino acids and Poly(Amino Acid)s

1.4.3.a. Introduction to Amino Acids

Amino acids are bi-functional compounds that contain a carboxylic group (-COOH), a basic amino group (-NH_2), and a side chain that is unique to each type of amino acid. In general, amino acids can be one of three types: alpha, beta, or gamma, with α- amino acids being the most common form found in nature. In the 20 standard α-amino acids, with the exception of glycine, the α-carbon is chiral and optically active in the levorotary configuration. More specifically, an α-amino acid has the general formula of $H_2NCHRCOOH$, where R is an organic substituent.

Some amino acids have the amine group attached to the β or γ-carbon, and are referred to as beta or gamma amino acids (Figure 1.3).

The 20 standard amino acids can be incorporated into polypeptides, and are directly encoded by the genetic code. In addition to these standards amino acids, two others can be encoded by the standard genetic code but require unique synthetic methods; pyrrolysine and selenocysteine. These 22 amino acids are referred to as proteinogenic amino acids, but only 21 are found in eukaryotes [66], [67]. Pyrrolysine is not encoded or expressed by eukaryotic organisms. Humans, however, can only synthesize 11 of these 20. The remaining nine are termed essential amino acids, and must be consumed as part of their dietary requirements [67], [68].

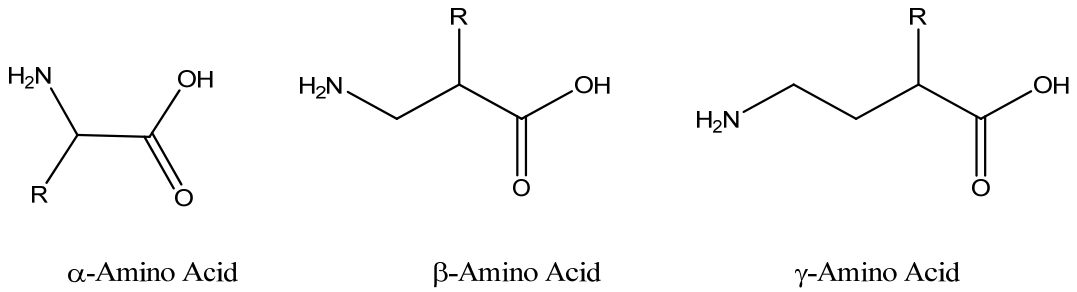

Figure 1.3. General structure of α-amino, β-amino, and γ-amino acids.

When α-amino acids are joined via a peptide bond (or amide bond), the alpha-carboxylic group of one amino acid is connected to the alpha-amino group of the next amino acid. This forms a chain of amino acid residues that will generally form an unbranched chain. It has directionality, which begins at the amino end, and terminates at the carboxyl end. The chain of paas is referred to as the backbone, while the R group substituents are referred to as the side chain [69]. The peptide bonds of the backbone are rigid and planar due to their partial double bond character. There is, however, some flexibility due to rotational degrees of freedom around other bonds of the backbone [68–70].

The interactions of the side chain groups, the backbone of the polypeptide, and the aqueous environment it is placed in, causes the polypeptide chain to fold into a variety of three-dimensional (3D) structures [71], [72]. The relationship between the amino acid sequence and the 3D structure was studied by Christian Anfinson (1958) on ribonuclease [72], [73]. A major driving force in secondary structure formation is the hydrophobic or hydrophilic nature of the side groups in the chain, and how they interact with the aqueous environment [69]. In water, hydrophilic side groups form hydrogen bonds with one another, and with the water. This is a major factor contributing to the molecule's structural stability [69], [72], [74].

It has been concluded that the 3D structure of a protein is held in place by hydrogen bonds, Van der Waals interactions, and electrostatic interactions, which are all non-covalent types of bonds. The hydrogen bond is an attractive interaction of a hydrogen atom with a nitrogen or oxygen atom from another molecule, and has bond strengths between 5 and 30 kJ/mole. Hydrogen bonding can occur inter or intra-molecularly [75]. Additionally, electrostatic interactions occur between positively and negatively charged groups to further advance the stability of the folded structure.

Van der Waals interactions are much weaker than either hydrogen bonds or electrostatic interactions, but are highly effective in large numbers [72]. Van der Waals interactions often form between the hydrocarbon side chains of the amino acid residues when the transient charge asymmetry around an atom induces an opposite asymmetry in the atom it is adjacent to [69]. The attraction, however, is lost if the atoms are far away, but contrary to this, a repulsion is created when an overlap of electrons occurs [69], [70], [73].

Due to the fact that α-amino acids are found as naturally occurring compounds and are present in molecules that exhibit biological activity, the synthesis of biodegradable, biocompatible, and nontoxic poly(α-amino acid)s are of extremely high interest [15], [27], [31],

[51], [76–78]. Poly (α-amino acid)s have been used as protein models for the study of a variety of biological processes [76]: drug delivery vehicles , polymer therapeutics [76], [79], and were used as coatings to render implanted devices biocompatible, and suppress any antigenic response [15], [16], [27–29], [33], [58], [65], [76], [78], [80].

1.4.3.b. Introduction to Poly(Amino Acid)s

In general, poly(amino acid)s are synthetic polymers comprised of α-amino acid residues that are linked by peptide bonds. The term poly(amino acid) is often used synonymously, but incorrectly, with the term polypeptide. The latter, however, is more accurate when describing naturally synthesized molecules, as opposed to poly(amino acid)s synthesized by the polymerization process *in vitro* [73].

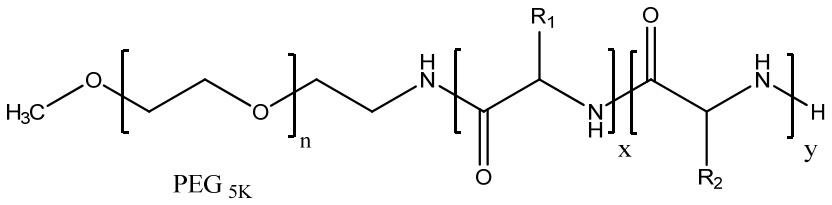

R_1= benzyl-L-Glutamate or TFA/Cbz-L-Lysine

R_2= Cbz-L-Cystiene

Figure 1.4. General PEGylated poly(amino acid) chemical structure.

In this study paas investigated will have identical backbone structure, but vary with regard to functional side chain composition. In all cases PEG will be used as the macroinitiator, however the poly (amino acid)s chain will be comprised of protected poly(L-glutamate) (PLG) or

poly (L-lysine) (PLL) with poly(L-cysteine) (PLC) in a random or block copolymer configuration (scheme 1.5 and 1.6).

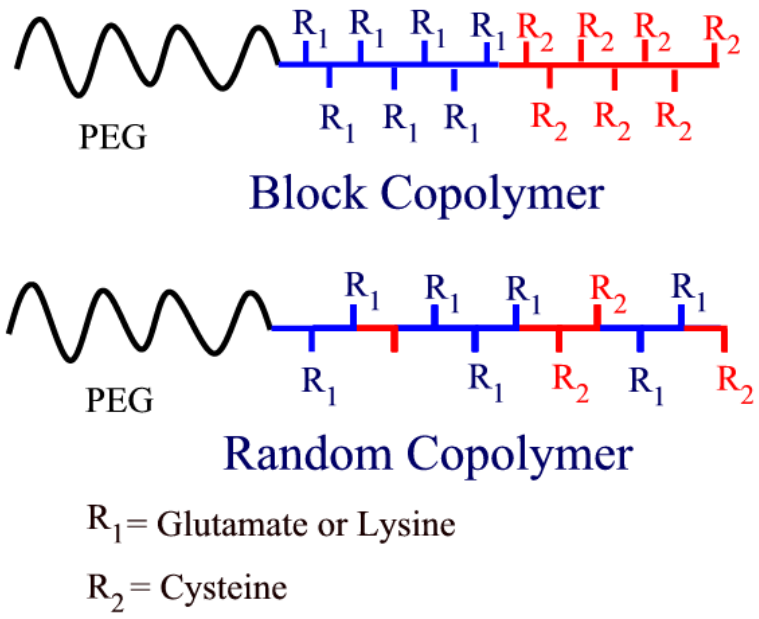

Figure 1.5. General structure of NCA based PEGylated random and block copolymers.

As PLG and PLL will be utilized as a connecting block in this study, it is important to compare one with the other, as they have different chemical properties and may affect the viability of the surface coating process differently. Both PLG and PLL have two different structures, one derived from naturally occurring synthesis in bacteria (*Bacillus* strains and *Streptomyces albus* respectively), and the other being chemically synthesized [81–83]. Poly(α-lysine) and poly(α-glutamate) are both synthesized chemically, whereas, poly(γ-glutamate) and poly(ε-lysine) are synthesized naturally in microorganisms (Figure 1.7) [81].

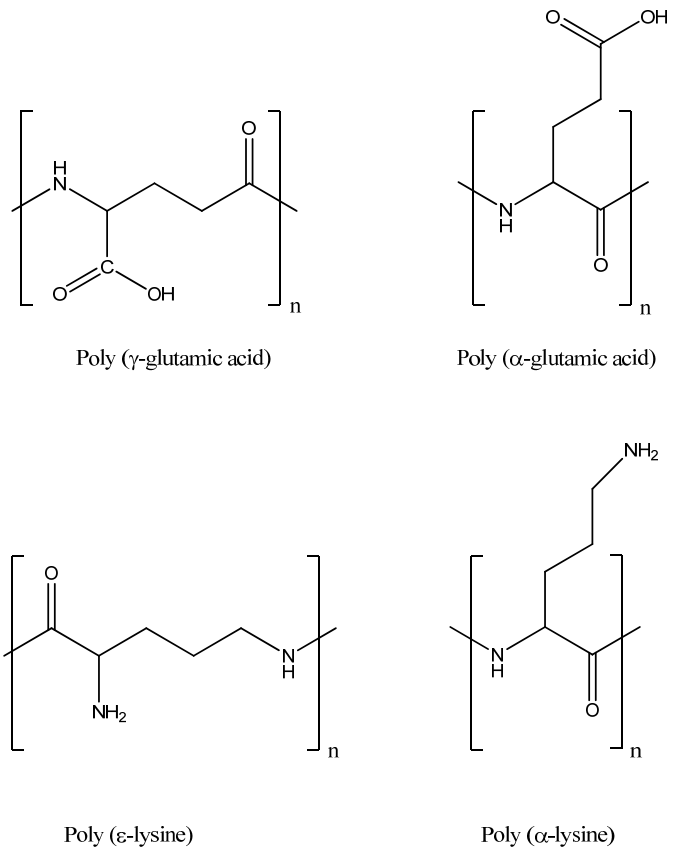

Figure 1.6. Structures of poly-glutamic acid and poly-lysine

1.4.3.c. Introduction to Protected Poly (Amino Acid)s

As discussed above, amino acids have reactive moieties at the amino and carboxyl terminus, which facilitate peptide bond formation during polymer synthesis. The side chain functional groups may also be highly reactive and can interact with the free termini of other side chain groups. This negatively affects control over peptide growth, yield, and purity. To counter these undesired reactions, reactive sites may be selectively shielded with a removable protective group at specific positions in a given compound [45]. These protective groups must fulfill a variety of requirements as outlined by Green (2007) [45]. As summarized by Kricheldorf, the protective group should:

- "React in a manner that is stable with regard to the projected reactions and be in a high enough yield to sufficiently protect the substrate" [28].
- "Must be capable of being selectively removed and readily available" [28].
- "Should not be toxic or attack the regenerated functional groups" [28].
- "It ought to form a derivative that is easily separated from side products that are created by its addition or cleavage from the functional site" [28].
- Finally, "it should have a minimal amount of functionality to avoid further site reactions" [28].

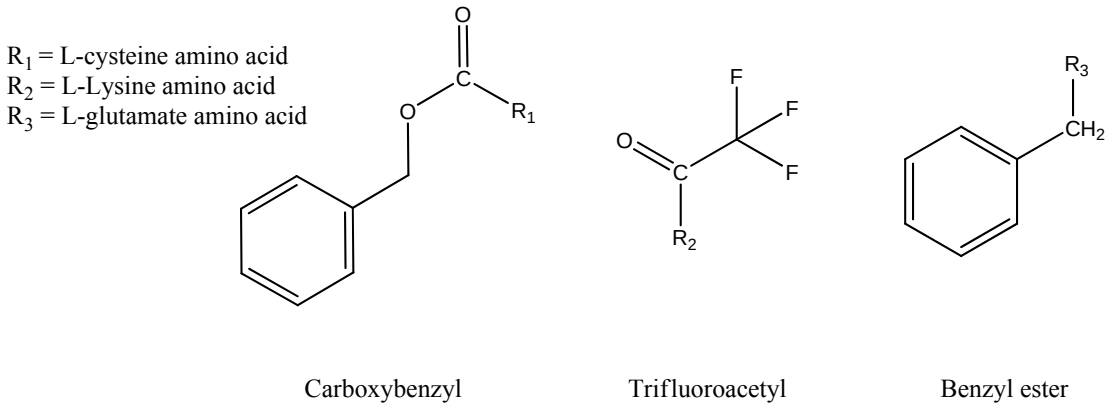

Figure 1.7. Protective groups that will be used to facilitate a more efficient and effective ring opening polymerization process.

These protective groups are usually added to the amino acids reactive sites prior to synthesis and purification, and then are selectively removed at specific steps in the peptide synthesis procedure. More specifically, trifluoroacetyl (TFA), carboxybenzyl (Cbz), and benzyl protective groups (Figure 1.7) will be utilized to prevent side reactions, thiol dimerization, and

polymer network formation from occurring. There are a vast variety of protective groups, however, that may be selected and utilized based on the criteria listed above.

1.4.4. Polymerization

1.4.4.a. Definition of Living Polymerization

Polymer synthesis methods generate products that are comprised of long chains with molecular weights that can be measured in the hundreds of thousands [84]. Conventional polymerization techniques create products with terminal ends that cannot be reactivated, therefore continued elongation of the chain is impossible. Also, conventional polymerizations generally do not have controlled molecular weights or architectures. Most conventional polymerizations exhibit a very slow initiation step, which may require a catalyst, but demonstrate rapid chain propagation and chain transfer reactions [84–86].

The two types of conventional polymerization are stepwise and addition polymerizations. Step polymerization is one that involves a random reaction of two molecules that propagate from a monomer, to a dimer, trimer, oligomer, and then finally a polymer [84]. All that is necessary for chain growth is the meeting of the appropriate functional groups in space [84]. Conversely, chain-growth polymerization is such that a monomer may only attach to an "active" chain in a chain-extension reaction and the active end may be an ionic or a free radical site [85].

The expression "living polymers" was first described by Michael Swarc (1956), where its original definition combined two properties of polymers [28], [87]. First, there should not be any change in the reactive end groups of the polymer once the reaction has finished. Thus, the active end should remain "alive" once polymerization stops. Second, the molecular weight distribution of the polymers must be narrow and have a PDI of 1.2 or less [28], [30], [31]. It has been shown,

however, that a low PDI can only be achieved if the propagation step is slower than that of the initiation step, which is most likely due to the fact that primary aliphatic amines are sterically unhindered [28], [35]. Due to this fact, primary amine based ring opening polymerization has been widely used for the production of poly (amino acid)s.

The use of primary α-amino acids in itself is not enough to achieve a low PDI, as it does not depend solely on the reactivity of the initiator, but also depends on the solubility and the secondary structure of the growing polymer chain [27], [34], [73]. Additionally, inert reaction media must be used, more specifically, copiously dry and inert reaction media must be used when synthesizing paas with NCA monomers [27], [28], [32], [35], [40]. Any contamination by strong nucleophilic molecules, such as water or alcohols, can propagate rapid polymerization and generate a broad distribution of molecular weights. Furthermore, narrow distributions require practically identical propagation rates of all the polymer chains, and a minimal amount of β-sheet formation in the growing polymer chain. β-sheet formation can create a high degree of steric hindrance, and cause chain growth to stop before all of the monomer units have been consumed [27], [28].

1.4.4.b. Polymerization of *N*-terminal Carboxyanhydrides.

Recent advances in biological and chemical syntheses of α-amino acids have enabled the preparation of increasingly complex polymers of controlled molecular weight (Mw) and sequence. As previously addressed, chemical syntheses, using α-amino acids, yield poly(amino acid)s (paa)s that may contain only a limited number of monomer unit types in the polymer chain. Chemical methods typically only give a statistical distribution of chain lengths on the order of thousands of monomer units. Some applications, however, require paas that have a length of less than 100 monomer units, yet still exhibit a strictly controlled Mw. The source of the problem is that upon polymerization initiation, the growing oligopeptides phase separate on a molecular

level and β-sheet formation can occur between oligopeptides [1-3, 8]. The formation of a secondary structure will cause a loss in control of the reaction and yield products of erratic Mw and polydispersity [8]. Additionally, control over chain growth and architecture of block copolymers has been hindered by the complexity of the polymerizations, which can proceed through several mechanistic pathways. In general, there are two major categories of NCA polymerization based on the type of initiator employed [1-3, 8]. When a nucleophile initiator is used, the mechanism followed will be either the carbamate or the amine mechanism (Scheme 1.1.A). When a base initiator is used, the activated monomer mechanism is seen (Scheme 1.1.B).

1.4.4.c. A Brief Review of the Kinetics of Living Ring Opening Polymerization

Kinetic studies for nucleophile initiated polymerizations, with primary amines used as the macroinitiator, have often presented contradictory results. This is due, in part, to the fact that the mechanisms for such reactions are often quite complicated, and often require the ability to facilitate a termination reaction [9, 10], cyclization reactions [10], or the phenomenon of auto-acceleration [11-13]. It was shown by Hadjichristidis, *et al.,* that the application of a high vacuum system during the purification of each of the reaction components would eliminate side reactions [14]. Also, Dimitrov and Schlaad demonstrated that a monodisperse product could be synthesized using an amine salt as a macroinitiator [15]. Originally, results from NCA polymerization kinetic studies were based on less than optimal methods, such as the determination of CO_2 emissions.

Recent kinetic studies of α-amino acid N-carboxyanhydrides, by Vayaboury *et al.*, were performed on N_ε-triflouroacetyl-L-lysine under standard conditions, at 0 and 50°, and again at 0° C with urea [33]. The use of N-hexylamine initiator was used in a variety of *M/I* ratios. It was found that after synthesis under standard conditions, a carboxylic acid terminated species was

detected [65]. This polymeric species was termed dead (or inactive), as no further polymerization could occur when additional monomer was added to the reaction vessel. This reaction termination was originally described by Sela and Beger [88], and verified experimentally by Vayaboury *et al.* [80]. Additionally, under standard conditions, the amine terminated species reacted with DMF to produce another inactive species that was found to be an N-formyl terminated polypeptide. Both species of inactive polymer were determined, originally, by nonaqueous capillary electrophoresis (NACE), coupled with online mass spectroscopy (NACE-MS) under acidic conditions [42], [65].

Successive to the aforementioned method, a newer NACE method has been exploited. The novel NACE method utilizes basic electrophoretic conditions rather than acidic conditions [9]. Each method was used to determine the percentage of inactivated polymer for each *M/I* ratio. Furthermore, the use of CE was used to derive the kinetic data necessary to determine the rate-limiting step for the N-hexylamine initiated polymerization with TFA-Lys based NCA.

1.4.4.d. Classes of Cyclomonomers

N-carboxyanhydrides are readily accessible by synthesis of protected $_{L}$-amino acids using a technique involving phosgenation in the presence of an HCl scavenger, such as α-pinene or tri-ethyl amine. These NCA cyclomonomers differ from the γ-lactams with the addition of a oxygen atom on the molecule (Figure 1.8). One major drawback to NCA is that it is a highly reactive nucleophile, and polymerization can be initiated with water. Therefore, it is crucial that the NCA monomers be handled under copiously dry conditions [28], [30], [34], [89].

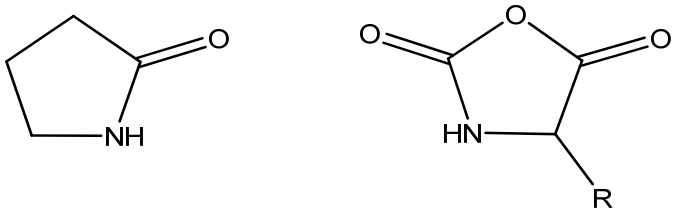

γ–Lactam N-carboxyanydride

Figure 1.8. Two classes of cyclomonomers: Lactams (γ-lactam shown) and N-Carboxyanyhydride

1.4.5. New Technologies in Synthesis of Living Poly(Amino Acid)s

Previous research in the synthesis of PEG-b-paa block polymers yielded significant and novel contributions to the field of NCA living ring opening polymerization (LROP) of amino acids, but some required the use of metal catalysts to achieve a monodisperse product. Metal catalysts can be difficult to remove during purification, and incomplete removal can render a product useless for bio-applications. Scholz *et al.* (2008) developed reaction conditions that allow for the use of macroinitiators, more specifically α-methoxy-ω-amino PEG, and were able to achieve control over the reaction without the need for metal catalysts [29]. They were able to use thiourea in combination with lowered reaction temperatures to prevent the formation of β-sheet secondary structure in the oligomers. Thus, allowing the propagation rate to remain at a level that prevented the activated monomer mechanism from taking over. The new synthesis technique allowed for strict control over molecular weight, PDI, and architecture, while keeping the reaction in line with a true living polymer state [28], [29], [65]. Without the addition of thiourea, the growing polymer chains would be truncated, and ultimately terminated, eradicating any living character from the paa chain.

1.4.6. Conclusion

Biodegradable, biocompatible, non-antigenic, and nontoxic materials are very useful in a wide range of biotechnical and biomedical applications. One example of such a material is PEGylated poly(amino acid) which may be synthesized by living ring opening polymerization of α-amino-*N*-Carboxyanhydrides (NCA) to create poly(amino acid)s. This polymerization technique can produce biocompatible polymers that are of a well-defined architecture and a controlled molecular weight. The use of polyethylene glycol (PEG) serves two roles in the project. First and foremost, PEG has been shown to be biocompatible, which makes it highly attractive in biomedical implants, drug delivery, and gene therapy. Second, the functionalized form, α-methoxy-ω-amino (mPEG-NH_2), can be used as a nucleophilic macroinitiator for living ring opening polymerization of NCAs to synthesize block and randomized co-poly(amino acid)s.

The living ring opening polymerization (LROP) of NCAs must be performed under optimal conditions to obtain a product that exhibits a high yield, while being of a well-defined architecture, controlled molecular weight, and show a true living nature. Therefore, the use of metal complexes and high vacuum techniques had been previously employed, but are practical in a general sense. The use of urea, to prevent β-sheet formation in the growing polymer chain, has made the synthesis and purification process much more cost effective and less time consuming. Additionally, the use of urea has shown that the aforementioned criteria of synthesizing a paa of controlled molecular weight and monodispersity can be achieved.

Once synthesized and purified, the PEGylated poly(α-amino acid) protective groups can be selectively removed from the side chains to reinstate their functionality. This allows the paas to be used as surface coatings, drug delivery vehicles, or for use in gene therapy. It is projected that when combined, the PEG and the amino acid regions can yield a product that is both stable and biologically feasible for use in mammalian tissues in a wide variety of roles.

One such application for the paas that are being studied is for use on a retinal implant prosthesis that may lead to a solution for people suffering from retinitis pigmentosa and age-related macular degeneration. Currently, there are no cures for these diseases and an implantable device is a promising solution that may help restore vision to those affected. The paas being studied will render the implantable device biocompatible, and quench both tissue damage from implantation and the immune-mediated responses often seen with implantable devices. However, it is first necessary to produce a biocompatible polymer product, which is of a desired architecture and chain length that will maximize the degree of coating, for which the specific surface application requires. It is with this focus that the present study has been undertaken.

CHAPTER 2

Synthesis of α-Amino-*N*-Carboxy Anhydrides (NCA)

2.1. Introduction

This part of the project required the successful synthesis and purification of the NCA monomers of L-Glutamate, L-Lysine, and L-Cysteine α-amino acids for successive synthesis of the PEGylated poly (amino acid) oligomers and polymers. During the synthesis of the NCA monomers, the buildup of hydrochloric acid (HCl) was addressed with α-pinene to reduce the formation of amino acid hydrochlorides. It was shown that NCA monomers could be synthesized and purified to give yields greater than 86%. The purity of the NCA was subsequently determined by proton nuclear magnetic resonance.

2.1.1 A Brief Review of NCA Synthesis History

Nature has the unique ability to produce an intricate and diverse range of structures that provide functionality by synthesizing precisely tailored macromolecules [90]. A protein's biological activities are derived from nature's ability to precisely arrange the 20 amino acids into specific sequences, which in turn, create well-defined secondary structures such as coils, α-helices, and β-sheets [40], [90], [91]. The self-assembly of the secondary structures relies on finding a conformation of the lowest energy possible, and gives rise to tertiary and quaternary structures [27], [70].

Chemists and biologists, however, do not currently have the technology to create structures with a fidelity as high as those that are produced in nature. Synthetic chemistry can,

however, create a wide variety of macromolecules. The challenge is to be able to create biomimetic macromolecules that contain conformational and hierarchical structures that reveal the link between synthesis, structure, properties and interaction of biomacromolecules [31], [92]. Poly(amino acid)s are a class of materials that can act in a biomimetic fashion by taking advantage of the vast array of NCA-based material available. Careful consideration of a paa product's amino acid selection and composition, as well as molecular weight can elucidate the functionality of the polymer for a variety of purposes.

Two methods for the synthesis of α-amino acids-*N*-carboxy anhydrides (NCA) have been established. These are the Leuchs method and the Fuchs-Farthing method [27], [28], [36]. The Leuchs method is based on the cyclization of *N*-alkoxycarbonyl amino acid halides to form oxazolidine-2,5-dione. The second method is the Fuchs- Farthing method, which uses phosgene to synthesize the amino acid based cyclic anhydride [28].

2.1.2. Leuchs Method of NCA Synthesis

NCA was first unintentionally discovered by Herman Leuchs in 1906 when he attempted to purify *N*-ethoxycarbonyl and *N*-methoxycarbonyl amino acid chlorides by distillation. He originally termed them "anhydrides of amino acids," but later renamed them "α-lactams of amino acids" [28] as he concluded that they were polymeric modifications of α-lactams. By 1921 Curtius *et al.* and Wessely *et al.* used water, alcohol, or primary amines to initiate polymerization and assumed, for the first time, that high molar mass polypeptides could be synthesized from NCAs [28], [93].

The Leuchs method uses a halide to form NCAs at lower temperatures, which has the advantage of lowering the possibility of high temperature decomposition of certain NCAs. Some halide byproducts, however, may interfere with the crystallization of the NCA product from

solution [94]. It is proposed that the rate determining step, of the Leuchs method, is the nucleophilic attack by the halide group on the alkyl group. Scheme 2.1 shows the proposed mechanism of the NCA formation using an acid halide, as outlined by Krichedorf (2006) [28], [31]. It is suggested that the halogenide group attacks the carbonyl oxygen of the carbamate group forming a cyclic ion intermediate [31], [94].

The type of halogenating agent used is an important factor with regard to how easy it is to synthesize NCA. For example, a bromide ion is a better nucleophile in the rate determining step than a chloride ion. Additionally, the nature of the NCA groups influences the rate of cyclization, and increases this rate when the electrophilicity of the alkyl group increases [31].

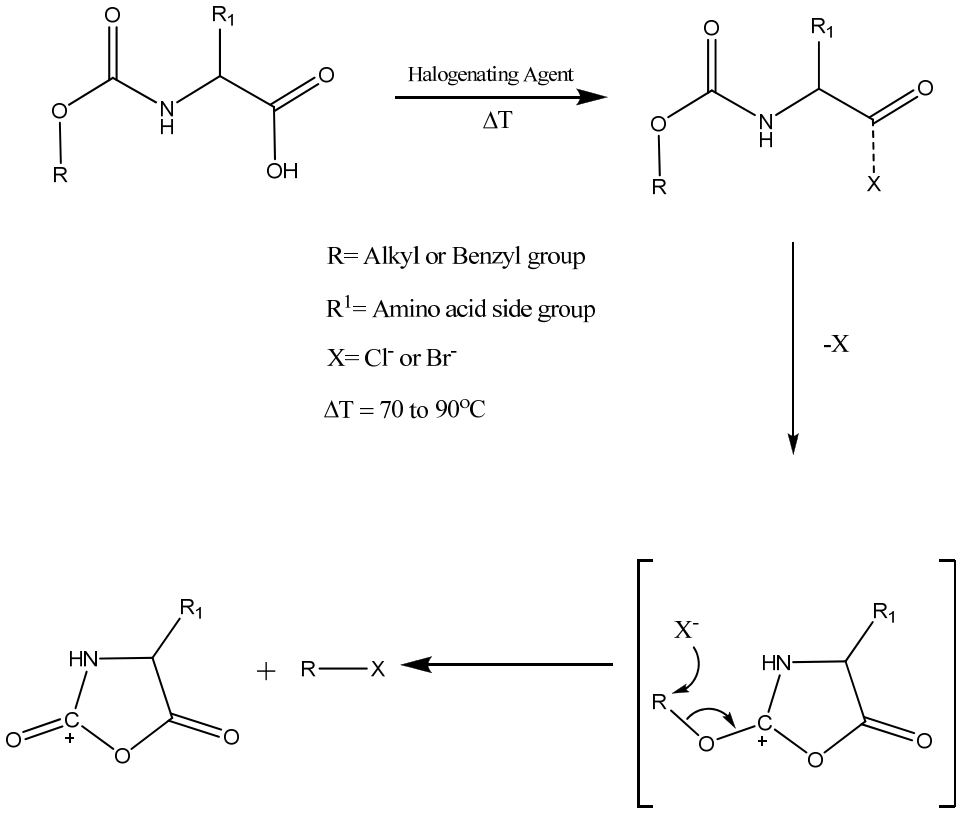

Scheme 2.1. The original version of the Leuchs method for the cyclization of NCAs

2.1.3. NCA Synthesis Using the Fuchs-Farthing Method

The Fuchs-Farthing method of NCA synthesis is probably the most widely used method today. This method is fairly straight forward and involves phosgenation of free α- amino acids. This method was first used by Fuchs (1922) for the preparation of N-phenyl-Gly-NCA and was applied to a broad range of NCAs by Farthing *et al*. (1950), Coleman (1950) and Levy (1950) [31]. This method promotes cyclization through the formation of *N*-chloroformyl amino acid intermediates after the loss of a hydrochloric acid (HCl) molecule. This is followed by the loss of a second HCl molecule to complete the NCA formation as depicted in Scheme 2.2.

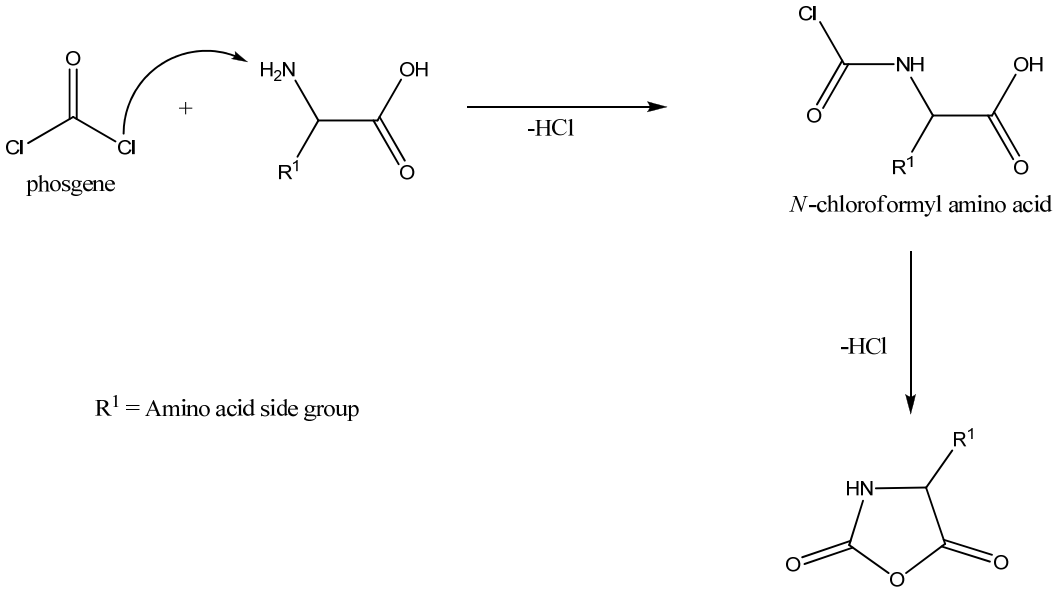

Scheme 2.2. Fuchs-Farthing method for NCA synthesis using phosgene

In principle, any reaction media that is inert against phosgene may be used in the synthesis of NCAs. It has been shown that non-polar solvents such as chloroform, carbon tetrachloride, toluene, or 1,4-dioxane , and polar aprotic solvents such as ethyl acetate and

tetrahydrofyran, are acceptable solvents for NCA synthesis. Chloroform (Dielectric constant (D) = 1.04), carbon tetrachloride (D=0.00), toluene (D=0.36), and ethyl acetate (D=1.78), nevertheless, can increase reaction times by a factor of 10 to 30 times [31]. Tetrahydrofuran (D=1.75) and 1,4-dioxane (D=0.45) are the most widely used reaction media, but they can exhibit side reactions that may make amino acid hydrochlorides when exposed to HCl for several hours [31], [95–97]. Amino acid chloride hydrochlorides can then be phosgenated in a second step to form α-isocyanato acid chloride (Scheme 2.3) [42].

Previous methods called for passing phosgene gas through the reaction mixture, but the gas does not allow for control over the stoichiometry. Excess amounts of phosgene gas can cause the formation of α-isocyanato acid chloride as mentioned above. To evade stoichiometric problems, diphosgene and triphosgene have been used. Diphosgene is available in liquid form, and supplies two molar equivalents of phosgene to the reaction [36], [95]. Triphosgene is available in a crystalline form and supplies three molar equivalents of phosgene to the reaction [97]. Di- and triphosgene require elevated temperatures to liberate reactive phosgene molecules from dimer and trimer molecules $\leq$ 50°C [31], [36], [97–99].

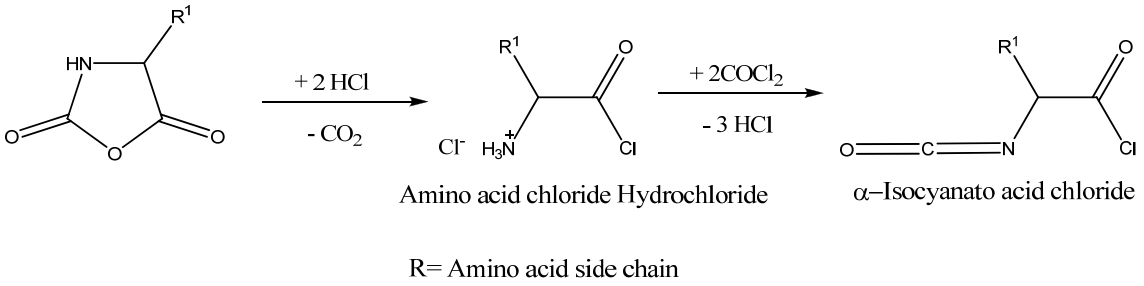

Scheme 2.3. Contaminant formation from presence of excess phosgene and HCl.

2.1.4. Methods to Address Excess HCl Byproducts During NCA Synthesis

Several methods have been investigated to alleviate the effects of HCl in the NCA reaction solution. Some methods investigated have attempted to mitigate the HCl content in solution, or abandoned HCl from the solution altogether.

Poché *et al.* washed the reaction mixture with water and aqueous bicarbonate at 0°C to remove HCl and the hydrochloride salts. The sensitivity of *N*-carboxy anhydrides to water negates this process in NCAs that are conventionally crystallized from solution. The method is applied to NCAs derived from oils [100].

Mobashery *et al.* and Kricheldorf *et al.* made use of silylated amino acids to eliminate the HCl generated in the reaction mixture. Kricheldorf *et al.* (1989) demonstrated a novel method that was based on the Fuchs-Farthing method [28], [42]. Kricheldorf's group showed that HCl could easily be avoided in solution when performing a phosgenation of silylated amino acids. Additionally, it was established that the hydroxyl groups were easily protected during cyclization via removal of the trimethylsilyl group [28].

Mobashery's (1985) method took advantage of silylated amino acid intermediates in a modified Luechs synthesis [101]. First, tBoc-α-*N*- amino acids were silylated in ethyl acetate with *tert*-butyldimethylsilyl chloride with triethylamine in solution to create triethylamine HCl, which was removed from solution by filtration. The filtrate was then evaporated to yield an oil which was dissolved in dichloromethane, chilled to 0°C, and then had a few drops of DMF added as an activator [101].

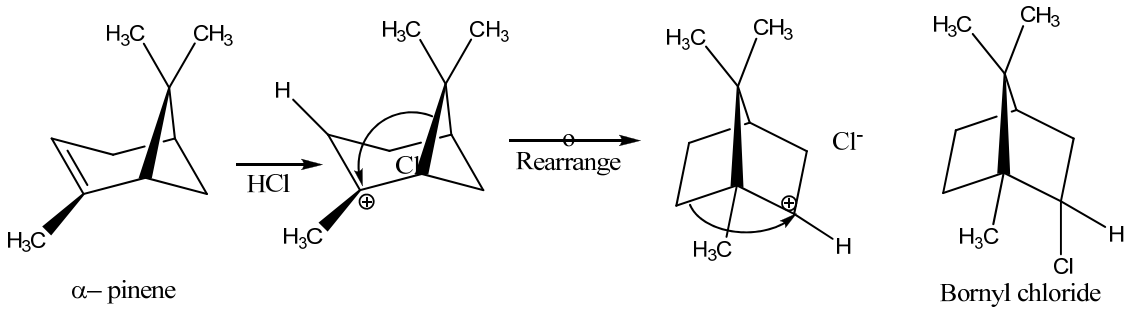

Scheme 2.4. α-pinene used as a hydrochloric acid scavenger during the production of NCAs.

Another method to combat the production of HCl in solution, upon phosgenation of α-amino acids using a modified Fuchs-Farthing method, is the addition of (+)-limonene or α-pinene [31], [37], [102]. α-pinene initially produces an unstable isomer, pinene hydrochloride, but rapidly isomerizes into bornyl chloride (Scheme 2.4) [103].

The compounds act as HCl scavengers, thus preventing side reactions. The use of a proton scavenger quenches the buildup of HCl, thereby speeding up the reaction. In addition to preventing side reactions, the use of α-pinene can allow for production of NCAs on a larger scale than was previously capable [37].

The use of an HCl scavenger, more specifically α-pinene (Scheme 2.5), is most appealing to our study, and was used extensively to produce all of the NCAs of choice. This technique is relatively inexpensive and not time consuming. There is no real need for special equipment to conduct the synthesis, and removal of pinene from the final product is straight forward. The phosgene and pinene were easily removed from the NCA product by way of no less than two crystallizations (discussed in detail later in this chapter).

2.2. Experimental

2.2.1. Materials

The solvents, including ethyl acetate (EtOAc) and n-hexanes, and the (1S)-(-)-alpha-pinene, 98% (α-pinene) were purchased from Fisher Scientific (Waltham, MA). The solvents were distilled just prior to NCA synthesis as described below. The triphosgene was purchased from Tokyo Chemical Industry Co., LTD. (Tokyo, Japan) and stored in the refrigerator at 5°C, per the manufacturer's specifications.

The γ-benzyl-L-glutamate was purchased from Bachem (Torrence, CA), stored at room temperature and used as received from the manufacturer. N^6-trifluoroacetyl-L-lysine was purchased from Chem-Impex International (Wood Dale, IL), stored at room temperature, and used as received. Finally, the S-carboxybenzyl-L-cysteine was purchased from Sigma Aldrich (St. Louis, MO), and Chengdu Unibiochem CO., LTD. (Schichuan, China), and stored at -20°C in a sealed container, as recommended by the manufacturer.

2.2.2. Modified Fuchs-Farthing Method for the Synthesis of NCAs

The most reasonable method for production of NCAs for the work, presented herein, is a modified Fuchs-Farthing method. This procedure will be applicable to all NCA syntheses, with the only deviation being in the relative stoichiometric amounts of solvents used to crystallize the NCAs during purification. This is due in part to the chemical properties of the side groups and the protective groups that have been attached to the side chains of the α-amino acids.

First, a Schlenk air free flask, containing a magnetic stir bar, was placed under vacuum for 2 hours. Then, α-amino acid (0.1g/mL) was added and suspended in freshly distilled ethyl acetate. Next, 2.1 equivalencies of α-pinene was added to the suspension. Subsequently, 0.5

equivalencies of triphosgene was dissolved in a small amount (between 1/2 and 1/3 equivalencies) of freshly distilled EtOAc. It was then added to the suspension, and the round bottom flask was fitted with a condenser. The reaction mixture was stirred for 2.5 to 4.5 hours (depending on the α-amino acid used) at 110°C. The reaction mixture was then filtered through a glass Buchner funnel that has a fritted disk (10-15 μm pore size), to remove any unreacted amino acid. The filtrate was concentrated, under vacuum, on a rotary evaporator at 35°C, and finally crystallized by adding n-hexane and left to precipitate/crystallize in the freezer (repeated 3 times). The crystalline product was filtered from solution, and placed in a clean/dry Schlenk air free flask fitted with a silicone septum, then dried under vacuum. The following amino acids were prepared by the above mentioned procedure: γ-benzyl-L-glutamate, N^6-trifluoroacetyl-L-lysine, and S-carboxybenzyl-L-cysteine.

Amino Acid	Mw AA (g/mol)	Mw NCA (g/mol)	Molecular Formula (NCA)	Average RXN Time (hrs)	Starting Weight NCA (g)	Theoretical Yield (g)	Actual Yield (g)	Yield (%)
Glu	237.26	265.25	$C_{13}H_{13}NO_5$	2.5± 0.17	1.0 ± 0.10	1.1± 0.13	0.970± 0.04	88 ±4.1
Cys	255.29	283.28	$C_{12}H_{11}NO_5S$	4.5± 0.37	0.5± 0.02	0.5± 0.03	0.480± 0.07	86 ±1.9
Lys	242.20	270.19	$C_8H_{11}F_3N_2O_3$	3.0± 0.30	1.0± 0.09	1.1± 0.14	1.04± 0.04	93 ±2.3

Table 2.1. Physical properties and yields of the amino acid (aa), and NCA monomers.

2.3. Results

Each of the α-amino acids was synthesized by a modified Fuchs-Farthing method, as discussed above. H^1 nuclear magnetic resonance (NMR) spectra were obtained on a Varian Unity Inova 500 MHz instrument equipped with a 5 mm Penta (H,C,N,P,D) PFG VT probe for each of the purified products. The ^{1}H-NMR of the crude product was obtained (Figures 2.1 and Appendix Figures B.2.and B.3), and a secondary purification was performed prior to synthesis of

block and random copolymers. Each NCA sample was dissolved, at a concentration of 5mg/mL, in dimethyl sulfoxide-d_6 (DMSO-d_6) and measured at 35°C with 16 scans and a 2 second relaxation delay time. Table 2.2 outlines the typical NMR chemical shift values obtained for each monomer molecule, which showed that the NCA products were easily distinguishable, and purity was readily observed.

^{1}H								
	Side Chain ^{1}H Assignments						Protecting Group ^{1}H Assignments	
NCA	α-carbon	β_α-carbon	β_β -carbon	β_γ -carbon	β_δ -carbon	α-NH	Phenyl	NH
Lysine	4.43	1.36	1.49	1.73	3.17	9.08		9.4
Glutamate	4.45	1.93	2.04		5.09	9.08	7.36	
Cysteine	4.80	3.31	5.28			9.24	7.38	

Table 2.2. Chemical shift data obtained from ^{1}H-NMR in DMSO

Highly purified NCA products were obtained after crystallization and drying of the NCA products, and kept in an air free environment until used in polymerization. All handling of NCA was done under an inert gas such as argon, including product mass determination. This minimized the initiation of polymerization by humidity in the air, as it known that water can act as a nucleophile [28].

Figure 2.1 shows the ^{1}H NMR of purified S-Cbz-L-cysteine immediately after NCA purification. The spectrum is very clean, and all peaks are well-defined and have integration ratios that agree with the NCA structure. The spectrum shows a definitive production of protected cysteine NCA with no evidence of contamination by solvents or α-pinene. It should

also be noted that there is no evidence of polymer formation that can result from exposure to humidity or other sources of contaminants.

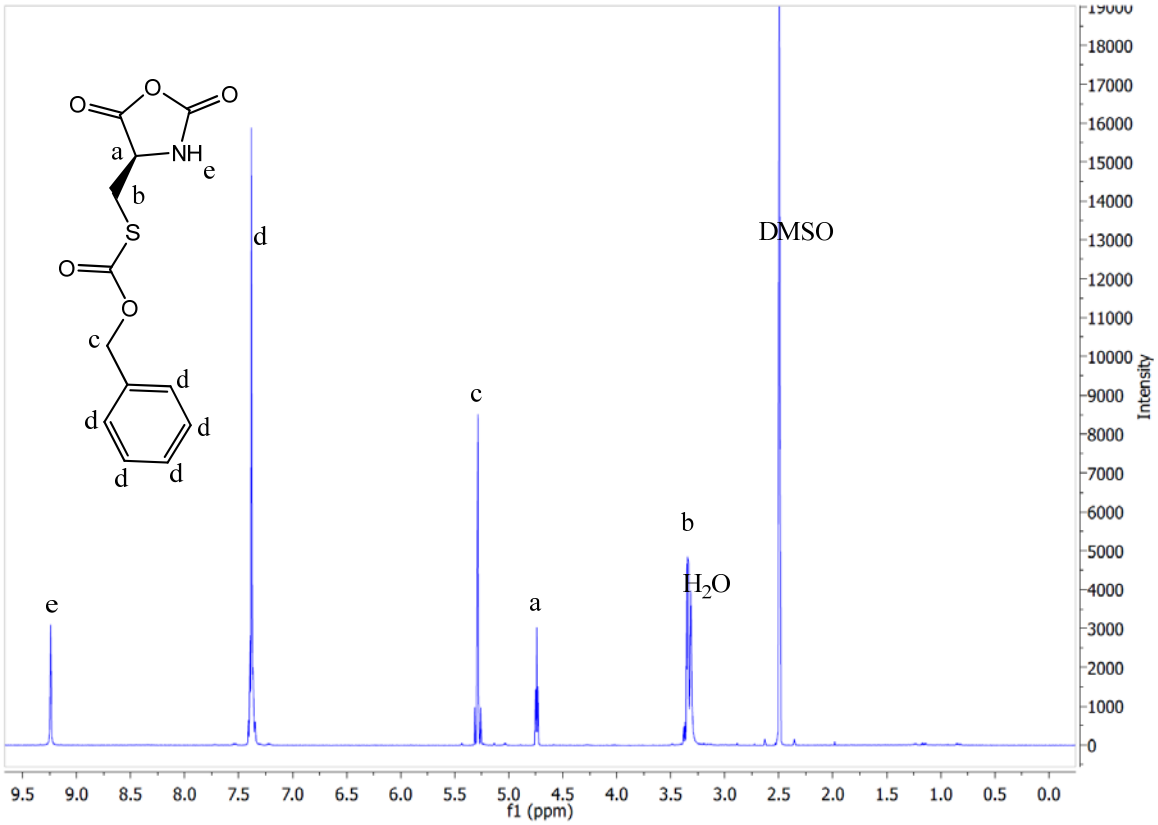

Figure 2.1. ^{1}H NMR spectrum of S-Cbz-l-cysteine NCA in DMSO-d_6, on a Varian 500 MHz instrument at 35°C): δ/ ppm = 3.34 (2H, CH_2-S-CO), 5.29 (2H, -O-CH_2-), 7.36 (5H, aromatic *H*), 9.1−9.24 (1H, -N*H*-).

Refer to Appendix B

Figure B.2 and B.3 for ^{1}H-NMR spectra data for the N^{6}-TFA-L-lysine and γ-Bnl-L-glutamate NCAs.

2.4. Discussion.

Phosgenation of the protected amino acid (aa) derivatives by way of a modified Fuchs-Farthing method proved to be successful. The purified products all yielded greater than 85%

(Table 2.1), and synthesis times were less than 5 hours. ^{1}H NMR experiments showed that NCA products of high purity could be synthesized.

It should be noted that S-Cbz-L-Cys proved to be the most difficult molecule to work with. It took much longer to synthesize and approximately 10% of the amino acid from Unibiochem CO., LTD was found to be non-reactive with the phosgene by a persistent turbidity of the solution, and weight determination of dried unreacted amino acid. The reactions, therefore, were halted at 4.5 hours as degradation of the cysteine NCA was a concern at such an elevated temperature [31]. Regardless, the cysteine amino acids that were reactive with phosgene yielded a superior quality product as observed in the ^{1}H-NMR in figure 2.1. The α-carbon was observed at 4.74 ppm and the phenyl ring of the protecting group at 7.38 ppm in DMSO (35°C).

The γ-benzyl-L-glutamate amino acid gave very high yields, and demonstrated a very high reactivity during phosgenation. It was visually evident once glutamate NCA synthesis was nearly complete, as the solution became almost completely clear. Only a very small amount of unreactive amino acid was observed in solution prior to removal by filtration. Appendix Figure B.3 shows a very pure γ-benzyl-l-glutamate NCA product. The ^{1}H-NMR spectrum shows the benzyl ring at 7.36 ppm, and a chemical shift of 4.45 ppm for the α-carbon in DMSO at 35°C.

The N^{6}-TFA-L-lysine required a slightly longer reaction time than that of γ-benzyl-L-glutamate; however, it still yielded a superior product. The lysine was easily purified, per the aforementioned technique and gave ^{1}H-NMR spectrum, as seen in Figure B.2. The chemical shifts for the α-carbon and the protective group's amide were observed at 4.43 and 9.08 ppm respectively. Had the amine of the side group not been protected, the chemical shift would have been expected around 2.0 ppm in DMSO at 35°C.

CHAPTER 3

Effects of Urea on Oligomer Secondary Structure Formation

3.1. Introduction

Oligomers of L-Lysine, L-Glutamate, and L-Cysteine were synthesized at 5, 10, and 20 repeat units with N-hexylamine as the macroinitiator. The purpose of this study was to determine secondary structure content of the oligomers during the first few iterations of polymerization of α-amino acids N-carboxy anhydrides. Circular dichroism, and attenuated total reflectance infrared spectroscopy were performed to determine the α-helix and β-sheet secondary structure in the liquid and crystalline state, respectively. Additionally, experiments were performed on hexylamino-poly-L-cysteine to observe how the use of urea during polymer synthesis affects the β-sheet secondary structure content of the growing chain. It was shown that L-Cysteine adopts a β-sheet structure at all oligomer chain lengths, and that β-sheet content could be reduced with the addition of urea to the reaction media. Additionally it was shown that at chain lengths of 5 repeat units L-Glutamate and L-Lysine exhibit predominantly β-sheet secondary structure with some α-helix content. However, when the chain lengths were 10 and 20 repeat units, α-helical secondary structure was predominantly adopted, while some β-sheet structure was retained.

3.1.1. Review of Oligomer Secondary Structure Formation in Living Ring Opening Polymerization

Living ring opening polymerization sets itself apart from other polymerization techniques as it allows for the synthesis of block copolymers of desired molecular weight. Most polymerization techniques do not yield such control over the reaction and have undefined chain

lengths. The living polymerization reaction of NCA occurs under conditions that allow for the primary amine mechanism, as discussed in section 1.2.

The ring opening polymerization, of N-carboxyanhydrides of α-amino acids, may deviate from the primary amine mechanism if the rate of propagation is faster than the rate of decarboxylation. This will form an acidic end group on the growing polymer chain and cause the polymer chain to terminate [28], [38].

Blout (1960) conducted infrared (IR) spectroscopic analysis of a variety of synthetic polypeptides to determine the secondary structure and derived [104]:

1. "High molecular weight polypeptides of α-amino acids prefer β-sheet structure, when the side chains are branched in the β position."
2. "Heteroatoms in the γ position prefer a β-sheet structure when synthesizing high molecular weight polymers from α-amino acids."
3. "All other high molecular weight α-amino acids form α-helices."
4. "Oligopeptides of all α-amino acids form β-sheets".

Blout's work, in tandem with many others, has solidified the theory that all amino acid oligomers can take on a β-sheet conformation, however, some amino acid paas adopt an α-helical structure when the chain length is long enough [28], [104]. This raises the questions: How does the secondary structure of the polymer chain influence the course of polymerization, and how can the reaction conditions be optimized to reduce unfavorable secondary structure formation?

Kawai *et al.* (1974) [105] found that crystalline β-sheet lamellae precipitate from solution during the first stages of synthesis. Chain growth still proceeds, but is very slow due to steric hindrance of the active chain end [28], [105]. Chain death may ultimately occur in these polymer chains, as propagation rates are so slow that the kinetics of the reaction pushes the system to

follow the carbamate mechanism. Thus, the chain ends will no longer be reactive and polymerization will cease altogether.

The hypothesis of chain death is in agreement with experimental findings that show high molecular weight paas are only obtainable in growing chains that can adopt an α-helical structure. These paas are helicogenic, and usually have molecular weights >10,000 Da [28].

Blout and Doty (1956) [104] ; found that primary amine initiated polymerization of γ-Bnl-L-glutamate NCA follow the subsequent route [28], [106]:

1. Initially, soluble di-, tri-, and tetra-peptides form.
2. Oligomers with a $\overline{DP}_n$ of >4 associate into extended β-sheets and may precipitate from solution in the form of crystalline lamellae.
3. Longer chains that are comprised of helicogenic amino acids may adopt an α-helical form and continue chain growth until all monomer molecules are consumed.

Additional work was also done using L-alanine and L-leucine NCAs, which showed the route of polymerization listed is, in principle, valid. The degree of polymerization ($\overline{DP}_n$) for the formation of β-sheets in L-alanine and L-Leucine is between three and five [28], but this number may vary slightly depending upon the solvent used. Helicogenic NCAs of γ-benzyl-L-glutamate and N^{ε}-Cbz-L-lysine were found to form stable α-helices when $\overline{DP}_n$ was equal to 9±1 and 12±1 respectively [28], [107], [108]. It has been determined that soluble oligopeptides of a $\overline{DP}_n < 5$ are usually the precursors of β-sheets, and β-sheets are the precursors of α-helices [28]. There is some debate, however, as to how these secondary structure formations occur. The most feasible hypothesis is that the formation and precipitation of β-sheets are in equilibrium and the soluble fraction of oligomers is the precursor of α-helices [28], [52].

This hypothesis is supported by several observations made during experimentation by Blout *et al.* First, bimodal molecular weight distributions, reported for primary amine initiated

polypeptides, demonstrated that living polymerization of NCAs do not always necessarily result in a narrow molecular weight distribution [28]. It was shown that β-sheet formation reduced the reactivity of the growing chain due to steric hindrance. Yet, those chains that can reach the threshold length for random coil to α-helix transition grew faster, thus yielding a bimodal molecular weight distribution[28], [41106106]. Second, the use of ^{13}C cross-polarization/magic angle spinning (CP/MAS) showed that α-helix and β-sheet structures can be determined in a qualitative and quantitative manner. This method allowed for the detection of β-sheet structures at <5% in the presence of a 90% α-helix structure. This demonstrated that β-sheets do not necessarily convert completely to α-helices and are thermodynamically stable, as the ratios of β-sheet to α-helix remained intact after being dissolved and re-precipitated [28], [108], [109]. Finally, the purified oligomers, with a $\overline{DP}_n < 10$, constituted poly(L-glutamate), poly(L-alanine), or Poly(L-leucine) [28], [41], [106], [109].

Secondary structure, molecular weight, and polydispersity may be influenced by the polymerization mechanism that the reaction follows. This is due to a role played by the association equilibrium of the growing paa chains and depends upon the mechanism that is employed [28]. Primary amines, as discussed above, generally exhibit fast initiation followed by slow propagation, which can cause a high concentration of oligopeptides which yield low α-helix/β-sheet ratios, low molecular weights, and a bimodal molecular weight distribution[28], [30], [84], [92]. The problem then exists; how to minimize β-sheet secondary structure in the oligomer chains?

Several groups have found methods to deal with secondary structure formation of α-amino acid oligomers. Deming *et al.* used metal catalysts and Hadjichristidis *et al.* employed high vacuum techniques (refer to section 1.2.1 for further explanation of their work). Vayaboury *et al.* (2008) used urea and low temperatures to gain control over the polymerization reaction and reduce the bimodal response of the molecular weight distribution [33].

The first two methods are quite cumbersome and have drawbacks with regard to purification, and expense of glassware and equipment. The third method, however, simply utilizes urea to reduce secondary structure formation (β-sheet) of the oligomers, and gaining control over the reaction. The method is quite simple and appears, from previous works, to facilitate the production of paas that meet the criteria necessary to be considered a living ring opening polymerization [29], [65].

3.1.2. Urea's Effect upon Secondary Structure in Poly(Amino Acid)s

Urea is a small organic molecule with the chemical formula $(NH_2)_2CO$ and a molecular weight of 60.06g/mol. It is highly soluble in water (107.9g/100ml water at 20°C), and when dissolved in water, does not act as an alkali or a base. Urea may also be called carbamide and has a wide variety of uses in biology, chemistry, industry, and agriculture. More specifically, urea is used to denature protein and poly(amino acid)s by interrupting the secondary structure. The molecular basis of denaturation is poorly understood, however [110], [111].

The driving force for β-sheet prevention, during paa synthesis, is chemical in nature. The secondary bonds (hydrogen bonds) holding the paa segments together are disrupted by the urea. The urea should be capable of forming equally strong, if not stronger bonds, with the group holding the conformation together. For example, urea or guanidine hydrochloride, at high enough concentrations, can break hydrogen bonds and interrupt the formation of β-sheets and α-helices.

It is widely accepted that urea interrupts intra- and inter-molecular hydrogen bonding in aqueous environments, and as previously mentioned, the mechanism is not fully understood. To further complicate the issue, water cannot be present in the reaction, and LROP must be performed under anhydrous conditions. It is assumed, however, that the disruption of hydrogen bonding in alternate solvent will be similar the effects seen when urea is used in water. Here, *N*-

N-dimethylformamide (DMF) will be used, and has a dipole moment of 3.86 D, and urea has a dipole moment of 4.42 D, and is soluble in the DMF [112]. The effects of inter-molecular bond disruption are of interest when looking at short chain oligomer secondary structure formation.

3.1.3. Research Goal

The aim of this portion of the research project was to show that the use of urea in dimethylformamide reduces the β-sheet secondary structure of the growing oligomer units, thus promoting kinetic conditions that favor living ring opening polymerization. Additionally, it was anticipated to confirm the secondary structures hypothesized for oligomers of poly(L-lysine), poly (L-glutamate), and poly(L-cysteine) oligomers.

The elimination of β-sheet formation during the first few iterations of polymerization will help eliminate side reactions, and lead to monodisperse products. This will demonstrate the feasibility of urea in DMF solution in lieu of high vacuum techniques or metallic catalysts.

3.2. Experimental

3.2.1. Materials

Acetonitrile, N, N-Dimethylformamide (DMF), tetrahydrofuran (THF), Drierite™ and urea were purchased from Fisher Scientific (Waltham, MA). The DMF was distilled and stored on 4Å molecular sieves to prevent water contamination prior to use. The urea and THF were used as received. Argon gas was purchased from Airgas (Huntsville, AL) and passed through a desiccator trap containing Drierite™ to remove any water vapor from the argon gas prior to

entering the reaction vessel. N-hexylamine was purchased from Sigma Aldrich (St. Louis, MO), dried and fractionally distilled over KOH prior to use.

3.2.2. Methods

3.2.2.a. Living Ring Opening Polymerization for the Production of α-Amino Acid Oligomers with Urea.

Living ring opening polymerization was carried out by first synthesizing and purifying the respective NCAs to be used in the reaction (please refer to section 2.2.2). The NCAs was dried under vacuum in a Schlenk air free flask, closed with a silicone stopper, to remove all residual solvents and minimize exposure to atmospheric humidity. Then urea was ground using a mortar and pestle to increase surface area for drying, and the appropriate amount of urea (to yield a final conc. of 0.2M) was placed in a second Schlenk, with a silicone stopper and a magnetic stir bar, to dry under vacuum for not less than one hour. Then the appropriate amount of distilled DMF (necessary to yield an NCA concentration of 0.1M) was added to the Schlenk containing the urea, and placed under vacuum to degas for approximately 15 minutes. Once degassing was complete, the DMF/urea solution was added to the NCA, along with a stir bar, under a flow of argon. Finally, a needle and syringe was used to inject the freshly distilled and dry N-hexylamine into the Schlenk containing the NCA, to initiate polymerization under a flow of argon. The flask was then evacuated of all air, which was replaced by argon. The flask was closed, and allowed to react at ambient temperatures while stirring until all apparent evolution of CO_2 subsided.

Twice daily the flask was evacuated of all air and replaced with fresh CO_2. This served a twofold purpose. First, the evolution of CO_2 is a direct indication that the reaction is occurring. Once the reaction is complete, no gas should be apparent upon evacuation of the reaction flask. Second, as discussed earlier, increased levels of CO_2 can cause the kinetics of the reaction to slow

to the point where the carbamate mechanism is initiated. By venting off CO_2 it was assumed the amine mechanism remained intact.

3.2.2.b. Ring Opening Polymerization for the Production of α-Amino Acid Oligomers without Urea.

Ring opening polymerization was carried out using an identical method as outlined in section 3.2.2.a. except the use of urea was omitted. Therefore, there was no need to weight and dry this chemical. The DMF (amount to necessary to yield a final NCA conc. of 0.2M) is placed into a Schlenk air free flask and degassed for 15 minutes. The DMF is added to the NCA under a flow of argon, and the remaining synthesis and purification steps are identical as those outlined in section 3.2.2.a.

3.2.2.c. Oligomer Isolation and Purification

The synthesis process of the α-amino acid oligomers, under living conditions, will only stop once the supplies of monomer units have been exhausted. One caveat, however, is that an alternate mechanism could be followed due to impurities in the flask, which lead to truncated or dead polymer chains. It is thought that oligomers synthesized without urea will not follow the primary amine mechanism; therefore ring opening polymerization may follow an alternate mechanism to synthesize the oligomer products. These oligomers were synthesized with no intent to control the reaction as they are short chain molecules and it is difficult to adequately affect dispersity under standard conditions.

To purify the oligomers, the mixture was transferred to a round bottom flask, and the DMF was removed on a Labconco rotary evaporator, with an inline vacuum pump attached, at

35°C until dry. Then, THF was added in an equivalent volume of the DMF that was used during the polymerization step. The solution was left to stir for $\leq$ 2 hours. This was done to reproduce identical conditions as those samples synthesized with urea. The THF solution was filtered on a Buchner funnel fitted with a glass frit (10-15 μm) to remove the precipitated urea. The filtrate was collected in a clean round bottom flask, and reduced on the rotary evaporator to a volume $\geq$ 1mL or until it became highly viscous. The concentrated solution was then placed into a Spectra/Por 6 regenerated cellulose dialysis tubing (Mw cutoff (c/o) 1,000) and distilled against 4 liters of de-ionized water (dH_2O) (changed with fresh dH_2O three times). This was done to remove any remaining urea, and residual THF/DMF. Finally the dialysate was placed in a beaker, flash frozen with liquid N_2, and lyophilized. The resulting product was stored in a vacuum chamber until needed.

3.3. Experimental Methods

3.3.1. Nuclear Magnetic Resonance (NMR) characterization

The purified samples of oligomeric paa products were dissolved, at a concentration of 5mg/mL, in D_6-Dimethyl sulfoxide (DMSO-D_6). NMR experiments were performed on a Varian Unity Inova 500 MHz spectrometer equipped with a 5 mm Penta (H,C,N,P,D) PFG VT probe. All experiments were performed at 35°C to lower the viscosity of the solvent, 32 scans, with a 10 second relaxation delay.

3.3.2. Circular Dichroism

Circular Dichroism (CD) measurements were carried out using an Olis CD spectrometer (Model RSM-100). The oligomer samples were dissolved into acetonitrile or EtOH, at a concentration of approximately 0.1 and 0.2mg mL^{-1} respectively, and filtered through a 0.2µm nylon syringe filter. All measurements were performed in a cylindrical quartz cuvette (path length of 0.1cm) at 20°C in the far UV range (195 to 260 nm). The scan rate was set to 10nm/min, at 0.1 nm increments. Acetonitrile was specifically selected as it has properties similar to dimethylformamide (DMF), which is the solvent that all polymerization reactions were performed in. It is required, herein, that the secondary structure of the growing oligomer chain be observed in conditions similar to that of the reaction flask. Ethanol was used to observe solvent effects of the oligomer chain in the CD experiment.

All secondary structure predictions were determined using CDPRO software, and reported results were averages based on percentile data given from the integrated data packages. The CD secondary structure determination method for CD (CDSSTR), Johnson's convex constraint method for minimal basis-random selection (CONTIN/LL), and self consistent method (SELCON3) software packages were all intrinsic to CDPRO, and used to calculate secondary structure content for each oligomer. Secondary structure prediction using all three software packages should improve the reliability of the predicted structures, as they each have different reference sets over varying wavelength algorithms [113–115]. The prediction software utilizes basis sets to determine the fit of the raw data, which must be entered in the software in per residue molar absorbance units (De M^{-1} cm^{-1}). The outputs from the three methods were averaged and presented in Tables 3.2 and 3.3 (see sections 3.4.2.a. and 3.4.2.b.) with the deviations presented being derived from the variation in the outputs resulting from using IBasis sets in each of the aforementioned methods.

More specifically, CDPRO software package uses large reference sets of proteins in the CD data analysis to determine secondary structure using more than one method of analysis. A larger reference set gives a better representation of secondary structure variance in a given protein and its influence on the CD spectrum itself [113], [115]. By using multiple methods of analysis with a variety of algorithms highlights the association between the protein's structure and the CD spectrum. Analysis of the results from different methods can yield a measure of reliability of the analysis, as well as determine the error present in the analysis [113], [114].

CDPRO's algorithms; CDSSTR, CONTIN/LL, and SELCON3 were used to determine the secondary structure of the oligomers. CDSSTR contains eight reference proteins that are used for a single value decomposition algorithm, and five single value decomposition components. Only the solutions from this algorithm that satisfy three basic selection rules for CD prediction are acceptable. First, the sum of the fractions must be between 0.95 and 1.05. Second, each fraction is greater than -0.03. Third, the rout mean square deviation between reconstructed and experimental CD is less than $0.25\Delta\varepsilon$. Additionally, a certain number of solutions are subjected to another rule based upon α-helical content. The helical content determined from the α-helix fraction estimate of the full reference set and the helix fraction content from the acceptable solutions. The solutions that satisfy these four criteria are then averaged to present a final solution to yield the predicted secondary structure. A draw back in this method is that one does not know which poly(amino acid)s are essential for the CD analysis, and are therefore selected at random [113–115]. This can generate a prediction that does not meet the aforementioned criteria, thus presenting results that are not in agreement with the other two methods.

The CONTIN/LL is a variation of the CDSSTR method, but it arranges the poly(amino acid)s in order of increasing root mean square deviation from the poly(amino acid) analyzed. The more distant poly(amino acid)s are deleted in a systematic manner to construct a smaller reference set. This creates a set of solutions, the number that is determined based upon the

number of reference poly(amino acid)s and the minimum number of poly(amino acid)s used for a solution [113]. The selection rules, based on α-helical content, are used to screen the solutions, and the final solution is the average of all the solutions that are found to satisfy the selection rules outlined in the CDSSTR section above [113], [115].

The SELCON3 algorithm is a self consistent method where the spectrum of the poly(amino acid) analyzed is included in a CD spectral data matrix, and an initial guess based upon the secondary structure of a reference poly(amino acid), having a CD spectrum most similar to that of the analyzed poly(amino acid) analyzed, is made for the unknown secondary structure [114], [115]. The solution replaces the initial guess and the process is iterated for convergence. The matrix equation relating to the CD spectra to the secondary structure is solved by the singular value decomposition algorithm, and variable selection in the locally linearized model. The solutions are obtained by varying the reference poly(amino acid) and/or the singular value deviation coefficients. The solutions are deemed acceptable is the following criteria are met: First, the sum of the fractions must be between the sum of the fractions must be between 0.95 and 1.05. Second, each fraction is greater than -0.025. Third, the rout mean square deviation between reconstructed and experimental CD is less than $0.25\Delta\varepsilon$. These criteria are similar to that seen with CDSTR including the necessity for α-helix content fraction estimation based upon the maximum/ minimum helix fraction from acceptable solutions [115]. The final solution is the average of all the solutions that follow the aforementioned rules.

The three aforementioned algorithms were used to analyze the CD data, as mentioned above, and the fractional secondary structure out puts from each algorithm was compared to the other output files. If the three outputs were similar ($< \pm$ 10% difference), then the results were determined to be “reliable”. The three results were averaged, with the deviation annotated to reflect the variance between the three outputs. However, if the results exhibited greater than 10% variance, an alternate basis set was used in an attempt to find a convergence for the three outputs.

It was discussed in the CDPRO software that a considerable difference in the results could be caused by a problem with the input data, or that the CD spectrum was not well represented in the reference poly(amino acid)s [113].

3.3.3. Infrared Spectroscopy

Attenuated total reflectance (ATR) Fourier transform infrared (FTIR) spectra of bulk *N*-hexylamino-poly(amino acid)s were obtained on a Perkins-Elmer Spectrometer. A total of 126 scans were signal-averaged over the range of 4000 to 650 cm^{-1}. A background measurement was obtained prior to recording the sample spectra with a resolution of 1 cm^{1-}.

3.4. Results

The oligomers of N^6-TFA-L-lysine, γ-benzyl-L-glutamate, and S-Cbz-L-cysteine were synthesized by initiation of *N*-hexylamine. Table 3.1 summarizes the data obtained samples that were synthesized. Each oligomer was synthesized on once, and no additional syntheses were performed as the goal was aimed at creating short chain molecules for the determination of secondary structure in oligomers $\overline{DP_n} \geq$ 20mers in length for comparison to theoretical information stated in the paper by Kricheldorf *et al.* [28]. Nuclear magnetic resonance data was used to determine chain length, and no further reactions were determined necessary as the oligomer chain lengths were sufficient for the circular Dichroism and Fourier transform infrared spectroscopy experiments. The shortest chain target length was a 5mer, which was readily synthesized within ± 1 repeat unit. The longer chain (20mer) showed a higher degree of error, and ranged from 16 to 20 repeat units long.

The most difficult oligomer to synthesize proved to be the *N*-hexylamino-poly(L-cysteine), as it was found to only be a 16mer when synthesized without urea. This apparent lack

of control could be indicative of the core problem hypothesized with regard to β-sheet structure formation in growing oligomer chains. In addition, the *N*-hexylamino-poly(L-lysine) was three repeat units shorter than the desired 20mer chain length ($\overline{DP_n}$= 16) (see Table 3.1). This shortened chain length could also be due to a lack of control in the growing polymer chain due to β-sheet secondary structure content. It has been discussed, in literature [36], [50], that N^{ε}-Cbz-L-lysine does not begin to adopt a well defined α-helical structure until $\overline{DP_n}$= 12 ±1. Therefore the β-sheet formation in the shorter chain oligomer of N^{ε}-TFA-L-lysine could also have caused a reduction in the kinetic rate of the reaction to induce chain truncation [28].

DP_n	Oligomers	Actual $\overline{DP_n}$ (Reaction time in days)	Theoretical M_w (g/mol)	Starting weight NCA (g)	Actual Mw (g/mol) (NMR)	Theoretical Yield (g)	Actual Yield (g)	Yield (%)
5	N-Hex-p(Glu)	6 (2)	1201	0.251	1421	0.254	0.234	92
5	N-Hex-p(Lys)	5 (2)	1195	0.255	1195	0.261	0.232	89
5	N-Hex-p(Cys)	4 (2)	1296	0.248	1057	0.256	0.22	86
10	N-Hex-p(Glu)	11 (3)	2521	0.254	2521	0.255	0.232	91
10	N-Hex-p(Lys)	12 (3)	2361	0.247	2813	0.248	0.221	89
10	N-Hex-p(Cys)	10 (3.5)	2491	0.255	2491	0.256	0.236	92
20	N-Hex-p(Glu)	20 (4)	4501	0.253	4501	0.253	0.223	88
20	N-Hex-p(Lys)	17 (4)	4621	0.250	3943	0.250	0.215	86
20	N-Hex-p(Cys)	16 (4.5)	4881	0.254	3925	0.257	0.234	91
5	N-Hex-p(Cys)[a]	4 (2)	1296	0.247	1057	0.255	0.214	84
10	N-Hex-p(Cys)[a]	9 (3)	2491	0.245	2252	0.247	0.222	90
20	N-Hex-p(Cys)[a]	18 (4)	4881	0.249	4403	0.249	0.222	89

Table 3.1. Physical properties and yields of the N-hexylamine initiated oligomers. (a) indicates that the oligomers were synthesized with urea in the reaction solution. All reactions were performed at room temperature.

Table 3.1 shows that all oligomers were synthesized and yielded 84% or greater purified product. Only 0.25 grams of product was synthesized to perform ^{1}H-NMR, CD, and ATR-FTIR experiments. The molecular weights of the oligomers ranged from 1057 g·mol^{-1} for to 4327

g·mol^{-1} for protected *N*-hexylamino-p(L-cysteine). The yields obtained for the oligomers were higher than anticipated for the low M_w products, as loss of product during dialysis was a concern. There does not appear to be a substantial trend, however, the low molecular weight products do exhibit slightly lower yields than those of higher molecular weight oligomers (Table 3.1). The 5mers of L-cysteine and L-lysine had molecular weights of 1057 to 1195 g·mol^{-1}, respectively, and gave 84 and 86% yield of purified product. The 5mer of L-glutamate was somewhat heavier at 1421 g·mol^{-1} and gave a yield of 92% indicating fewer products loss during dialysis.

3.4.1. Nuclear Magnetic Resonance Spectroscopy Results

The data obtained from NMR spectroscopy showed that all desired oligomers were synthesized within ±3 residues of the desired chain length (Table 3.1). The molecular weight calculated from NMR data allowed for a more accurate determination of molar concentration, as was necessary to properly determine apparent secondary structure formation using circular dichroism. The theoretical molecular weight was calculated based upon desired oligomer chain length. Oligomer yields were well above 80%, and a majority product loss was likely due in part to transfer from one vessel to another during purification, and during dialysis. All theoretical yields were based upon the molecular weights calculated upon target chain lengths.

The ^{1}H-NMR spectra of the oligos were obtained in d_6-DMSO to determine the number of repeat units present for each of the three types of oligomer molecules (see Table 3.1). A representative ^{1}H-NMR spectra of *N*-hexylamino-p(L-glutamate) ($\overline{DP_n}$= 20) is shown in Figure 3.1. The methyl group of *N*-hexylamino-p(L-glutamate) ((a) δ= 0.81 ppm) was normalized to 3 and used to integrate the peaks used for the determination of the oligomer chain length. The protecting group methyl proton peak (j) was integrated and showed that the oligomer had 20 repeat units (2H; -O-CH_2-C_6H_5; δ=5.02), and the phenyl protons (h) confirmed the 20mer chain

length (5H; -O-CH_2-C_6H_5, δ= 7.25 ppm). Additionally, the backbone methine protons (f) showed were integrated to yield 19 protons, which is in good agreement with the aforementioned peak integration values (1H; -CO-C*H*(NH_2)-CH_2-, δ= 3.8-4.4 ppm).

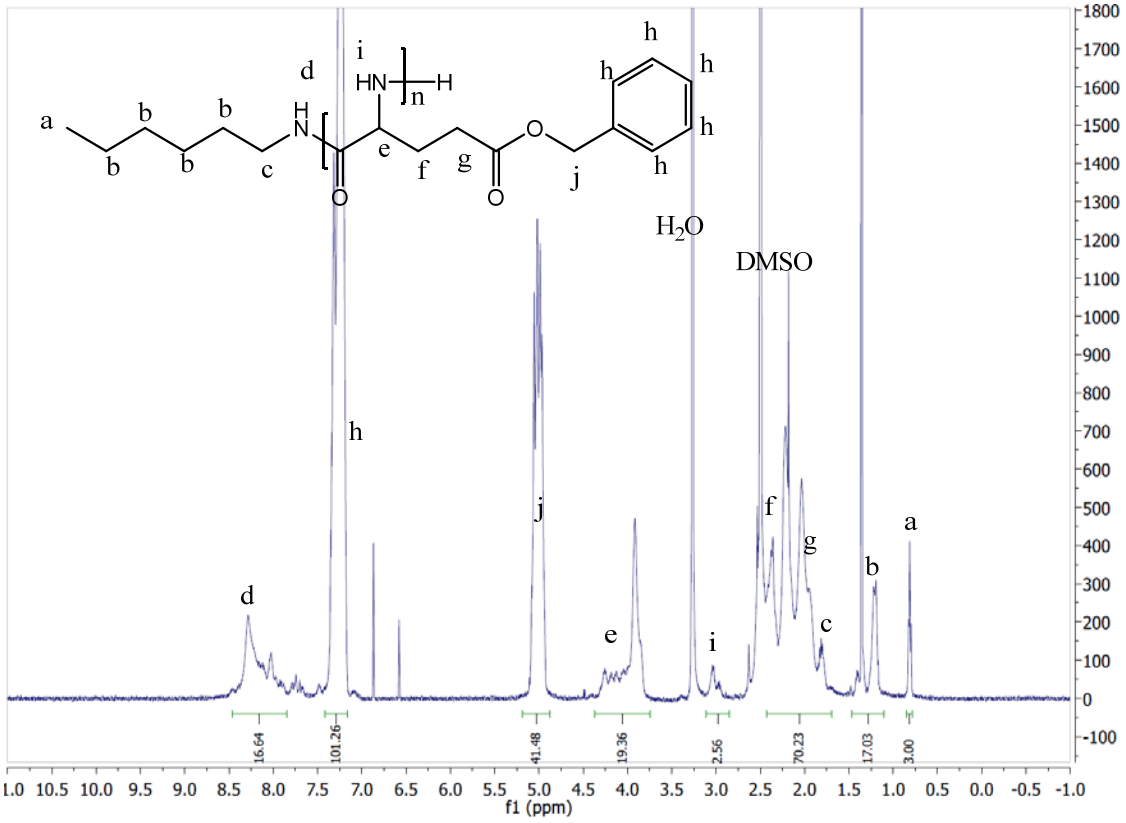

Figure 3.1. ^{1}H-NMR of *N*-hexylamino-poly(glutamate$_{20}$). ^{1}H NMR (500 MHz): *δ*/ ppm = 0.81 (3H, C*H*$_3$-), 3.8-4.4 (1H; -CO-C*H*(NH_2)-CH_2-), 5.02 (2H; -O-C*H*$_2$-C_6H_5), 7.25 (5H; -O-CH_2-C_6H_5), 8.27 (2H; -N*H*). *The peaks located at δ= 6.87, 6.58, and 2.32 ppm are residual solvent from the cleaning process of the NMR tubes.

1H- NMR Peak assignments for *N*-hexylamino-p(L-cysteine) can be seen in Figure 3.2. The methyl protons (a) were easily observed at δ=0.81 ppm, and normalized to 3. The remaining peak integration and assignments were based upon this initial value. The methylene peaks (b) of *N*-hexylamine were observed (8H; CH_3-(C*H*$_2$)$_4$-CH_2-NH-, δ= 1.20 ppm). The methylene protons (f) , adjacent to the thiol group, were determined (2H; C*H*$_2$-S-, δ= 2.85- ppm), but only yielded 6

residues as it was difficult to integrate the peak because of peak splitting and subsequent overlap into the water peak at δ= 3.27 ppm. However, the benzyl (g) protons, adjacent to the phenyl group, indicated that 11 residues were present in the oligomer (2H; -O-CH_2-C_6H_5, δ= 5.24ppm). Additionally, the benzyl protons (h) were integrated (5H, -O-CH_2-C_6H_5, δ= 7.34ppm) and found to be in good agreement with the number of residues derived from the methyl peak (f). The terminal amine peak (i) was observed and integrated to yield 2 protons (2H; -CH_2-NH_2, δ= 5.03 ppm), and the backbone methine protons (e) were integrated to 11.04 (1H; -NH-CO-CH_2-, δ= 4.25-4.68).

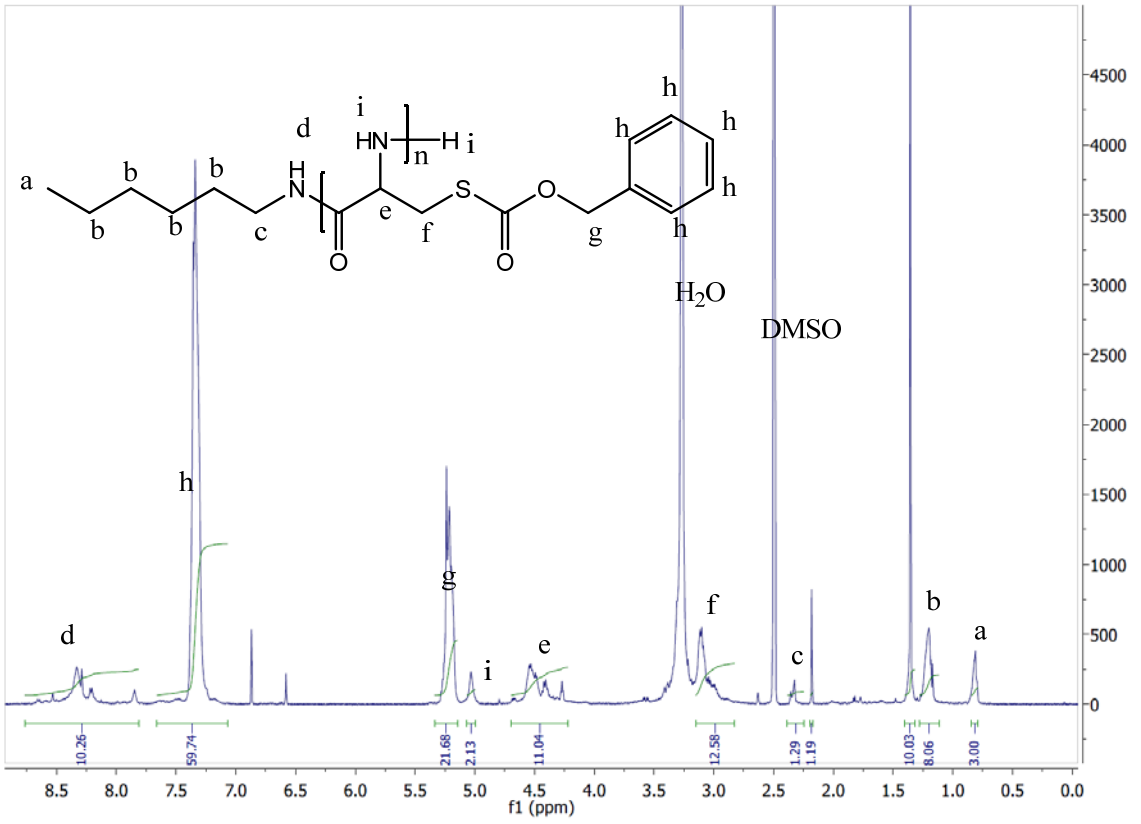

Figure 3.2. ^{1}H-NMR of *N*-hexylamino-poly(Cystiene$_{11}$). ^{1}H NMR (500 MHz): *δ*/ ppm = 0.81 (3H; CH_3-), 1.20 (8H; (-CH_2-(CH_2)$_4$-CH_2-NH-), 2.85 (2H; -CH_2-S-), 4.25-4.68 (1H; -NH-CO-CH_2-), 5.03 (2H, -CH_2-NH_2), 5.24 (2H, -O-CH_2-C_6H_5), 7.34 (5H; -O-CH_2-C_6H_5), 8.33 (1H; CH2-N*H*-CO), 9.35 (1H; -CH_2-N*H*-CO-). *The peaks located at δ= 6.87, 6.58, and 2.32 ppm are residual solvent from the cleaning process of the NMR tubes.

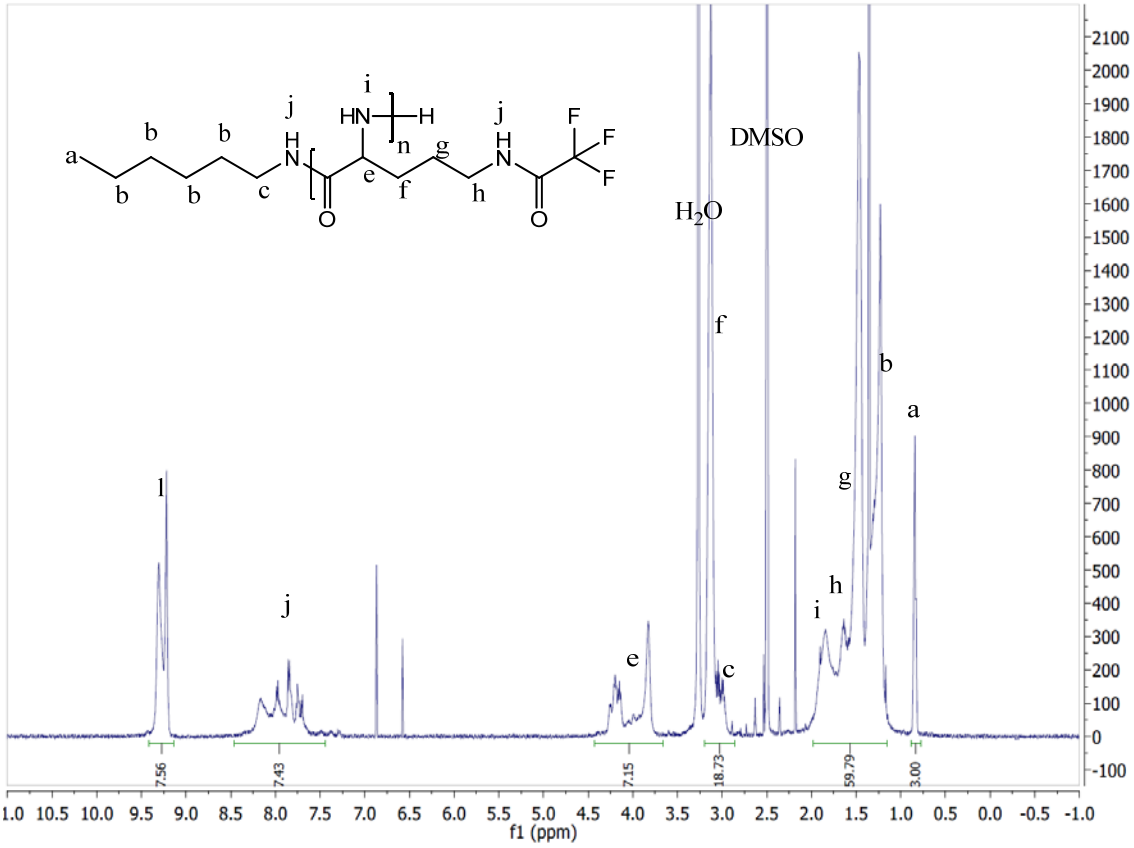

Figure 3.3. [1]H-NMR of *N*-hexylamine poly(TFA-L-lysine) in D_6-DMSO at 35°C. (The peak observed at δ=2.18 ppm is residual acetone). [1]H NMR (500 MHz): *δ*/ ppm = 0.78 (3H, C*H*$_3$-), 1.16-1.79 (10H, (C*H*$_2$)$_5$-NH-), 1.52-1.67 (4H, -NH-C*H*$_2$-C*H*$_2$-), 3.13 (2H, -C*H*$_2$-NH-CO-CF$_3$), 3.82-4.18 (2H, -C*H*-(CH$_2$)$_4$-NH), 7.6-8.5 (1H, -N*H*-CO), 9.22 (1H, CH2-N*H*-CO), 9.35 (2H, -N*H*$_2$). *The peaks located at δ= 6.87, 6.58, and 2.32 ppm are residual solvent from the cleaning process of the NMR tubes.

[1]H- NMR Peak assignments for *N*-hexylamino-p(L-lysine) ($\overline{DP_n}$= 7) (Figure 3.3). The methyl peak (a) was observed at δ=0.85 ppm, and was normalized to 3 to integrate the remaining peaks in the spectrum. The CH-N*H* peak and backbone amide peaks (l), at $\delta = 9.22$ ppm was in good agreement with the amide protons on the protective group (j) which lead to the conclusion that a 7mer was synthesized (1H, -CH$_2$-N*H*-CO-CF$_3$; δ=7.87) . The methylene peaks (g-i) were in such close proximity to one another that it was difficult to integrate them separately (δ=1.5-2.5ppm). The target DP_n, however, was 5 repeat units, but the synthesized molecule is reasonable due to the small quantity of liquid *N*-hexylamine initiator needed to achieve the correct M/I ratio.

Furthermore, support for derivation of the oligomer chain length, of 7 repeat units, was based upon the integration of the backbone methyl peak (e) (1H, CO-C*H*-NH, δ= 3.82 and 4.18ppm and integration found or be 7.15) (Figure 3.3).

3.4.2. Circular Dichroism Study of the Oligomers

Circular Dichroism (CD) experiments were performed in EtOH prior to Acetonitrile. However, EtOH proved to be less suited as a solvent for the synthesized protected oligomers due to their low hydrophilic character. Nevertheless, as a whole, the results could be interpreted in the CD spectra and verified the data obtained in acetonitrile.

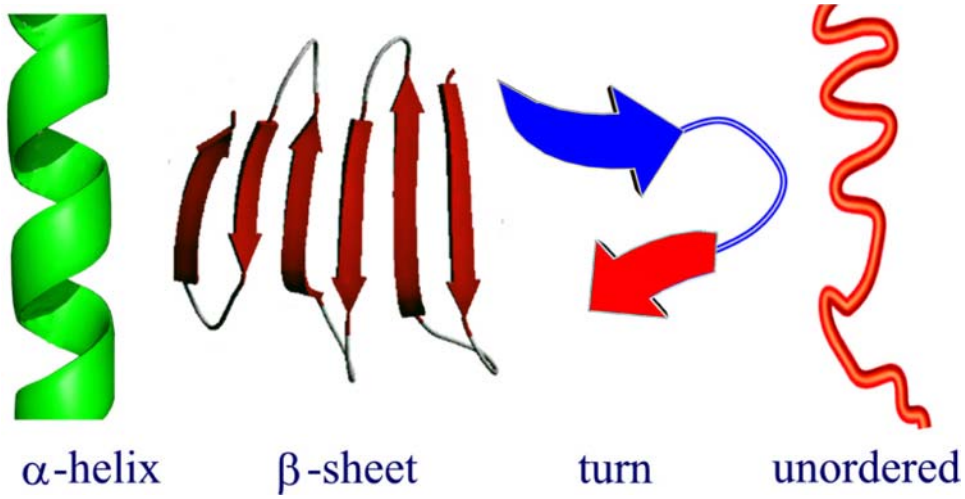

Figure 3.4. Secondary structures that can be derived from circular dichroism experiments.

The secondary structures of the prepared oligomers: N-hexylamino-p(L-glutamate) (NPLG), N-hexylamino-p(L-lysine) (NPLL), and N-hexylamino-p(L-cysteine) (NPLC) at $\overline{DP}_n$s of 5, 10, and 20 repeat units, were examined in solution by circular dichroism (CD) spectroscopy

(EtOH CD spectra can be found in Appendix A). There are three main types of structures in CD spectroscopy: α-helix, β-sheet, and random coil and there are also turns and unstructured regions that can be determined by circular dichroism experiments (Figure 3.4). The occurrence of them all can vary with respect to measurement conditions (pH, solvent, and temperature).

3.4.2.a. Circular Dichroism of Oligomers in Acetonitrile.

The oligomers were dissolved in acetonitrile, and as stated earlier, solvents play a role in secondary structure observance in CD. CD experiments in EtOH showed it to be a less than optimal solvent with regard to the solubility of the oligomers. Therefore, acetonitrile was used. Additionally, acetonitrile has similar properties to dimethylformamide (DMF), which was the solvent used during ring opening polymerization. It was hoped that the synthesis conditions could be replicated, in part, to observe the possible oligomer secondary structures formed during synthesis. In addition, acetonitrile had to be used in place of DMF, as DMF is a poor solvent for use in CD at far UV ranges. DMF has a useable wavelength cutoff of 250nm, in a 0.1cm path length; and could not be used to derive any secondary data. Acetonitrile, however, has a wavelength cutoff, in a 0.1 cm cuvette, of 175nm and allows for a full range CD scan from 260 to 195 nm (see Figures 3.5-3.8).

The acetonitrile yielded spectra with a lower signal to noise ratio than those obtained when the samples were run in EtOH (refer to Appendix A for EtOH CD spectra). As can be seen in Table 3.2, the degree of error is lower in acetonitrile in comparison to the samples run in EtOH (Table 3.3 Section 3.4.2.b). The presentation of lowered signal to noise ratios could be attributed to the fact that the oligomers were more soluble in acetonitrile and did not require filtering prior to CD experiments.

CDPRO prediction software was used to calculate the amount of secondary structure in each sample as derived from the raw data obtained on the Olis CD instrument. Table 3.2 shows results of samples dissolved in acetonitrile, which were similar to those seen in EtOH, but there are some differences that require discussion. The degrees of error were based upon the deviance from the average percentage of secondary structure determined by each of the CDPRO software's built in algorithms (CDSSTR, CONTIN/LL, and SELCON3).

Oligo	Helix (r)	Helix (d)	β Sheet (r)	β Sheet (d)	Turn	Unordered
Cys 5	0.000	0.000	0.635±0.022	0.112±0.013	0.122±0.009	0.130±0.025
Cys 10	0.000	0.000	0.487±0.018	0.287±0.011	0.118±0.015	0.112±0.041
Cys 20	0.000	0.000	0.221±0.007	0.535±0.017	0.000	0.143±0.036
Lys 5	0.000	0.036±0.013	0.232±0.013	0.413±0.01	0.043±0.005	0.276±0.022
Lys 10	0.381±0.016	0.224±0.012	0.201±0.019	0.001±0.001	0.053±0.005	0.140±0.015
Lys 20	0.581±0.011	0.224±0.009	0.000	0.004±0.003	0.054±0.006	0.151±0.018
Glu 5	0.018±0.008	0.020±0.004	0.341±0.004	0.272±0.01	0.194±0.011	0.171±0.028
Glu 10	0.332±0.012	0.253±0.014	0.181±0.013	0.014±0.005	0.054±0.003	0.146±0.012
Glu 20	0.429±0.009	0.280±0.008	0.000	0.110±0.003	0.181±0.013	0.000
Cys 5*	0.000	0.000	0.000	0.150±0.01	0.164±0.017	0.686±0.021
Cys 10*	0.000	0.000	0.243±0.009	0.067±0.005	0.110±0.018	0.576±0.012
Cys 20*	0.000	0.000	0.344±0.014	0.053±0.004	0.199±0.015	0.404±0.023

Table 3.2. Secondary structure prediction from CD data for oligos in Acetonitrile. (*) indicates the synthesis was carried out with the addition of urea. (r) indicates regular structure, and (d) is indicative of a distorted structure.

N-hexylamine-poly(L-cysteine) (NPLC) showed no α-helix formation in any of the oligomers, synthesized with or without urea. The cysteine oligomers synthesized with urea showed a dramatic decrease in regular β-sheet formation (Figure 3.5), and an increase in unordered regions compared to that of the cysteine oligomers synthesized without urea (Table 3.2). The regular β-sheet formation decreased from an average of 44.7% (for the urea free synthesized products) to an average 19.6% in the oligomers synthesized with urea. The

unordered structure was found to be an average of 12.8% in the urea free synthesis, and increased to an average of 55.5% in the oligomers synthesized with urea.

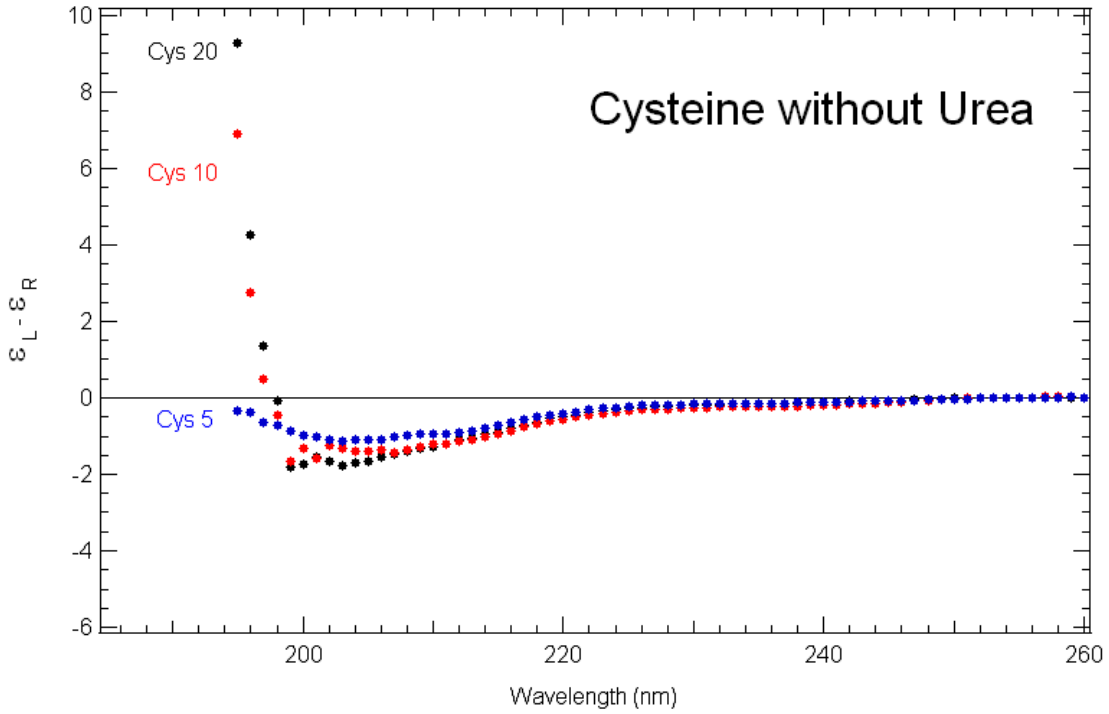

Figure 3.5. CD spectra of poly(L-cysteine) in acetonitrile (0.2mg/mL)

It was originally assumed that there would be a total reduction in secondary structure formation of all NPLC oligomers synthesized with urea, presenting a globally unordered molecule. The purification process, however, removed urea by dialysis in water and could have allowed a re-formation of β-sheet structure in the oligomers. Interestingly, CDPRO determined that $NPLC_5$, synthesized with urea, only contained 15% distorted β-sheet and there was no regular β-sheet structure. The majority of the secondary structure was reduced in this sample and became generally unordered (68.6%). Likewise, the 10mer and 20mer NPLC samples synthesized with urea showed an increase in unordered molecular structure, with the 10mer having 57.6% and the

20mer yielding over 40%. These findings support the claim that urea will reduce β-sheet secondary structure content in short chain oligomers. Additionally, the data shows that as chains grow longer, the impact of urea becomes more pronounced.

Figures 3.5 and 3.6 show comparative spectra of *N*-hexylamino-poly(L-cysteine) with and without urea utilized during the synthesis process. From visual inspection, it appeared that the 5 and 10mer oligomers synthesized with urea showed a no significant secondary structure, and contain mostly unstructured regions. The 20mer synthesized with urea does appear to exhibit a more pronounced negative peak at around 210nm, which could be indicative of more significant secondary structure (Figure 3.6), however it is still difficult visually ascertain any useful information.

The urea free *N*-hexylamino-p(L-cysteine) 5mer does not visually show any significant β-sheet formation (Figure 3.5). It is hypothesized in literature that short chain β-sheet structures are precursors to true β-sheets, at chain lengths below 5 repeats units, but there is no experimental data to verify this claim [28]. The NPLC 10 and 20mers exhibit very similar CD spectra in the urea free synthesized samples (Figure 3.5); however, the secondary structure prediction estimates the β-sheet content to be a total of 75%. This could be an indication that secondary structure in both oligomers is highly conserved and consistent. Furthermore, secondary structure prediction based upon output from CDPRO indicated both the 10mer and the 20mer for NPLC contained over 70% β-sheet. The 10mer, predicted in CDPRO, contained more regular β-sheet structure than the 20mer (48% and 22% respectively). The inconsistency here could be a result of an increase in differences of the experimental data from the basis set in the CDPRO software, as the basis sets are generally founded on α-helical structure containing poly(amino acid)s.

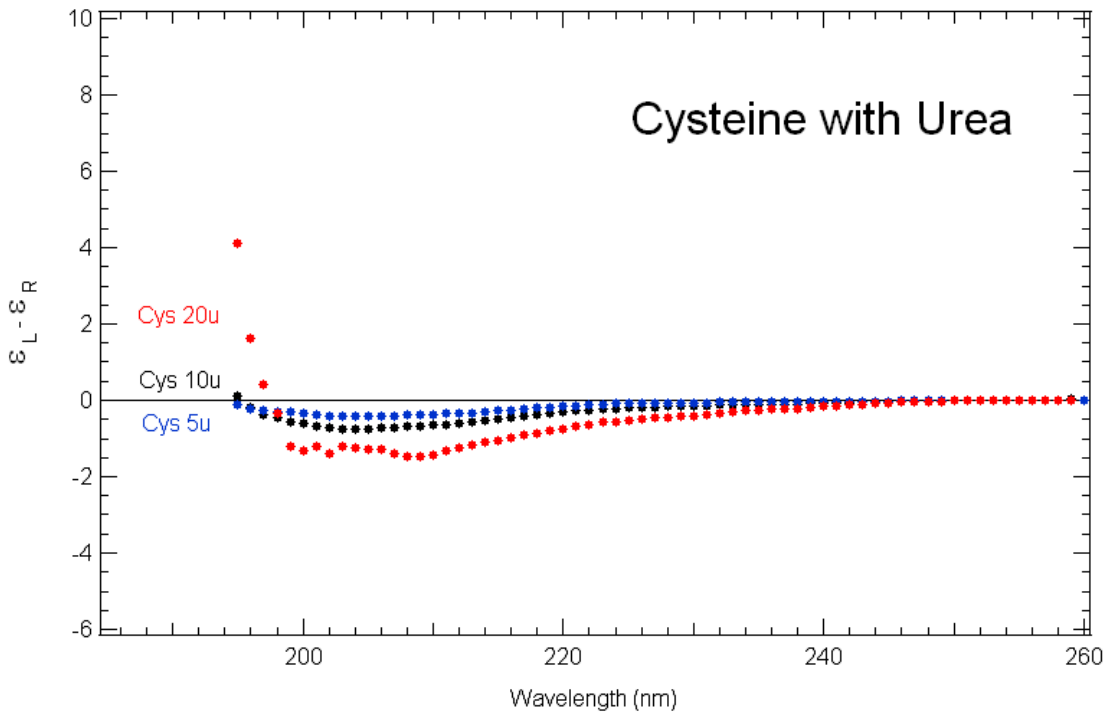

Figure 3.6. CD spectra of poly(L-cysteine) in acetonitrile, (0.2mg/mL) that was synthesized with urea.

N-hexylamine-poly(L-lysine) (NPLL) was synthesized without urea only, and investigated via circular dichroism experiments in EtOH and acetonitrile. The NPLL oligomers were synthesized in chain lengths of approximately 5, 10, and 20 repeat units to determine secondary structure in solution. The NPLL 5mer showed approximately 3.6% disordered α-helix, which was not expected. The NPLL 5mer presented with 23% regular β-sheet and 31% disordered β-sheet secondary structure in acetonitrile. Additionally, 27.6% unordered moiety, was predicted by using CDPRO. The α-helix structure in the 5mer was unexpected as it was hypothesized that the short repeat unit oligomers would all present close to 100% β-sheet structure as proposed in literature (Table 3.2).

The presentation of the unstructured α-helix moiety in the NPLL could be indicative of the precursor of a well order α-helical molecule. Additionally, the production a high degree of unordered structure in the molecule supports the assumption that the molecule is in a mid-state

transition form a well ordered β-sheet to an α-helix molecule (Table 3.2). It is possible that the high degree of distorted β-sheet structure in the NPLL 5mer is a result of solvent effects, or the presence of the side chain protecting groups. These groups may inhibit the ordered stacking necessary in well formed β-sheet and the subsequent formation of lamella.

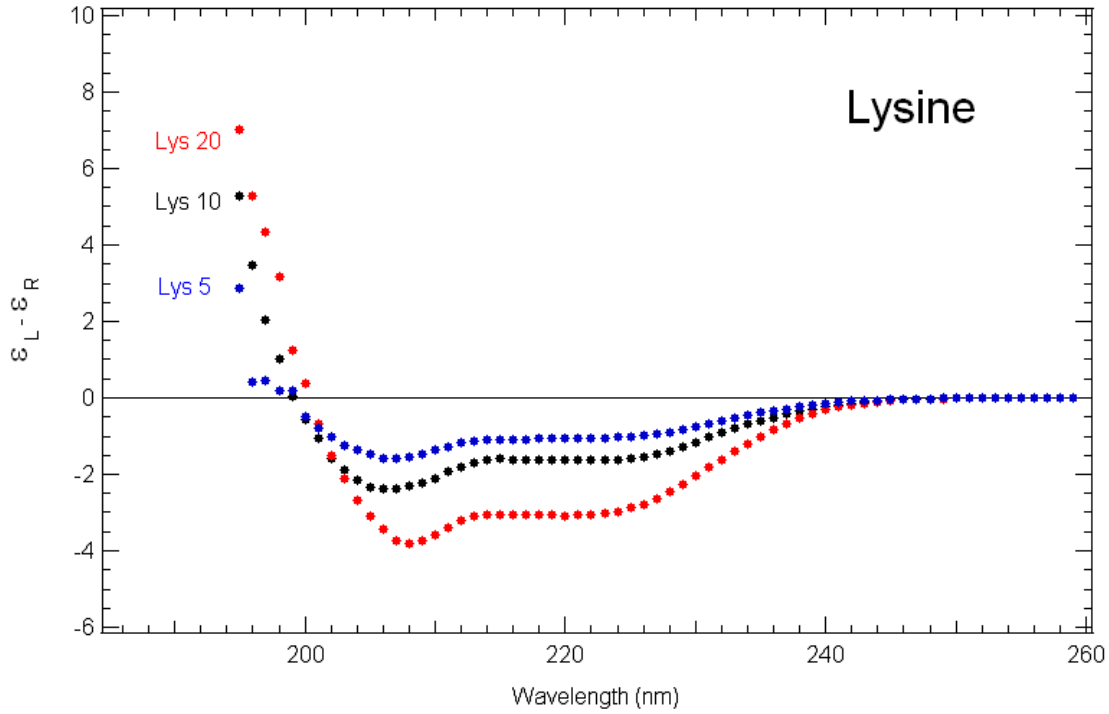

Figure 3.7. CD spectra of poly(L-lysine) in acetonitrile (0.2mg/mL)

The CD spectrum of NPLL 5mer appears to show the α-helical spectra with a negative peak at 230 nm and 209 nm (Figure 3.7). Additionally, the spectrum shows a slight positive peak at 201 nm that is usually characteristic of β-sheet secondary structure. The spectrum presented for the NPLL 5mer appears to be in good agreement with the data derived in CDPRO. The NPLL CD spectra of the 10 and 20mers show higher degrees of ordered α-helical structure as the chain

length is extended (Figure 3.7). The negative peak at 209 nm in the 20mer is very well pronounced, and is indicative of a well ordered α-helix in the NPLL oligomer chain.

The NPLL 10mer oligomer was predicted (Table 3.2) to have a total of 60.5% α-helix structure (38.1% regular 22.4% distorted), and there was a marked decrease in the regular β-sheet content to 20%. The unordered moiety also decreased, when compared to the NPLL 5mer from 27.6% to 14%. The distorted β-sheet was reduced from 32% to approximately 1% indicating that a stable β-sheet structure has been obtained, and the molecule is developing into a well defined α-helix structure. Kricheldorf [28] discussed that β-sheet structure does not completely disappear as the α-helix content continues to increase, and this appears to be supported by the data inferred from the CD spectrum obtained in acetonitrile.

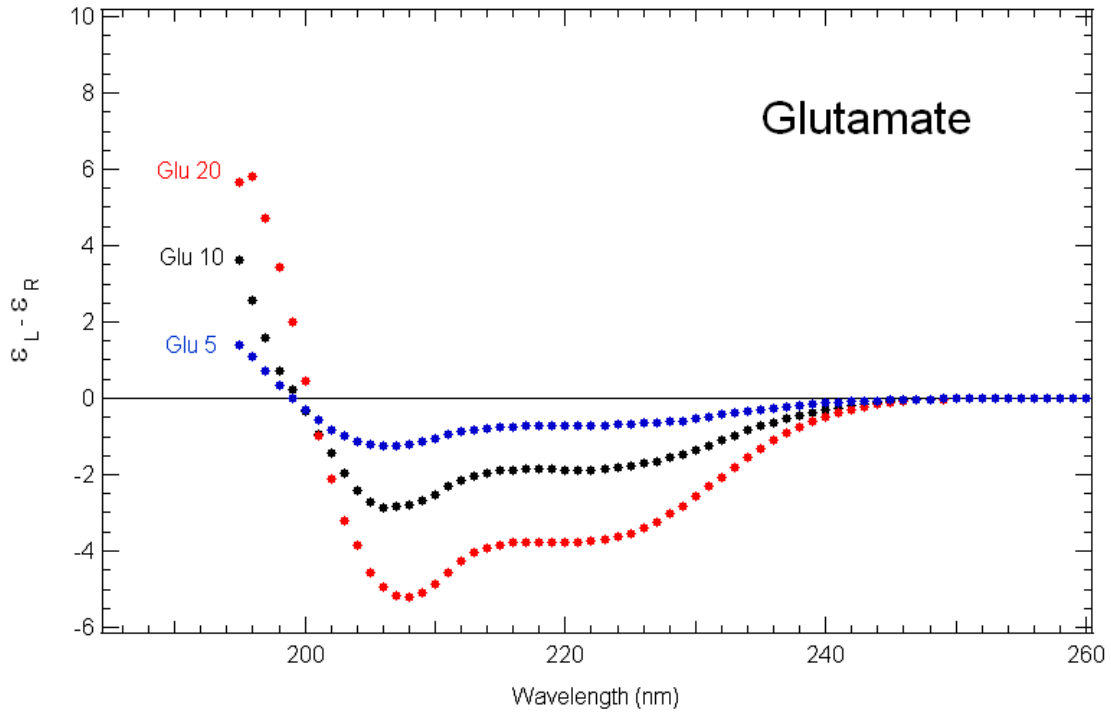

Figure 3.8. CD spectra of *N*-hexylamino-poly(L-glutamate) in acetonitrile (0.2mg/mL)

The NPLL 20mer was determined to contain 58% regular α-helix, and 22.4% distorted α-helix secondary structure, which indicated that the molecule is a well ordered helical chain. The β-sheet structure content was reduced to 0% for the regular structure and only contained about 1% or the disordered moiety in acetonitrile. The unordered structure present was determined to be approximately 15%, which is similar to the 10mer. These results support the proposition that α-helix becomes increasingly ordered in the longer oligomer chains, and that some β-sheet secondary structure is still retained.

N-hexylamine-poly(L-Glutamate) (NPLG) was also synthesized with *N*-hexylamine as the initiator to yield oligomers of 6, 11 and 21 repeat units in length, as determined by ^{1}H-NMR experiments. The samples were examined by circular dichroism to determine secondary structure content. The spectra in Figure 3.8 showed well defined α-helical structure formation at the 10 and 20mer chain lengths. The NPLG oligomer synthesized with 5 repeat units showed α-helical content as well, but the signal was not as intense as seen in the longer chain lengths, and could indicated much less ordered secondary structure.

NPLG 6mer was determined to contain approximately 2% α-helix structure, which is in agreement with visual inspection of the spectrum. The entire spectrum seems relatively flat, with some definition at 206 nm where a negative peak is seen. There appears to be a positive peak at 215nm but the intensity is very weak. However, a large amount of β-sheet content was predicted in CDPRO for the 6mer oligomer sample. Algorithms predicted 34% regular β-sheet and 27% disordered β-sheet content. This is not directly seen in the spectrum, but it appears that the positive peak exhibits a flattening trend below 200nm. Differences in the predicted secondary structure content and the apparent α-helical content of the oligomer could be due to a difference in the CDPRO's basis sets from the NPLG's data set. Literature does state, however, that well defined α-helixes may be present at $\overline{DP_n} \geq 9\pm1$. Therefore, L-glutamate, being an α-helix forming amino acid, could start developing distorted structure at much shorter chain lengths.

Additionally, the solvent effects upon the dissolved oligomer chain could have induced more defined secondary structure formation as the oligomer was readily soluble in acetonitrile.

NPLG 11mer was predicted to contain a much larger amount of α-helical secondary structure, totaling 58%. Approximately 33% was found to be regular structure, and 25% was disordered (Table 3.2). The spectrum (Figure 3.8) shows a more intense and better defined α-helical structure with a more pronounced negative peak observed at approximately 206nm. The total β-sheet content of the 11mer is greatly reduced from 58% to approximately 19.5%. This trend follows expected behavior for longer oligomer chains of L-glutamate, and the retained β-sheet content is in good agreement with proposed finding by Blout [104] and Kricheldorf [28]. The NPLG 11mer showed a less unordered structure than the 6mer, as well (27.6% for the 6mer and 14% for the 11mer). This data indicates that the 11repeat unit NPLG presents a molecule that is adopting a well ordered α-helical conformation. However, 25% unordered α-helical content could be indicative of steric hindrance due to the large benzyl protecting groups attached to the glutamate side chains.

The $NPLG_{21}$ oligomer spectrum (Figure 3.8) was clearly more α-helical in nature. There is a well defined negative peak at 208 nm, with a large positive peak formation below 200nm. Additionally, the formation of a negative peak region at 225 nm shows the formation of a classical helical spectrum observed in literature and texts. CDPRO predicted a total lack of regular β-sheet content, and approximately 11% distorted β-sheet structure. These findings are in good agreement with literature [28], which states that there was not a complete disappearance of β- sheet secondary structure upon the formation of α-helices in previously studied poly(amino acid) copolymers.

The NPLG 21mer showed a large total α-helical content of 71%, of which only 28% of this was determined to be distorted. Again, this could result from improper folding due to

protected side chain hindrance or solvent effects. The NPLG presented no unordered regions, and only 11% distorted β-sheet content. These results indicate that a well defined α-helical molecule has been synthesized, but still retains some β-sheet stricter.

3.4.2.b. Circular Dichroism of Oligomers in EtOH.

The oligomers of NPLL and NPLG were found to be more readily soluble in EtOH than the NPLC oligomers at all chain lengths, as was expected. The EtOH had a lower useful wavelength cutoff, than DMSO, which was originally used, but it still was difficult to obtain useful data at frequencies lower than 210 nm. This caused a larger degree of error in the CD spectra (see Appendix A for EtOH spectra). Acetonitrile proved to be a more useful solvent, and increased the degree of certainty in the secondary structure prediction (Table 3.2).

Table 3.3 shows that the oligomer chains contain a high degree of β-sheet structure formation at $\overline{DP_n} \leq 5$ in all three oligomer species. A more α-helical structure is observed in NPLG and NPLL oligomers between 5 and 10 monomer units, with some β-sheet being conserved. NPLC, however, maintains a strictly β-sheet structure in all samples, and does not show any apparent conformational changes at higher degrees of polymerization that would indicate the propensity to adopt an α-helical conformation.

Interestingly, $NPLG_{20}$ exhibits no β-sheet structure in the 20mer, but did show 17% unordered structure. In contrast, $NPLL_{17}$ maintained approximately 12% β-sheet structure (Table 3.3). However, NPLL showed approximately 13% turn structure, but no unstructured regions. NPLG had approximately 18% unstructured secondary structure formation. This difference could be in part to the NPLL being 4 residues shorter than NPLG, but it has been previously shown that a stable α-helical structure required 12±1 residues of N^{ε}- Cbz-L-lysine residues whereas γ-*O*-Bnl-L-glutamate only required 9±1 residues [28]. It should be noted that the nature of the end groups,

side chains, and solvent used, can play a role in the stability of α-helical secondary structures [28]. Therefore, the information found for N^{ε}-Cbz-L-lysine may not strictly apply to the N^{ε}-TFA-L-lysine used in this study.

Each of the NPLL and NPLG oligomers contained a distorted α-helix structure in EtOH. This could be indicative of a conformation change of the molecule from β-sheet to preferentially become a α-helix as chain growth continues (Table 3.3). Table 3.3 shows that β-sheet formation never completely disappears, and in some instances is only observed in the disordered form, but is still present. This observance is in good agreement with previous works discussed by Kricheldorf (2006) which states that β-sheet to α-helical transition cannot occur in the absence of hydrogen bond breaking solvents [28]. In addition, temperature also plays a role with regard to the solvents hydrogen bond breaking capabilities.

The increase in the distorted structures of all the NPLL and NPLG could be caused by the effects of the EtOH solvent upon the protected amino acids in the oligomers. The carboxybenzyl and benzyl protective groups are more hydrophobic than the native amino acids, and could have adopted slightly alternate structures due to differences in solubility. Additionally, the unexpected CDPRO based structure prediction may be caused by a larger difference between the experimental data and the basis sets provided in the software.

Each oligomer chain length, derived from NMR spectra, gave good confidence regarding the number of residues in the oligomer chain. Similar results were achieved with the remaining oligomer molecules when analyzed by ^{1}H-NMR spectroscopy. Additional spectra can be seen in Appendix A, and oligomer data is summarized in Table 3.3.

Oligomer	DP_n	Helix (r)	Helix (d)	β Sheet (r)	β Sheet (d)	Turn	Unordered
Cys 5	4	0.000	0.000	0.527±0.018	0.000	0.110±0.020	0.363±0.029
Cys 10	10	0.000	0.000	0.349±0.023	0.004±0.020	0.223±0.013	0.414±0.027
Cys 20	16	0.000	0.000	0.742±0.033	0.100±0.025	0.000	0.158±0.024
Lys 5	5	0.000	0.008±0.011	0.858±0.002	0.108±0.012	0.026±0.014	0.000
Lys 10	13	0.138± 0.013	0.279±0.0140	0.039±0.002	0.000	0.211±0.017	0.333±0.013
Lys 20	17	0.214± 0.017	0.583±0.012	0.115±0.011	0.000	0.133±0.0013	0.000
Glu 5	6	0.000	0.009±0.015	0.889±0.014	0.015±0.013	0.106±0.014	0.000
Glu 10	11	0.171±0.023	0.132±0.020	0.622±0.004	0.075±0.016	0.000	0.000
Glu 20	20	0.750±0.012	0.073±0.014	0.000	0.000	0.000	0.177±0.018

Table 3.3. Secondary structure prediction from CD data for oligos in EtOH. (r) indicates regular structure, and (d) is indicative of a distorted structure.

3.5. Attenuated Total Reflectance (ATR) Fourier Transform Infrared (FTIR) Spectroscopy

ATR-FTIR spectroscopy was performed to further verify secondary structure present in the oligomers of *N*-hexylamine initiated poly-L-cysteine, poly-L-glutamate, and poly-L-cysteine. ATR-FTIR is a very powerful technique for the determination of secondary structure of poly(amino acid)s. This is accomplished by exposing the sample to IR radiation and observing which wavelengths of radiation are absorbed by the sample to induce a variety of vibrational modes. Each compound exhibits characteristic bands that yield information about its chemical composition and may provide information regarding its secondary structure.

Characteristic bands of the synthesized oligomers were found at 696, 742, and 1733 cm^{-1} and were attributed to the benzyl and carboxybenzyl groups. The band observed at 2944 was characteristic of the aliphatic methylene groups, and 3303 $cm^{-1}$was due to a NH stretch. The band at 3126 cm^{-1} was determined to be secondary amide resulting from an overtone of the NH deformation of the main chain amide group in the poly(amino acid) repeat unit [116]. The band at 1700 cm^{-1} was the carboxylate stretch. Finally, the notable peaks observed between 1520 and 1560 cm^{-1} were typical for the amide II (NH stretch) and bands between 1620 and 1650 cm^{-1} were characteristic of the amide I (C=O). Both the C=O and the N-H bonds were involved in

secondary structure formation by way of hydrogen bonding. Therefore, the amide I and amide II bands are sensitive to secondary structure content of poly(amino acid) molecule [116].

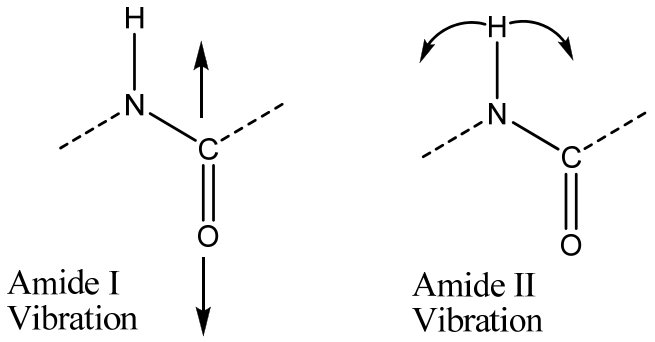

Figure 3.9. The vibrations responsible for the amide I and amide II bands in the infrared spectra of poly(amino acid)s, polypeptides, and proteins. The amide I band is due to carbonyl stretching vibrations and the amide II band is due to NH bending vibrations [1].

The relative positioning of the Amide I and Amide II bands yielded a wealth of information, regarding secondary structure, in the poly(amino acid)s. The Amide I band is a result of carbonyl stretching vibrations, while the amide II is due to amine NH bending vibrations (3.9). Previous studies have assigned the secondary structure character of amide I and amide II bands, summarized below [1], [116], [117] :

- Amide I
    - α-helices are found at approximately 1650 cm^{-1}.
    - β-sheet bands are located between 1620 and 1630 cm^{-1}.
    - Unordered moieties are characteristic of bands located at ~1520 cm^{-1}.
- Amide II
    - α-helices are located between 1540 and 1550 cm^{-1}.
    - β-sheet bands are located at approximately 1520 cm^{-1}.

Table 3.4 summarizes the data obtained from the spectra from ATR-FTIR experiments, are in agreement with circular dichroism studies (section 3.4.2.a and 3.4.2.b). It was observed that the *N*-hexylamino-p(L-Lysine) (NPLL) and *N*-hexylamino-p(L-Glutamate) NPLG both exhibited a combination of α-helix and β-sheet secondary structure at $\overline{DP_n}$ = 5 and 10. The 5mers of NPLL and NPLG exhibited respective amide I bands at 1654 and 1650cm^{-1} and amide II bands at 1548 and 1545 cm^{-1} (Table 3.4 and Figure 3.10), which are indicative of α-helical secondary structure [117]. Additionally, amide I stretching bands were present at 1633 cm^{-1} for NPLL and 1632 cm^{-1} for NPLG (Table 3.4 and Figure 3.10), which are indicative of β-sheet secondary structure [117].

The ATR-FTIR data shows that the 5mer NPLL and NPLG oligomers contain β-sheet secondary structure, and are both in the preliminary phases of α-helix formation. CD prediction suggested that NPLL and NPLG 5mers contained 64% and 61% β-sheet with approximately 2.5% α-helical structure. The presentation of amide I bands at approximately 1630 cm^{-1} (β-sheet) and 1650 cm^{-1} (α-helix) in both 5mers confirms the CD experiments findings (Figure 3.10 and Table 3.4).

Figure 3.10 shows a characteristic shift of the α-helix bands when compared to the β-sheet bands. The NPLL shows a small shoulder at 1648 indicating that the α-helix secondary structure is present in the oligomer and is becoming more ordered. The NPLG band at 1645 cm^{-1} is a shift toward values determined to indicate unstructured moieties (1640 cm^{-1}) [1], which is in agreement with CD data that suggests a distorted α-helical structure is present rather than a well defined α- helix.

Target DP_n	Oligomer	Actual DP_n	Secondary Structure*	Amide I Position cm^{-1}	Amide II Position cm^{-1}
5	N-Hex-p(Cys)	4	β-sheet	1631	1522
10	N-Hex-p(Cys)	10	β-sheet	1630	1522
20	N-Hex-p(Cys)	16	β-sheet	1629	1517
5	N-Hex-p(Glu)	6	α-helix + β-sheet	1632/1651	1545
10	N-Hex-p(Glu)	11	α-helix + β-sheet	1626/1645	1546
20	N-Hex-p(Glu)	21	α-helix	1650	1546
5	N-Hex-p(Lys)	5	α-helix + β-sheet	1633/1654	1558
10	N-Hex-p(Lys)	13	α-helix + β-sheet	1627/1648	1551
20	N-Hex-p(Lys)	17	α-helix	1648	1557
5	N-Hex-p(Cys)[a]	4	unordered	1639	1516
10	N-Hex-p(Cys)[a]	9	unordered	1638	1518
20	N-Hex-p(Cys)[a]	18	Unordered	1639	1517

Table 3.4. Summary of amide I and amide II bands as observed in ATR-FTIR experiments performed on *N*-hexylamine initiated oligomers of protect α-amino acids. (a) indicates samples that were synthesized with urea.

This finding is not unanticipated as the oligomer is short and may be sterically hindered by the large carboxybenzyl protecting group. From the data, it appears that NPLL can form an α-helix, in the 5mer, more readily than was observed in the NPLG. This could be due to less steric crowding of the trifluoroacetyl protecting group in comparison to the large Cbz on the glutamate amino acids.

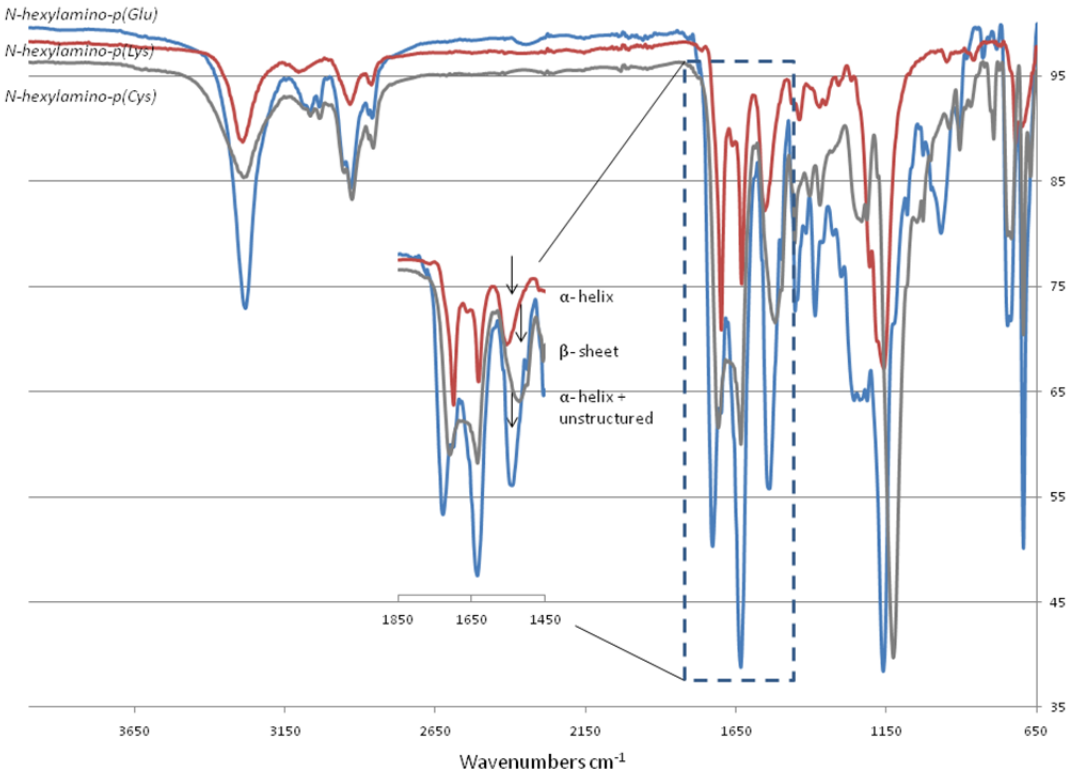

Figure 3.10. ATR-FTIR spectrum of *N*-hexylamino-p(lysine$_5$) (grey line), *N*-hexylamino-p(cysteine$_4$) (red line), and *N*-hexylamino-p(glutamate$_6$) synthesized without urea (blue line). The arrow indicates the position of amide II band.

Figure 3.11 shows that the NPLL and NPLG 10mers both exhibit more α-helical structure, but retain some β-sheet moiety. NPLL amide I bands were observed at 1627 and 1648 cm^{-1} (Table 3.4) which indicates the presence of both helical and sheet structure, as was determined in CD experiments. Circular dichroism showed an increase in α-helix structure from 3% to 58% in the NPLL 10mer. Likewise, the NPLG 10mer presented bands at 1626 and 1645 cm^{-1} (Table 3.4) which signify the α-helix and β-sheet moieties are both present in this oligomer as well. Additionally, the NPLG (blue) spectrum in Figure 3.11 shows a shoulder at 1626 cm^{-1}, which demonstrates that there is β-sheet structure present as was predicted by circular dichroism experiments. The spectra in Figure 3.11 show that the NPLL and NPLG 10mer oligomers are α-helix structures and are decidedly more ordered than observed in the 5mers. The propensity

towards a characteristic α-helix banding pattern, when compared to the β-sheet band exhibited by *N*-hexylamino-p-(L-Cysteine) (NPLC) oligomer, is readily observed in the spectra (Figure 3.11, red line).

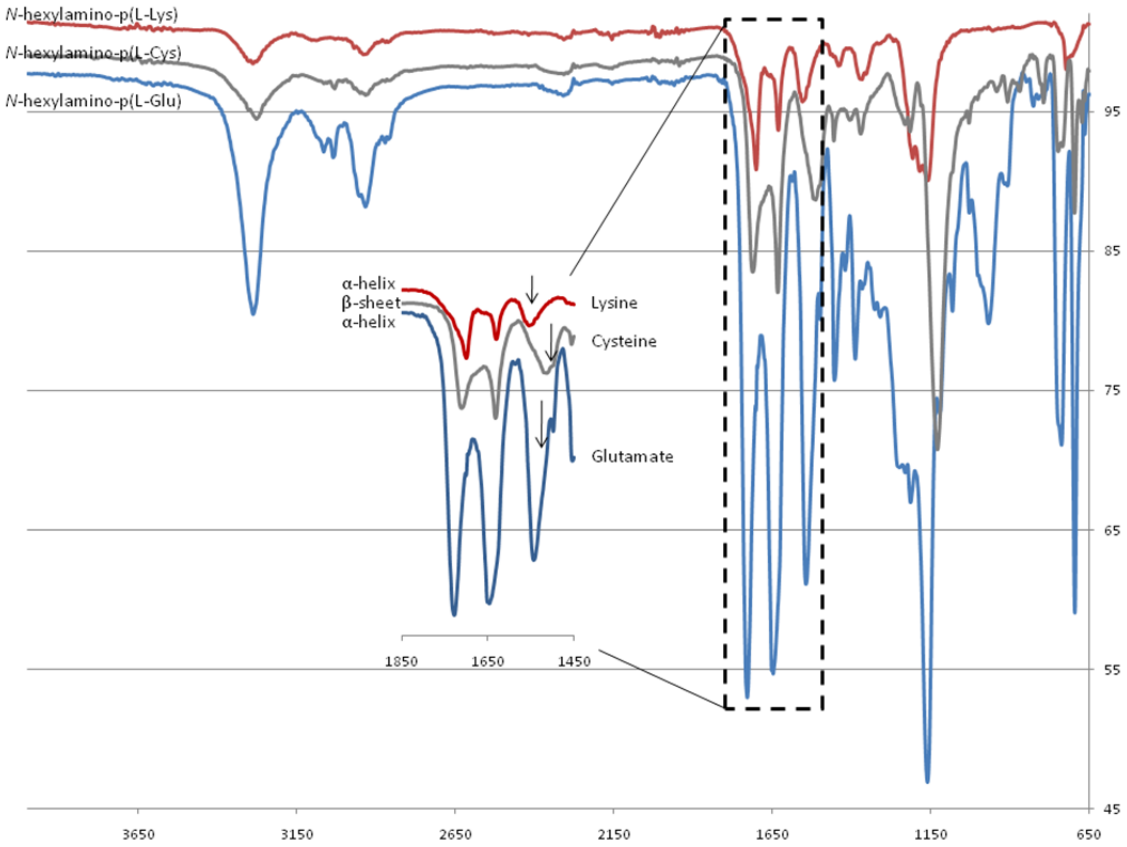

Figure 3.11. ATR-FTIR spectrum of *N*-hexylamino-p(lysine$_{17}$) (grey line), *N*-hexylamino-p(cysteine$_{16}$) (red line), and *N*-hexylamino-p(glutamate$_{21}$) synthesized without urea (blue line). The arrows show the amide I stretching band.

Furthermore, the 20mer NPLL and NPLG oligomers present bands solely in the α-helix regions for amide I, at 1648 and 1650 cm^{-1} respectively. The amide II also shows α-helix moieties for NPLL and NPLG at 1546 and 1557 cm^{-1} (Table 3.4). This data demonstrates that the NPLL and NPLG oligomers form well structured α-helixes as their chain lengths grow. The CD determined that NPLL contained 80% α-helix and NPLG contained 71% α-helix secondary

structure at = 20. Conversely, the NPLC oligomer maintained strictly β-sheet structure at all chain lengths. In the 20mer, the absorption bands observed at 1629 cm^{-1} (amide I), and 1517 cm^{-1} (amide II), were indicative of strictly β-sheet secondary structure. This finding is also in agreement with the CD data, which determined that the NPLC 20mer contained 76% β-sheet secondary structure (Table 3.2 and Table 3.4).

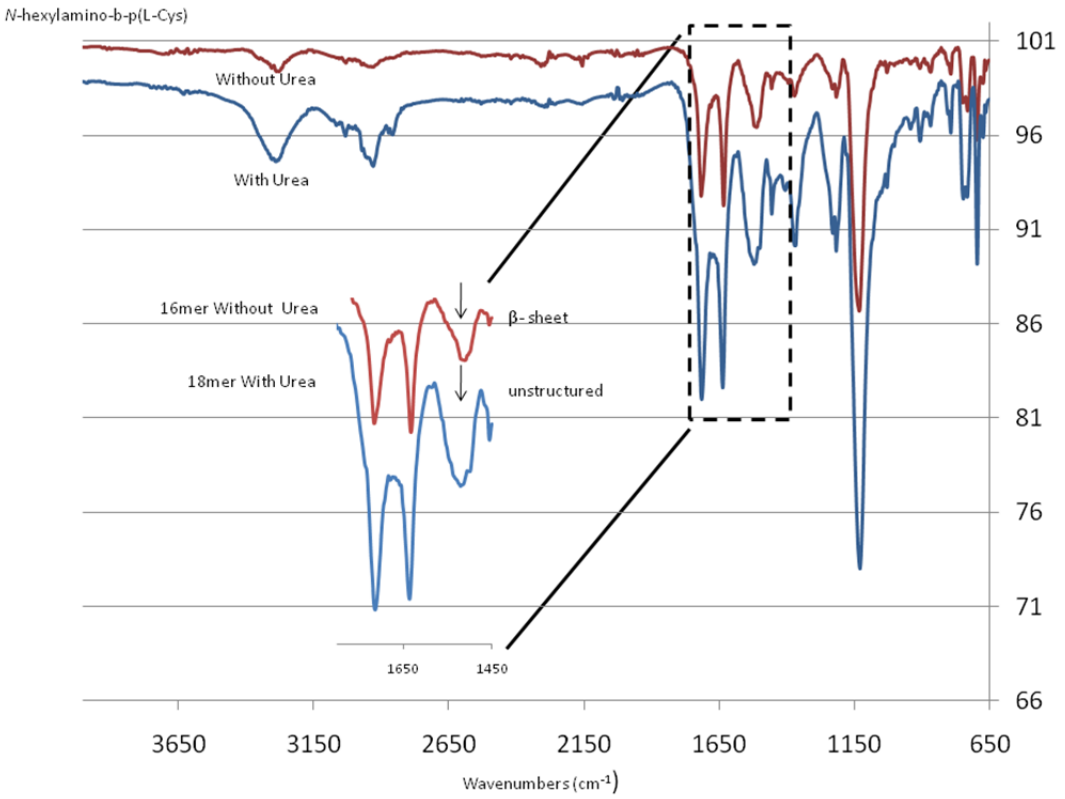

Figure 3.12. ATR-FTIR spectrum of *N*-hexylamino-p(cysteine$_{16}$) synthesized without urea (red line), and *N*-hexylamino-p(cysteine$_{18}$) synthesized with urea (blue line).

Finally, the *N*- hexylamino-p(L-Cysteine) NPLC oligomers were examined using ATR-FTIR. The oligomers were synthesized both with and without urea in analogous chain lengths of 5, 10 and 20mers. The CD data showed that there was absolutely no α-helix structure present in any of the cysteine based moieties. However, there was a large degree of unordered structure

present in the samples synthesized in the presence of urea; between 40% and 70% (Table 3.2). The ATR-FTIR was used to verify these findings.

The urea free NPLC samples showed secondary structure in the amide I bands as follows: 5, 10 and 20mers had bands at 1631, 1630, and 1629 cm^{-1}, respectively, which are all characteristic of β-sheet structure. In addition, the amide II bands were observed at 1522, 1522, and 1517 cm^{-1} for the 5, 10, and 20mers respectively, and also indicate β-sheets have formed. This information indicates that the oligomers secondary structure in agreement with information obtained by CD, and that there were no α-helical bands observed at, or around, 1650cm^{-1} (Figure 3.12, red line).

The NPLC samples synthesized without urea, presented amide I bands in the 1640 cm^{-1} range, which indicated an unordered structure, as per literature [1], [116], [117]. Urea free 5, 10 and 20mer yielded bands at 1639, 1638, and 1639 cm^{-1}, respectively. The amide II bands showed β-sheet structure as the bands for the 5, 10 and 20mers were located at 1516, 1518, and 1517, respectively (Table 3.4). This data indicated that the β-sheet secondary structure was reduced by the presence of urea, but was no completely eliminated. This is in agreement with the information extracted from CDPRO, which showed that the NPLC synthesized with urea retained between 7% and 53% β-sheet structure, while presenting more unordered regions than was observed in the urea free NPLC oligomers (Table 3.2). Figure 3.12 clearly shows the difference in the amide I band of the NPLC synthesized with urea (blue) and the urea free NPLC (red). There is an apparent shift from the β-sheet band at 1630 to the unstructured band at 1640. Interestingly the Amide II band shows a broadening, when compared to that of the urea free oligomer. This is an additional indication that the structure is becoming less ordered with the addition of urea, even though the peak minimum is at 1517 cm^{-1} [117].

3.6. Discussion

Circular dichroism and attenuated total reflectance Fourier transform infrared spectroscopy of *N*-hexylamine initiated amino acid oligomers yielded interesting information with regard to secondary structure of short chain molecules. The CD spectra obtained in EtOH had fairly high signal to noise ratios that made data analysis rather difficult. CDPRO analysis of the EtOH CD data showed that all forms of the *N*-hexylamino-p(cysteine) (NPLC) yielded no α-helix secondary structure and β-sheet structures were between 35% and 84%. The 5mer and 10mer oligomers had unordered moieties of 36% and 41% respectively, which could indicate an inability to fold due to either insufficient chain length or solvent effects.

N-hexylamino-p(L-lysine) (NPLL) and *N*-hexylamino-p(L-glutamate) (NPLG) both showed a large percentage of β-sheet structure in the oligomers with approximately 5 repeat units. Both NPLL and NPLG showed a marked increase in α-helical secondary structure content as the oligomer chains became longer. The NPLL 10mer showed a 33% unordered region indicating that it was in the process of becoming a well ordered α-helical molecule, but true α-helical structure had not been achieved until it was synthesized in the 20mer species. The NPLG 20mer showed 17% unordered structure content in EtOH, which may indicate steric hindrance effects from the side chain protecting groups or undesired solvent effects.

The CD spectra obtained in acetonitrile yielded much better results, and the signal to noise ratio was markedly reduced, thus allowing for more accurate secondary structure determination. The NPLC CD data obtained from the samples in acetonitrile yielded similar results. There was no α-helical secondary structure observed and β-sheet content was predicted to be approximately 75% for each species synthesized without urea. Additionally, the α-helical content of the NPLL and NPLG ($\overline{DP}_n \leq 6$) was minimal, and may have been derived in error by the CDPRO software (approximately 13% distorted for NPLL and about 2% distorted for NPLG). It is possible,

however, that the presentation of distorted helical structure could indicate the initial stages of a transformation from β-sheet to α-helices.

The 10 and 20mer oligomers for NPLL and NPLG demonstrated that chain length clearly affect α-helical formation in amino acids that prefer this configuration. The 10mer NPLL and NPLC oligomers yielded total α-helix contents of 60% and 58% respectively. In these oligomers β-sheet content fell to roughly 20% total. The NPLL and NPLG 20mers contained α-helical structures of 80% and 70%, with distorted β-sheet content of 0.4 and 11%. This demonstrates that the pre-polymers of amino acids do indeed form β-sheet secondary structure that can inhibit chain growth, and that some β-sheet secondary structure is retained even in well defined α-helices forming amino acids.

N-hexylamino-p(L-cysteine) (NPLC) was also synthesized with urea and CD analysis was performed in acetonitrile. The results showed that the β-sheet secondary structure was diminished in each of the L-cysteine based oligomers. The 5mer β-sheet content was only 15% whereas the urea free synthesis yielded a product that contained 74% β-sheet. The 5mer with urea in turn developed almost 69% unstructured character, as determined by CDPRO software. The 10mer contained slightly more β-sheet formation, at 30%, but the unordered region still occupied 58% of the molecule. The trend continued, where the 20mer showed almost 40% β-sheet moiety, however, it still exhibited 40% unordered structure. These results show that urea does in fact reduce the presence of β-sheet secondary structure content in oligomer chains, even in amino acids that preferentially adopt a β-sheet structure.

Attenuated Total Reflectance (ATR) Fourier Transform Infrared (FTIR) Spectroscopy was performed on all of the *N*-hexylamine initiated oligomers synthesized in the bulk state. Only the cysteine based oligomers were synthesized both with and without urea. This was due to the

inherent nature of cysteine to preferentially adopt a β-sheet conformation, and it was desired to observe if urea reduced β-sheet secondary structure formation via CD and ATR-FTIR.

Analysis of the amide I and amide II bands, at 1581 and 1609 cm^{-1} facilitated the determination of secondary structure in each of the oligomer samples. The NPLG and NPLL both presented α-helical structure in the bulk state at $\overline{DP_n} \geq 9$, which was expected. NPLG appeared to contain both α-helical and β-sheet structure at $\overline{DP_n}$=6, which was not expected, but can be explained by looking to the CD data. The CD showed that the α-helical moiety is actually unstructured at this chain length, and it is known that the retention of β-sheet structure is not unusual even when well defined α-helical structure is present in long chain molecules.

NPLL at all chain lengths showed a propensity towards α-helical secondary structure, even at $\overline{DP_n}$=5. At first glance this was puzzling as it was expected that the NPLL oligomer at this length would present a β-sheet structure in bulk, based on previous work [28], [104] performed on N^{ε}-Cbz-L-lysine. It was determined that α-helix formation would be well defined for N^{ε}-Cbz-L-lysine at $\overline{DP_n}$ =12±1. N^{ε}-TFA-L-Lysine, however, can apparently form α-helixes at lower at $\overline{DP_n}$ than Nε-Cbz-L-lysine. This observation is most likely due to less steric hindrance of the TFA protecting group, and the lack of special crowding allows the TFA protected L-lysine to adopt an α-helical moiety more easily than the Cbz protected L-lysine. The CD data obtained in acetonitrile predicted a higher percentage of α-helical structure in the NPLL 5mer than was predicted for NPLG, which is in good agreement with the ATR-FTIR findings.

The NPLC oligomers were also analyzed using CD and ATR-FTIR, which showed that all lengths of the oligomers definitively exhibited β-sheet conformation in the urea free synthesis. However, when urea was added to the synthesis protocol, the amount of β-sheet secondary structure was greatly impacted. There was a readily apparent reduction in β-sheet from a total of 74.7% in the urea synthesis to 15% when urea was used. The percentage of unordered structure

in the urea synthesized NPLC increased to five times that of the urea free NPLC. Similar results were seen in the 10mer an d 20mer NPLC molecules, where β-sheet structure was reduced by at least 40% overall. Additionally, ATR-FTIR spectra showed that the amide I band was no longer skewed toward the lower wavelengths, but became more symmetrical. This indicates that the amide linkage is still present in the molecule, but the secondary structure has been reduced from a true β-sheet structure to an unordered configuration. This study confirms that urea can effectively be used to reduce the β-sheet secondary structure in the first iterations of amino acids based polymer synthesis, and that N^{ε}-TFA-L-lysine can adopt an α-helix conformation at a lower degree of polymerization than that of N^{ε}-Cbz-L-lysine.

CHAPTER 4

Synthesis and Characterization of PEGylated α-Amino Acid Random and Block Copolymers for Solid Surface Modification

4.1. Introduction

This investigation required that living ring opening polymerization (LROP) be successfully employed to yield poly(amino acid)s of either random or block architecture. Polymer products of low polydispersities were not required for surface coating in this study; however, by definition a polydispersity index (PDI) close to unity were required to conclude that true living polymerization was achieved. Additionally, it was desired to achieve a mono disperse population. It was also proposed that polymer chains of desired molecular weights could be synthesized to demonstrate control over the LROP technique using α-amino acid *N*-carboxyanhydrides.

Here, PEGylated poly(amino acid) random and block co polymers were synthesized, at a variety of lengths and amino acid monomer ratios, with mPEG-NH_2 as the macroinitiator. The PEGylated-poly(amino acid) polymers were purified, then characterized using gel permeation chromatography (GPC) and proton nuclear magnetic resonance (^{1}H- NMR). Results from GPC experiments showed that the polymer products were monodisperse, but shoulder presentation in the co-polymers indicated that a blocky formation occurred in lieu of a truly randomized product. Polydispersity indexes (PDIs) for the random copolymers were all greater than 1.2, whereas the block copolymers were monodisperse with a PDI of less than 1.2, but all indices indicated that PEGylated paas of desired molecular weights had been achieved.

4.1.1. Review of Methods of Poly(Amino Acid) Synthesis

Many biological and chemical approaches are being developed for the synthesis of poly(amino acid)s. Biological methods offer superior control over polymer chain purity, architecture, sequence, and stereochemistry [79], [118], [119]. Chemical synthesis exhibits limited versatility due to the inability to synthesize poly peptide molecules that use many different monomers in a specific sequence. Natural synthesis can synthesize proteins that incorporate specific sequences of monomer units into a polymer chain. Twenty amino acids are present in natural peptides, but advances in biochemistry are broadening the flexibility of biopolymer science by synthesizing amino acid analogues that can be incorporated into functional poly(amino acid)s chains [27], [36], [118], [120].

4.1.2. Biological Methods for PAA Synthesis

Three approaches have been investigated to incorporate non-natural amino acids into functional biosynthesized polymer chains [118]. One technique is the use of an *in vitro* system where an amino acid analogue is supplemented into a cell free paa synthesis of proteins and poly (amino acid)s [121], [122]. Another tactic is the *in vitro* binding of a suppressor tRNA with an unnatural amino acid to synthesize site specific chemically modified natural polymer analogues [118], [123], [124]. Last, the incorporation of unnatural amino acids *in vivo* is probably the most challenging method. It is well known that certain amino acid analogues can be incorporated into bacterial proteins, and poly(amino acid) chains [124–126]. Cellular paa synthesis requires that the aminoacyl-tRNA synthetase enzymes recognize an amino acid and "charge" it with respect to its particular tRNAs for incorporation into a paa chain in the ribosome [125], [127]. To incorporate an unnatural amino acid into a protein; the microorganism's (such as *E. Coli*) gene encoding the natural amino acid must be cloned into an expressed plasmid. The new codon sequence may also be inserted at the desired locus by site directed mutagenesis [71], [127].

4.1.3. Chemical Methods of PAA Synthesis

Chemical methods, on the other hand, are generally limited to synthesis of polymers that do not have sequence specificity. While these polymers may have narrow Poisson distributions, their chain lengths may be in the tens of thousands of monomer units long. Current chemical methods do allow for the creation of paas that have a small number of amino acid types that can make block or random copolymers. Chemical synthesis methods are also useful; however, as they can easily incorporate D-amino acids and amino acid analogues into the growing paa chain [128].

Solid phase synthesis of paas takes root from the pioneering works of Robert Merrifield (1963) [129], which involves a solid phase synthesis process that involves a stepwise addition of *N*-protected amino acids to a peptide chain that was anchored to a polymeric support [32], [129–131]. Merrifield synthesis yields products that are of defined specificity, but require at least four steps per monomer addition. These steps are necessary to ensure a high fidelity sequence, purity, and completion of the reaction [118]. Furthermore, expensive reagents are necessary to prevent racemization during the coupling and protection of the amino acids [118].

Polymerization of *N*-carboxyanhydrides is currently one of the most commonly used techniques for large scale preparation of paas. This method has traditionally exhibited limitations due to chain termination and chain transfer reactions, and generally produces polymers that are homopolymers or random copolymers that lack sequence specificity [27], [36], [40], [42], [93], [118]. The side reactions create products of broad molecular weight distributions, and inhibit the formation of well-defined block copolymers [118]. Living polymerization of NCA has generated products with extensive use in a wide variety of applications, which can rival biologically synthesized polymers [2], [27], [28], [31], [32], [40].

NCA polymerizations have been initiated with a wide variety of nucleophiles and bases, and the effectiveness of these initiators correlates to their relative nucleophilic/basic ratios (as discussed above) and the specific monomer being polymerized. Primary amines are good nucleophiles, have a low basicity and are good general initiators for many NCA monomers [27], [28], [32], [39], [118]. The use of primary amines under optimal conditions will follow the amine mechanism where the polymer chain grows in a linear fashion with the absence of side reactions. The capability of producing conditions that yield a true amine mechanism allows for the synthesis of di and tri block copolymers under living conditions as there are no termination or other side reactions. This process will yield paas with low Mw distributions, low PDIs, and well-defined architecture[27], [32], [35], [36], [42], [77], [118].

4.1.4. Research Goal

The aim will be to use primary amine initiators to synthesize poly(amino acid)s of varying Monomer/Initiator (M/I) ratios and specific architecture via living ring opening polymerization. It will be shown that copolymers can be synthesized in good yields with low polydispersity indexes (PDI)s based on low molecular weight distributions. It is possible that differences in chemical reactivities could exhibit a broadening in the molecular weight distributions of the paas, and lead to the formation of blocky regions instead of a synthesis of a true randomized paa.

Additionally, it will be shown that syntheses of block and random PEGylated copolymers, with PDIs of less than 1.2 can be obtained, thus a true living nature has been achieved. Previous works by Vayaboury *et.al.* [65] showed the use of urea in LROP facilitated the amine mechanism and reduced the production of dead copolymer chains. Based on this work,

urea will be incorporated into the synthesis to reduce the β-sheet formation, and allow propagation to continue at a kinetic rate that favors the normal amine mechanism.

Protected amino acids will be used to prevent cross-linking of the PEGylated polymer chains, thus preventing the formation of a network structure via cross-linking or disulfide bridges. The protective groups will not interfere in the polymerization process, as they have been previously shown to be inert, and are commonly used in poly(amino acid) syntheses [28], [118], [132].

4.2. Experimental Methods

4.2.1. Materials

N, N-Dimethylformamide (DMF), tetrahydrofuran (THF), Drierite™ and urea were purchased from Fisher Scientific (Waltham, MA). The DMF was distilled and stored on 4Å molecular sieves to prevent water contamination prior to use. Urea and THF were used as received. Argon gas was purchased from Airgas (Huntsville, AL) and passed through a desiccator trap containing Drierite™ to remove any water vapor from the argon gas prior to entering the reaction vessel. α-methoxy-ω-amino PEG (mPEG-NH_2) 5000 Da was purchased from Laysan Bio (Huntsville, AL), and stored at -20°C per the manufacturer's directions.

4.2.2. Methods

4.2.2.a. Living Ring Opening Polymerization Synthesis of PEGylated Random Copolymers

Living ring opening polymerization was carried out by first synthesizing and purifying of the respective NCAs to be used in the reaction (please refer to section 2.2.2). The NCAs were

combined and dried under vacuum in a Schlenk air-free flask, closed with a silicone stopper, to remove all residual solvents and minimize exposure to atmospheric humidity. The appropriate amount of mPEG-NH_2 was placed in a second clean/dry Schlenk, along with a magnetic stir bar, and allowed to dry under vacuum for no less than one hour. Then urea was ground using a mortar and pestle to increase surface area, to facilitate drying, and the appropriate amount was determined (to yield a final conc. of 0.2M). The urea was placed in a third Schlenk, with a silicone stopper and a magnetic stir bar, to dry under vacuum for not less than one hour. Then the appropriate amount of distilled DMF (necessary to yield an NCA concentration of 0.1M) was added to the Schlenk containing the urea, and placed under vacuum to degas for approximately 15 minutes. Once degassing was complete, an aliquot of DMF/urea solution (4mL/ 250mg mPEG-NH_2) was added to dissolve the mPEG-NH_2 under a flow of argon gas. Slight heating with a heat gun was necessary to fully dissolve the mPEG-NH_2. The remaining DMF/Urea solution was added to the NCA, along with a stir bar, under a flow of argon. Finally, a syringe was used to inject the mPEG-NH_2 solution into the Schlenk containing the NCA, to initiate polymerization, under a flow of argon. The flask was then evacuated of all argon and CO_2, which was replaced by fresh argon. The flask was closed, and allowed to react at ambient temperatures while stirring until all apparent evolution of CO_2 subsided.

Twice daily the flask was evacuated of all CO_2 and replaced with fresh argon. This served a twofold purpose. First, the evolution of CO_2 is a direct indication that the reaction is occurring. Once the reaction is complete, no gas should be apparent upon evacuation of the reaction flask. Second, as discussed earlier, increased levels of CO_2 and pressure can cause the kinetics of the reaction to slow to the point where the carbamate mechanism is preferentially followed. By removing the CO_2 it was assumed the amine mechanism remained the predominant mechanism of the reaction.

4.2.2.b. Polymerization of PEGylated Block Copolymers

Di-block copolymers had already been synthesized and required a third block to be added to the paa under living conditions. This method is very similar to that outlined in section 4.2.2.a. When synthesizing the block copolymers, however, it was necessary to allow the PEGylated di-block copolymer to completely polymerize all monomer amino acids prior to addition of the NCAs used to create the third block. The necessary amount of the third amino acid NCA was stochiometrically calculated to determine the paa/monomer ratio. The appropriate amount of NCA was pre-weighed and placed under vacuum in a Schlenk until needed.

Once the synthesis of the di-block copolymer was determined to be complete, the Schlenk containing the paa was evacuated of all CO_2/argon, and then refilled with fresh argon gas. The stopper was removed, and under a high flow of argon the pre-weighed NCA was added to the reaction media. The flask was then sealed with a silicone stopper, evacuated of all air with a vacuum line system, and the Schlenk was again filled with fresh argon gas. The reaction was allowed to proceed as outlined above. CO_2 was removed from the flask and evolution was monitored as outlined above.

4.2.2.c. Polymer Isolation and Purification

To purify the PEGylated paas, the reaction solution was transferred to a round bottom flask, and the DMF was removed on a Labconco rotary evaporator, with an in-line vacuum pump attached, at 35°C until dry. Then, THF was added in equivalent volume as the DMF that was used during the polymerization step. The solution was left to stir for $\leq$ 2 hours to facilitate precipitation of urea from the system. The THF solution was filtered on a Buchner funnel fitted with a glass frit (10-15 μm) to remove the precipitated urea. The filtrate was collected in a clean round bottom flask, and reduced on the rotary evaporator to a volume of approximately 1 to 2 mL

or until it became highly viscous. The concentrated solution was then placed into a Spectra/Por 3 regenerated cellulose dialysis tubing (Mw c/o 3,500) and distilled against 4 liters dH_2O (3x). This was done to remove any remaining urea, and residual THF/DMF. Finally the dialysate was placed in a beaker, flash frozen with liquid N_2, and lyophilized. The resulting product was stored in a vacuum chamber until needed.

4.2.3. Methods of PEGylated Poly(Amino Acid) Characterization

4.2.3.a. Gel Permeation Chromatography (GPC) Characterization

The purified PEGylated paa samples were characterized by GPC. A purified sample of each PEG-b-paa was dissolved in 0.1M LiBr dimethylformamide by vortexing with slight heating. All samples were passed through a 0.2 μm nylon syringe filter and injected into a Waters 1515 High Pressure Liquid Chromatography (HPLC) system equipped with a Waters 2414 Refractive Index detector. The column used was a Waters Styragel HR 5E column running at a flow rate of 1.0 mL/ min at 50°C. The system was calibrated with monodisperse PEG standards of various molecular weights (177,500, 73,500, 25,300, 5,500, and 1,750 $g \cdot mol^{-1}$) prior to injection of samples. The Waters Corporation's Breeze software (version 3.30) was used to determine the physical properties of the mPEG-NH_2 and the PEGylated block and random copolymers.

4.2.3.b. Nuclear Magnetic Resonance (NMR) Characterization

The purified samples of PEGylated paa products were dissolved, at a concentration of 5mg/mL, in D_6-Dimethyl sulfoxide (D_6-DMSO). NMR experiments were carried out using a Varian Unity Inova 500 MHz spectrometer equipped with a 5 mm Penta (H,C,N,P,D) PFG VT

probe. All experiments were performed at 35°C to lower the viscosity of the solution, 32 scans, with a 10 second relaxation delay.

4.3. Results

4.3.1. Characterization of the α-methoxy-ω-amino Polyethylene Glycol (5kDa)

The mPEG-NH_2 was characterized before use as a polymerization initiator. This was done to determine its purity and to give a reference standard for use in subsequent GPC and ^1H NMR experiments. The mPEG-NH_2's was normalized by integration of the ethylamine (2H, -CH_2-NH_2) peak (e) at δ= 3.57ppm to 2.0. Peak splitting of the main peak at 3.65 ppm is due to scalar coupling. The peak integration for the main chain yielded approximately 464 protons, which indicated 116 repeat units. This integration was subsequently used for all PEGylated polymer product NMR spectrum analysis. Based upon this information the PEG was determined to have a molecular weight of approximately 5197g mol^{-1}, which was used for all calculations necessary for determination of molar quantities of monomer units needed to achieve proper monomer/ initiator ratios during polymer synthesis (list of synthesized polymers are tabulated in Table 4.2).

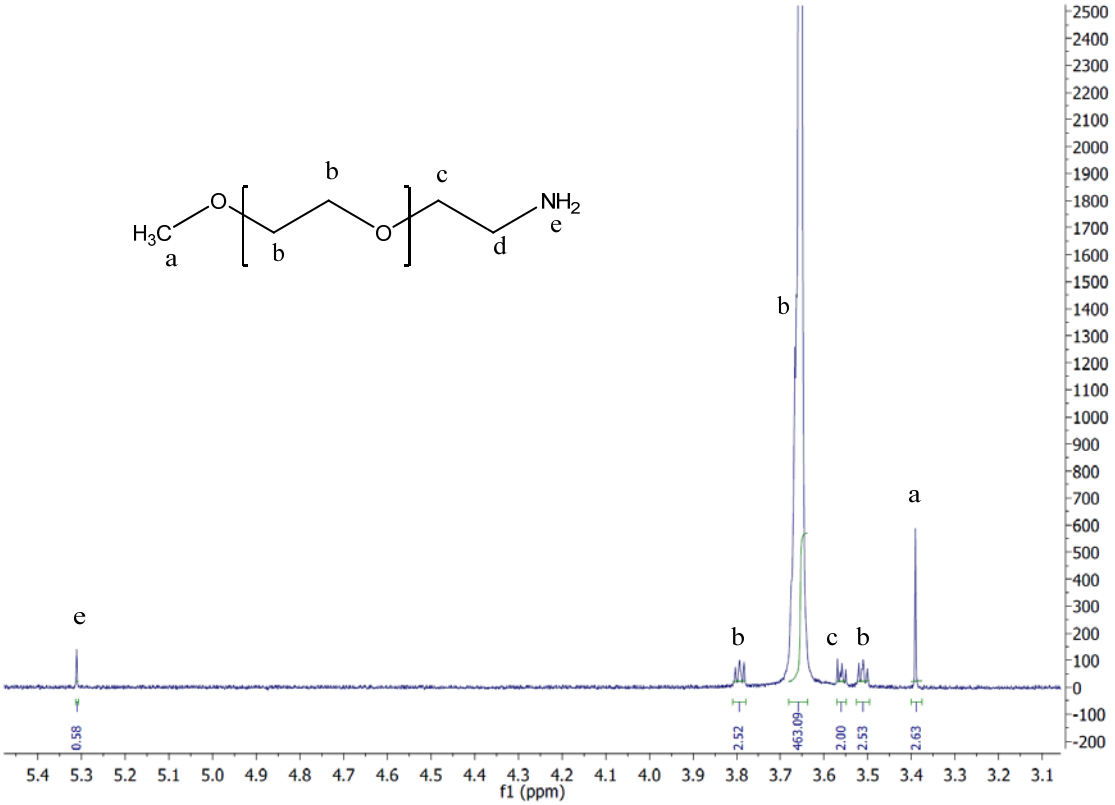

Figure 4.1. ^{1}H NMR spectrum of α-methoxy-ω-amino PEG in $CDCl_3$. ^{1}H NMR (DMSO-*d*6, 500 MHz): *δ*/ ppm = 3.39 (3H; C*H*$_3$-), 3.65 (8H; -C*H*$_2$-C*H*$_2$-O-C*H*$_2$-C*H*$_2$-) with satellite peaks at 3.51, and 3.79 due to scalar coupling, 3.57 (2H; CH_2-N*H*$_2$).

The representative ^{1}H-NMR was performed on the Laysan Bio mPEG$_{5k}$ (Figure 4.1) in $CDCl_3$ and chemical shifts were assigned using TMS as an internal reference. Characteristic PEG peaks were observed at the appropriate chemical shifts including the ethylene oxide main chain –C*H*$_2$-C*H*$_2$-O- structure of PEG at δ=3.6ppm, with satellite peaks at δ=3.51 and 3.79 ppm (b,c). The CH_2-C*H*$_2$-NH- methyl protons (e) were observed at δ=3.57ppm, integration normalized to 2 and used to determine the molecular weight of the mPEG-NH_2. The methoxy group was observed at δ= 3.39 ppm (a), and the amine group was observed at δ=5.30ppm (f). The PEG product appeared to be pure, and yielded a NMR calculated molecular weight of approximately 5197g/mol.

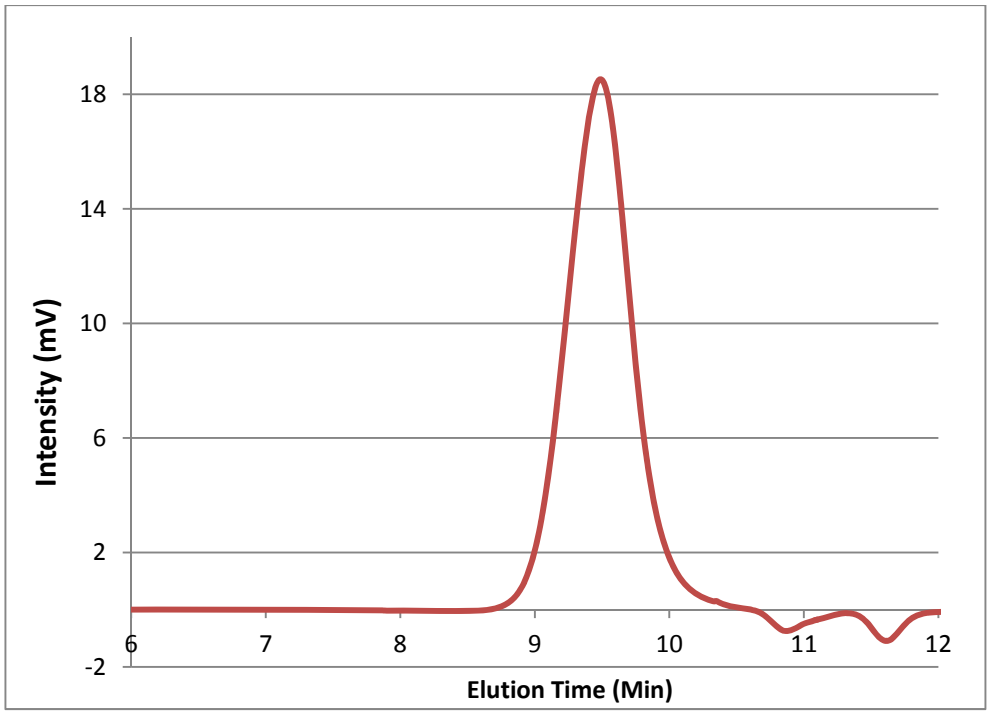

Figure 4.2. GPC chromatogram of α-methoxy-ω-amino PEG (5 mg/mL) in 0.01M LiBr DMF.

GPC was performed on the mPEG-NH_2 to determine the polydispersity of the macroinitiator. The GPC chromatogram for the α-methoxy-ω-amino PEG yielded a narrow monodisperse peak and the PDI was determined to be 1.02. The M_w for the PEG was found to be 5087g/mol, with a M_n of 4987g/mol, and the GPC trace showed the PEG was monomodal and exhibited narrow dispersivity (Figure 4.2). This indicated the mPEG-NH_2 was pure, and was subsequently used for all PEGylated poly(amino acid) synthesis, and the NMR and GPC results in good agreement as to the size of the PEG from Laysan.

4.3.2. Characterization of PEG-b-Poly(Amino Acid) Block and Random Copolymers

The goal of this segment of the investigation was to synthesize a variety of PEGylated block and random copolymers using α-methoxy-ω-amino PEG (Mw 5000Da) as the nucleophilic macroinitiator. Table 4.1. summarizes the results from random and block copolymers produced. The molecular weights and yields were calculated based upon theoretical polymer chain lengths, prior to NMR and GPC characterization, and give a good estimate as to yield of each polymer product. The poly(amino acid)'s molecular weights are calculated assuming the monomer/initiator ratios were achieved as desired to yield the $\overline{DP_n}$ specified for each polymer sample listed in Table 4.1. Actual molecular weights and $\overline{DP_n}$ data can be found in Table 4.2., and are derived from experimental data.

The synthesis of PEGylated block copolymers mPEG-b-p(L-lysine-b-L-cysteine) and mPEG-b-p(L-glutamate-co-cysteine) was carried out via ring opening polymerization under living ring opening polymerization conditions (LROP) in DMF, with urea, at ambient temperatures. These samples were initially characterized with the protecting groups intact.

Each block copolymer has an A-B-C architecture where the A block was mPEG, the B block was considered a linker region made of either L-lysine or L-glutamate. The C block, in the block copolymers, was always designed to be the L-cysteine block, which was intended to be the anchor for the paa chain when applied to gold surfaces.

The random copolymers were synthesized with an A-(BC)- architecture. Where A was the mPEG block and BC was a randomized amino acid block consisting of L-lysine/ L-cysteine, or L-glutamate/ L-cysteine. It was proposed that the BC block would not contain any sort of sequence specificity, and anticipated to have L-cysteine residues inter-dispersed between the L-glutamate and L-lysine residues in a non-specific order. This was to promote paa adhesion to the gold along the entire amino acid block, rather than just at the N-terminus of the poly(amino acid).

Sample No.	Sample (Target repeat units)*	Mass [g] NCA 1 Added	Mass [g] NCA 2 Added	Paa Mw [g] (Calc)
7	PEG-b-p(Lys_{50}-b-Cys_{10})	1.14	0.239	18,700
10	PEG-b-p(Lys_{100}-b-Cys_{10})	0.988	0.104	30,000
11	PEG-b-p(Lys_{100}-b-Cys_{20})	1.23	0.258	32,400
13	PEG-b-p(Lys_{50}-co-Cys_{10})	0.993	0.208	18,700
14	PEG-b-p(Lys_{100}-co-Cys_{10})	1.12	0.118	30,000
17	PEG-b-p(Lys_{100}-co-Cys_{20})	1.17	0.245	32,400
28	PEG-b-p(Lys_{50}-b-Cys_{10})	0.976	0.205	12,600
32	PEG-b-p(Lys_{100}-b-Cys_{10})[a]	1.11	0.116	16,800
33	PEG-b-p(Lys_{100}-b-Cys_{20})[a]	1.31	0.275	15,200
29	PEG-b-p(Lys_{50}-co-Cys_{10})[a]	1.08	0.227	12,400
35	PEG-b-p(Lys_{100}-co-Cys_{10})[a]	0.983	0.103	18,300
36	PEG-b-p(Lys_{100}-co-Cys_{20})[a]	0.876	0.187	19,700
8	PEG-b-p(Glu_{50}-b-Cys_{10})	0.977	0.209	18,500
9	PEG-b-p(Glu_{100}-b-Cys_{10})	1.14	0.122	29,500
12	PEG-b-p(Glu_{100}-b-Cys_{10})	1.1	0.235	31,900
19	PEG-b-p(Glu_{50}-co-Cys_{10})	0.995	0.198	18,500
20	PEG-b-p(Glu_{100}-co-Cys_{10})	0.986	0.105	29,500
26	PEG-b-p(Glu_{100}-co-Cys_{20})	0.999	0.213	31,900
37	PEG-b-p(Glu_{130}-co-Cys_{20})[a]	1.07	0.176	22,800
30	PEG-b-p(Glu_{50}-b-Cys_{10})[a]	1.11	0.237	12,600
28	PEG-b-p(Glu_{100}-b-Cys_{10})[a]	1.2	0.120	16,800
31	PEG-b-p(Glu_{100}-b-Cys_{20})[a]	1.08	0.231	15,200
38	PEG-b-p(Glu_{50}-co-Cys_{10})[a]	0.993	0.199	12,400
40	PEG-b-p(Glu_{100}-co-Cys_{10})[a]	1.08	0.115	18,300
41	PEG-b-p(Glu_{100}-co-Cys_{20})[a]	0.991	0.212	19,700

TABLE 4.1. List of theoretical data for the prepared polymers, properties and yields of analyzed samples. ([a]) indicates the protective groups have been removed from these polymers. *All samples were synthesized at room temperature.

Table 4.1 is a summarization of the PEGylated poly(amino acid) (PEG-paa) random and block copolymers and the reactants that were used during the synthesis of each PEG-paa in this study. Preparations of the paas were based upon monomer 1 (NCA1)/initiator ratios to yield paas of desired chain lengths. Subsequently, monomer 2 (NCA2) was then calculated based upon the molar content of monomer 1. The desired degrees of polymerization ($\overline{DP_n}$) are shown in Table 4.1, as well as the molecular weight that should be obtained it the desired paa chain lengths are achieved.

The reaction times listed in Table 4.2 indicate the amount of time (in days) that was required for the LROP to come to completion. Each reaction was carried out at room temperature, and was not strictly controlled. The synthesis times were between 3 and 6 days. The block copolymers were synthesized in two steps, as it was necessary for the di-block paa synthesis to reach completion before adding monomer 2 for the ter-block copolymer formation. Therefore, times in Table 4.2 are cumulative for the block copolymers. The longest reaction time observed was that of the PEG-b-p(Glu_{130}-b-Cys_{20}), and the shortest synthesis of three days was seen in both block and random copolymers of 60 repeat units long. The PEGylated polymers with a $\overline{DP_n}$= 110 were found to take between 4 and 5 days for the reactions to terminate. All of the products that contained 120 amino acid repeat units terminated on day 5. This data indicates that chain length plays a role in reaction time, whereas, the difference between block and random copolymer design does not.

Table 4.2 summarized the yields obtained for each of the PEG-paa samples. All of the PEG-poly(amino-acid)s gave 78.2% or better yields. The polymers with $\overline{DP_n}$=60 showed the highest yields and averaged 88.5%, for PEG-paas with $\overline{DP_n}$= 110 average yield was found to be 87.8%, and the samples with a $\overline{DP_n}$= 120 had an average yield of 87.7%. The average yield for the random copolymer was found to be 88.2%, and the block copolymer had an average yield of 87.7% . The PEG-paa polymers that had lysine had average yields of 87.7%, whereas the glutamate based PEG-paas had an average yield of 88.2% (all calculations were averaged from Table 4.2). These results indicate that the LROP synthesis does not prefer one amino acid type or sequence over another, and that all polymer types can be consistently produced under the aforementioned conditions. Variances in yields are most likely a result of loss during transfer from one vessel to another, during dialysis, or even loss during lyophilization.

Sample No.	Sample (Target repeat units)*	Reaction Time (Days)	Theoretical Yield [g]	Actual Yield [g]	% Yield
7	PEG-b-p(Lys_{50}-b-Cys_{10})	4	1.396	1.21	86.8
10	PEG-b-p(Lys_{100}-b-Cys_{10})	5	1.013	0.79	78.2
11	PEG-b-p(Lys_{100}-b-Cys_{20})	5	1.353	1.23	91
13	PEG-b-p(Lys_{50}-co-Cys_{10})	3	1.216	1.08	88.4
14	PEG-b-p(Lys_{100}-co-Cys_{10})	4	1.149	1.04	90.2
17	PEG-b-p(Lys_{100}-co-Cys_{20})	5	1.287	1.08	84.3
28	PEG-b-p(Lys_{50}-b-Cys_{10})	3	1.196	1.09	90.8
32	PEG-b-p(Lys_{100}-b-Cys_{10})[a]	5	1.138	1.01	88.6
33	PEG-b-p(Lys_{100}-b-Cys_{20})[a]	5	1.440	1.22	84.9
29	PEG-b-p(Lys_{50}-co-Cys_{10})[a]	4	1.323	1.23	93.2
35	PEG-b-p(Lys_{100}-co-Cys_{10})[a]	5	1.008	0.87	86.4
36	PEG-b-p(Lys_{100}-co-Cys_{20})[a]	5	0.968	0.86	89.2
8	PEG-b-p(Glu_{50}-b-Cys_{10})	4	1.199	1.04	86.5
9	PEG-b-p(Glu_{100}-b-Cys_{10})	4	1.168	1.04	89.3
12	PEG-b-p(Glu_{100}-b-Cys_{10})	5	1.211	1.06	87.9
19	PEG-b-p(Glu_{50}-co-Cys_{10})	3	1.221	1.11	90.8
20	PEG-b-p(Glu_{100}-co-Cys_{10})	4	1.011	0.87	86.4
26	PEG-b-p(Glu_{100}-co-Cys_{20})	5	1.099	0.98	88.8
37	PEG-b-p(Glu_{130}-co-Cys_{20})[a]	6	1.107	0.91	82.3
30	PEG-b-p(Glu_{50}-b-Cys_{10})[a]	4	1.363	1.15	84.5
28	PEG-b-p(Glu_{100}-b-Cys_{10})[a]	5	1.211	1.13	93.5
31	PEG-b-p(Glu_{100}-b-Cys_{20})[a]	5	1.188	1.08	90.7
38	PEG-b-p(Glu_{50}-co-Cys_{10})[a]	3	1.193	1.04	87
40	PEG-b-p(Glu_{100}-co-Cys_{10})[a]	5	1.106	0.99	89.6
41	PEG-b-p(Glu_{100}-co-Cys_{20})[a]	5	1.090	0.98	90.2

TABLE 4.2. List of experimental data for prepared polymers, properties and yields. ([a]) Indicates the protective groups have been removed from these polymers. * All samples were synthesized at room temperature.

The gel permeation chromatography (GPC) and nuclear magnetic resonance (NMR) data are summarized in Table 4.3. This table is derived from data discussed in sections 4.3.2.a. and 4.3.2.b. As can be seen, the PEG-paas were synthesized fairly close to the target lengths desired (from Table 4.1). Each sample was synthesized based on molar ratios of the monomers and the initiators, and any large deviation from the desired $\overline{DP_n}$ is most likely a result of inaccurate weight determination of the monomer or initiator prior to addition to the reaction flask.

Sample No.	Polymer (Actual Composition)	DP_n (NMR) Lys/Cys	M_n (NMR)	M_w (GPC)	M_n	PDI
7	PEG-b-p(Lys_{49}-b-Cys_9)	49/9	18,600	18,700	15,800	1.18
10	PEG-b-p(Lys_{104}-b-Cys_8)	104/8	31,400	31,300	27,700	1.13
11	PEG-b-p(Lys_{109}-b-Cys_{15})	109/15	34,000	34,100	29,400	1.16
13	PEG-b-p(Lys_{53}-co-Cys_{10})	53/10	19,800	20,000	15,700	1.27
14	PEG-b-p(Lys_{101}-co-Cys_7)	101/7	30,500	29,700	21,500	1.38
17	PEG-b-p(Lys_{105}-co-Cys_{14})	105/14	32,700	33,100	25,100	1.32

Sample No.	Polymer	DP_n (NMR) Glu/Cys	M_n (NMR)	M_w (GPC)	M_n	PDI
8	PEG-b-p(Glu_{57}-b-Cys_9)	57/9	19,700	19,500	16,800	1.16
9	PEG-b-p(Glu_{101}-b-Cys_7)	101/7	29,100	29,200	25,000	1.17
12	PEG-b-p(Glu_{108}-b-Cys_{14})	108/14	32,300	32,100	28,200	1.14
19	PEG-b-p(Glu_{50}-co-Cys_8)	50/8	18,000	18,300	14,500	1.26
20	PEG-b-p(Glu_{102}-co-Cys_7)	102/7	29,400	29,200	21,800	1.34
26	PEG-b-p(Glu_{100}-co-Cys_{19})	100/19	31,600	31,700	23,800	1.33

*****Extensive GPC chromatogram data is located in Appendix B. Replicate synthesis NMR and chromatogram data is located in Appendix B.

Table 4.3. Physical properties of the PEGylated block and random copolymers derived from GPC and NMR data.

Polydispersity index (PDI) data (table 4.3) was determined from the M_w/M_n ratio obtained using the Waters GPC instrument. The PDIs for the PEGylated poly(amino acid)s does not appear to show any apparent difference with regard to lysine or glutamate content. The average PDI for PEG-paas containing lysine was 1.24, and the average of those synthesized with glutamate was 1.23. The PDIs averaged for random and block copolymers, on the other hand, does show a marked difference. The average PDI for the random copolymer was calculated to be 1.32, but the block copolymer had an average PDI of only 1.16. This indicates that the block copolymer has a low molecular weight distribution and the synthesis process is closely followed the primary amine mechanism (see section 1.2.1), and the reaction kinetics facilitated living ring opening polymerization. Additionally, narrow molecular weight distributions were seen in the GPC chromatograms (see Appendix B for additional data), with no shoulder, as previously

discussed. Additionally, replicate synthesis data is presented in Appendix B for a variety of random and block copolymers that were synthesized more than once..

The random copolymers, had significantly higher PDIs, and some GPC chromatograms showed shoulder formation indicating that the polymerization kinetics were skewed from that present in the block copolymers. The differences in monomer chemical reactivities could have cause the randomization of the cysteine to be diminished, lending to shoulder formation in the random PEG-paa GPC chromatograms. The molecular weight distributions are still quite narrow in the random copolymers; however, the data indicates that the random copolymers show a "blocky" distribution.

It should be noted that the protected PEGylated paas were not water soluble due to the hydrophobicity of the protective groups. Therefore, it was necessary to use DMF as the mobile phase, and 0.01M LiBr was added to reduce the polymer-solvent interaction that can occur. This interaction may yield a shoulder in high molecular weight polymers, giving an apparent bimodal response [133] .

4.3.2.a Gel Permeation Chromatography of PEGylated Random and Block Copolymers

It was initially assumed that the block copolymers would yield a more disperse product, as it required an additional step when adding the cysteine monomer to the reaction media. However, as can be seen in Figure 4.3, the representative GPC traces of mPEG-b-p(Lys-b-Cys) ($\overline{DP}_n$= 110), and α-methoxy-ω-amino PEG_{5k} gave monomodal distributions. The narrow distributions are indicative of a lack of side reactions, and a PDI of < 1.2 generally indicates a true living polymerization [28], [30].

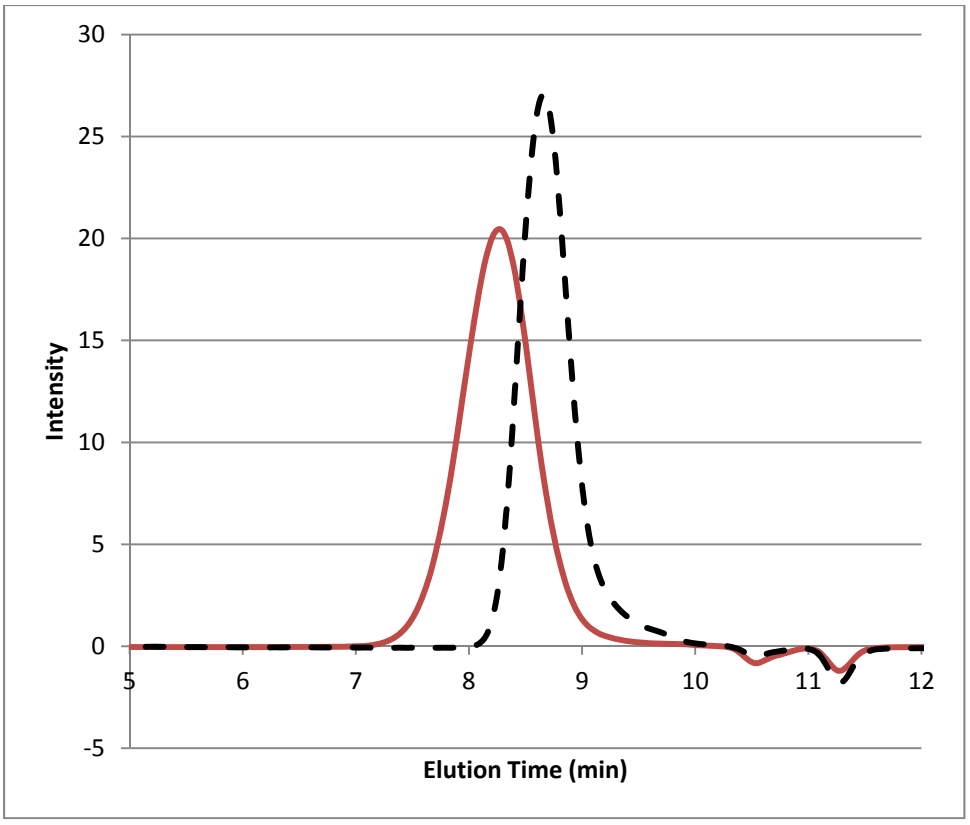

Figure 4.3. GPC chromatogram of mPEG-b-p(Lys_{100}-b-Cys_{10}) (solid line) α-methoxy-ω-amino PEG_{5k} (dashed line).

Furthermore, the α-methoxy-ω-amino PEG peak was placed as a reference to demonstrate that the addition of the amino acid blocks increased the molecular weight from that seen in the PEG alone. The PEG-paa peak appears to be slightly broader than that of the mPEG; however, this is not usual given that a ter-block copolymer has been synthesized by the addition of the cysteine residues in a secondary reaction (see Appendix B for additional GPC chromatograms).

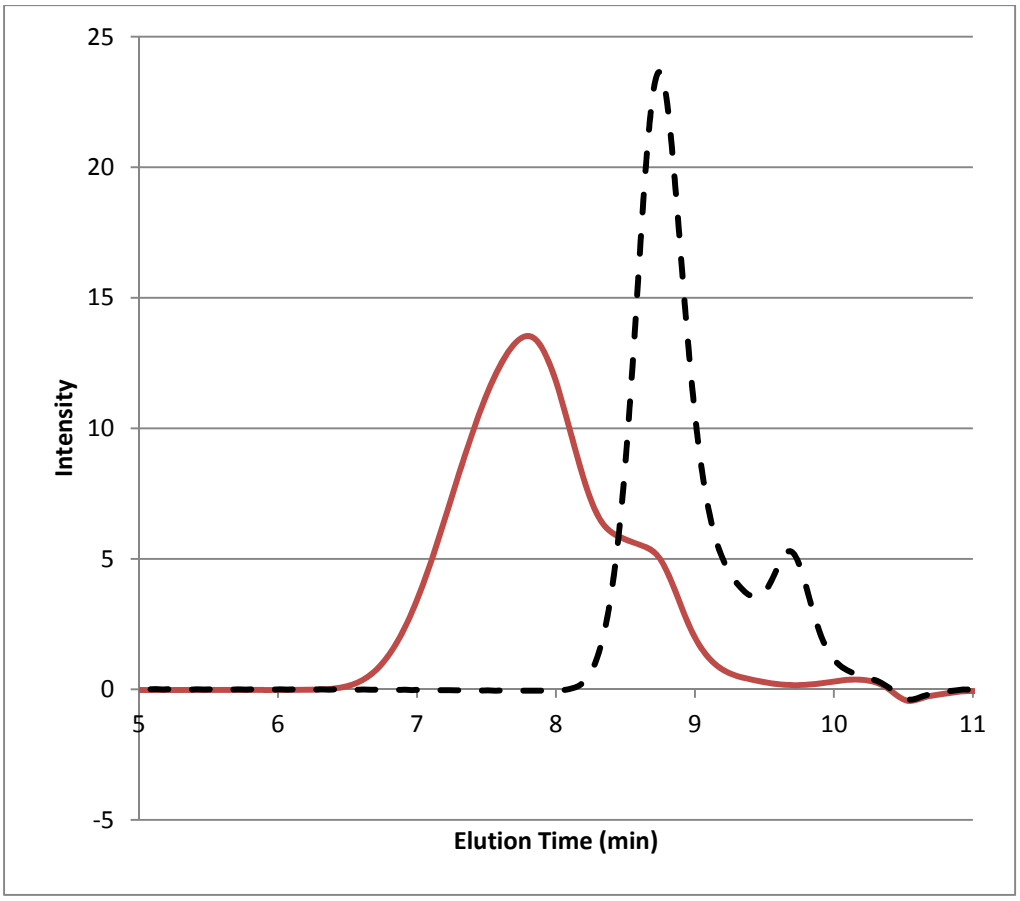

Figure 4.4. GPC chromatogram of mPEG-b-p(Lys_{100}-co-$_{Cys20}$) (solid line) and mPEG-b-p(Lys_{50}-co-Cys_{10}) (dashed line).

From the data present in Figure 4.4, it can be seen that the random copolymers of mPEG-b-p(Lys-co-Cys) $\overline{DP_n} = 60$ and 120, have a bimodal distributions with PDIs of 1.27 and 1.32 respectively. The shoulder that appears in the low molecular weight region could be caused by side reactions of the paa polymerization due to impurities being present, which would cause truncation of the paa chain. A difference in reactivities of the monomer units can cause a lack of true randomized polymer. This can cause a blocky product that will exhibit a broader molecular weight distribution. The chromatogram in Figure 4.5 shows that there is not a large enough molecular weight shift, when comparing the random copolymer with the block copolymer, to undoubtedly support this conclusion. Regardless, Figure 4.5 shows that the PEG-paa products

were synthesized to yield polymers of similar molecular weights despite the fact that one was a block copolymer and the other was a random copolymer.

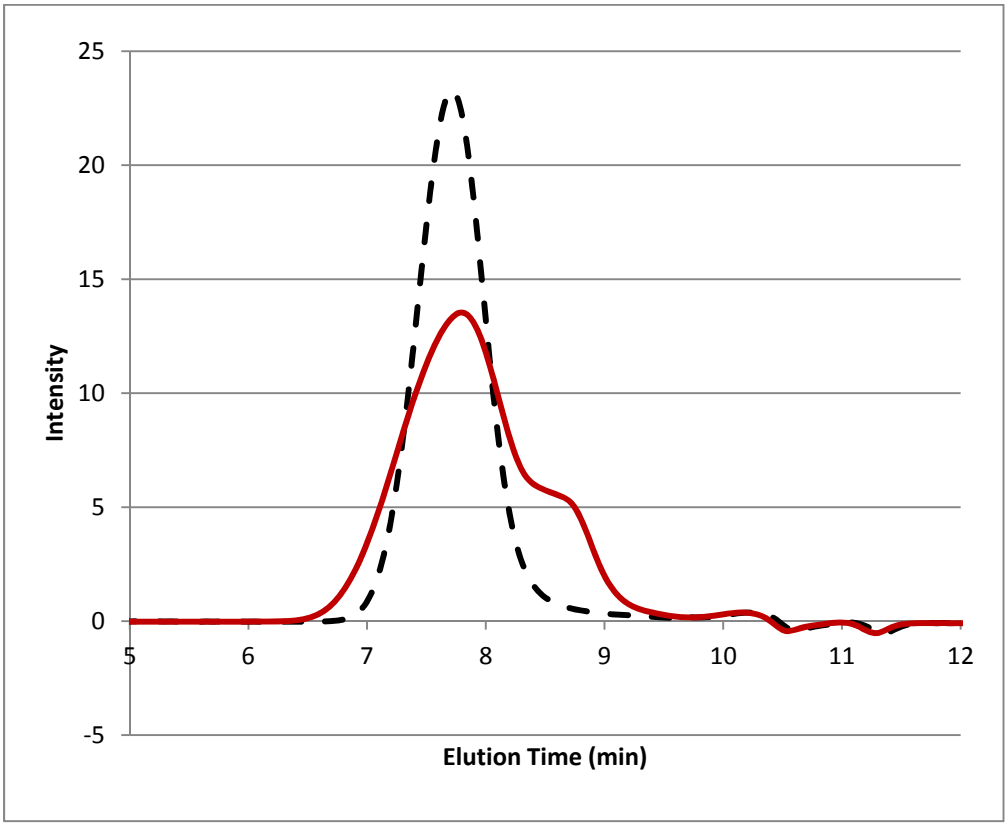

Figure 4.5. GPC chromatogram of mPEG-b-p(Lys_{100}-co-Cys_{20}) (solid line) and mPEG-b-p(Lys_{100}-b-Cys_{20}) (dashed line).

Figure 4.5 is indicative of results observed, on a consistent basis, in the random copolymerization. The PDI for the PEG-b-p(Lys_{100}-co-Cys_{20}) and the PEG-b-p(Lys_{100}-b-Cys_{20}) yielded PDIs of 1.32 and 1.16 (Table 4.3) respectively. As mentioned above, the lack of a shoulder (Figure 4.3) and low PDI in the block copolymer shows that there is a greater amount of control over the reaction. Additional experiments and analysis would be necessary to determine the exact cause of the shoulder formation in the GPC traces for the random copolymers. It should

be noted, however, that all of the block copolymers yielded a lower PDI than that of the random copolymers (Table 4.3), which could lead to the conclusion that a truly randomized polymer has not been synthesized.

In summary, the PEGylated copolymers that were produced by LROP exhibited a low polydispersity (between 1.13 and 1.38 and the number of repeat units found in each polymer varied slightly from the desired monomer/initiator ratios (Table 4.1). The variances in control of the degree of polymerization are most likely due to a lack of precision of the scale that was used to weigh the calculated amount of monomer and initiator being used. Small variances in mass can have a fairly large impact upon the final $\overline{DP_n}$ of the product. Regardless, the chain length of the amino acids varied from the target lengths by only ±4 monomer units overall.

As mentioned above, this increase in PDI is due to a difference in reactivities of the lysine/glutamate and cysteine monomers. It is not probable that solvent effects or secondary structure formation effected the polymerization reaction, as the use of DMF has been shown to reduce aggregation and auto-acceleration of the chains [29], [33], [65].

4.3.2.b. Nuclear Magnetic Resonance of PEGylated Random and Block Copolymers

The proton NMR results for the PEGylated copolymers exhibited broad peaks when short relaxation delay times are used, as is expected for large polymer products. The methoxy groups of the PEG and the amino acids were difficult to resolve, as there was often a large amount of peak overlap between 1.5 and 2.5 ppm. Peak assignments could be generally assigned, however, but not definitively quantified in the alkane region of the spectra (see Appendix B for additional NMR spectra).

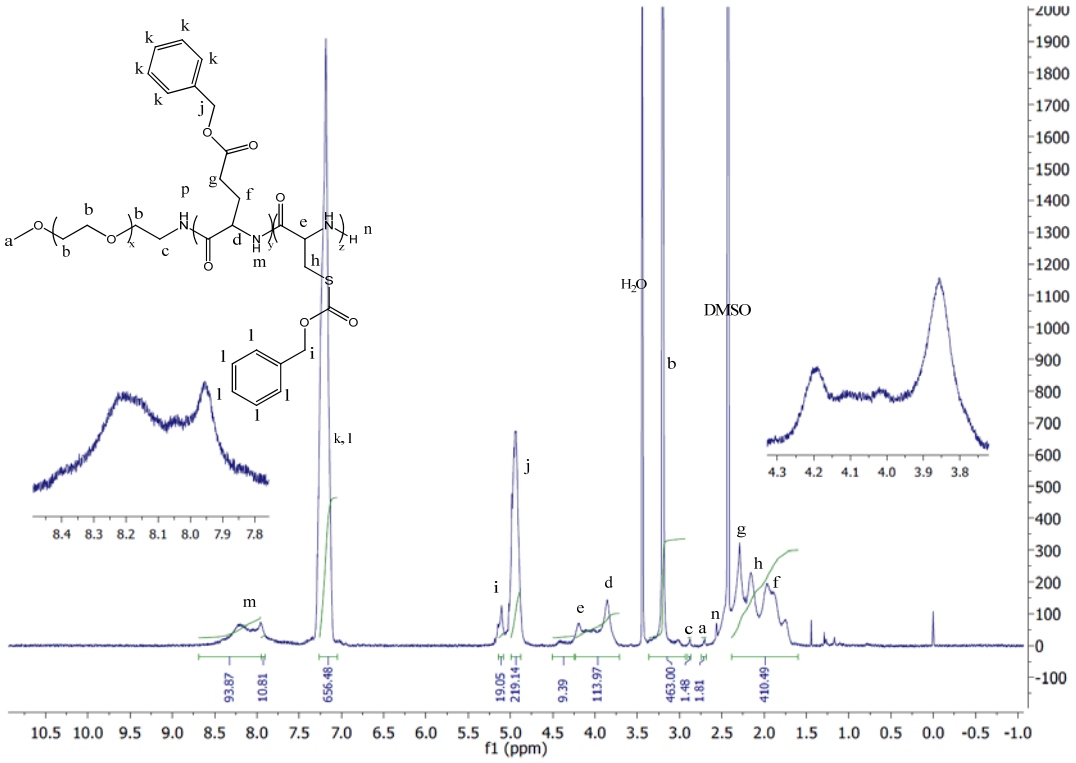

Figure 4.6. Representative ^{1}H-NMR of PEG-b-p(Glu$_{100}$-b-Cys$_{10}$) (DMSO-*d*6, 500 MHz): *δ*/ ppm = 1.75-2.31 (2H; -C*H*$_2$-), 3.26 (4H; CH$_3$-O-C*H*$_2$-C*H*$_2$-O-), 3.83 and 4.19 (1H; CO-C*H*-NH-), 4.97 and 5.15 (2H; O-C*H*$_2$-C$_6$H$_5$), 7.95 and 8.4 (5H; O-CH$_2$-C$_6$*H*$_5$).

Peak assignments and quantification of monomer units were derived from the methylene protons adjacent to the aromatic protecting groups on glutamate (j) and cysteine (i) at 4.97 and 5.15 ppm respectively (Figure 4.6). Additionally, the backbone methine protons for the monomer units could be quantified for glutamate (e) and cysteine (d) at 4.19 and 3.83 ppm respectively. Amide protons could be quantified and give the overall chain length of the amino acid region, and were found in a very broad peak (n) between 7.95 and 8.4 ppm for the glutamate and cysteine amides. The methylene peaks on the glutamate and cysteine side chains (f-h) were difficult to integrate as there was a high degree of peak overlap. The methylene group (h) adjacent to the thiol (-C*H*$_2$-S-CO) showed characteristic peak splitting due to the electronegativity of the sulfur atom present in the chain. PEG-b-p(Glu-b-Cys) and PEG-b-p(Glu-co-Cys) copolymers molecular weights were determined by finding the number of residues by integration numbers observed in

peaks d, e, i, and j. In addition, the peak integration of n and m was used to verify the probably number of repeat units by dividing the total integrated value by the five protons found in the benzyl ring.

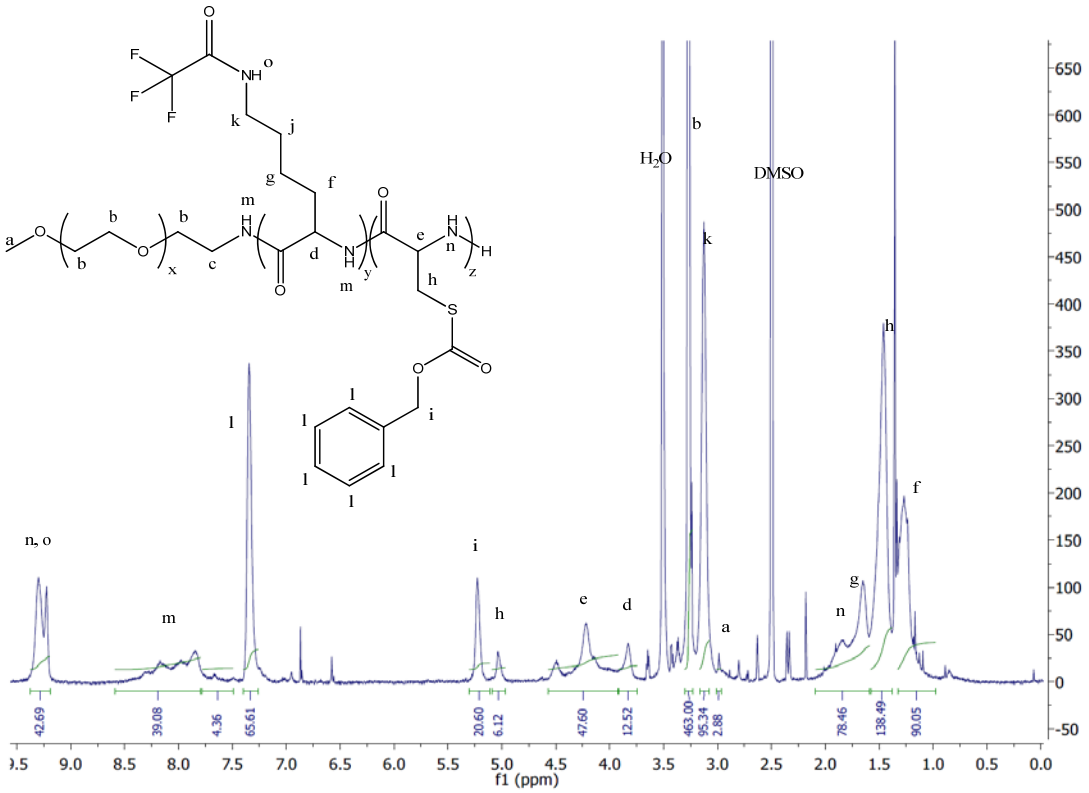

Figure 4.7. Representative ^{1}H-NMR of PEG-b-p(Lys$_{46}$-b-Cys$_{13}$) (DMSO-*d*6, 500 MHz): *δ*/ ppm = 1.28-1.83 (2H; -C*H*$_2$-), 3.13 (6H; CH$_3$-C*H*$_2$- C*H*$_2$-O- C*H*$_2$-), 3.83 and 4.23 (1H; CO-C*H*-NH-), 7.40 (2H; O-C*H*$_2$-C$_6$H$_5$), 7.92- 8.21,(CH$_2$-N*H*-CO-), 9.30 (1H; CH$_2$-N*H*-CF$_3$). *The peaks located at δ= 6.87, 6.58, and 2.32 ppm are residual solvent from the cleaning process of the NMR tubes.

The lysine based polymers (Figure 4.7) yielded a broad peak spectrum as well. The phenyl peak (l) (δ= 7.35 ppm) gave a direct indication as to the number of cysteine amino acids that were integrated into the paa chain. As with the glutamate/cysteine paa product, the alkane region was very difficult to quantify (f-h). Peak assignments could be generally assigned, but no useful data could be extracted regarding number of protons in the polymer chain. It was necessary to look, again, to the amino acid backbone protons for lysine (e) and cysteine (d) at

3.83 and 4.23ppm respectively (Figure 4.7) to determine the number of repeat units in the PEG-paa chain. Previous NMR data yielded the base integration of the PEG region of the polymer, which was used to normalize the spectra. This allowed for the integration of the remaining peaks to facilitate determination of the quantity of lysine and cysteine residues. It was possible, therefore, to determine more accurate degrees of polymerization, molecular weights, and number average molecular weights for each sample (Table 4.3). Figure 4.7 shows that the number of protons in the peak at δ=3.83 ppm could be compared with those of the carboxybenzyl aromatic ring (l) found at δ ~7.4ppm to conclude if they are in good agreement. Also, Figure 4.7 shows some residual solvent from insufficient dialysis during purification, but as the alkyl region is not well resolved; the need for additional purification was moot.

4.4. Discussion

The implementation of poly(amino acid) living ring opening polymerization using a nucleophilic initiator has allowed for the successful synthesis of a variety of PEGylated poly(amino acid)s. The methods, outlined above, facilitated the production of random and block copolymers of desired molecular weight. The polydispersity of the block copolymers was quite narrow from 1.13 to 1.18. The random copolymers demonstrated a broader molecular weight distribution from 1.26-1.38, and a multimodal distribution. This is possibly due to differences in chemical reactivities of the amino acids being used.

Shoulders seen in the GPC chromatograms were present only in the copolymers, and points more towards differences in reactivities than impurities in the reaction. This cannot be definitively determined, however, without further investigation. Still, it should be noted that several steps were taken to reduce a multi- or bi-modal response and reduce a possibility for loss of control over the reaction. First, urea was used to reduce β-sheet secondary structure. This can

occur during early iterations in paa chain growth and sterically hinder the reaction causing an alternate mechanism to predominate. Second, NMR data was obtained on all purified monomer units to check for impurities and contamination from atmospheric humidity or solvents. Also, secondary purifications were performed on each of the NCAs just prior to polymerization initiation. Third, Dimethylformamide was used as the reaction medium to reduce the possibility of auto-acceleration or aggregate formation. During GPC characterization of the purified products, 0.01M LiBr was used in DMF to reduce solvent -polymer interactions that can cause a bimodal chromatogram.

The PDIs of the block polymers were all less than 1.2, which would indicate a living polymerization environment. The molecular weight distributions were in good agreement with the target chain lengths, and showed that monomer/initiator ratios could adequately be used to synthesize polymers of desired molecular weight and allow control over paa architecture when a living nature of the polymer chain was achieved. More importantly, the addition of the cysteine block to the PEGylated-paa chains showed that the polymers chains were still reactive, thus living. The production of ABC block copolymers, with low PDIs and narrow molecular weight distributions, demonstrated the feasibility of the use of the above technique to synthesize small chain length paas when a nucleophilic macroinitiator was used.

CHAPTER 5

Removal of Protective Groups from Amino Acid Side Chains

5.1. Introduction

The ability to make linear poly(amino acid)s random and block copolymers via living ring opening polymerization (LROP) required the use of α-amino acid N-carboxyanhydrides (NCA) that have protective groups on the side chains. In the absence of protecting groups, functional groups could inhibit polymerization, leading to an uncontrolled reaction mechanism [45], [134]. Therefore, it is necessary to select protective groups that can temporarily mask the functional groups to facilitate regioselective bond formation. Emil Fischer (1918) was one of the first researchers who used protective groups to synthesize the carbohydrates [134].

The main characteristics of protective groups are [134]:

1. They should be easily introduced to the functional group
2. They should be stable in a broad range of reaction conditions
3. They should be capable of being removed after the reaction is completed, or when functional group manipulation is required, without damaging the functional group.

Another feature of protective groups is orthogonality, which was described by Barany *et al*. (1977). This concept states that the use of two or more protecting groups belonging to independent classes should be capable of being selectively removed by independent and distinct mechanisms [134–136]. The groups, therefore, can be removed in any order and in the presence of the other protecting groups without affecting the remaining groups [134].

However, this study did not require selective deprotection of the functional groups and a "one pot" method was developed to remove the carboxybenzyl (Cbz), benzyl ester (Bnl), and trifluoroacetyl (TFA) protective groups in a single reaction. A novel method has been introduced that was based upon a method originally used to remove only the TFA protective groups. The modified reaction conditions showed that all the protective groups could be removed at the same time, and were verified by ^{1}H-NMR.

5.1.1. Protective Groups for the Side Groups of α-Amino Acids

In this study, three types of protective groups will be used: Carboxybenzyl (Cbz), Benzyl (Bnl), and trifluoroacetyl (TFA). These are only a small sample of protective groups that are used to shield; alcohol, amine, carbonyl, carboxylic, phosphate, thiol, and terminal alkyne groups. The protective groups may protect any of the reactive sites on α-amino acids, including the N and C termini, as well as the side chain of the amino acids. This will allow for selective polymerization using chemical methods. Conversely, biological synthesis of paas in cells does not require the use of protected α-amino acids as tRNAs and ribosomes selectively conduct the paa assembly.

Here the Cbz will protect the thiol group of L-Cysteine NCA to prevent inter and intra molecular disulfide bond formation. The Bnl is used to shield the carboxylic end of the L-Glutamate (Figure 5.1), and prevent anhydride formation in the presence of the activated amino acids, enhancing solubility in non-polar solvents. The TFA will protect L-Lysine's amine end of its side chain, thus preventing its activation during polymerization (Figure 5.1) [137]. Failure to use protected amino acids can cause undesired branched and network copolymer formation and yield very low quantities of paas of a desired architecture [138].

5.1.2. Standard Deprotection Methods and Uses of the Amino Acid Protecting Groups

5.1.2.a. The Benzyl Group

The benzyl groups are generally used as a carboxyl protecting group (Figure 5.1), and can be easily added or removed making it a very popular choice for poly(amino acid) synthesis [45], [139]. Benzyl groups are susceptible to cleavage by acid or base hydrolysis. One simple method for Bnl cleavage is hydrogenolysis, and is typically accomplished by using palladium on carbon (Pd/C) in ethanol or ethyl acetate. [45]. One alternate method of interest, however, facilitates cleavage by using K_2CO_3, H_2O, in THF, and been shown to give a 75% yield of the purified deprotected product. This method is similar to the method used, herein, to cleave trifluoroacetyl protective groups as discussed below.

5.1.2.b. The Trifluoroacetyl Group

Amide derivative protecting groups are generally not used as they require harsh conditions to facilitate removal, which can cause degradation of the host molecule they are attached to [139]. However, the N-trifluoroacetyl (TFA) protecting group is an exception, as it is readily removed by base hydrolysis from primary and secondary amines. It has been shown in previous works that an 86% yield of the purified deprotected product can be achieved when TFA is removed with potassium carbonate in aqueous methanol (1:20 ratio of H_2: MeOH) without affecting the remaining ester. This is feature is very useful for deprotection of L-lysine protected with TFA.

5.1.2.c. The Carboxybenzyl Group

The carboxybenzyl (Cbz) protecting group is primarily used to protect amines from electrophiles. And can be conventionally cleaved by three main methods: acidolysis, catalytic hydrogenation, and reduction with a dissolved metal [140].

5.2. Research Goals

The focus of this part of the research project was to demonstrate that the deprotection of Bnl, Cbz, and TFA protective groups from their respective amino acids, can be performed using a one pot method. As mentioned above, it is usually desired that protective groups be selectively removed from the copolymer, however, this was not a concern in this research. It was desired, however, that simultaneous removal of hetero-functional groups could be achieved in all PEGylated poly(amino acid) products without degrading the main poly(amino acid) chain.

The central focus of the deprotection is the removal of protecting groups of the thiol so the paas may be used to modify gold on silica surfaces for possible use as a biomedical prosthesis. The thiols on the cysteine are necessary to anchor the paa securely to the surface, and it has been shown that the gold-thiol bond has dissociation energy of approximately 20 to 40 kcal mol^{-1} [141]. It is possible that the poly(ethylene glycol) may have a weak affinity for the gold surface, but this nonspecific interaction is much too weak to yield a surface coating that would be resistant to chemical and mechanical stress [142].

Furthermore, there are two reasons to investigate the deprotection of lysine and glutamate amino acids. First, their deprotection will allow the paa to become soluble in water. It has been observed that the addition of the Bnl and TFA protective groups lowers the overall solubility of the polymer chain in water even in the presence of high molecular weight PEG. The removal of

the non-polar functional groups will increase solubility of the PEGylated polymers and render them water soluble for non-selective application to gold surfaces by simple diffusion. Second, deprotection of these amino acids stems from their implications with regard to their potential use in drug delivery [46]. This second postulate will not be investigated at this time.

5.2.1. Description of the Novel Deprotection of Carboxybenzyl and Benzyl Protective Groups Simultaneously with TFA Protective Group Deprotection.

Previous methods for deprotection have demonstrated that trifluoroacetyl (TFA), carboxybenzyl (Cbz), and benzyl (Bnl) protective groups could be selectively removed by very different methods. It is proposed, however, that it's possible to cleave all three functional groups from the PEGylated poly(amino acid) polymers by one method. For the purposes of this study, selective removal of the protective groups is not necessary, and will not be investigated herein. Therefore, it was preferred that the elimination of multiple deprotection steps be found to mitigate unnecessary product loss, and reduce deprotection/purification time.

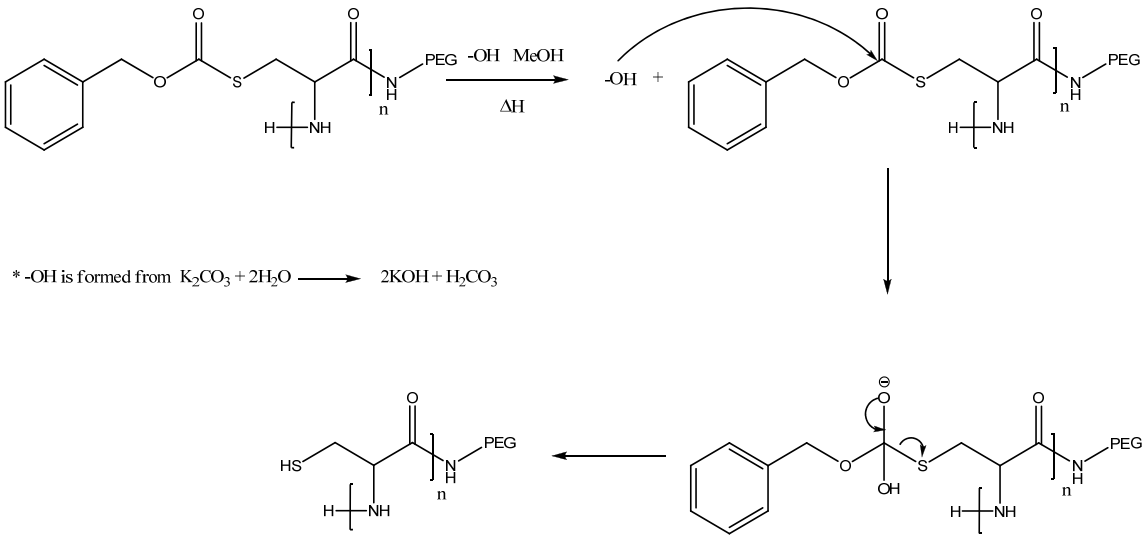

Scheme 5.1 S-Cbz-L-Cysteine deprotection scheme

Similar to the standard method, discussed above, for removal of TFA and Bnl; a reaction solution containing K_2CO_3, H_2O, and MeOH was used (Scheme 5.2 and 5.3). However, the method was modified to adjust the MeOH /H_2O ratio from 10:1 to 20:1, and the reaction was refluxed between 60° and 70°C, as opposed to 0° to 25°C for the original Bnl protocol. Additionally, tetrahydrofuran (THF) was not used to facilitate solubility of the polymer product, as was done in previous methods. Here, heat was used to relax the secondary structure and speed up the reaction process. It was observed early that cleavage of the Cbz and Bnl protective groups was extremely slow (projected to be on the order of days to weeks depending on chain length and composition) at ambient temperatures which prompted the increase of the reaction temperature.

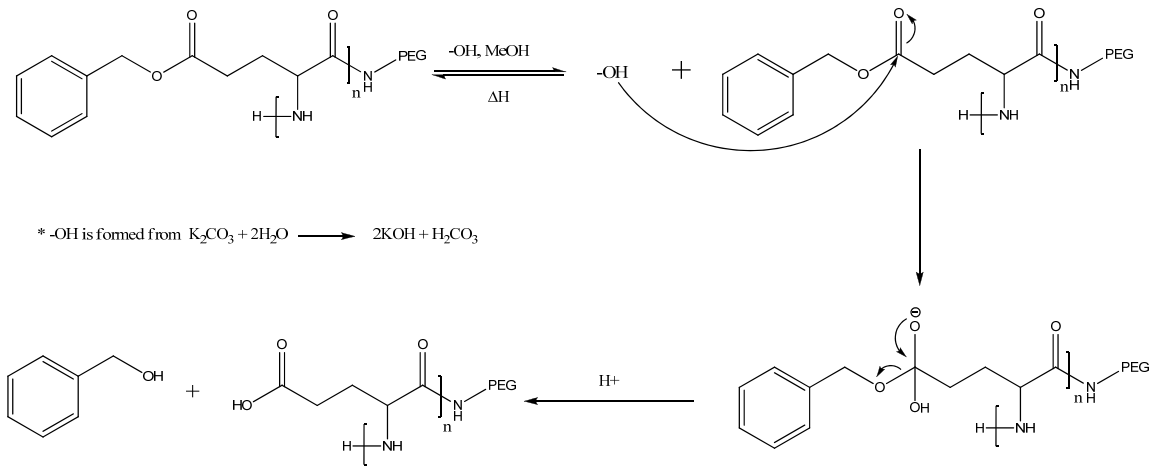

Scheme 5.2. γ-Bnl-L-Glutamate deprotection scheme

The glutamate and lysine amino acid residues deprotection occurs as the hydroxide nucleophile attacks the carbon of the ester C=O, creating the tetrahedral intermediate. The intermediate gives way and reforms the C=O resulting in the loss of the leaving group, the alkoxide, RO-, yielding a carboxylic acid of the glutamate (Scheme 5.2) and the amide for lysine (Scheme 5.3).

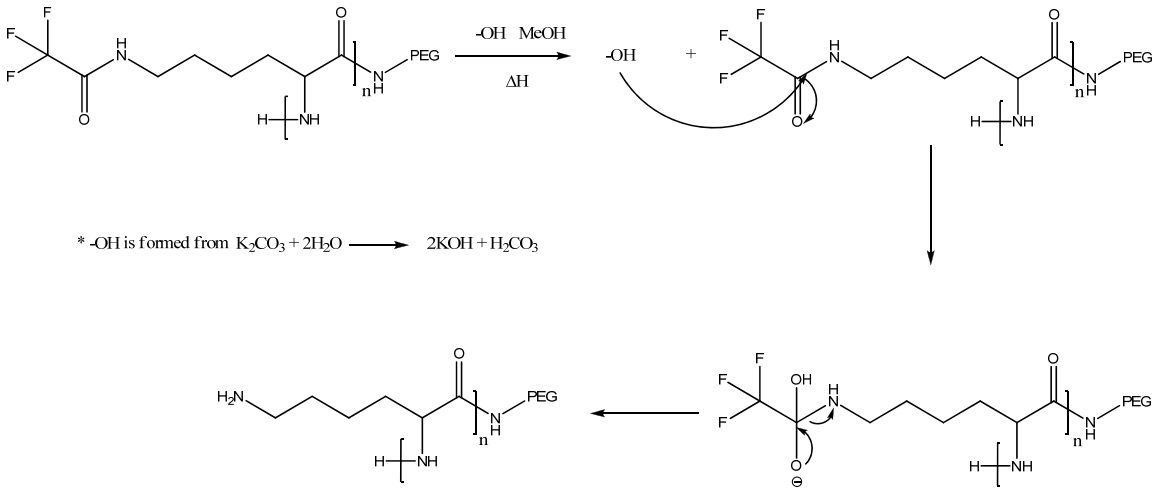

Scheme 5.3 N^6-TFA-L-Lysine Deprotection scheme

5.3. Experimental

5.3.1. Materials

The K_2CO_3 was purchased from Sigma Aldrich (St. Louis, MO), and the MeOH was purchased from Fischer Scientific (Waltham, MA). The Spectra/Por 3 dialysis membrane was (3,500 M_w cutoff) was purchased from Spectrum Laboratories (Rancho Dominguez, CA) and stored in the 37°C refrigerator until needed.

5.3.2. Methods

5.3.2.a. Deprotection of PEGylated Poly(Amino Acid)s

The polymers were insoluble in MeOH and water due to the hydrophobicity of the protecting molecules on the glutamate and lysine despite, the presence of hydrophilic PEG. The deprotection was carried by base hydrolysis while heating. First, magnetic stir bars, 9.5mL of MeOH, 0.5mL dH2O (to yield a 20:1 ratio), 150mg K2CO3, and 100mg of PEGylated paa were

combined in a round bottom flask. The mixture was allowed to reflux between 60°C and 70°C until the solution became clear.

Then, the solution was filtered through a Buchner funnel fitted with a fritted disk (5-10μm pore size) to remove any un-reacted polymer. The filtrate was collected in a round bottom flask, and reduced on a Labconco rotary evaporator at 35°C until the solution volume was approximately 1 to 2mL. The concentrated polymer solution was then dialyzed against 5L dH_2O (3X) to remove the K_2CO_3 and any residual small molecules that were generated during the deprotection process. The dialysate was then flash frozen in liquid N_2 and lyophilized. The resulting deprotected product was stored in a vacuum chamber until needed.

5.3.2.b. Nuclear Magnetic Resonance

The purified PEGylated paa products were dissolved, at a concentration of 5mg/mL, in Deuterium Oxide (D_2O). NMR experiments were carried out using a Varian Unity Inova 500 MHz spectrometer equipped with an 5 mm Penta (H,C,N,P,D) PFG VT probe. All proton experiments were performed at 25°C, 32scans, and a 10 second relaxation time.

5.4. Results

Early attempts at deprotection yielded undesired results, as the paas were either only partially deprotected, or the reaction showed degradation of the main chain, as observed by ^1H NMR experiments. It was initially assumed that once the reaction solution became clear, the paas were completely deprotected. However, the lack of turbidity does not adequately reflect that all protective groups have been cleaved.

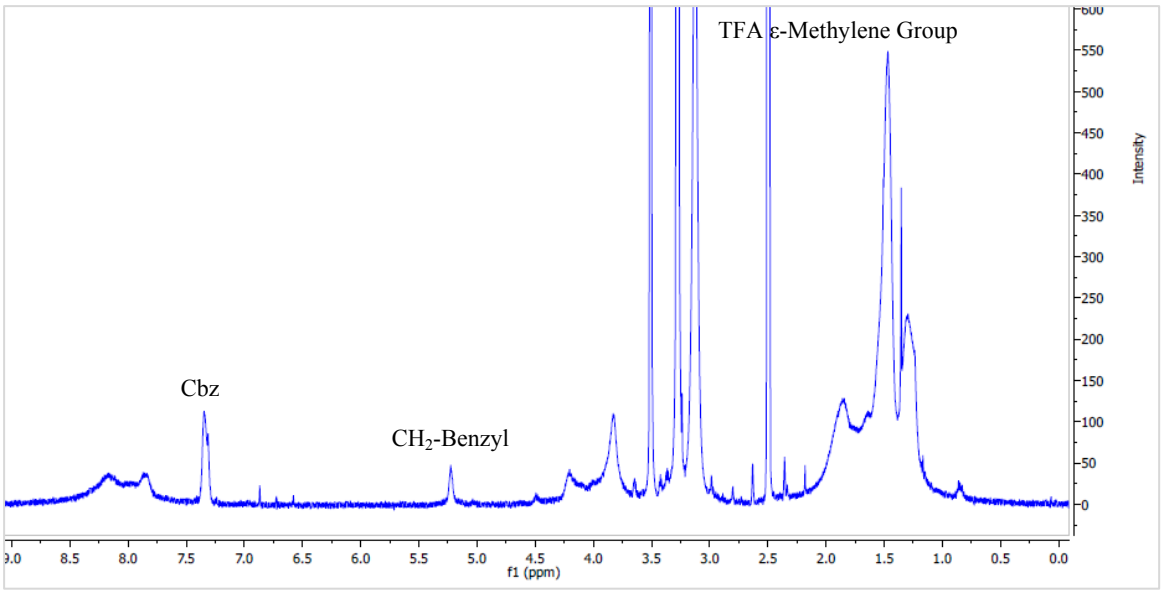

Figure 5.1 PEG-b-p(Lysine$_{60}$-co-Cys$_{20}$) showing incomplete removal of the protecting groups by the presentation of the characteristic carboxybenzyl peak at δ= 7.31ppm and the TFA's ε-methylene peak at δ=3.13 ppm.

Figure 5.1 shows that half of the protective carboxybenzyl groups and approximately a third of the trifluoroacetyl protective groups were removed. However, 100% removal was not been achieved in this reaction. Integration of the aromatic proton peak, at δ= 7.31 ppm, as well as the methylene protons of the C*H*$_2$- Benzyl peak, at δ= 5.21, shows that approximately five protected cysteine residues remain. The TFA-protected lysine's ε-methylene peak present at δ=3.13 ppm shows that approximately 40 of the original 60 residues remains protected. The overall hydrophilicity of the paas chain, however, was sufficient enough to render the molecule water soluble. This observation led to the premature termination of the reaction in the initial attempts at paa deprotection. It is well understood that PEG is water soluble, and the removal of some of the protective groups could have "pulled" the entire molecule into solution. It was desired, however, that all protecting groups be removed from the amino acids side chains prior to the application of the polymers to gold surfaces, therefore the reaction was allowed to proceed between 4 and 8 hours, depending upon polymer chain length and composition (Table 5.1). However, the paa main chain began to degrade as the basic conditions began to cleave the

backbone amide bonds. This was observed, in ^{1}H-NMR experiments, by a marked reduction in the observable backbone protons on the α-carbon (spectra not shown). Therefore, the reaction time was only allowed to continue approximately 60 minutes past the point of solution clarity. This yielded a product that exhibited no residual protective groups, and left the main polymer chain intact (Figures 5.2 and 5.3).

Sample No.	Polymer	Protective groups	DP_n (Actual)	M_w (g/mol)	Reaction Time (h)	Percent Yield
7	PEG-b-p(Lys_{49}-b-Cys_9)	TFA/ Cbz	58	9,596	5	88
10	PEG-b-p(Lys_{104}-b-Cys_8)	TFA/ Cbz	112	14,227	6	90
11	PEG-b-p(Lys_{109}-b-Cys_{15})	TFA/ Cbz	124	15,602	6	86
13	PEG-b-p(Lys_{53}-co-Cys_{10})	TFA/ Cbz	62	10,096	6	89
14	PEG-b-p(Lys_{101}-co-Cys_7)	TFA/ Cbz	108	13,915	7	93
17	PEG-b-p(Lys_{105}-co-Cys_{14})	TFA/ Cbz	124	14,446	8	91
8	PEG-b-p(Glu_{57}-b-Cys_9)	Bnl/Cbz	66	10,384	4	87
9	PEG-b-p(Glu_{101}-b-Cys_7)	Bnl/Cbz	108	14,011	5	89
12	PEG-b-p(Glu_{108}-b-Cys_{14})	Bnl/Cbz	122	15,026	5	89
19	PEG-b-p(Glu_{50}-co-Cys_8)	Bnl/Cbz	58	9,729	4	89
20	PEG-b-p(Glu_{102}-co-Cys_7)	Bnl/Cbz	109	14,096	5	92
26	PEG-b-p(Glu_{100}-co-Cys_{19})	Bnl/Cbz	119	14,636	6	91
45*	PEG-b-p(Lys_{109}-b-Cys_{11})	Cbz/Cbz	120	14,825	8	86

Table 5.1. Deprotection reaction data for calculated molecular weights, and reaction time in (h). (*) indicates this reaction was performed one time only and contained carboxybenzyl protecting groups on both types of amino acid residues.

Proton nuclear magnetic resonance (^{1}H-NMR) experiments were conducted to observe the removal of the protective groups from the PEGylated poly(amino acid) chains. The characteristic aromatic signal (generally observed at $\delta \approx 7.3$ ppm) produced by carboxybenzyl (Cbz) and benzyl (Bnl) protective groups proved to be the simplest means for determination of their removal (Figures 5.2 and 5.3).

^{1}H-NMR of PEG-b-p(Lys_{100}-co-Cys_{10}) in Figure 5.2 showed that the reaction time was adjusted sufficiently to allow for the removal of the protective groups, yet degradation of the polymer had not yet started. The aromatic protons of the Cbz protective group were completely absent in the deprotected sample (lower spectrum Figure 5.3. and inset) at δ=7.25 ppm.

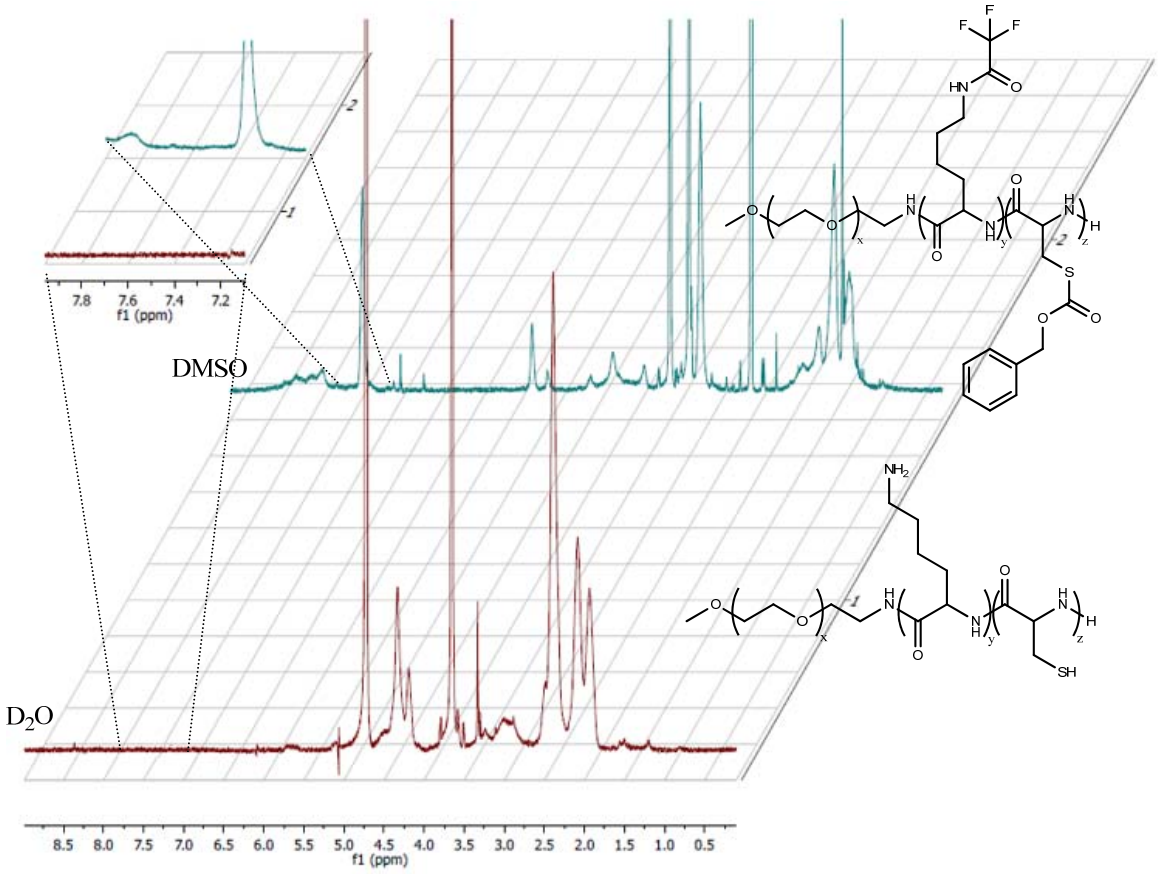

Figure 5.2. ^{1}H NMR of deprotected PEG-b-p(Lys_{100}-co-Cys_{10}) in red, and protected PEG-b-p(Lys_{100}-co-Cys_{10}) in blue. Chemical shift differences were induced by use of D_2O used in the deprotected sample versus D_6-DMSO in the protected sample. The inset, shows the removal of the carboxybenzyl protective group at δ= 7.25 ppm.

Additionally, the trifluoroacetyl (TFA) cleavage was determined by the disappearance of the ε-methylene peak that was observed at approximately δ= 3.4ppm (Figure 5.2). The carboxybenzyl protecting groups benzyl proton peak (δ=5.23) is slightly obscured in Figure 5.2

(top spectrum), however, the cleavage of the Cbz protective group clearly causes this peak to disappear in the bottom spectrum in Figure 5.2.

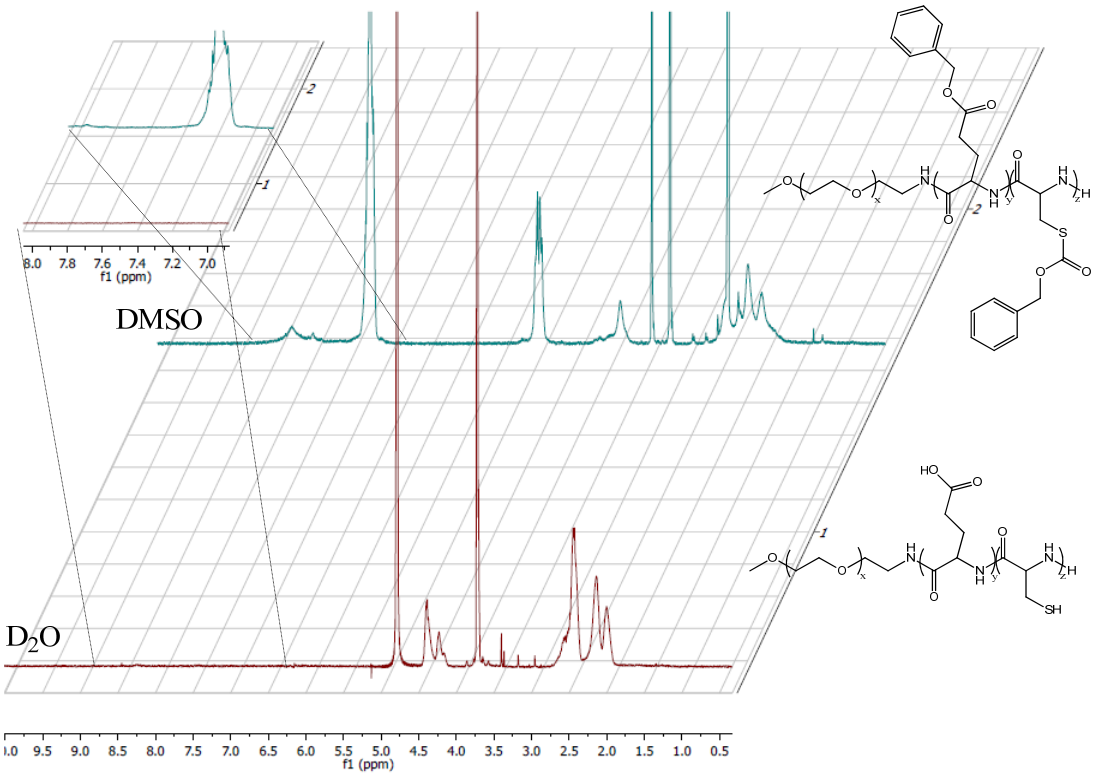

Figure 5.3. ^{1}H NMR of deprotected PEG-b-p(Glu_{100}-co-Cys_{10}) in red, and protected PEG-b-p(Glu_{100}-co-Cys_{10}) in blue. Chemical shift differences were induced by use of D_2O used in the deprotected sample versus D_6-DMSO in the protected sample. The inset shows the removal of the Cbz and Bnl aromatic protons from the cysteine and glutamate residues. Additionally, the benzyl proton adjacent to the phenyl ring (δ= 4.68) are no longer present in the lower spectrum.

Figure 5.3 shows a complete removal of all aromatic protons (δ=7.13) in the PEG-b-p(Glu_{60}-co-Cys_{10}) polymer chain. This indicated that there was a complete removal of the Cbz and the Bnl protective groups from the cysteine and glutamate residues, respectively. Additionally, as mentioned previously, the benzyl protons (δ=5.21 ppm) were also absent which indicated the complete removal of the Cbz benzyl protective groups from cysteine and glutamate.

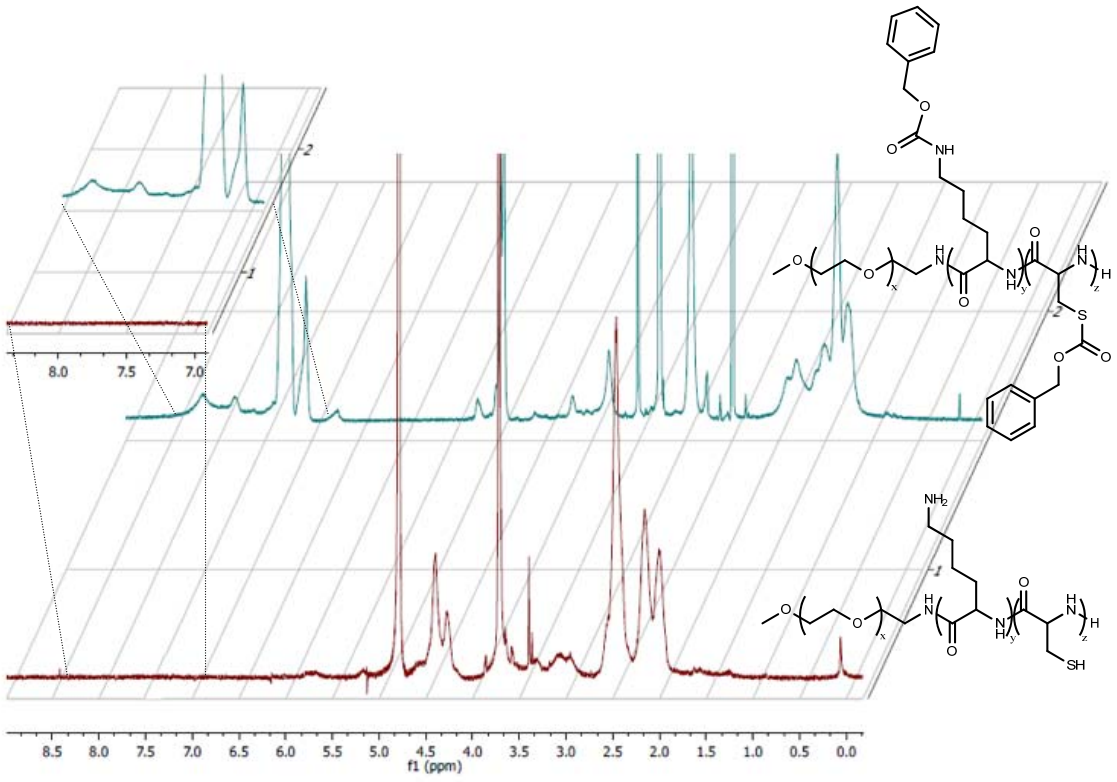

Figure 5.4. ^{1}H NMR of deprotected PEG-b-p(Lys_{100}-co-Cys_{10}) in red, and protected PEG-b-p(Lys_{100}-co-Cys_{10}) in blue. Chemical shift differences were induced by use of D_2O used in the deprotected sample versus D_6-DMSO in the protected sample. The inset, shows the removal of the carboxybenzyl protective group at δ= 7.25 ppm.

Figure 5.4 shows the results from a single synthesis that was performed using N^6-Carboxybenzyl-L-Lysine instead of N^6-TFA-L-Lysine. The L-Cysteine's aromatic proton peak at δ=7.1ppm and the L-Lysine's phenyl proton peak at δ=7.25ppm are both absent in the lower spectrum (Inset Figure 5.4). Additionally, the benzyl proton peaks for the L-Lysine and L-Cysteine (at approximately δ= 5.13 and 5.45 respectively) are no longer present. The PEG-b-poly(Lys_{100}-co-Cys_{10}) experiment demonstrated that Cbz protective groups can be completely removed from lysine amino acids. This shows; first, complete removal of Cbz protective groups is possible under the reaction condition outlined above, and seconds, additional amino acid analogues, that are protected with Cbz, can be used in future works to synthesis PEGylate-paas.

5.5. Discussion

Typically, selective deprotection of protective groups is desired, and different groups are chosen so that one group may be cleaved rendering the side chain functional, while the other is left intact and continues to protect the side group. There are times, however, when selective deprotection is not desired, but the use of multiple protective groups is necessary for later studies. Here, that problem is addressed with regard to carboxybenzyl, benzyl, and trifluoroacetyl protective groups on L-cysteine, L-glutamate, and L-lysine α-amino acids, respectively.

Each type of protective group has previously been selectively cleaved under a variety of independent conditions such as hydrolytic cleavages or hydrogenolysis. It has been shown herein, both hypothetically and experimentally, that a one pot method can be performed using K_2CO_3, H_2O, and MeOH to remove all three types of protective groups from the previously synthesized PEGylated poly(amino acid) products.

Extreme care must be taken to prevent back bone amide cleavage from occurring due to prolonged exposure under basic condition. This has been shown to degrade the polymer chain, rendering it virtually useless for future surface coating studies. Yet, when deprotection is performed with care, the amino acid side groups are exposed and functionality is reinstated. Most notably, for this study, the thiol groups are exposed and show promise for use as anchor points in gold-thiol based interactions, which will lead to the ultimate goal of surface modification for future use in chronically implanted biomedical devices.

CHAPTER 6

SURFACE COATING

6.1. Introduction

Surfaces and interfaces are very important in medicine and biology. All biological reactions involving biomedical implants occur at the surface, and therefore, require a modification to render it compatible in biological plasma and cellular environments [143]. The success of a bio-implant relies upon a number of different criteria; selectivity, specificity, sensitivity, and stability. The first three are legitimately connected with the need for a protein resistant surface.

There are a variety of different approaches to render a surface protein-resistant, or to reduce the non-specific protein interaction with a substrate. Some of these include the use of polyoxazolines, phospholipids, polyacrylates, polysaccharides, polyethers, amines/ammonium salts, amides sugars, and functional groups on self assembling monolayers such as hydrophilic groups.

This leads to the role of poly(ethylene glycol) (PEG), which is used to chemically modify surfaces involved in blood or tissue contacting environments [144]. PEG is known to be a highly biocompatible, hydrophilic polymer that is capable of decreasing protein adsorption, cell and platelet adhesion [16], [24], [57]. Additionally, PEG has been shown to be nontoxic and posses non-immunogenic properties. As mentioned previously, PEG has a large excluded volume on surfaces and its rapid chain motion helps to prevent protein and cell adhesion to the implanted surface [58], [145]. However, this point is under some debate, and requires further investigation. It is not clear whether protein penetration is an occurrence because high molecular weight PEG

creates large surface voids, or if protein adherence is due to a decrease in chain motion when PEG molecular weight becomes too high [145].

6.1.1. Possible Mechanisms of Protein Resistance of PEG

6.1.1.a. Charge Neutrality

PEG is not a charged molecule and therefore does not interact with proteins that carry a local or global charge. The lack of electrostatic interactions enables PEG to act as a barrier to protein-substrate interaction by shielding the substrates surface charge. The PEG layer must be of an adequate thickness to prevent the protein from "seeing" the substrate surface.

6.1.1.b. Osmotic Pressure and Steric Repulsion due to Excluded Volume

Mentioned previously, PEG chains have a high degree of mobility, which is believed to be important with regard to steric repulsion of proteins (sometimes referred to as excluded volume). The mobility of the chains (flexibility and rapid motion) acts as an entropic factor that reduces the compressibility of the PEG chain. When compressed by an approaching protein, entropy is reduced, as is the number of available conformations of the PEG chain. Therefore, the PEG's lack of free space causes a repulsion (or excluded volume) effect on the protein. This protein exclusion is dependent upon the PEG's chain length and density, on the substrate.

6.1.1.c. PEG- Water Interaction

The solubility of PEG in water is characterized by a closed immiscibility loop that contains both higher and lower critical solution temperatures. This lends to the unusual

temperature dependence of the molecular interaction of PEG with water. PEG has been shown to lose its solubility at elevated temperatures due to a "clouding effect". The cloud point occurs at the lower critical solution temperature (LCST) and depends upon PEG's molecular weight, concentration, and the pH of the solution. PEG shows an inverse solubility-temperature relationship. This means that at elevated temperatures the hydration shell around PEG becomes increasingly disordered. Additionally, the water solubility of PEG has been explained as it having a good structural fit between water and the polymer due to its hydrogen bonding capabilities [57]. It has been suggested that PEG's hydrogen bonding character and its low interfacial free energy helps prevent protein –substrate interaction. Furthermore, the PEG-water interface, at or near low interfacial energy boundaries, will effectively negate electrostatic attraction of the substrate. The proteins, therefore, do not feel any greater attraction from the surface than they do from the bulk solution.

6.1.2. Surface Deposition

6.1.2.a. PEGylation of Surfaces

PEG can be attached to a surface through a variety of different approaches. These include; plasma cross-linking, physi- and chemisorptions, silanization, as well as chemical grafting. However, the two main strategies employed are physical adsorption and chemical grafting. The strength of the interaction will affect the thickness and long term stability of the polymer layer.

PEG itself can be adsorbed onto a substrate, such as gold, but the adhesion is so weak that a biomolecule can easily displace the PEG layer from the surface. Therefore, for long term applications, it is necessary to use covalent means of binding the PEGylate polymer to gold.

Several techniques have been used to covalently attach PEGylated poly(amino acid)s to gold, including “grafting from”, and “grafting to” methods. The “grafting from” technique is achieved by initial immobilization of functional groups on to the surface, then using radical polymerizations to form a mono-layer. Conversely, “grafting to” is conducted by chemically coupling a single pre-synthesized molecule or polymer onto the surface. PEG is covalently coupled with a terminally reactive group that is chemically reactive with the gold surface. These pre-synthesized polymers can be characterized prior to attachment to the surface; and can be tailored with regard to composition and architecture. This method has been used to create surface coating that are of a high density when the immobilization is performed close to the cloud point for the PEG.

6.1.2.b. Gold-Thiol Interactions

The use of cysteine amino acids was implemented into this project to facilitate the adherence of the synthesized poly(amino acid) chain to the gold on silica surfaces based on the “grafting to” method. It was previously stated that there is a weak interaction of PEG with a specially prepared negatively charged gold surfaces. However, this bond is not strong enough to be useful in a proposed prosthetic device, and the PEG layer can be easily removed with little effort. Therefore, to enhance the adherence of the polymer to the gold surface, thiol based tethers have been investigated. The gold-thiol interaction has been described as an oxidative addition of the S-H bond to surface of Au(III), and may be followed by a reductive elimination of di-hydrogen or the presence of dissolved oxygen [146].

6.1.3. Poly(ethylene glycol) Deposition on Substrates

6.1.3.a. Large Molecular Weight Poly(ethylene glycol) Effects When Non-Selectively Bound to Surface Substrates

PEG chain length is inversely proportional to the rate of motion of the molecule on an axis. Therefore, shorter PEG molecules will rotate at a faster rate than that of longer chains. This point is well known, however, the debate is centered upon the efficiency of the excluded volume for long PEG chains (5k or greater). It is proposed that high molecular weight PEG shows an increased excluded volume effect when non-selectively bound to surfaces, and allows protein interpenetration to occur on the substrate. PEG chain length not only affects chain motion, but also density on surfaces. It has been shown that higher molecular weight chains lower the overall density of the PEG layer due to their extended chain lengths and greater chain motion which increases the excluded volume [61].

The low surface coating density seen with high molecular weight PEG is due in part to the fact that no two molecules may occupy the same space at the same time. More specifically, steric repulsion of one PEG chain from another cause the molecules to become more disperse across a surface as M_w of the PEG chain increases. Therefore, the length and density of the tethered PEG chain exhibits a tradeoff with respect to the relationship of sensitivity and selectivity of biomolecular repulsion [61], [147].

6.1.3.b. Low Molecular Weight Poly(Ethylene Glycol) Effects When Non-Selectively Bound to Surface Substrates

Low molecular weight PEG products ($\leq$ 1.5k) can negatively affect biocompatibility of substrates, as well as, PEG products that are of high molecular weight. As mentioned above, high

molecular weight PEGs exhibit slow chain motion which may induce low excluded volume effects and allow solute penetration and interaction with the substrate. Bergstrom *et al.* (1994) showed that PEG molecules with molecular weights below 1500 g mol^{-1} showed an increase in fibrinogen/protein adherence to a polystyrene surface [20], [148]. In addition to this, PEG chains with a M_w of 250g mol^{-1} exhibited no fibrinogen/protein rejecting ability, whatsoever [148].

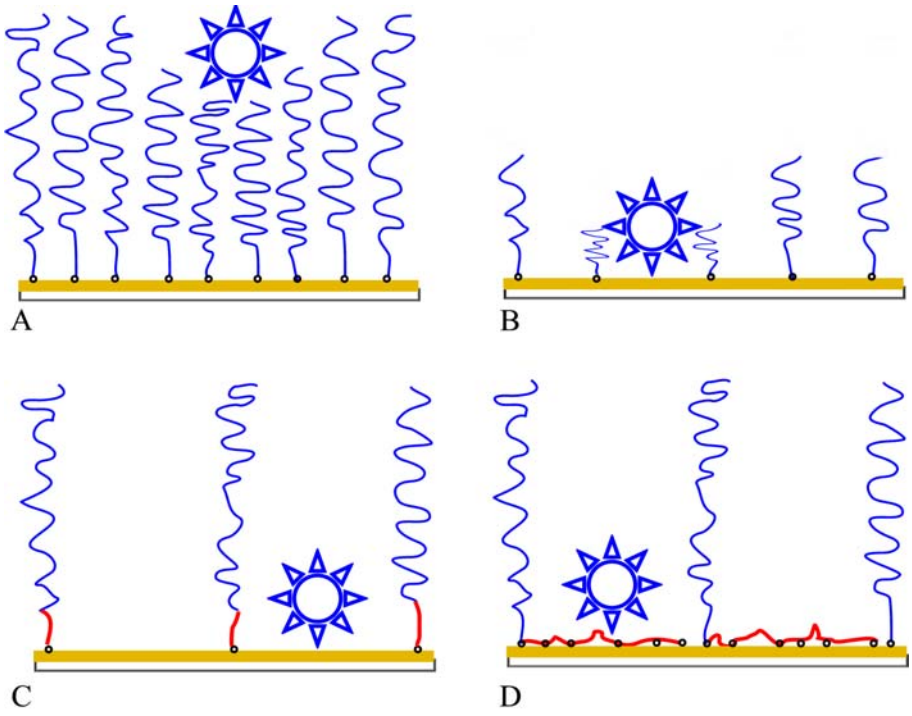

Figure 6.1. Shows non-specific binding of PEGylated paas on the gold on silica surfaces and possible protein (represented by the star-like structure) interaction with the surfaces under a variety of scenarios. (A) indicates a theoretical high molecular weight PEG coating under ideal conditions. (B) demonstrates the coating with low molecular weight PEG. (C) represents an increase in intermolecular space when high molecular weight PEG is used. (D) shows how the paa based under-fill will cover the Au surface and assist in protein/cellular rejection.

There are four factors that can contribute to the increase in protein adsorption when low molecular weight PEG is utilized. First, the small PEGs can inadequately hide the substrate surface from the approaching protein molecule and the protein can compress the surface bound

PEG to the point that is may be able to sense the surface [148]. Second, unfavorable entropic changes of the low M_w chain, when PEG is compressed by the approaching protein, can allow for interdispersion of the protein molecules. Third, prevention of protein adsorption can be due to a reduction of the low interfacial free energy of the PEG-water interface (see Figure 6.1 (d)) [148]. Finally, it has been shown by Nakagoa *et al.* (1985) that small PEG chains are more rigid and exhibit lower rotational freedom [148], [149]. This lack of mobility prevents the PEG from effectively repelling proteins because the adsorbed protein does not have sufficient contact time with the PEG molecules.

6.2. Research Goal

It is important to improve the biocompatibility of the implantable devices by modifying their surfaces so that they exhibit reduced plasma protein adsorption and cell adhesion. An effective approach is to modify the surfaces of the device with poly(ethylene glycol), which is non-toxic, non-immunogenic, and non-antigenic [16], [58]. We propose to use PEGylated poly(amino acid) based polymers as coatings on mock gold on silica surfaces for future studies of biomedically relevant implantable devices.

The thiol group of the cysteine amino acid will provide the anchor points for the PEGylated paas in random and block copolymers that have been synthesized by living ring opening polymerization (LROP). This study will be limited to preliminary surface coating studies with two types of polymers being used. One type of polymers will contain poly(lysine) and the other will have poly(glutamates), which are both water soluble poly(amino acid)s. The hydrophilic amino acids will be used to facilitate the incorporation of the hydrophobic cysteine amino acids to create an overall water soluble copolymers that will coat the gold on silica surfaces.

Different gold on silica surfaces were investigated to determine effectiveness of coating: a solid gold surface and a nano particulate gold on silica surface were used in this study. It was hypothesized that the surfaces would be uniformly coated on the solid surface, and only shows selective PEG-paa adhesion where gold is located on gold nano-particulate covered surfaces.

6.3. Experimental

6.3.1. Materials

Ethanol (EtOH) was purchased from Fischer Scientific (Pittsburg, PA), and Argon was purchased from Airgas (Huntsville, Al) and passed through a desiccator trap containing Drierite™ to remove any water vapor form the argon gas. The gold on silica wafers were obtained from Cornell University through the Boston Retinal Implant Project. The wafers were prepared by deposition of a 50nm titanium coating, followed by a 50nm gold coating, placed by electron beam evaporation in a CVC 6-pocket e-beam evaporator.

To make the nano particle on gold surfaces silica wafers were immersed in a 1:4 mixture of HNO_3 and H_2SO_4 for one hour; subsequently they were rinsed thoroughly with ethanol and de-ionized water. A previously described solution-based technique for the synthesis of gold nanoparticles has been modified to allow for their synthesis on solid substrates [150], [151]. Briefly, first a gold catalyst was prepared by adding 4.5 mL of ethylene diamine to a 10 wt% solution of $HAuCl_4$ in water. The resulting transparent brown solution was stirred for 30 min., then 70 mL of ethanol were added, which resulted in the formation of $Au(CH_2CH_2)_2Cl_3$, a yellow precipitate. The precipitate was collected by centrifugation (10 min at 4,000 rpm) and dried overnight at 40°C. A 0.25 wt% solution of the $Au(CH_2CH_2)_2Cl_3$ was prepared in water and the pH was adjusted to 10 with 5 wt% NaOH solution. This stock solution was diluted to 50% and 25%, yielding a 3.48×10^{-3} M (labeled Au2) and $1.74\ 10^{-3}$ M (labeled Au3) solution,

respectively. Silica wafers were immersed in solutions Au2 and Au3 for 2 hours dried in vacuum overnight and then reduced in a H_2/Ar stream at 150 °C for one hour.

6.3.2. Methods

6.3.2.a. Surface Coating

Prior to surface coating, the samples were cleaned by emersion in a 1:4 HNO_3 and H_2SO_4 solution for 1hour. Subsequently they were rinsed thoroughly with EtOH and deionized water. Then PEGylated poly(amino acid)s were deposited onto gold on silica surfaces by dissolving the deprotected poly(amino acid)s (paa) into 1mL of dH2O to yield a 50mM final concentration. The mock device was placed into a vial, and gently shaken for approximately 12 hours. The surface was removed from solution and rinsed with copious amounts of dH_2O, and then rinsed with 70% EtOH. The surface was then dried under a stream of argon gas, and stored until needed.

6.3.2.b. Atomic Force Microscopy

Surface morphologies of dip coating copolymer films on gold surface were studied using an atomic force microscope NanoWizard (JPK Instruments, Germany) working in tapping mode. The silicon cantilevers used were type Arrow (NanoWorld, Switzerland) and had resonance frequency of about 285 kHz and force constant of about 42 N/m. AFM measurements were performed by the group of Dr. J. Kressler at Martin Luther University in Halle, Germany.

6.4. Results

6.4.1. Atomic Force Microscopy

Surface characterization by atomic force microscopy (AFM) was used to observe the topography and apparent density of the coating of the PEGylated poly (amino acid)s on the gold on silicon (Au-Si) substrates. Prior to obtaining images of coated polymer samples a sample survey was obtained of the uncoated gold on silica surfaces to establish its topography. Figure 6.2 shows uncoated Au-Si at a resolution of $2\mu m^2$ and $5\mu m^2$, and showed the gold had a mean particle size of 184nm, with an arithmetic mean roughness (R_a) of 7.04 nm (70.4Å), and a root mean square roughness average (R_q) of 9.23nm (92.3Å), as determined by AFM spectroscopy. The "orange peel" topography observed in Figure 6.2 is characteristic of vapor deposited gold on silica surface.

Figure 6.3 shows the AFM images acquired for PEG-b-p(Glu_{100}-b-Cys_{20}) and PEG-b-p(Glu_{50}-co-Cys_{10}) that were dip coated onto the gold substrate. The phase and height images show that homogenous surface coatings were achieved, and that there were no pinholes present in either coating. This indicates that the block and random copolymers completely coat the surface and crystallize on the surface. There are apparent phase boundaries between the lamellae observed in the phase images of Figure 6.3 A and C, and as can be seen in both Figures 6.3, and 6.4, lamella formation is evident by large layered structures, with small button-like bumps present on the lamella surface. The structures present in the AFM images are indicative of self-seeding of the PEGylated (paas) on the surface by a large number of nucleation sites [152]. Since the thiol of the cysteine is the anchor point for the polymer chain, nucleation can be very non-specific and dense. This is readily apparent by the large number of nodules observed on the surface image.

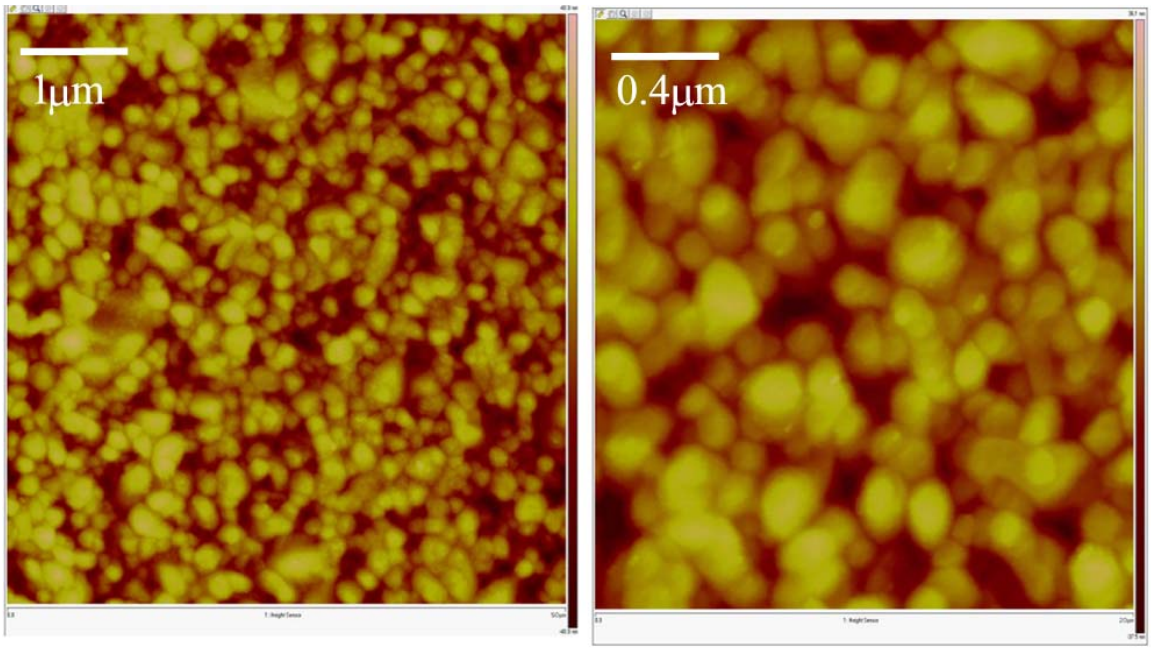

Figure 6.2. AFM of uncoated gold surfaces at 5μm^2 (left) and 2μm^2 (right).

AFM images show that there appears to be no significant difference in the PEG-b-p(Glu_{50}-b-Cys_{10}) and the PEG-b-p(Glu_{100}-co-Cys_{20}) copolymers. The PEG-b-p(Glu_{100}-b-Cys_{20}) AFM height images show light to dark colors which indicate the polymer from a thin to a thick coating on the gold surface. The lighter regions indicate where PEG-paas are present, and the darker regions indicate a thinner polymer coating. Black regions are on the scale of approximately 14 nm, and show where the PEG-paa surface is thin. In addition, the phase images, left side of Figure 6.3, are colored dark to light as well. The lighter regions signify that a softer surface has been encountered, and indicates where polymer coating is present on the gold on silicon surface.

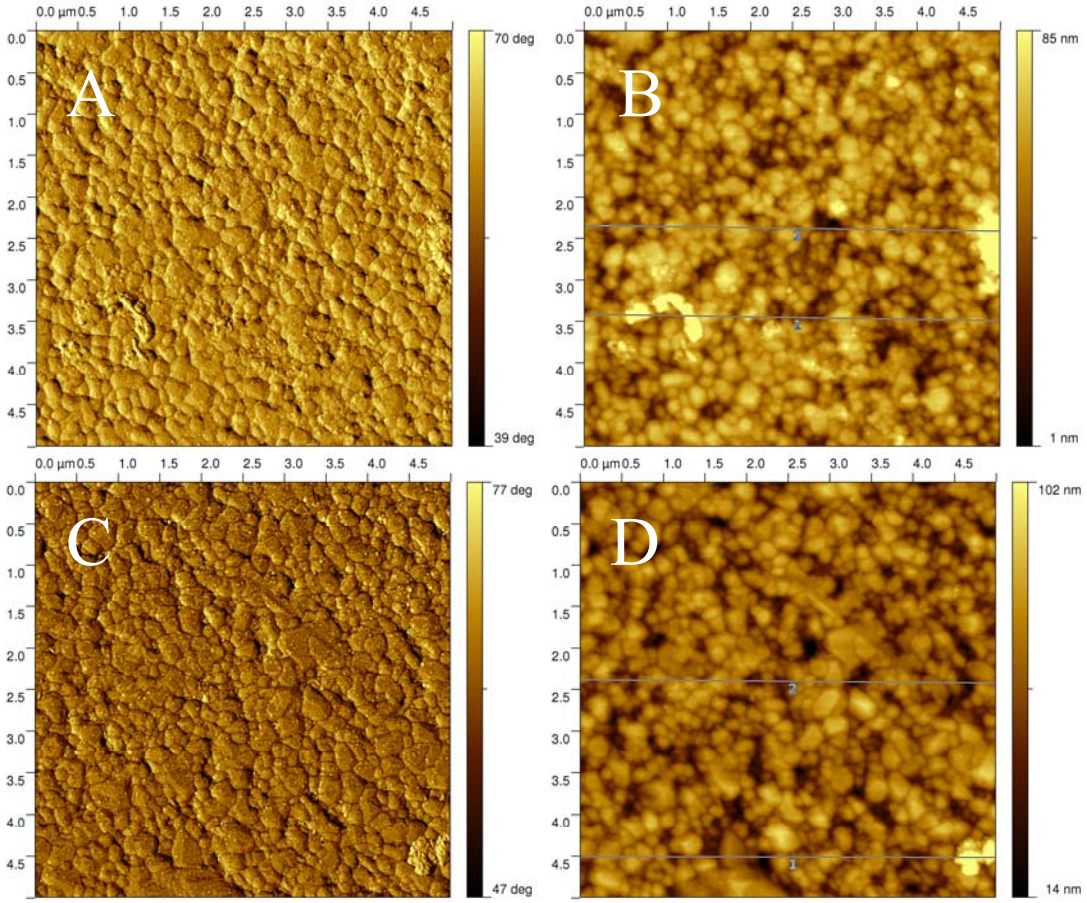

Figure 6.3. AFM height (right) and phase (left) images of PEG-b-p(paa)s coating on the gold on silica wafer. PEG-b-p(Glu_{50}-b-Cys_{10}) surface is shown at 5μm^2 (A and B), and PEG-b-p(Glu_{100}-co-Cys_{20}) coating was imaged at 5μm^2 (C and D).

The mean diameters of large and small crystalline regions were taken in a 2 μm^2 area by averaging five measurements. In the PEG-b-p(Glu_{50}-b-Cys_{10}) the small nodule average was found to be approximately 0.66nm, and the larger nodules were found to be an average of 3.48nm. The PEG-b-p(Glu_{100}-co-Cys_{20}) showed little difference as the large nodule measured an approximate average of 3.42nm, and the small nodules were found to be an average 0.45nm. The height profiles were obtained for both the random and block copolymers and determined to be an average of 0.6 and 0.5 μm respectively, with a height distribution of 0.7μm for the block

copolymer, and 0.6μm for the random copolymer. This indicates that a similar coating were achieved for both types of polymers on the gold wafers.

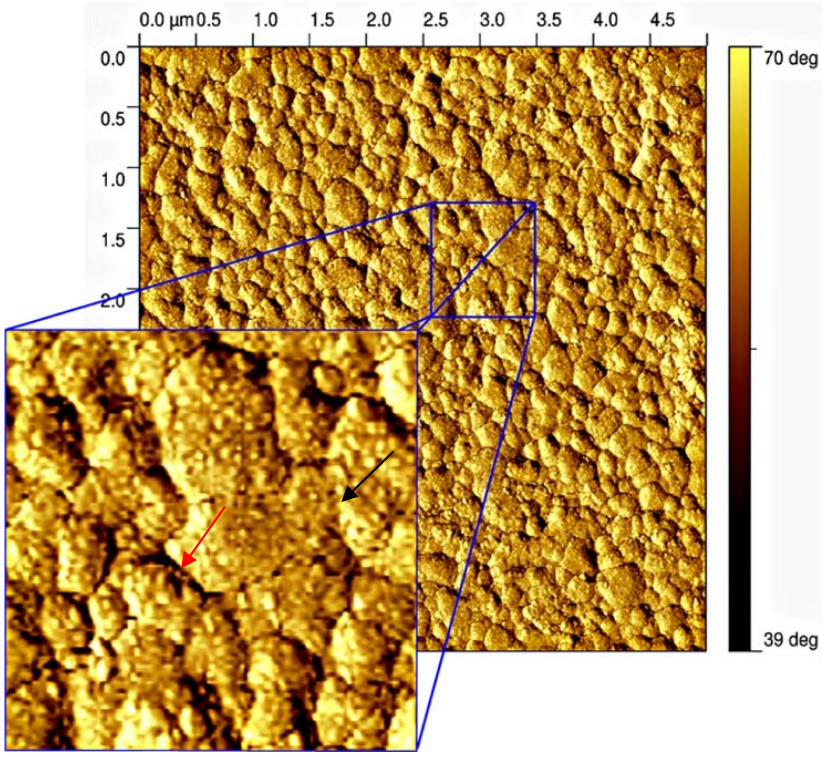

Figure 6.4. AFM height image of PEG-b-p(Glu_{50}-b-Cys_{10}) with 1μm^2 expanded view shows that the wafer is uniformly coated with polymer. The figure shows an impingement between nodules (black arrow), and where crystals grew separate and parallel to one another (red arrow).

Figure 6.4 shows an expanded view of the nodules for PEGylated block copolymers. The image illustrates individual crystallite growth that is independent of one another on the gold surface. Some nodules show parallel growth adjacent to one another, and are characterized by distinct margins around the entire perimeter (Figure 6.4 red arrow). This suggests that crystal growth occurs independently from one another at different nucleation sites [152], [153]. Additionally, continued growth may occur by edge dislocations [154], [155] as observed by impingement, or overlapping (indicated by the black arrow in Figure 6.4). This is not unusual in

crystallites that grow along a single layer, and is usually observed when primary re-crystallization is considered to be complete in a single plane [154].

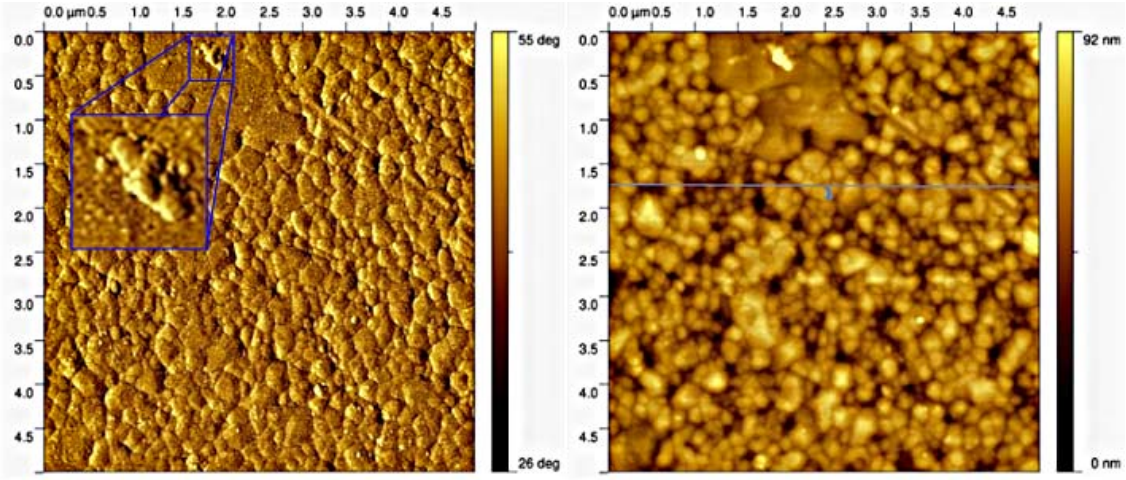

Figure 6.5. AFM height (right) and phase (left) images of PEG-b-p(Glu_{100}-co-Cys_{20}) coating on the gold on silica wafer. PEG-b-p(Glu_{100}-b-Cys_{20}) surface is shown at 5µm^2 , and the inset in the phase image is 0.5 µm^2.

Figure 6.5 shows the topography presented when PEG-b-p(Glu_{100}-co-Cys_{20}) is dip coated onto the gold on silica wafer, and is very similar to that of the block and random copolymers ($\overline{DP_n}$=120 and 60 respectively), but some large nodule formation has occurred. This agrees with the above discussion that states edge dislocation causes impingements, leading to complete crystallization to occur. Upon initial assessment of the large plateau, apparent in the phase image of Figure 6.5, it was assumed that the 2 µm long node was a single surface feature. However, close investigation shows that there is actually several sites of impingement present (Figure 6.6.), which are in good agreement with edge deformations generally seen during completed crystallite growth [154].

Additionally, a well formed screw dislocation is observed in the large nodule (inset Figure 6.5), which indicates that there is a stacking of the lamellae in this regions. This implies that the crystal structure of the PEG-b-p(paas) are parallel to the lamellar surface. However, the

individual PEG crystals cannot be observed, calls to question, where are the PEG crystals located in reference to the amino acid residues on the surface?

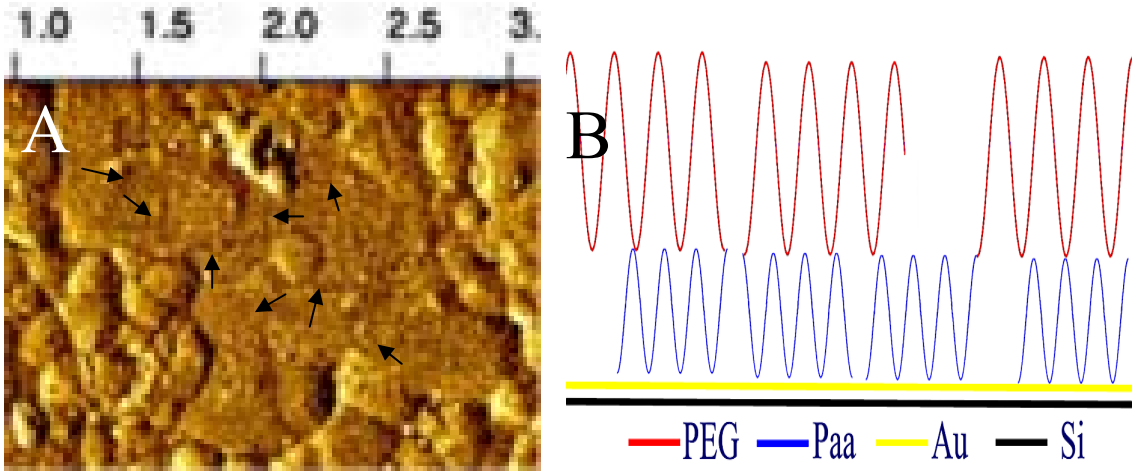

Figure 6.6. Expanded view of AFM phase image of PEG-b-p(Glu_{100}-co-Cys_{20}) coating on the gold on silica wafer large node (A). The black arrows in (A) indicate impingement margins. (B) shows how the PEG is arranged parallel to the poly(amino acid) block on the gold surface.

The topography observed in the AFM images is most likely due to the fact that PEG is covalently connected to the paa block, and the paa block is bound to the gold surface. The PEG-paas are bound to the surface via the thiol-gold interaction created by the use of cysteine residues in the paa chain. This bond arrangement, however, prevents PEG from being macroscopically phase separated from the paa block lamella. The arrangement of the PEG, covalently bound to the paa, on the surface creates the lamella structures that obstruct the observance of single PEG crystal as illustrated in Figure 6.6 (B). Figure 6.6 (B) exhibits how the PEG may form a crystal by adopting an orientation parallel to the gold surface. It is assumed that when placed in an aqueous environment, the PEG-paas will become more perpendicular in orientation and dissolve the crystal structure to facilitate freedom of movement, of the PEG, as discussed in chapter 5.

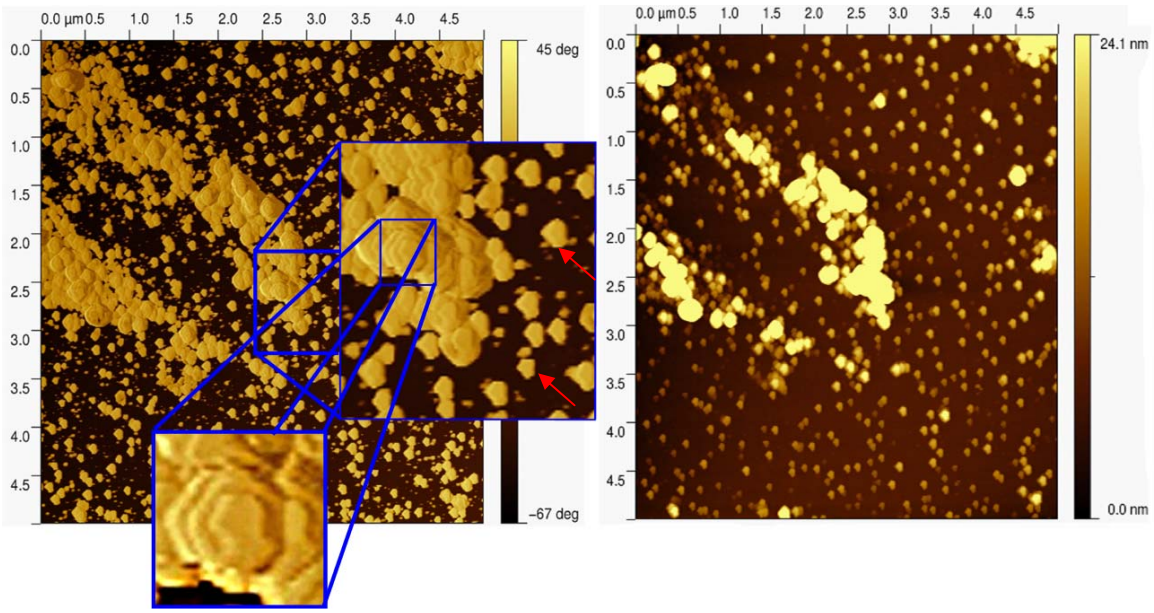

Figure 6.7. 5 µm^2 AFM phase (Left) image and height image (right) of PEG-b-p(Glu_{50}-co-Cys_{10})dip coated onto large size non-particulate Gold on Silicon surfaces. Insets show screw dislocation formation found by the stacking of lamella. The red arrow indicate single layer lamella on the gold nano particles.

Figure 6.7 shows PEG-b-p(Glu_{50}-co-Cys_{10}) that was dip coated onto a silicon surface that was covered with large size (200- 400nm) nano particulate gold. The image shows that PEG-paa polymer was localized and densely packed on the nano particulate gold. The dark regions represent the silicon wafer, and shows that the PEGylated paas do not adhere. This is in agreement with the hypothesis that the thiolated paas will form a polymer coating by anchoring to the gold on the silicon surface. The height image (Figure 6.7) shows the silicon in the darkest areas, and the lighter regions indicate structures that project from the surface, which are PEG-paas anchored on the gold substrate.

It is clear that single layer lamella are present (indicated by the red arrow, inset, Figure 6.7), and that the PEGylated paas form a thin layer with distinct margins. This is due to the presence of separate nucleation sites that do exhibit crystal overlap due to their dispersion across the gold surface. This is opposite to the information derived from the gold on silica wafer, where

the edge dislocations caused overlap and impingement of the crystallites. In addition, screw dislocations are readily apparent in figure 6.7. This is most likely an occurrence caused by gold nano particles that are in very close proximity to one another, which in turn causes a greater packing density of the PEG-paas, and leads to lamella stacking.

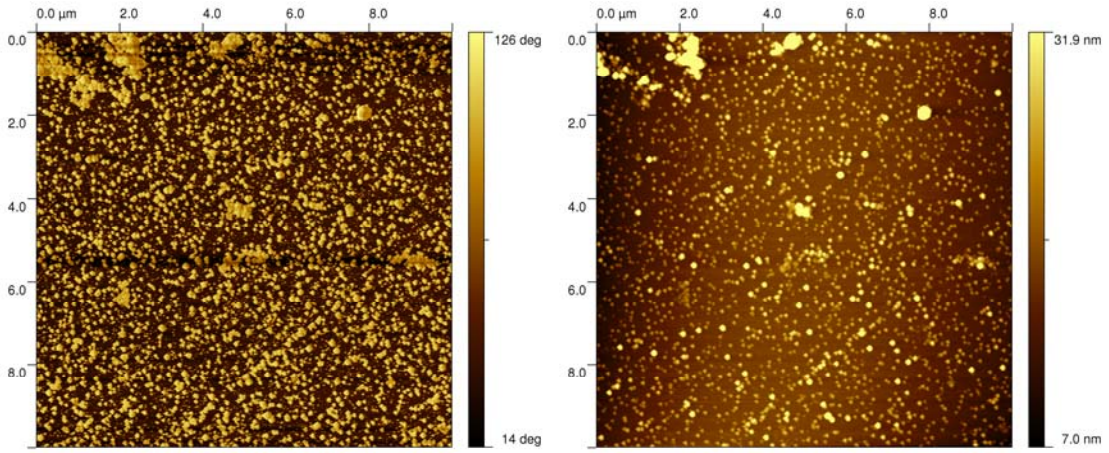

Figure 6.8. 10 μm^2 AFM phase (Left) image and height image (right) of PEG-b-p(Glu_{50}-co-Cys_{10}) dip-coated onto large size non-particulate Gold on Silicon surfaces.

The PEG-paa single layer lamellas (Figure 6.6) all contain a relatively similar orientation on the surface, with the most prominent point of the pentagon positioned to the left side of the nodule. The small localized lamellas are approximately 0.92 nm in diameter. Interestingly, PEG has been shown in previous work to form hexagonal or square crystal structures. The use of cysteine and glutamate appears to interrupt the native crystal structure of PEG and induces a pentagonal crystal structure instead (Figure 6.7). In addition, Figure 6.7 shows an appearance of small particulate nodes, which are too small to reliably be measured, that could be small size nano gold particles coated by a few PEG-paa molecules. A comparable occurrence is observed in Figure 6.8, which is an image obtained of a different region on the same surface.

Figure 6.8 shows a coating of PEG-b-p(Glu_{50}-co-Cys_{10}) on large nano particle gold, and indicates that the "caking" seen is due to crystallite extension from the gold nano particles. The

PEG-paa develops individual planar lamella that are consistently dispersed across the surface, where gold nano particles have been applied to the silicone. No PEG-paa adhesion appears to take place on the silicon surface itself, which is in agreement with the above findings. The silicone is indicated by dark regions in the height image of Figure 6.8 (right), and the polymer is indicated by the light regions of the height image. Some aggregation appears in the top of the frames of Figure 6.8 in both the phase and the height images. These structures are most likely due to localized high densities of nano particle gold, inducing both screw and edge deformations. These 10 μm^2 height and phase images clearly show how the PEG-paas build around the gold nano particles, and indicates selective coating of the solid matrix based upon the presence of gold on the silicon.

PEG-b-p(Glu_{50}-co-Cys_{10}) was also dip coated onto small (20 to 40nm) gold nano particle on silicon surfaces. However, the coating was inconsistent, and proved to be unsuitable for use as a substrate (AFM images are located in Appendix C).

6.5. Discussion

PEGylated block and random copolymers were successfully applied to gold on silicon wafers and nano particle gold on silica surfaces and analyzed by atomic force microscopy (AFM). Coating densities are directly related to the gold that is applied to the surface, and shows that the PEGylated poly(amino acid)s (PEG-Paa)s localize on the surface in regions where gold is present. This is important for biocompatibility of surfaces that may be used in the future for medical implant devices.

The surface coatings, on the gold on silica wafers, were very dense and exhibited edge dislocations based on impingement of adjacent crystallites. This indicated complete growth of the crystal as presented with large nodes on the gold surface. Additionally, parallel margin formation was observed indicating that crystallite growth had originated from individual nucleation sites, which is as expected based upon the thiol content of each PEG-paa molecule.

Neither the chain length, nor the block versus random arrangements of the PEG-paas appeared to play a role in the coating density of any of the surfaces.

The use of nano particulate gold on silicone induces a very different topography than was seen in the solid gold on silicon wafers. Small planar lamella were present in regions where the gold nano particles were well dispersed, but large screw dislocations were readily evident in area that gold nano particle aggregates were present. This induced a stacking of pentagonal lamella causing large vertical features to occur perpendicular to the gold surface.

It has also been shown that the PEGylated copolymers do not show a propensity towards binding onto the silicone. Any polymer that was on the silicone was easily washed away after dip coating, and did not appear to be bound in any of the AFM images. The inclusion of the cysteine amino acids in the PEG-paa chain made use of the strong thiol-gold interaction to keep the polymer bound to the surfaces.

The major impact of this part of the study was that it was shown that the synthesized block and random copolymers could be easily dip coated to create a dense covering on the gold on silica surfaces. The amino acid blocks arrangements and type do not appear to affect the coating density in any way. This will open the field of PEG-paa surface coatings to investigate a large number of other amino acid conjugate to render implantable surfaces biocompatible.

CHAPTER 7

Future Work

PEGylated Poly(amino acid) random and block copolymers were produced under living conditions to yield products whose properties were investigated. The gel permeation chromatograms suggested that the random copolymers are not truly randomized, and may contain a blocky structure. This may be due to the differences in chemical reactivities of the amino acids used. This should be investigated further by NMR to determine the architecture of the polymer chain. The determination of architecture could lead to the development of conditions that would allow for the synthesis of a truly randomized paa chain, and yield products of a lower PDI, and with more control over the molecular weight.

Second, further work needs to be done to investigate the secondary structure content of the oligomers at a variety of chain lengths, in their protected and deprotected states. A broad screening of a majority of the amino acids available could be conducted to verify the secondary structure content proposed in the publication by Kricheldorf et *al*. [31]. Additional techniques such as X-ray, Raman, and NMR techniques can be used to determine the α-helix and β-sheet content of not only the oligomers but the full length synthetic PEGylated poly(amino acid)s as well. Also, loss or retention of β-sheet content could be investigated by these means to determine if there is an apparent conformation change as the PEGylated paa chain grows and adopt an α-helical structure.

These secondary structures could lead to a wide range of applications where specific secondary structure of poly(amino acid)s is needed for drug delivery, gene delivery, and surface modification in biotechnological applications.

Third, the exact orientation of the PEGylated poly(amino acid)s should be investigated both in crystal form and wet AFM , which will show PEG extension from the gold on silica surface. This will definitively show that the anchor point for the PEGylated paas is indeed the thiols of the polymer, and not due to gold-PEG interactions. The definitive determination of the PEG-paa orientation on the surface will advance the probable use of these polymer products in biomedically relevant implantable devices.

Fourth, the biocompatibility of these PEGylated polymer products needs to be extensively studied. This research should include the use PEG-paa polymers that vary with regard to PEG chain length, and the number of poly(amino acid) repeat units. Once the polymers are applied to gold on silica substrates, protein adherence/rejection studies can be performed. These studies may be able to determine the optimal PEG weight necessary to yield a PEG-paa coating dense enough to render the surface "invisible" to proteins and fibrinogens. This could lead to highly biocompatible surfaces that can be chronically implanted in mammalian models.

CHAPTER 8

Conclusion

The current technology of living ring opening polymerization of α-amino acid *N*-carboxyanhydrides and is very useful for synthesizing polymer chains of desired molecular weight and composition. However, the technique is limited due to β-sheet secondary structure formation in the oligomer chain during the initial iterations of polymerization. The research conducted herein has shown that the use of urea can effectively reduce the β-sheet secondary formation when using N-carboxyanhydrides of α-amino acids as the monomer units.

Additionally, it has been determined that oligomers of α-amino acids present β-sheet secondary structure as short chains, and some adopt a preferential α-helix secondary structures when their chain length is long enough. Urea was shown to reduce the amount of β-sheet secondary structure present in *N*-hexylamino-p(cysteine) , a polymer proven to adopt a β-sheet conformation, of 5, 10 ad 20mer chain lengths. This secondary structure reduction has fortified the use of urea in living ring opening polymerization of protected α-amino acids NCAs using $mPEG_{5k}$-NH_2 as the macroinitiator.

Many PEGylated poly(amino acid) random and block copolymers were synthesized, and contained amino acid block ranging from 60 to 150 repeat units. It was shown that strict control was gained over the reaction and products were synthesized with controlled molecular weights and low PDIs. The copolymers were seen to have slightly broader distributions, and GPC data suggested that the PEGylated random copolymers yielded a bimodal distribution, where as the block copolymers yielded a strictly monomodal distribution. This was most likely due to the copolymers exhibition of the differences in the chemical reactivities of the amino acids used.

The PEGylated poly(amino acid)s were then subjected to removal of the side chain protective groups. Typical methods call for selective deprotection of the CBZ, TFA, and Bnl protective groups. It was shown that these protective groups could be efficiently removed in a one pot method. Novel contributions were made to the field by the cleavage of the Cbz and Bnl protective groups by using a modified method that has been traditionally used to cleave the TFA protective group. Initial experiments demonstrated that care was necessary when using the deprotection method, as premature stoppage of the reaction yielded products that were not completely deprotected. On the other hand, allowing the deprotection reaction to proceed for excessively long periods of time showed a degradation of the main polymer chain. Therefore, it was necessary to determine the conditions and times necessary to properly deprotect each block and random copolymer.

Finally, the deprotected PEGylated poly(amino acid)s were dip coated on to gold on silica surfaces. These consisted of gold on silicon coated wafers, and spattered large (200 to 400 nm) and small (20 to 40 nm) nano-particle gold on silica surfaces. Dip coating as performed and subsequent AFM analysis showed that the gold on silicon wafer yielded a homogenous coating of the PEG-paas regardless of the chain length or block/ random copolymer makeup. The PEGylated paas were anchored to the gold by way of the thiol group on the deprotected cysteine amino acids. The PEG-paas showed that a uniform coating could be created, and showed individual nucleation sites by evidence of parallel crystal margins. Also edge deformation and impingements of the crystallites upon one another implied that separate nucleation sited occurred and crystallite growth occurred to the point that a single layer was achieved. The nano-particle gold on silicon showed that lamella formation would form at sites where gold is present on the silicon surface. Single nodes indicated nucleation points, and a dense coating was observed with no apparent impingement due to the spacing of the gold particles. Regions where the nano-particle gold was densely concentrated gave way to screw deformation. This caused lamellar

stacking of the PEG-paas, and exhibited pentagonal crystalline structure. This was different from the typical square and hexagonal structure observed in PEG crystals, and was most likely due to the presence of the α-amino acids in the polymer chain.

This work showed that PEGylated poly(amino acid)s can be efficiently synthesized via living ring opening polymerization of α-amino acid NCAs, globally deprotected in a single step method, and efficiently applied to gold on silicone surface, which has great implications in the ever growing field of biocompatible implantable medical devices.

APPENDIX A

CD Spectra

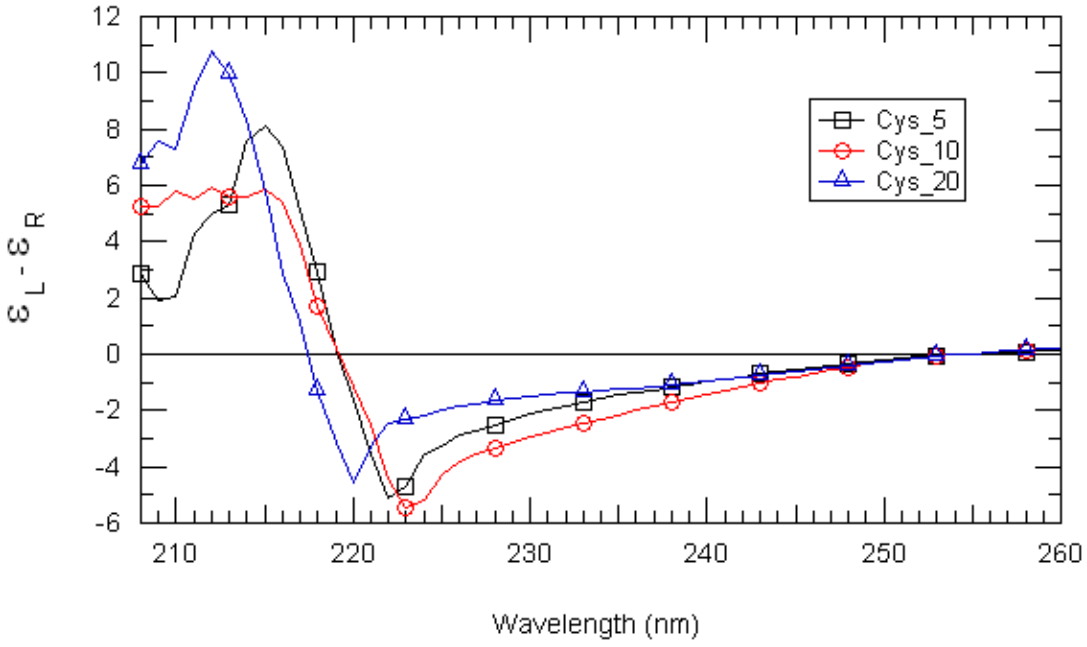

Figure A.1. Circular Dichroism Spectra of *N*-hexylamino-poly(L-cysteine) with 5, 10 and 20 monomer repeat units.

Parameters:

Frequency: 260 to 190nm

Experiment: Circular Dichroism Scan

Temperature: 20°C

Solvent: EtOH

Scan Rate: 1nm sec^{-1}

Conc.: 0.1mg/mL

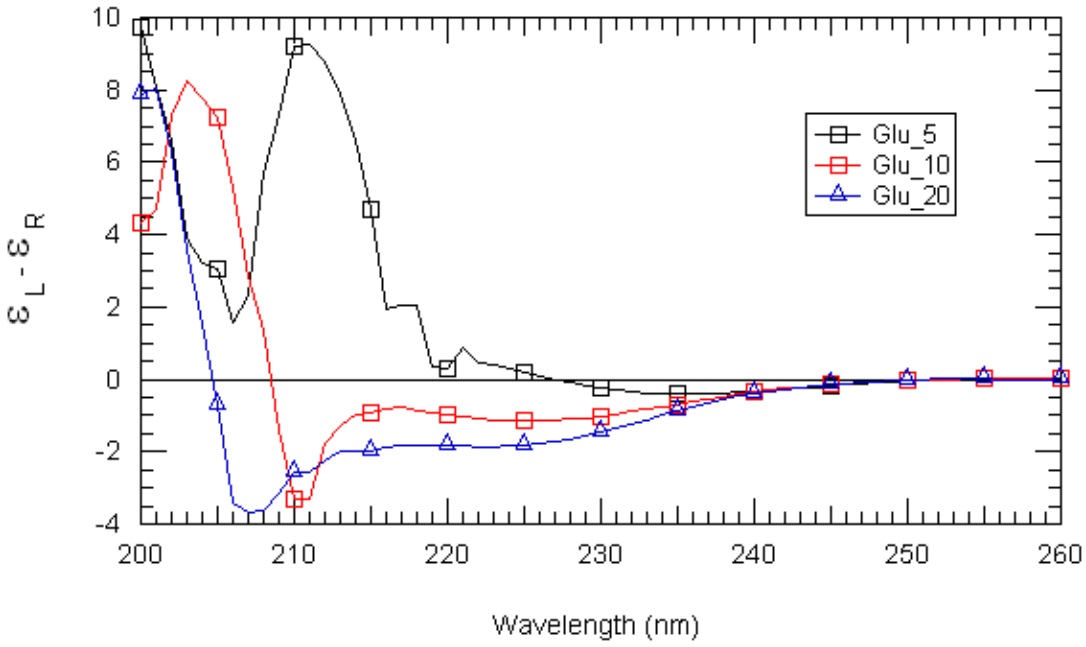

Figure A.2. Circular Dichroism Spectra of *N*-hexylamino-poly(L-glutamate) with 5, 10 and 20 monomer repeat units.

Parameters:

Frequency: 260 to 190nm

Experiment: Circular Dichroism Scan

Temperature: 20°C

Solvent: EtOH

Scan Rate: 1nm sec^{-1}

Conc.: 0.1mg/mL

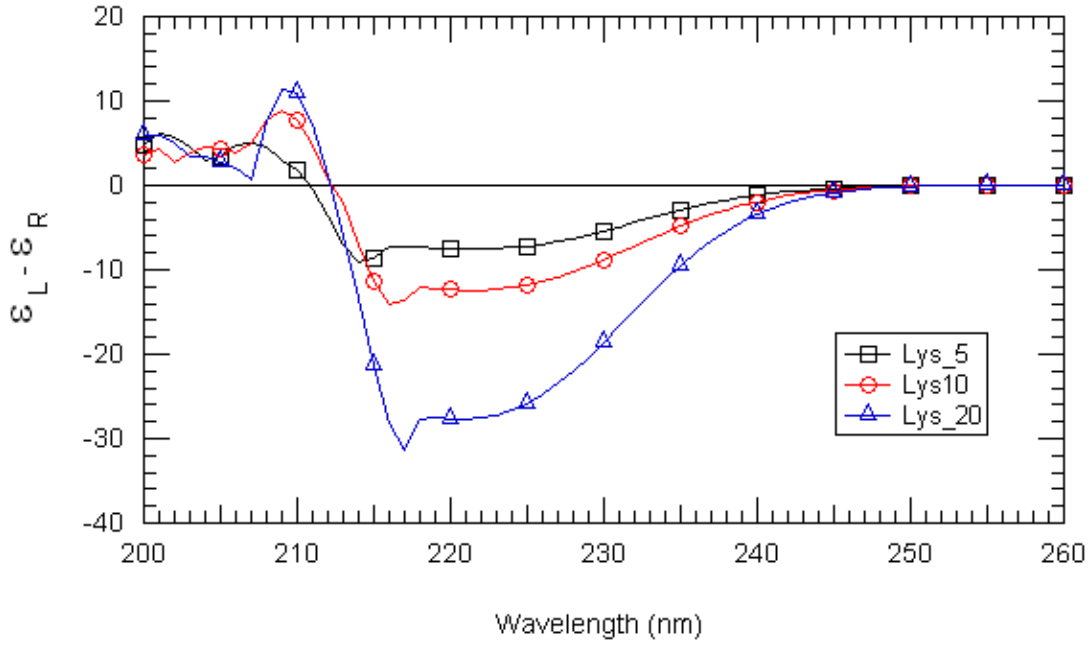

Figure A.3. Circular Dichroism Spectra of *N*-hexylamino-poly(L-lysine) with 5, 10 and 20 monomer repeat units.

Parameters:

Frequency: 260 to 190nm

Experiment: Circular Dichroism Scan

Temperature: 20°C

Solvent: EtOH

Scan Rate: 1nm sec^{-1}

Conc.: 0.1mg/mL

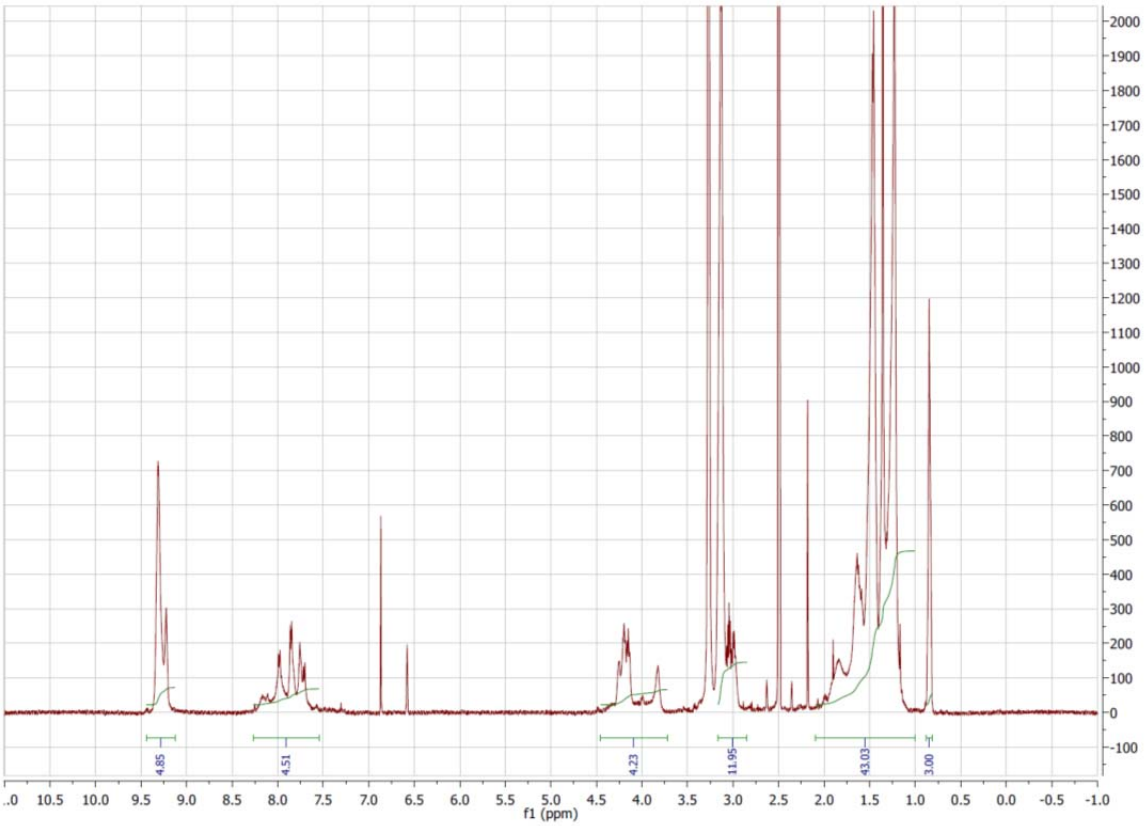

Figure A.4. ^{1}H NMR spectrum of *N*-hexylamino-p(L-Lysine$_4$) .

Parameters:

Frequency: 500 MHz

Experiment: ^{1}H

Temperature: 35°C

Solvent: D_6-DMSO

Scans: 32

Relaxation Delay: 10 Seconds

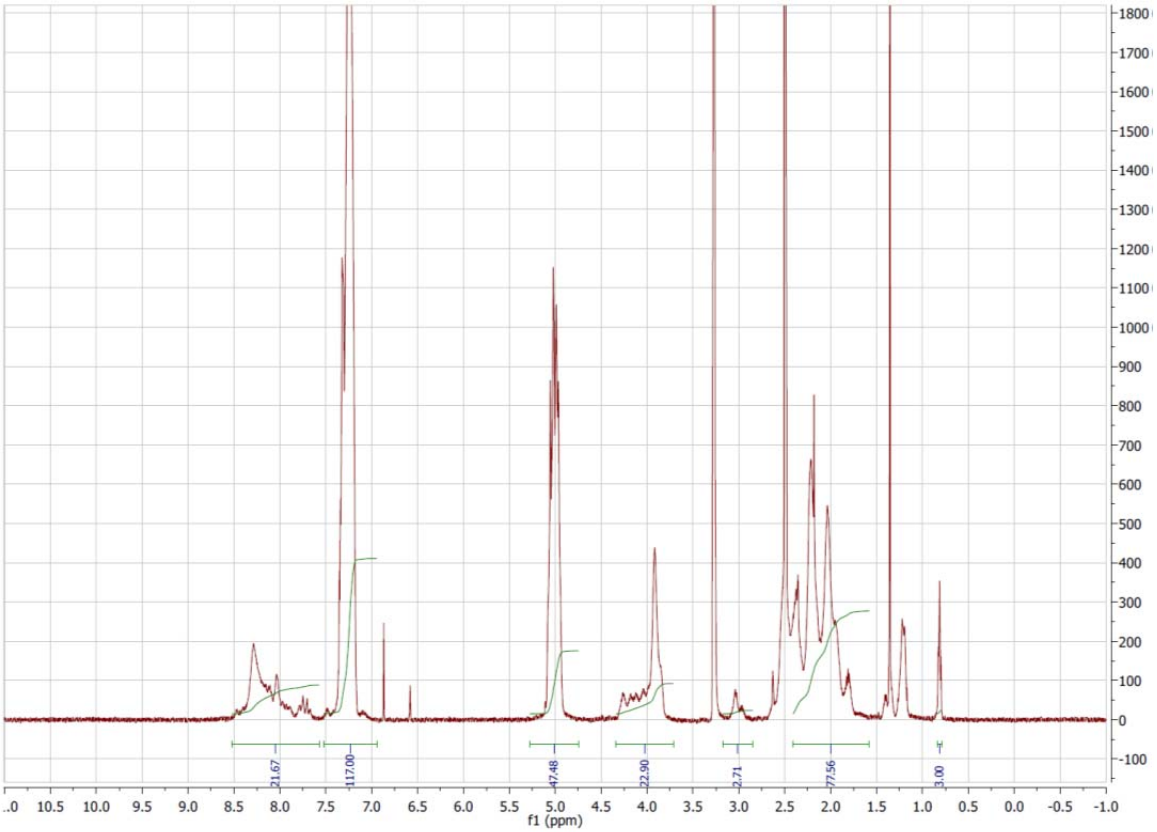

Figure A.5. ^{1}H NMR spectrum of *N*-hexylamino-p(L-Glutamate$_{22}$) .

Parameters:

Frequency: 500 MHz

Experiment: ^{1}H

Temperature: 35°C

Solvent: D_6-DMSO

Scans: 32

Relaxation Delay: 10 Seconds

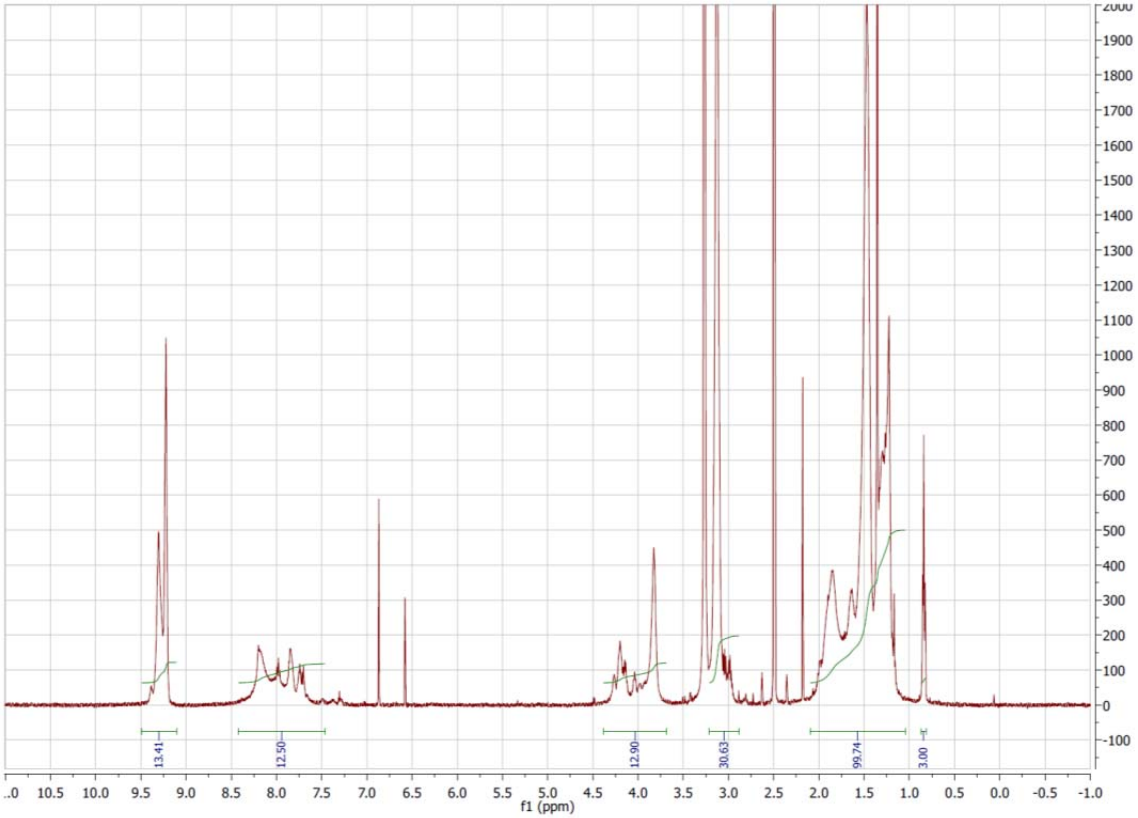

Figure A.6. ^{1}H NMR spectrum of *N*-hexylamino-p(L-Lysine$_{13}$) .

Parameters:

Frequency: 500 MHz

Experiment: ^{1}H

Temperature: 35°C

Solvent: D_6-DMSO

Scans: 32

Relaxation Delay: 10 Seconds

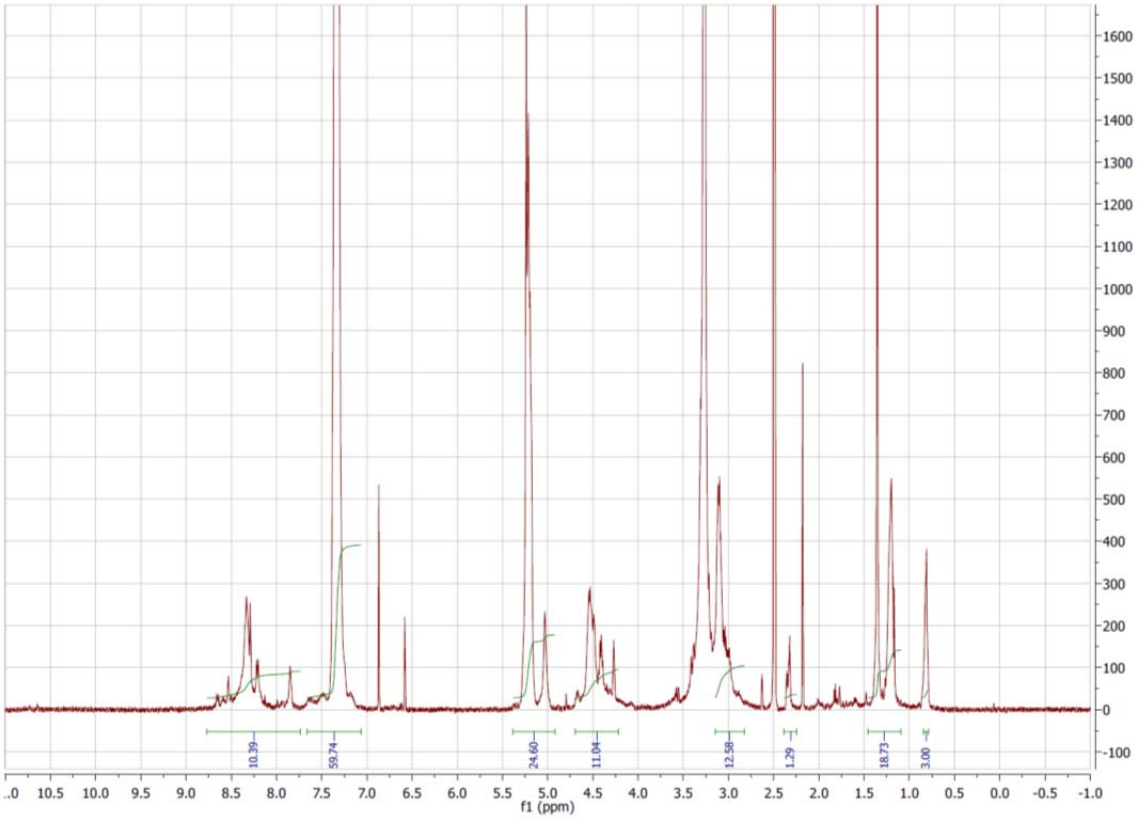

Figure A.7. ^{1}H NMR spectrum of *N*-hexylamino-p(L-cysteine$_{11}$) .

Parameters:

Frequency: 500 MHz

Experiment: ^{1}H

Temperature: 35°C

Solvent: D_6-DMSO

Scans: 32

Relaxation Delay: 10 Seconds

APPENDIX B

NMR and GPC Spectra

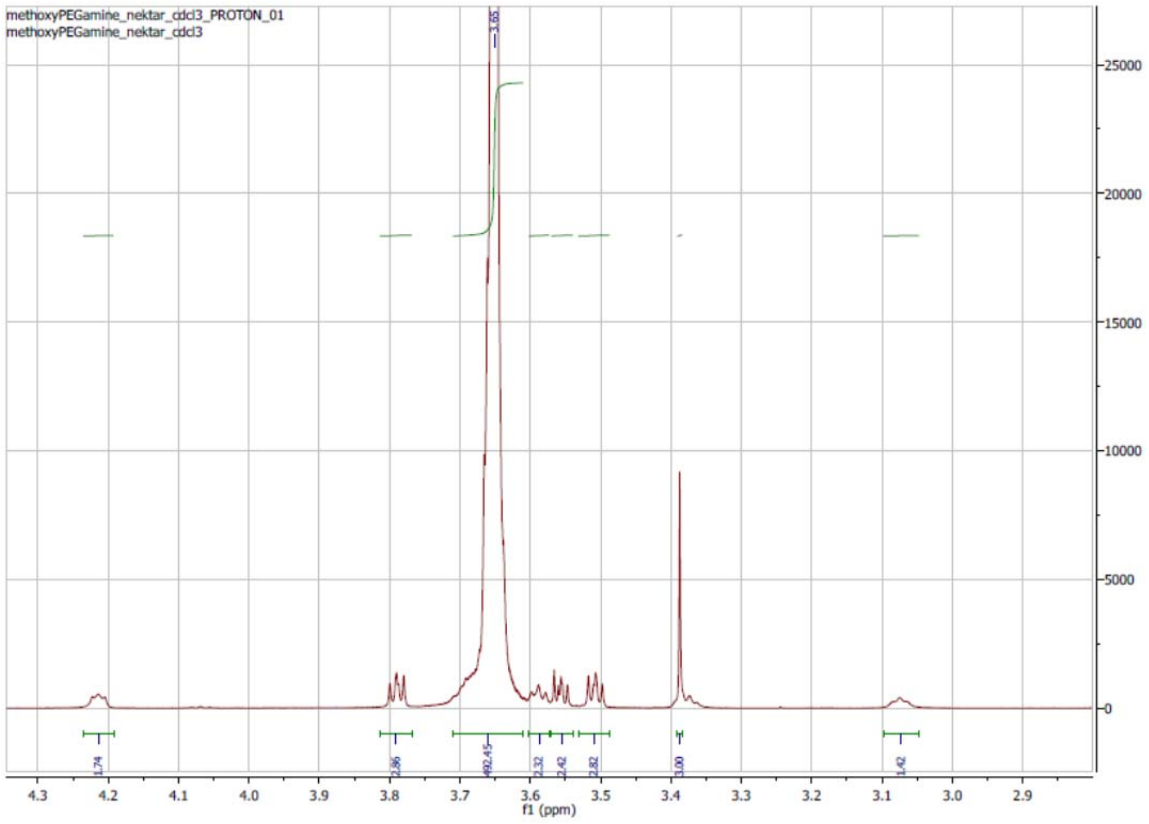

Figure B.1. ^{1}H NMR spectrum of Laysan-Bio α-methoxy-ω-amino.

Parameters:

Frequency: 500 MHz

Experiment: ^{1}H

Temperature: 25°C

Solvent: $CDCl_3$

Scans: 32

Relaxation Delay: 10 Seconds

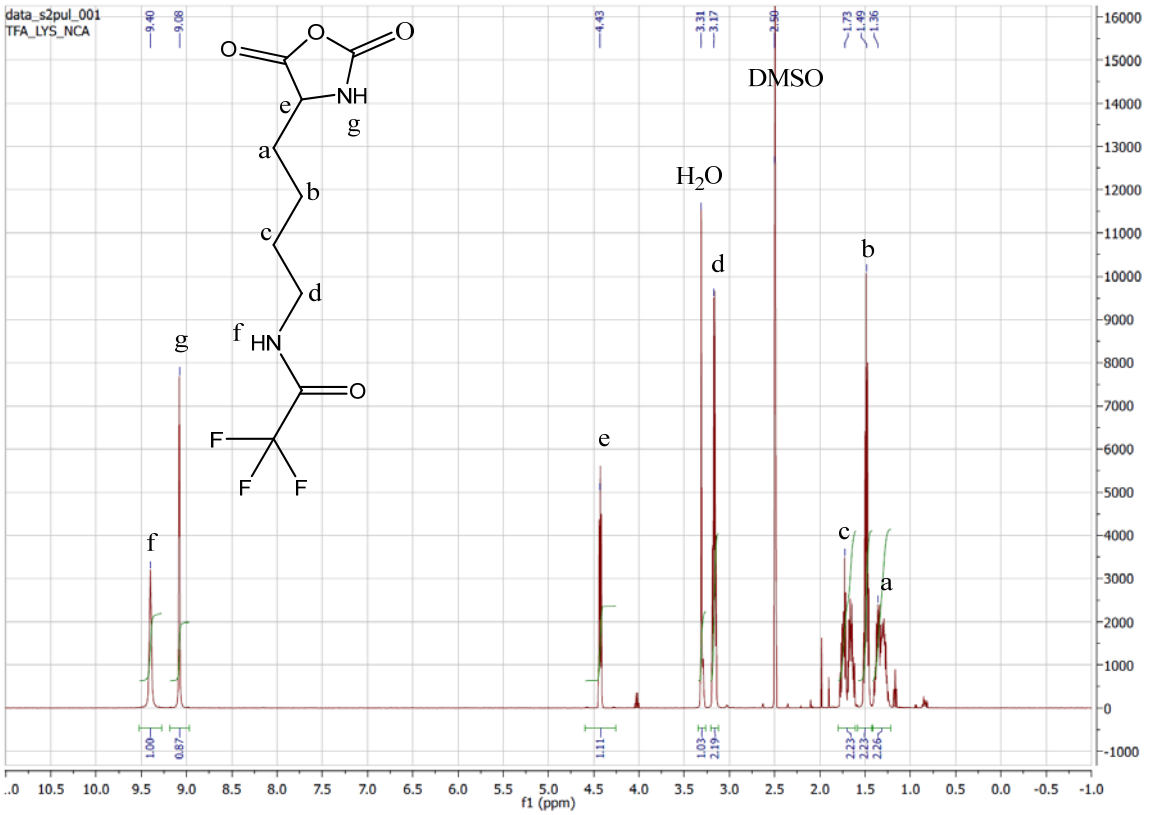

Figure B.2. ^{1}H NMR spectrum of N^{6}-TFA-l-Lysine NCA.

Parameters:

Frequency: 500 MHz

Experiment: ^{1}H

Temperature: 35°C

Solvent: D_6DMSO

Scans: 32

Relaxation Delay: 10 Seconds

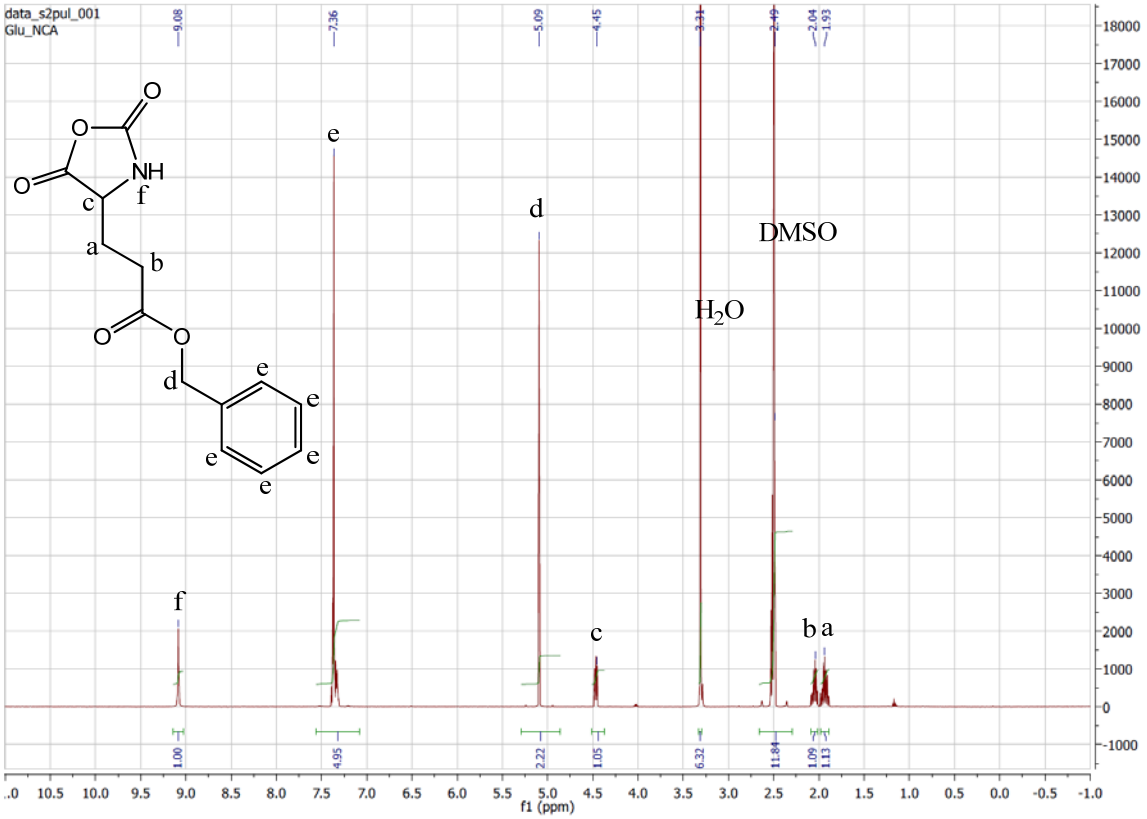

Figure B.3. ^{1}H NMR spectrum of γ-benzyl-l-Glutamate NCA.

Parameters:

Frequency: 500 MHz

Experiment. ^{1}H

Temperature: 35°C

Solvent: D_6DMSO

Scans: 32

Relaxation Delay: 10 Seconds

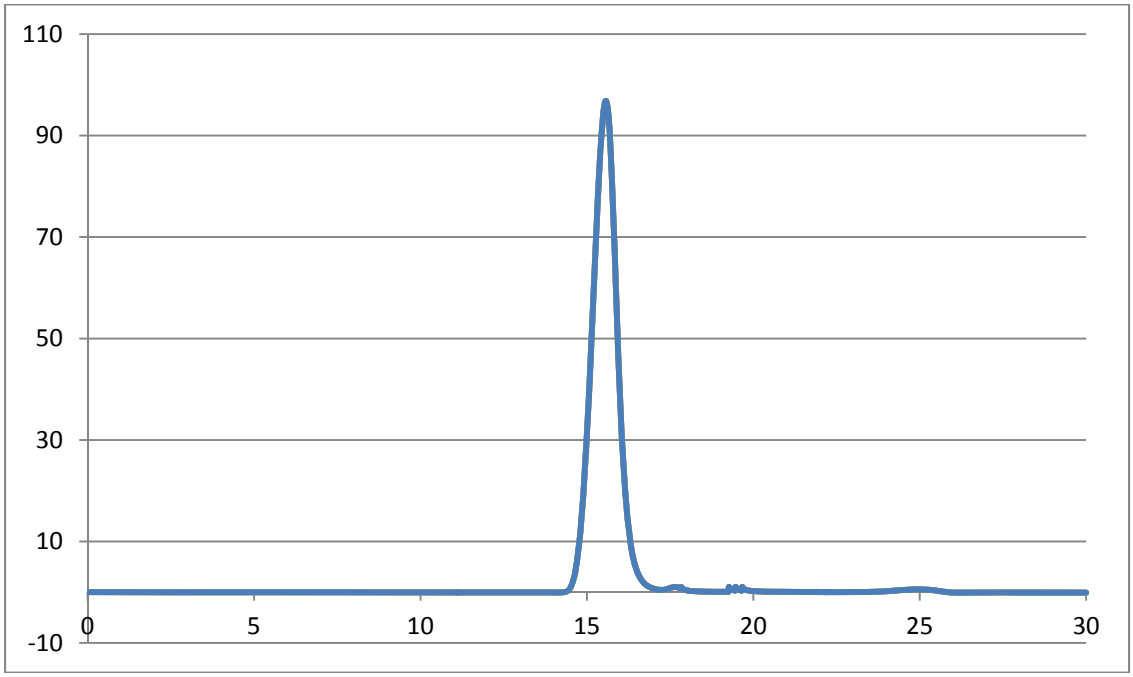

Figure B.4. GPC trace of mPEG-b-p(Glu-b-Cys) R=150

Parameters:

PDI: 1.12

M_w: 34,200 g/mol

Experiment. GPC

Temperature: 50°C

Solvent: DMF

Flow Rate: 1.0 mL/min

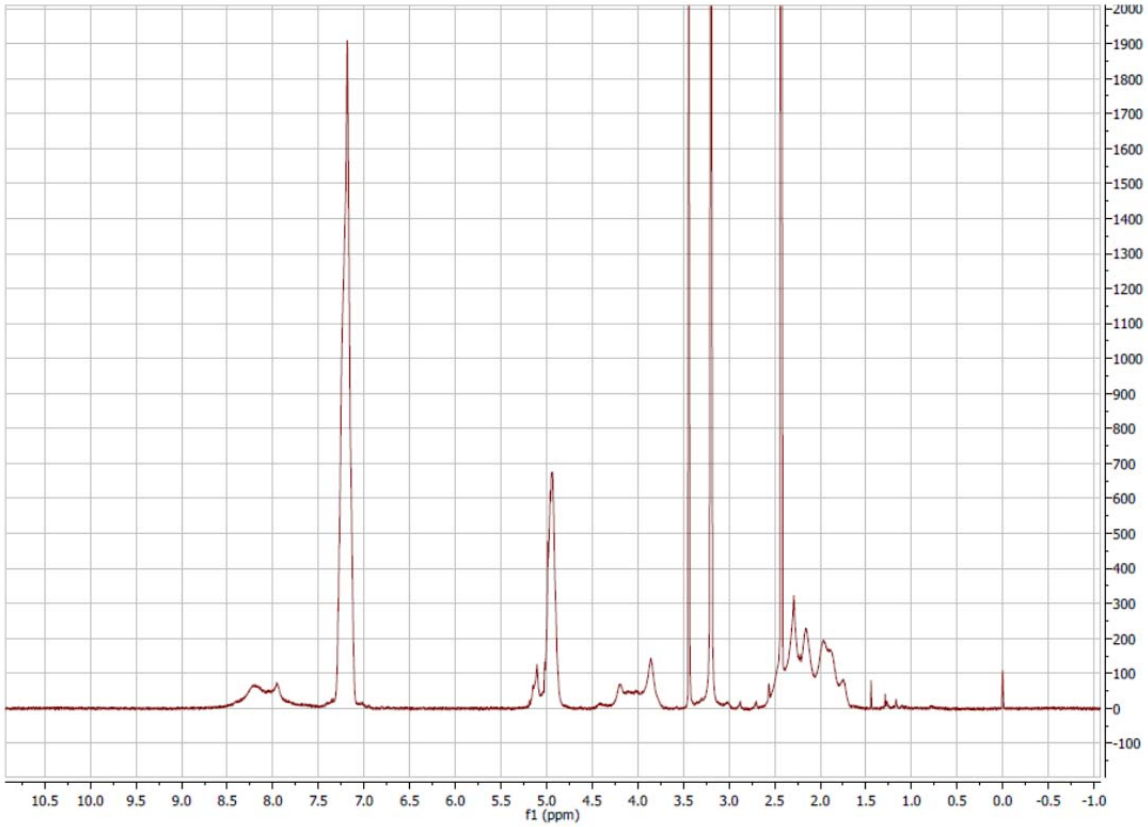

Figure B.5. ^{1}H NMR spectrum of mPEG-b-p(Glu-b-Cys) R=150

Parameters:

Frequency: 500 MHz

Experiment: ^{1}H

Temperature: 35°C

Solvent: D_6DMSO

Scans: 32

Relaxation Delay: 10 Seconds

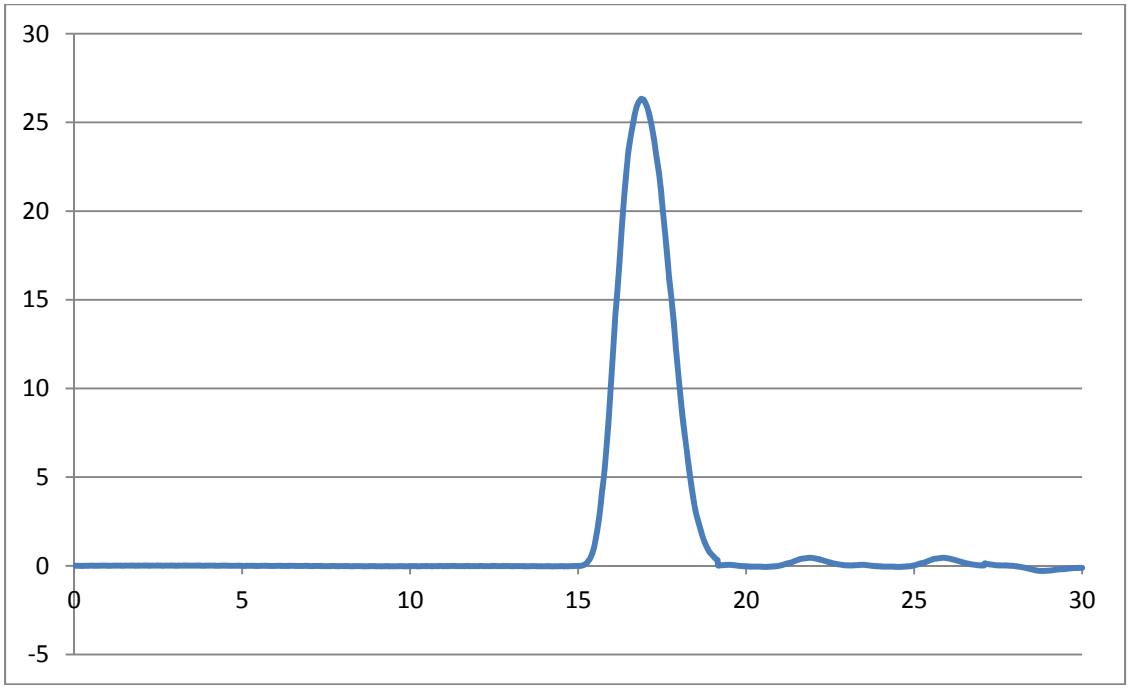

Figure B.6. GPC trace of mPEG-b-p(Glu-co-Cys) R=60

Parameters:

PDI: 1.27

M_w: 19,800 g/mol

Experiment. GPC

Temperature: 50°C

Solvent: DMF

Flow Rate: 1.0 mL/min

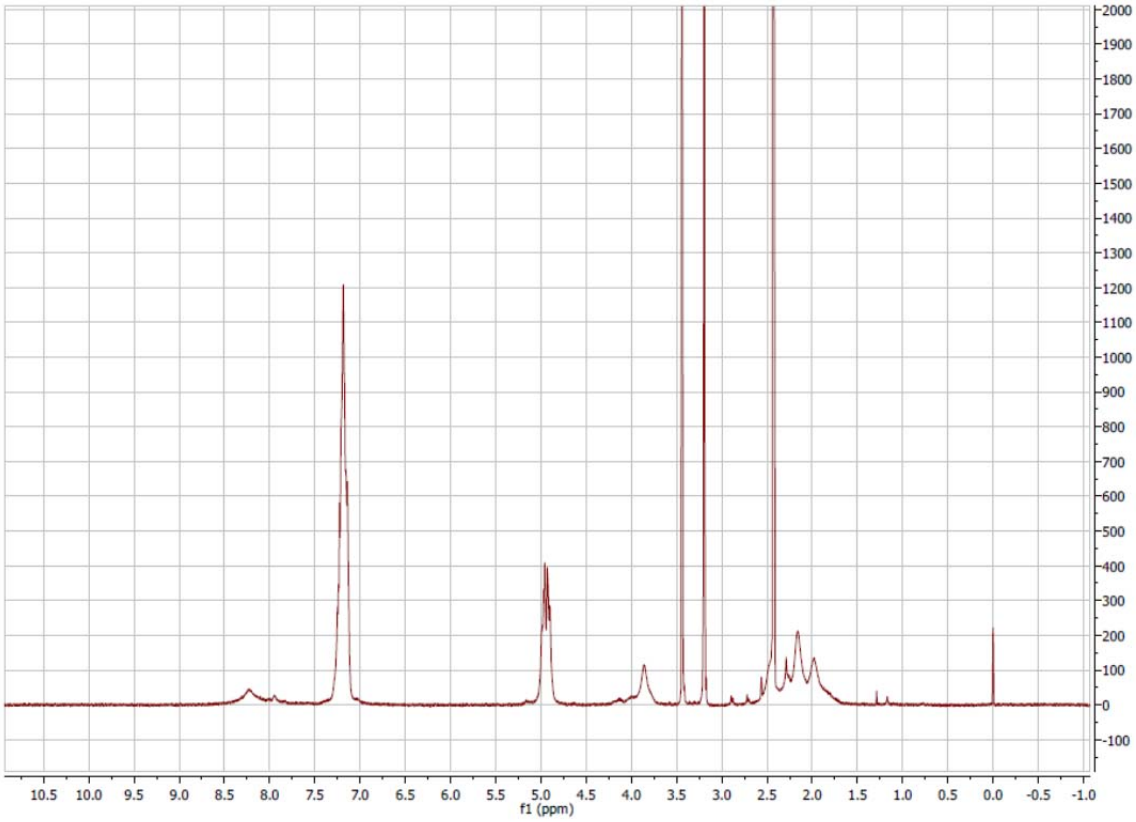

Figure B.7. ^{1}H NMR spectrum of mPEG-b-p(Glu-co-Cys) R=60

Parameters:

Frequency: 500 MHz

Experiment: ^{1}H

Temperature: 35°C

Solvent: D_6DMSO

Scans: 32

Relaxation Delay: 10 Seconds

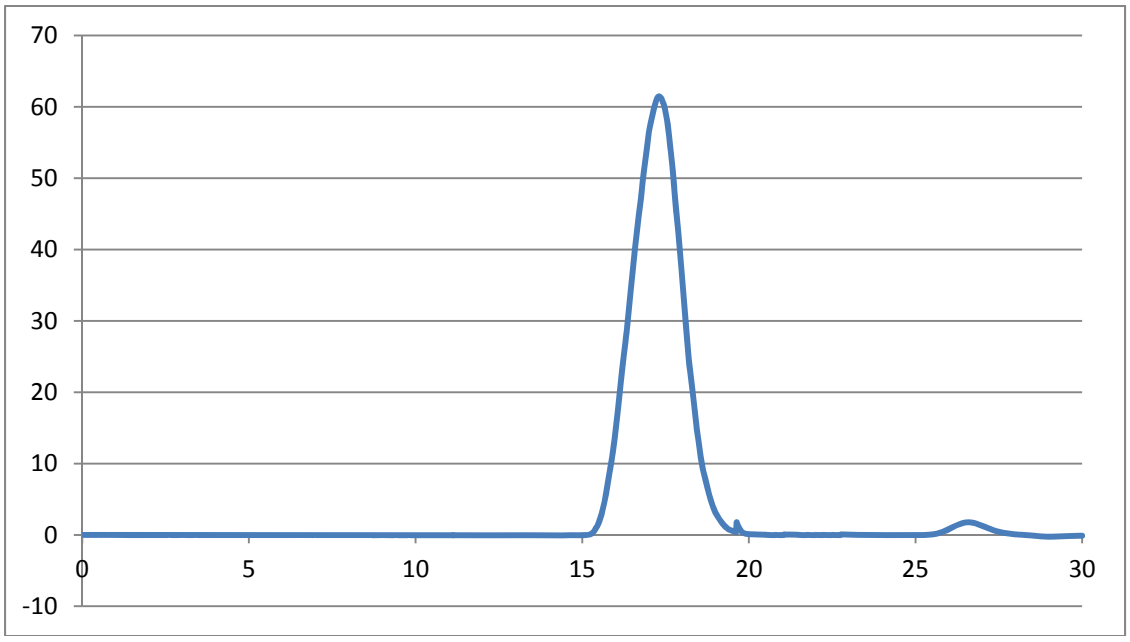

Figure B.8. GPC trace of mPEG-b-p(Glu-co-Cys) R=60

Parameters:

PDI: 1.26

M_w: 14,500 g/mol

Experiment. GPC

Temperature: 50°C

Solvent: DMF

Flow Rate: 1.0 mL/min

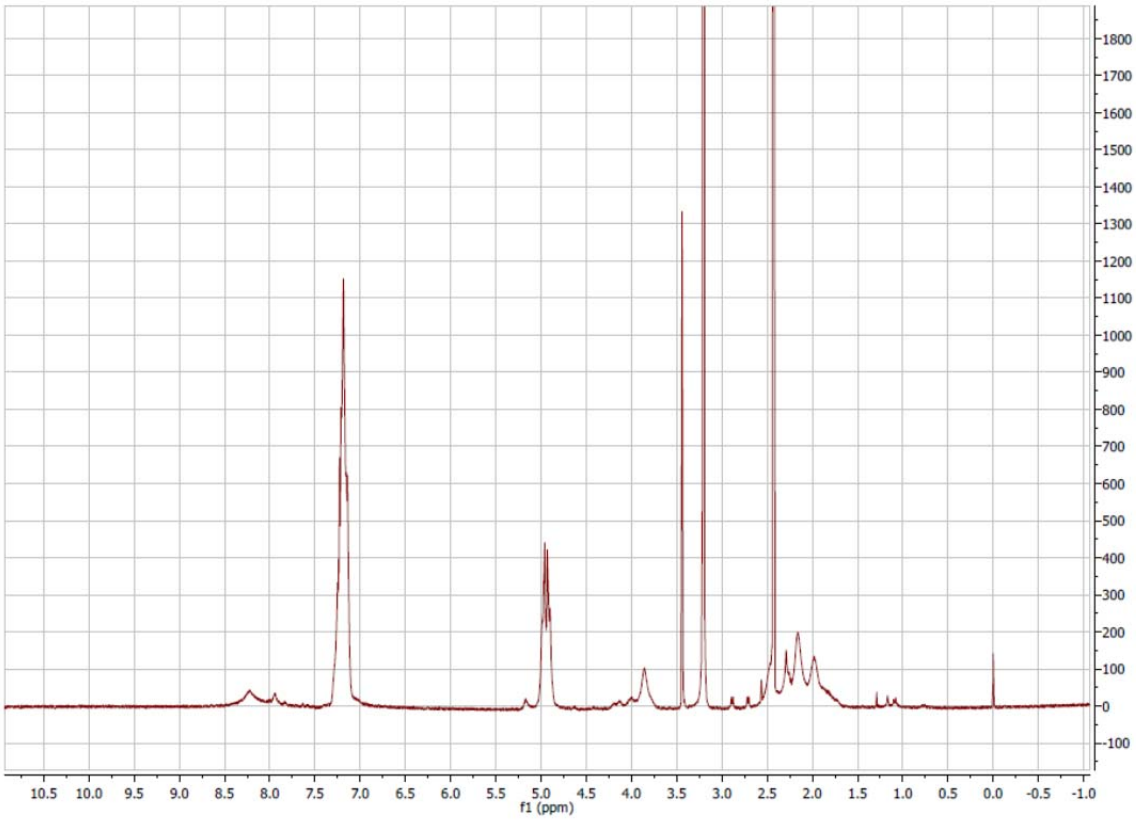

Figure B.9. ^{1}H NMR spectrum of mPEG-b-p(Glu-co-Cys) R=60

Parameters:

Frequency: 500 MHz

Experiment: ^{1}H

Temperature: 35°C

Solvent: D_6DMSO

Scans: 32

Relaxation Delay: 10 Seconds

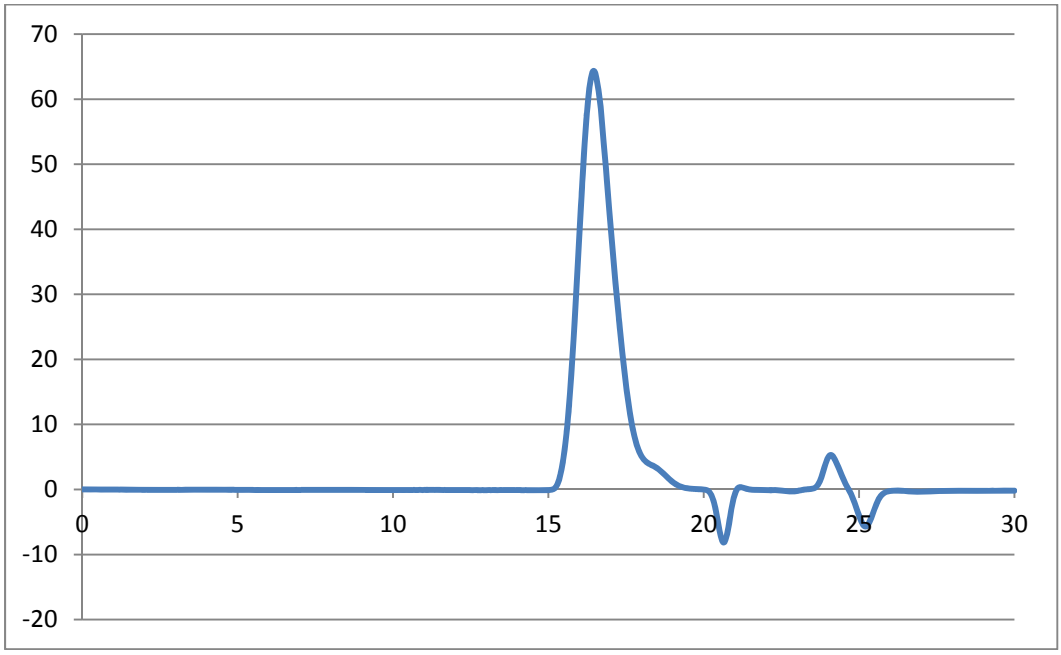

Figure B.10. GPC trace of mPEG-b-p(Glu-co-Cys) R=60

Parameters:

PDI: 1.25

M_w: 14,300 g/mol

Experiment: GPC

Temperature: 50°C

Solvent: DMF

Flow Rate: 1.0 mL/min

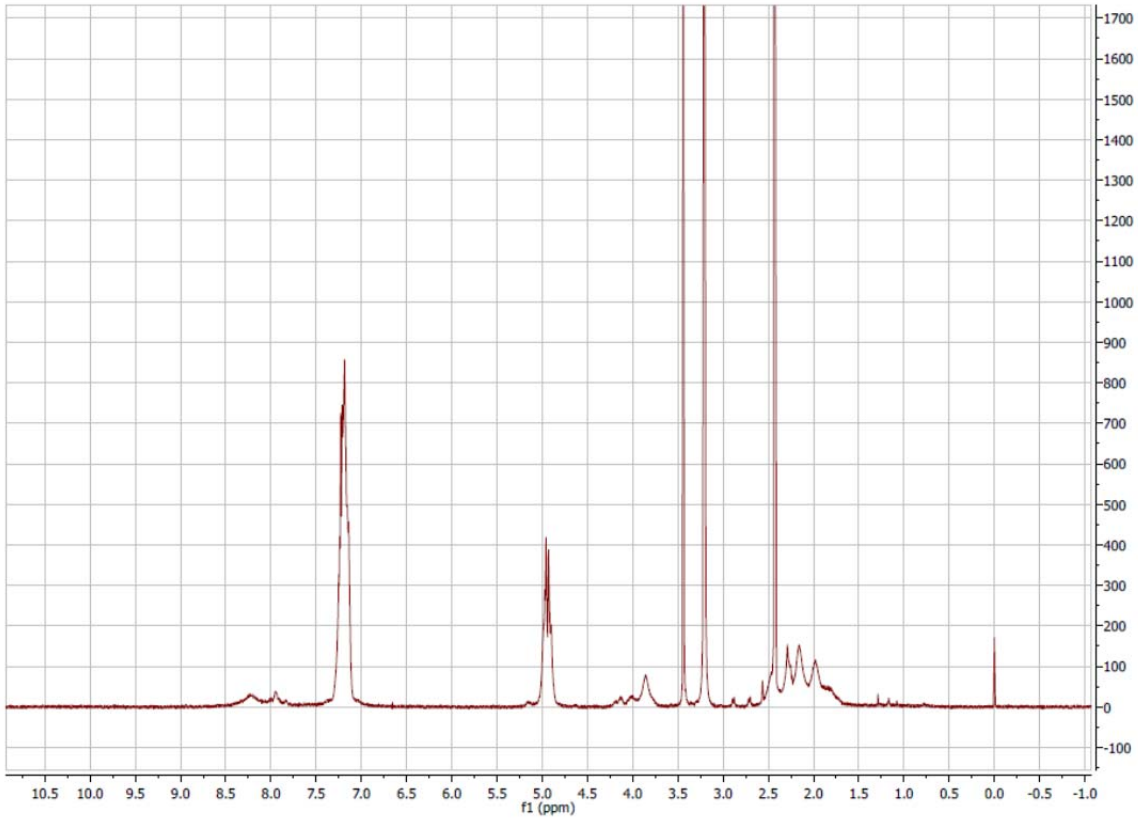

Figure B.11. ^{1}H NMR spectrum of mPEG-b-p(Glu-co-Cys) R=60

Parameters:

Frequency: 500 MHz

Experiment: ^{1}H

Temperature: 35°C

Solvent: D_6DMSO

Scans: 32

Relaxation Delay: 10 Seconds

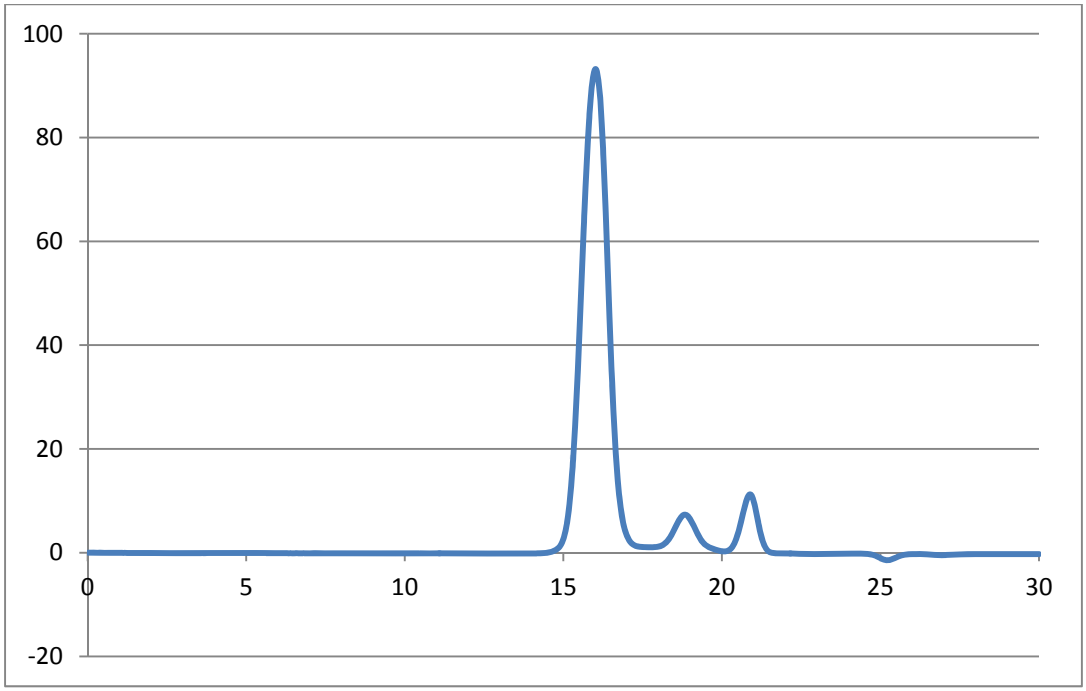

Figure B.12. GPC trace of mPEG-b-p(Glu-b-Cys) R=110

Parameters:

PDI: 1.16

M_w: 25,000 g/mol

Experiment: GPC

Temperature: 50°C

Solvent: DMF

Flow Rate: 1.0 mL/min

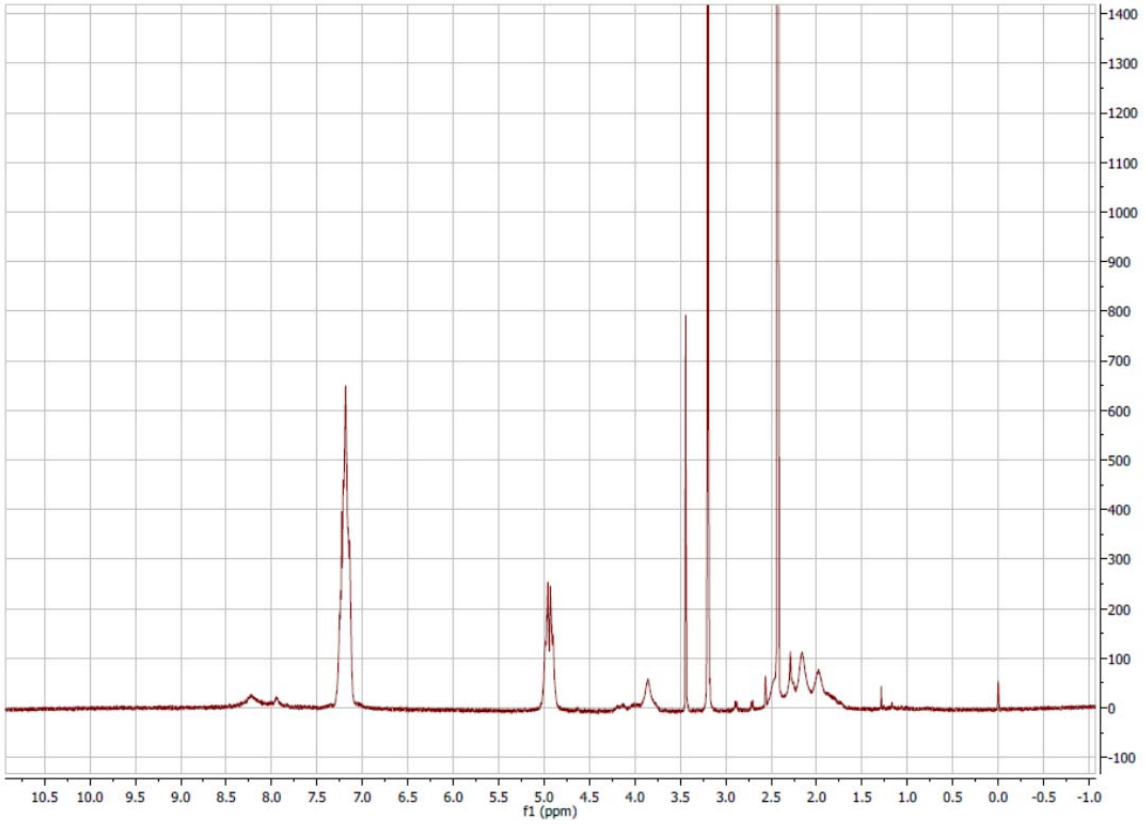

Figure B.13. ^{1}H NMR spectrum of mPEG-b-p(Glu-b-Cys) R=110

Parameters:

Frequency: 500 MHz

Experiment: ^{1}H

Temperature: 35°C

Solvent: D_6DMSO

Scans: 32

Relaxation Delay: 10 Seconds

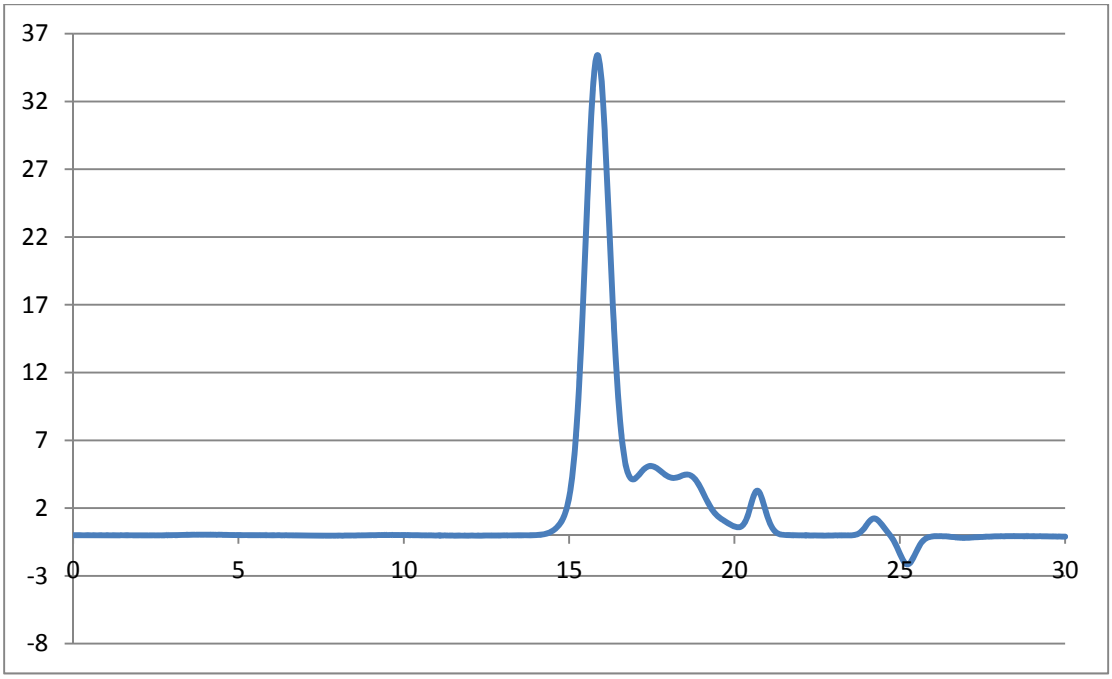

Figure B.14. GPC trace of mPEG-b-p(Glu-b-Cys) R=110

Parameters:

PDI: 1.14

M_w: 28,200 g/mol

Experiment: GPC

Temperature: 50°C

Solvent: DMF

Flow Rate: 1.0 mL/min

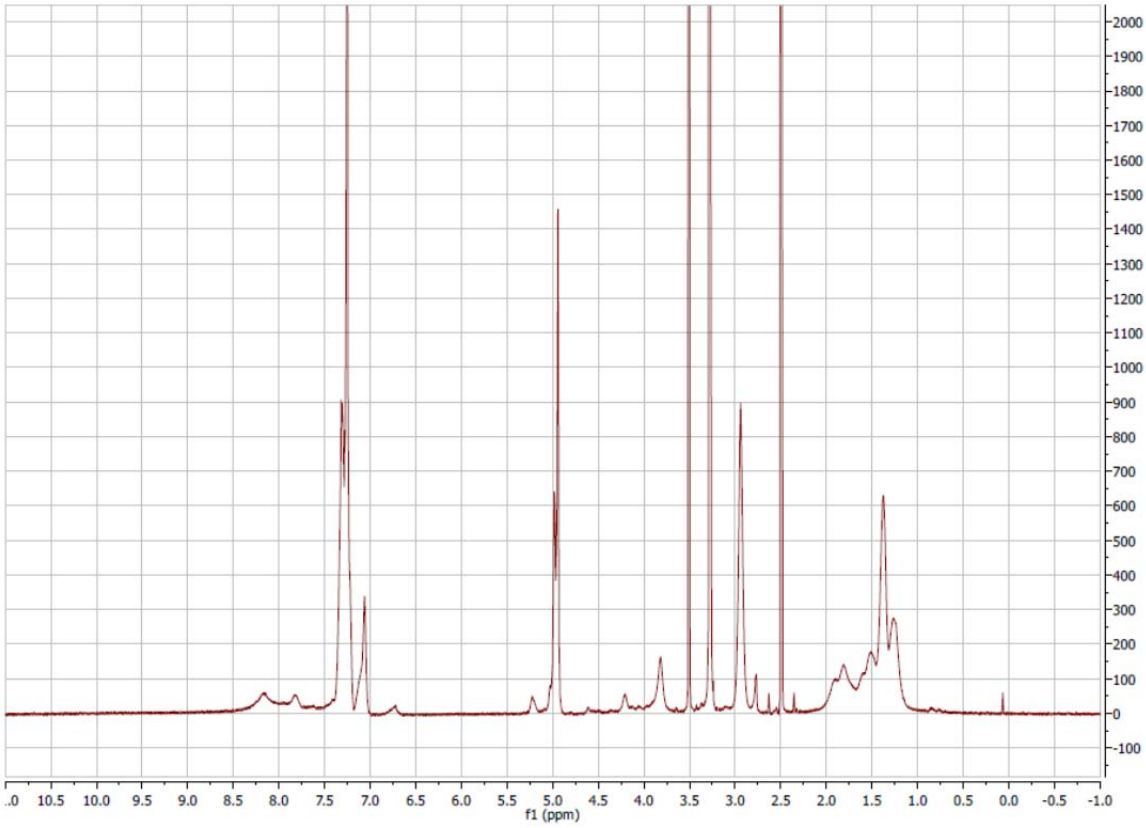

Figure B.15. ^{1}H NMR spectrum of mPEG-b-p(Glu-b-Cys) R=110

Parameters:

Frequency: 500 MHz

Experiment: ^{1}H

Temperature: 35°C

Solvent: D_6DMSO

Scans: 32

Relaxation Delay: 10 Seconds

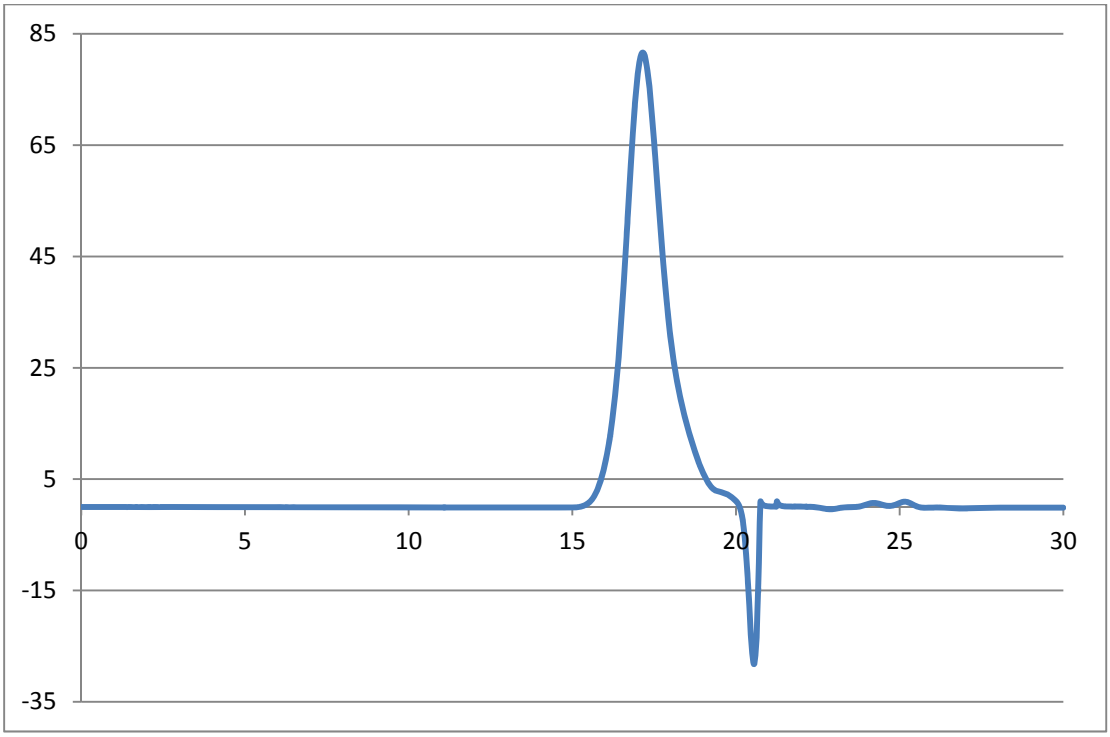

Figure B.16. GPC trace of mPEG-b-p(Lys-b-Cys) R=60

Parameters:

PDI: 1.17

M_w: 15,700 g/mol

Experiment: GPC

Temperature: 50°C

Solvent: DMF

Flow Rate: 1.0 mL/min

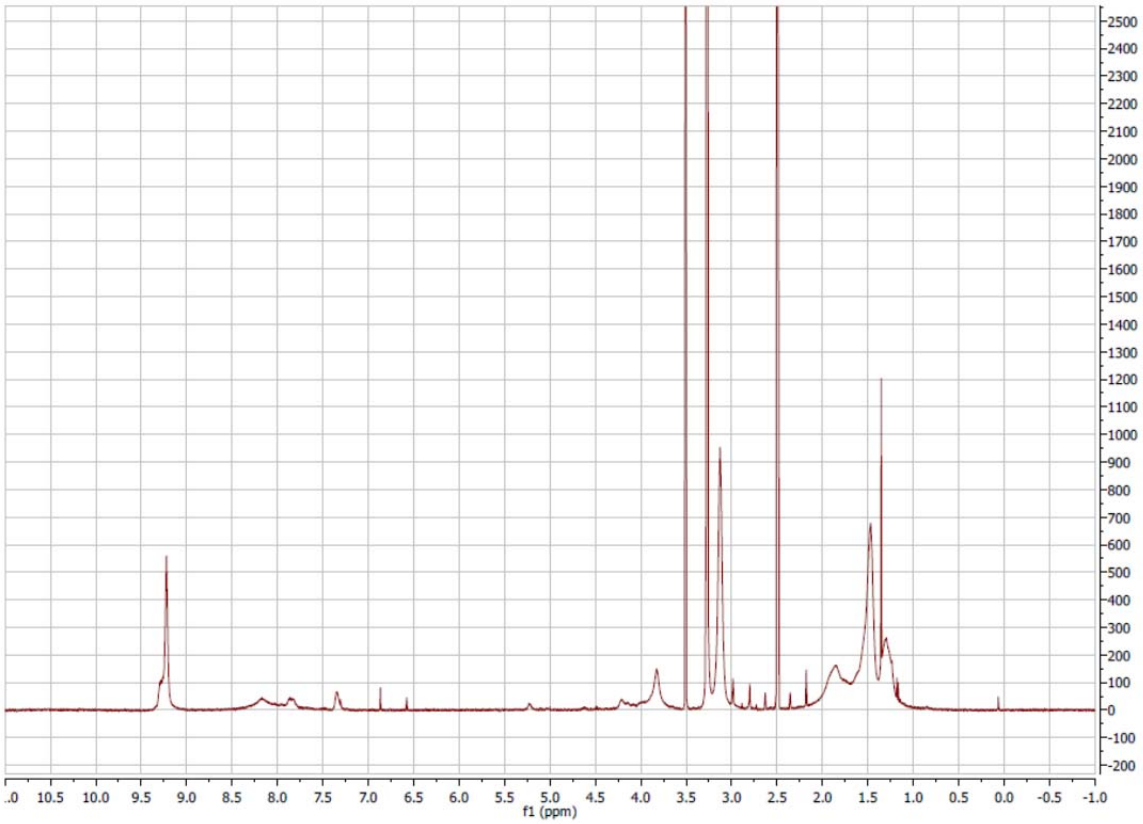

Figure B.17. ^{1}H NMR spectrum of incomplete deprotection of mPEG-b-p(Lys-b-Cys) R=60

Parameters:

Frequency: 500 MHz

Experiment: ^{1}H

Temperature: 35°C

Solvent: D_6DMSO

Scans: 32

Relaxation Delay: 10 Seconds

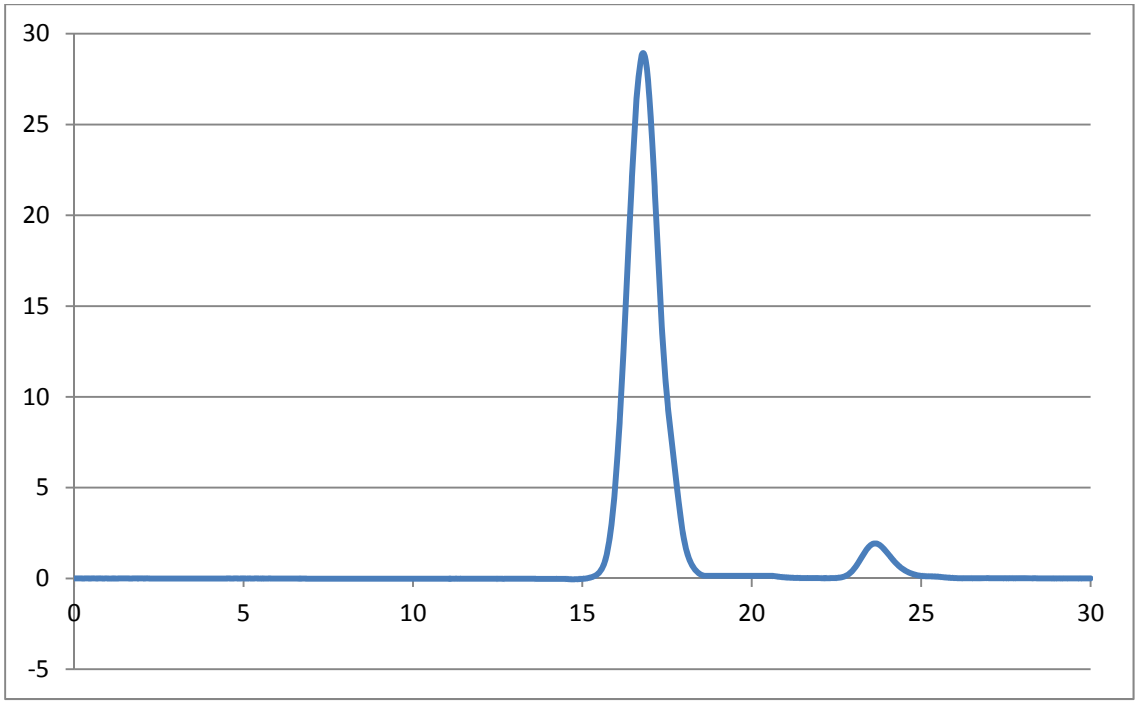

Figure B.18. GPC trace of mPEG-b-p(Lys-b-Cys) R=60

Parameters:

PDI: 1.18

M_w:

Experiment: GPC

Temperature: 50°C

Solvent: DMF

Flow Rate: 1.0 mL/min

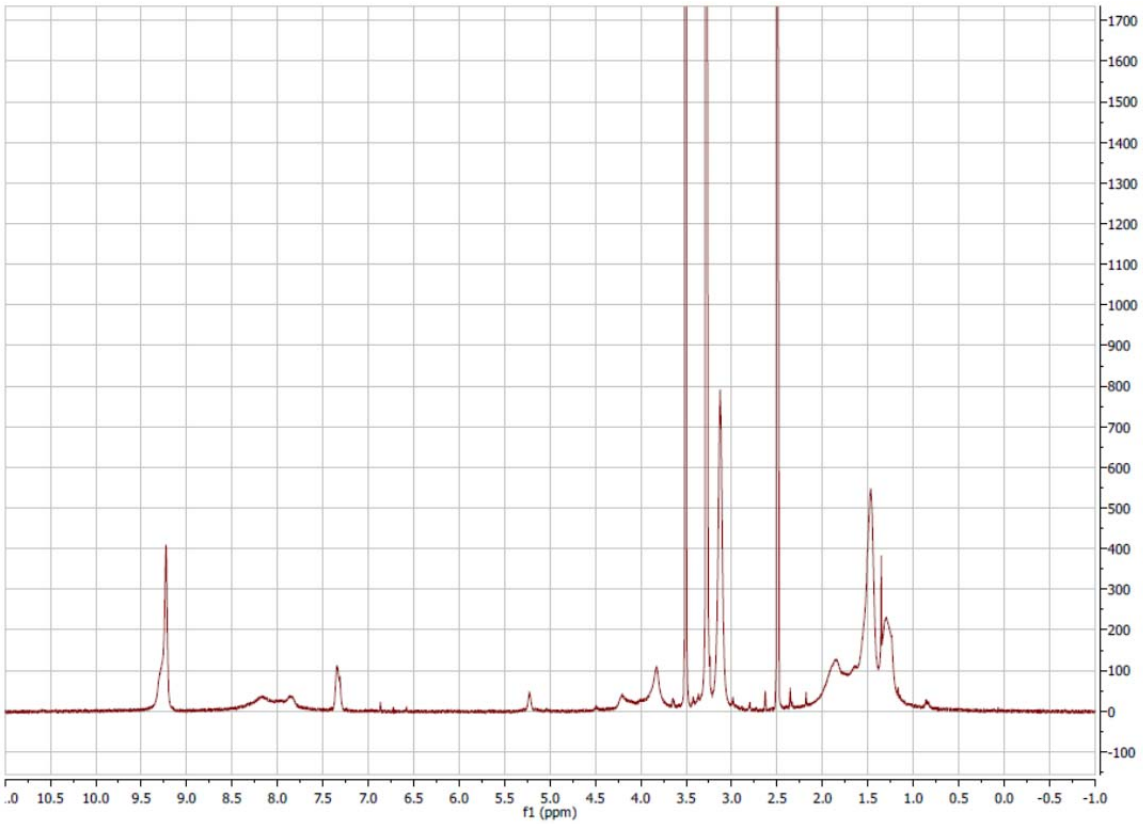

Figure B.19. ^{1}H NMR spectrum of mPEG-b-p(Lys-b-Cys) R=60

Parameters:

Frequency: 500 MHz

Experiment: ^{1}H

Temperature: 35°C

Solvent: D_6DMSO

Scans: 32

Relaxation Delay: 10 Seconds

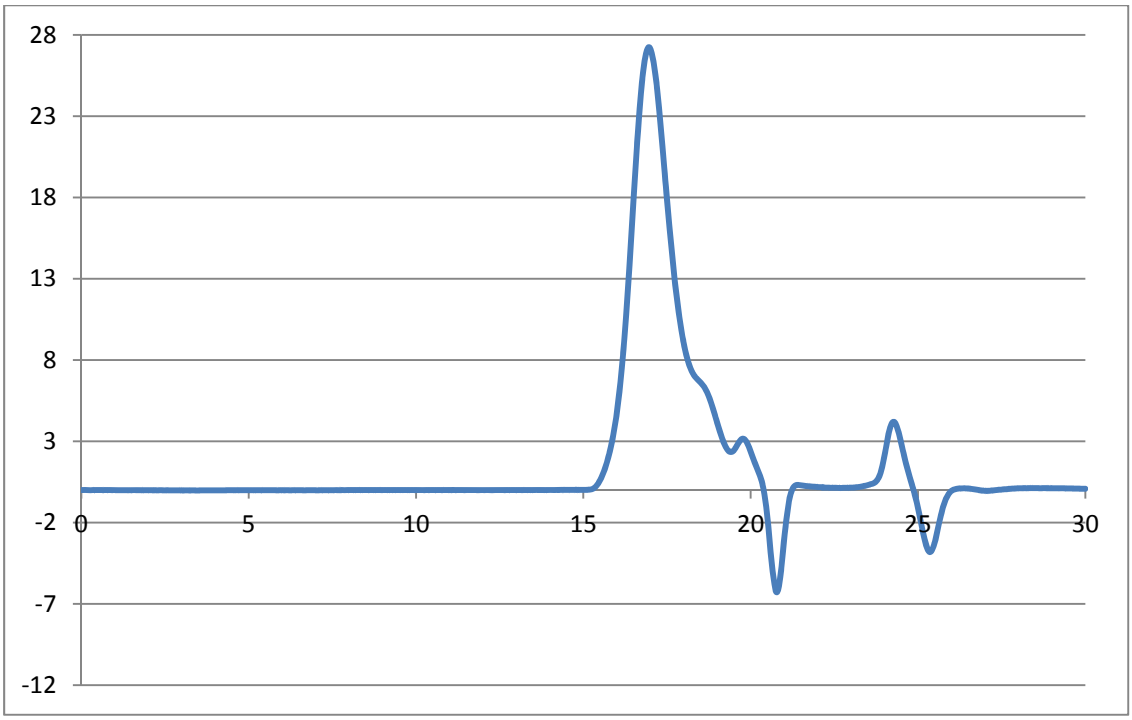

Figure B.20. GPC trace of mPEG-b-p(Lys-co-Cys) R=60

Parameters:

PDI: 1.20

M_w:

Experiment: GPC

Temperature: 50°C

Solvent: DMF

Flow Rate: 1.0 mL/min

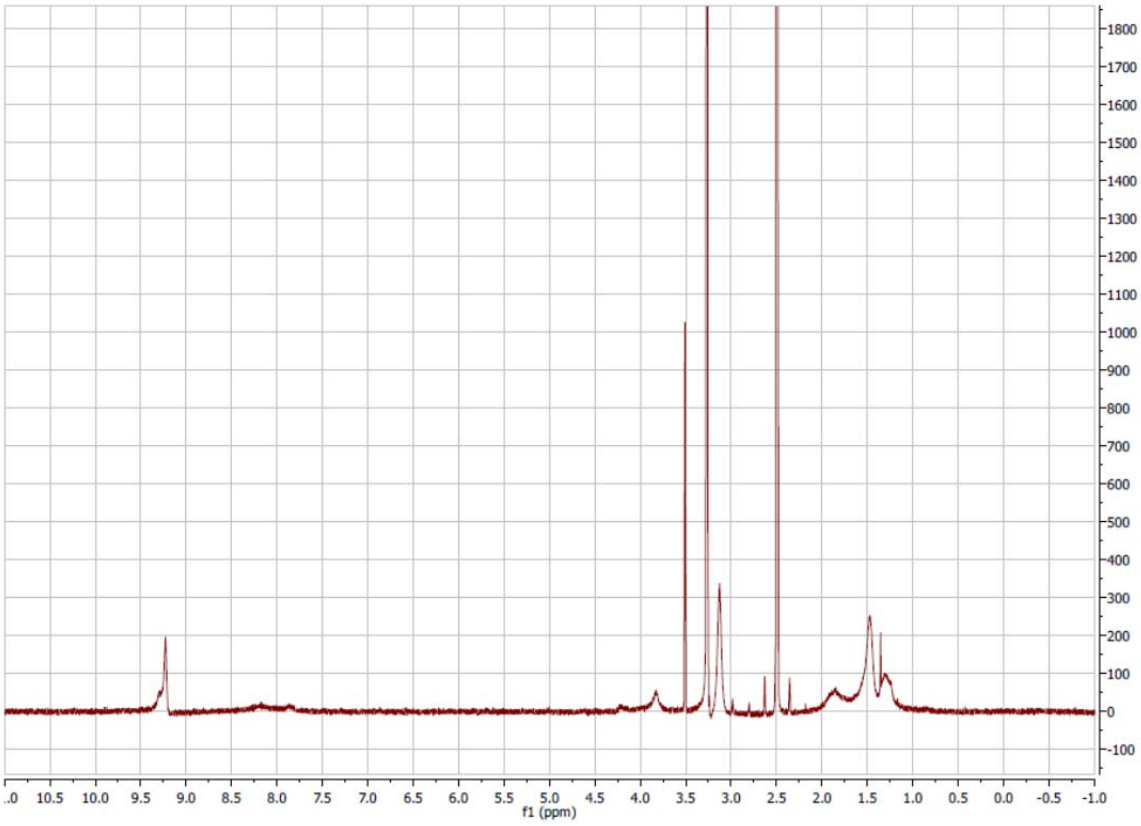

Figure B.21. ^{1}H NMR spectrum of mPEG-b-p(Lys-co-Cys) R=60

Parameters:

Frequency: 500 MHz

Experiment: ^{1}H

Temperature: 35°C

Solvent: D_6DMSO

Scans: 32

Relaxation Delay: 10 Seconds

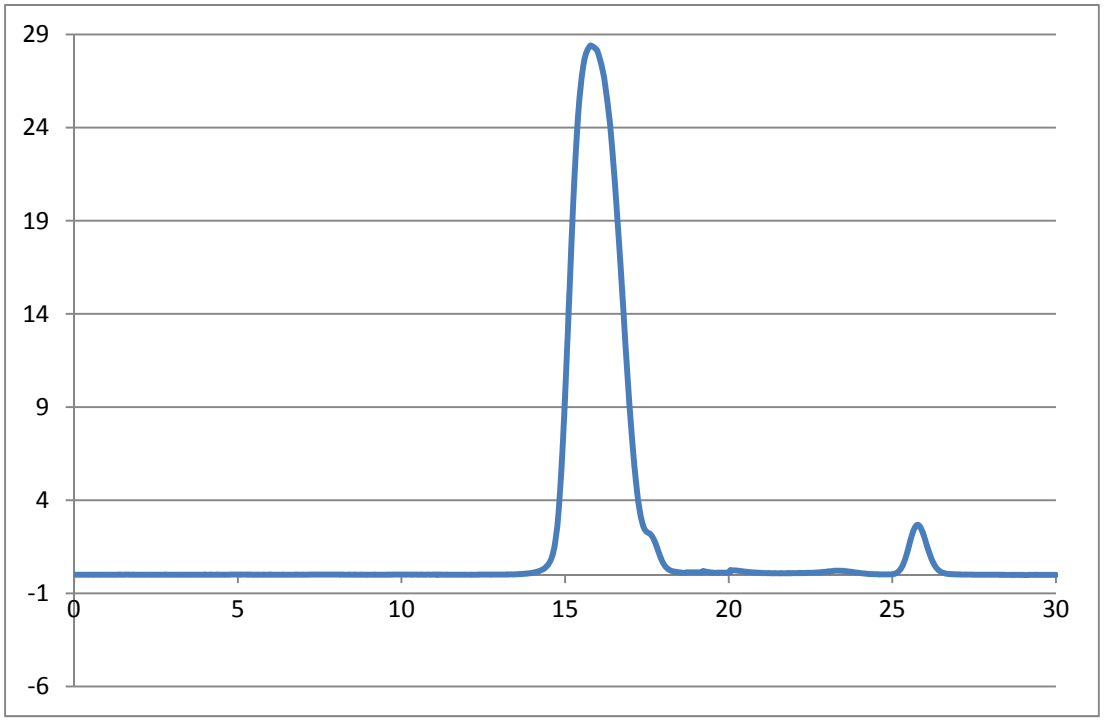

Figure B.22. GPC trace of mPEG-b-p(Glu-co-Cys) R=120

Parameters:

PDI: 1.33

M_w:

Experiment: GPC

Temperature: 50°C

Solvent: DMF

Flow Rate: 1.0 mL/min

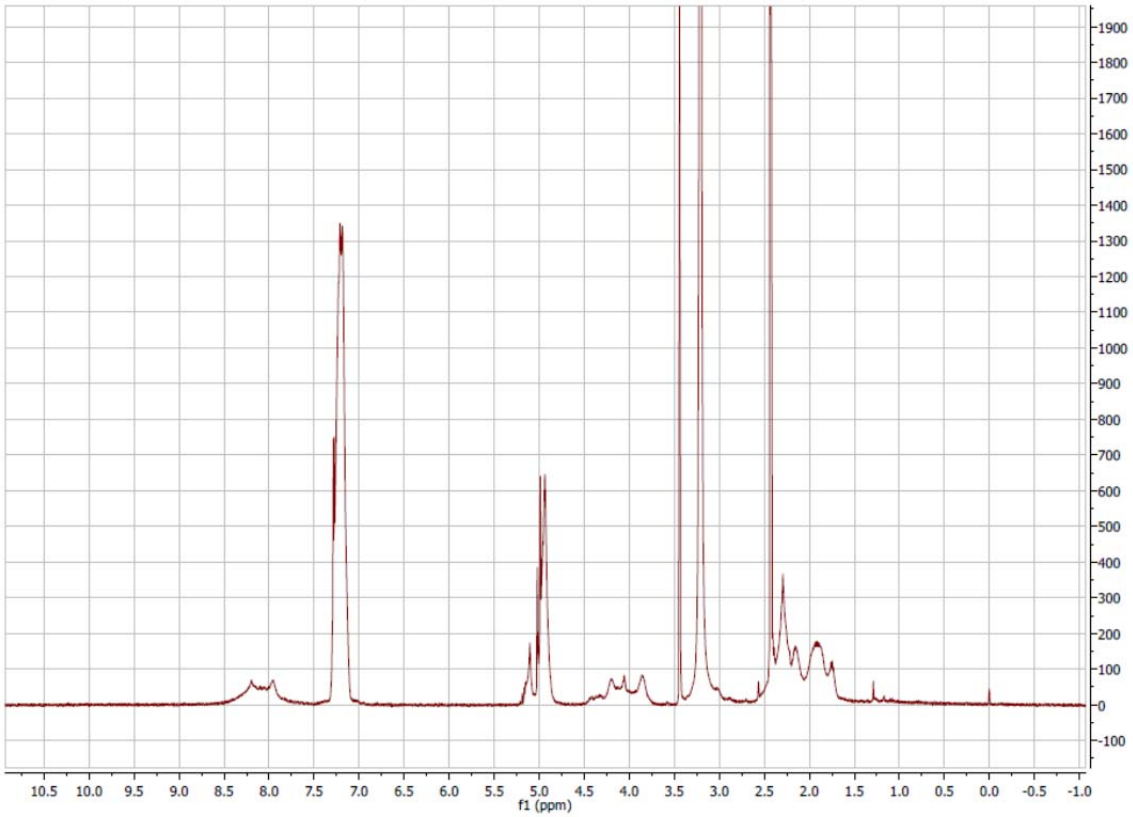

Figure B.23. ^{1}H NMR spectrum of mPEG-b-p(Glu-co-Cys) R=120

Parameters:

Frequency: 500 MHz

Experiment: ^{1}H

Temperature: 35°C

Solvent: D_6DMSO

Scans: 32

Relaxation Delay: 10 Seconds

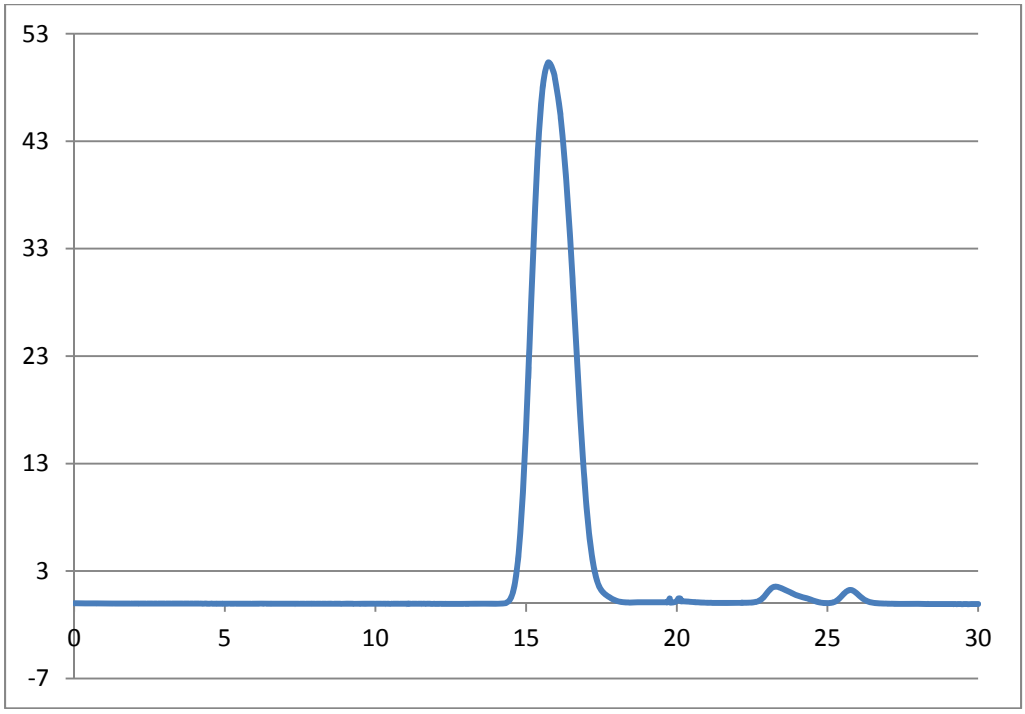

Figure B.24. GPC trace of mPEG-b-p(Lys-co-Cys) R=120

Parameters:

PDI: 1.32

M_w:

Experiment: GPC

Temperature: 50°C

Solvent: DMF

Flow Rate: 1.0 mL/min

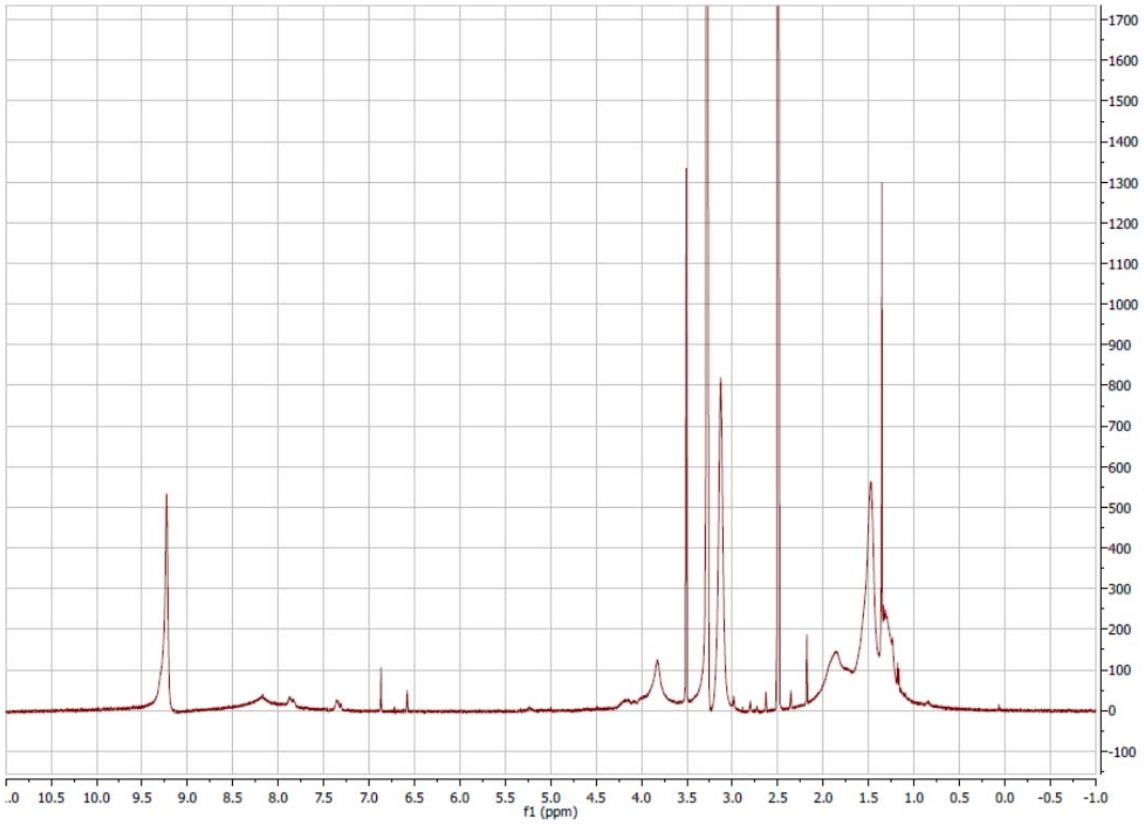

Figure B.25. ^{1}H NMR spectrum of mPEG-b-p(Lys-co-Cys) R=120

Parameters:

Frequency: 500 MHz

Experiment: ^{1}H

Temperature: 35°C

Solvent: D_6DMSO

Scans: 32

Relaxation Delay: 10 Seconds

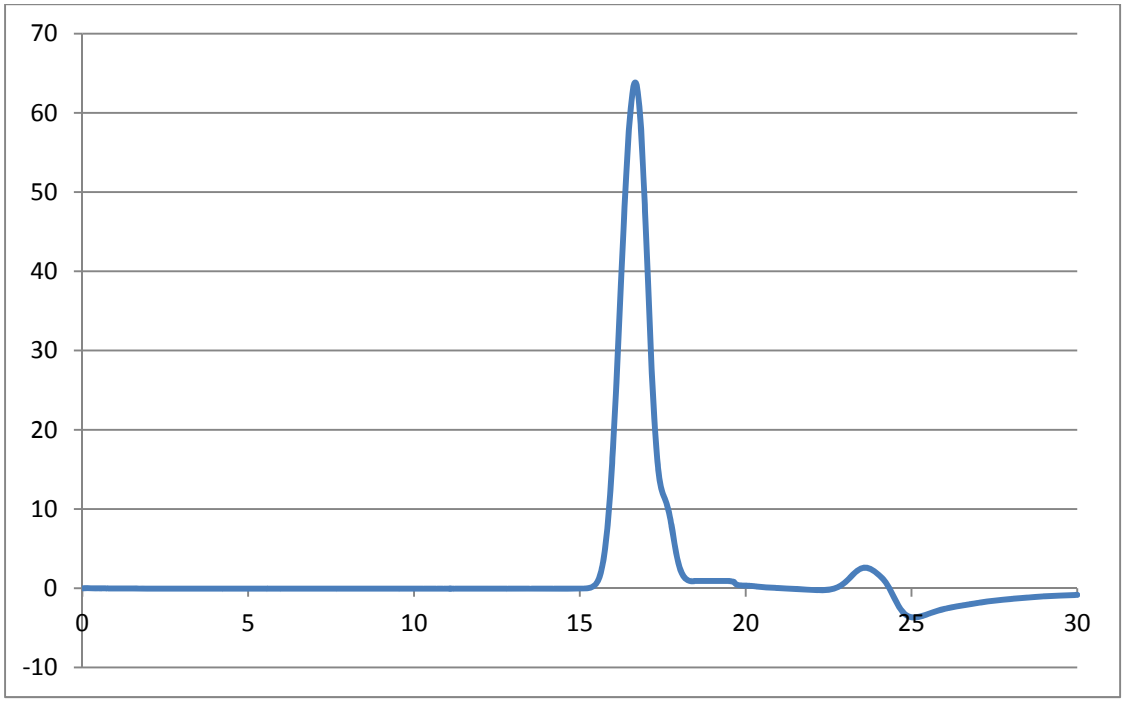

Figure B.26. GPC trace of mPEG-b-p(Lys-b-Cys) R=120

Parameters:

PDI: 1.16

M_w:

Experiment: GPC

Temperature: 50°C

Solvent: DMF

Flow Rate: 1.0 mL/min

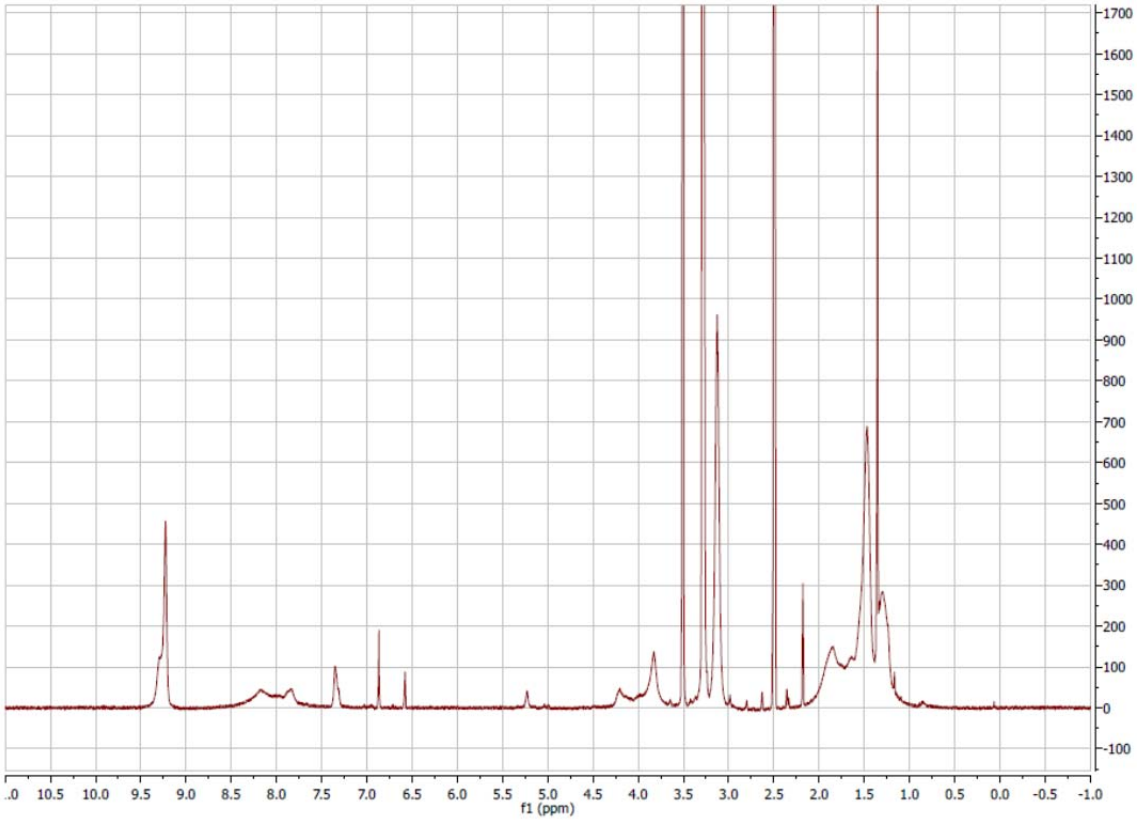

Figure B.27. ^{1}H NMR spectrum of mPEG-b-p(Lys-b-Cys) R=120

Parameters:

Frequency: 500 MHz

Experiment: ^{1}H

Temperature: 35°C

Solvent: D_6DMSO

Scans: 32

Relaxation Delay: 10 Seconds

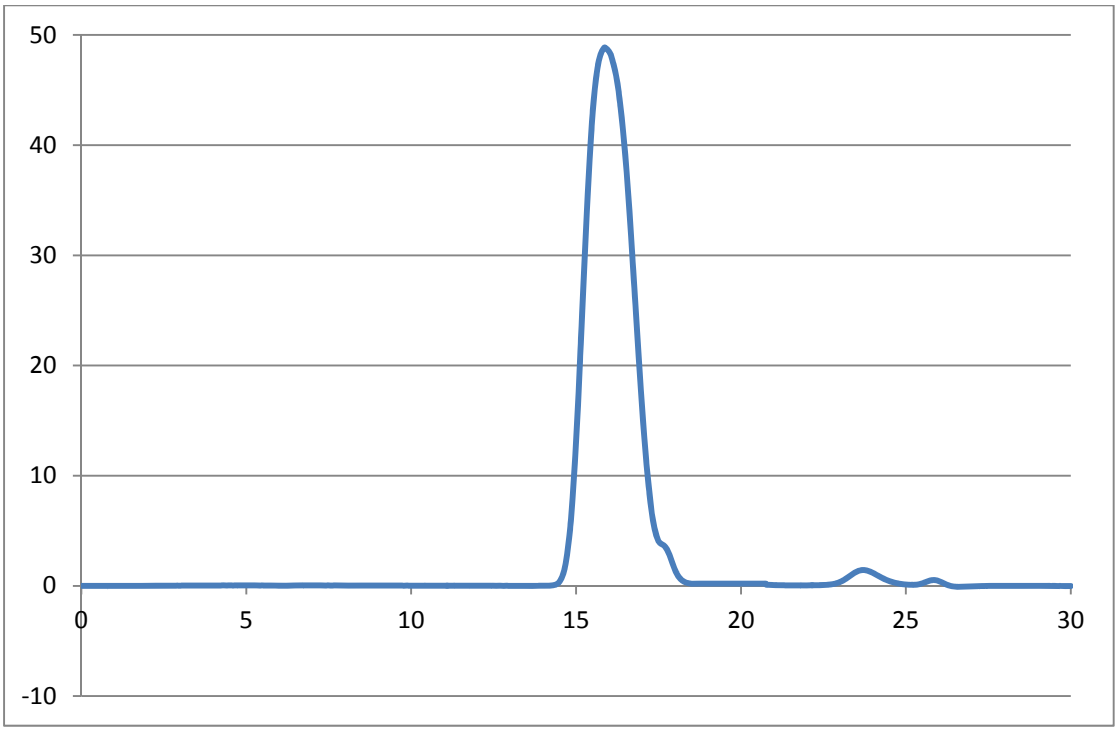

Figure B.28. GPC trace of mPEG-b-p(Lys-co-Cys) R=110

Parameters:

PDI: 1.38

M_w:

Experiment: GPC

Temperature: 50°C

Solvent: DMF

Flow Rate: 1.0 mL/min

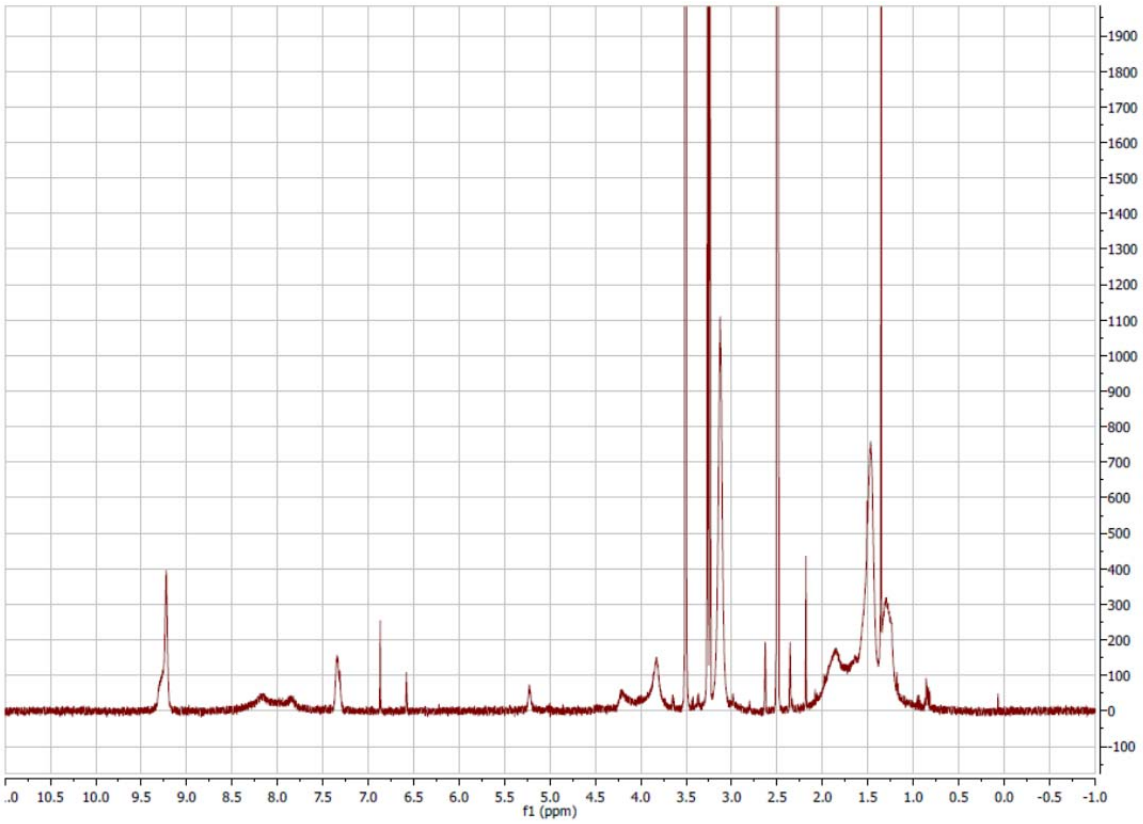

Figure B.29. ^{1}H NMR spectrum of mPEG-b-p(Lys-co-Cys) R=110

Parameters:

Frequency: 500 MHz

Experiment: ^{1}H

Temperature: 35°C

Solvent: D_6DMSO

Scans: 32

Relaxation Delay: 10 Seconds

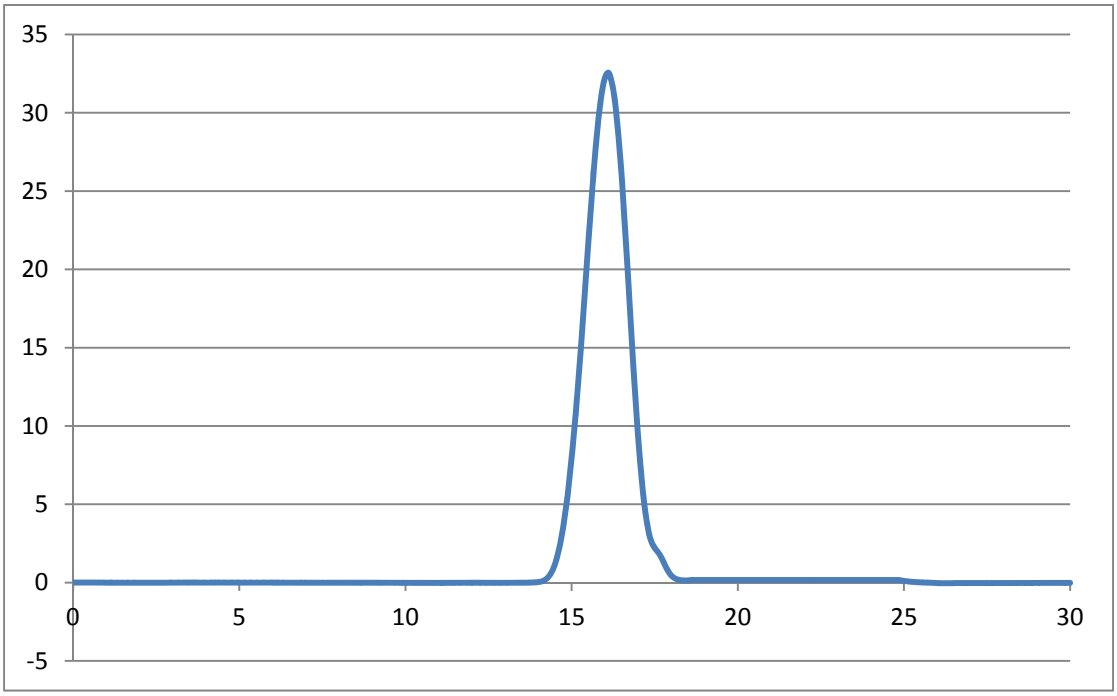

Figure B.30. GPC trace of mPEG-b-p(Glu-co-Cys) R=110

Parameters:

PDI: 1.34

M_w:

Experiment: GPC

Temperature: 50°C

Solvent: DMF

Flow Rate: 1.0 mL/min

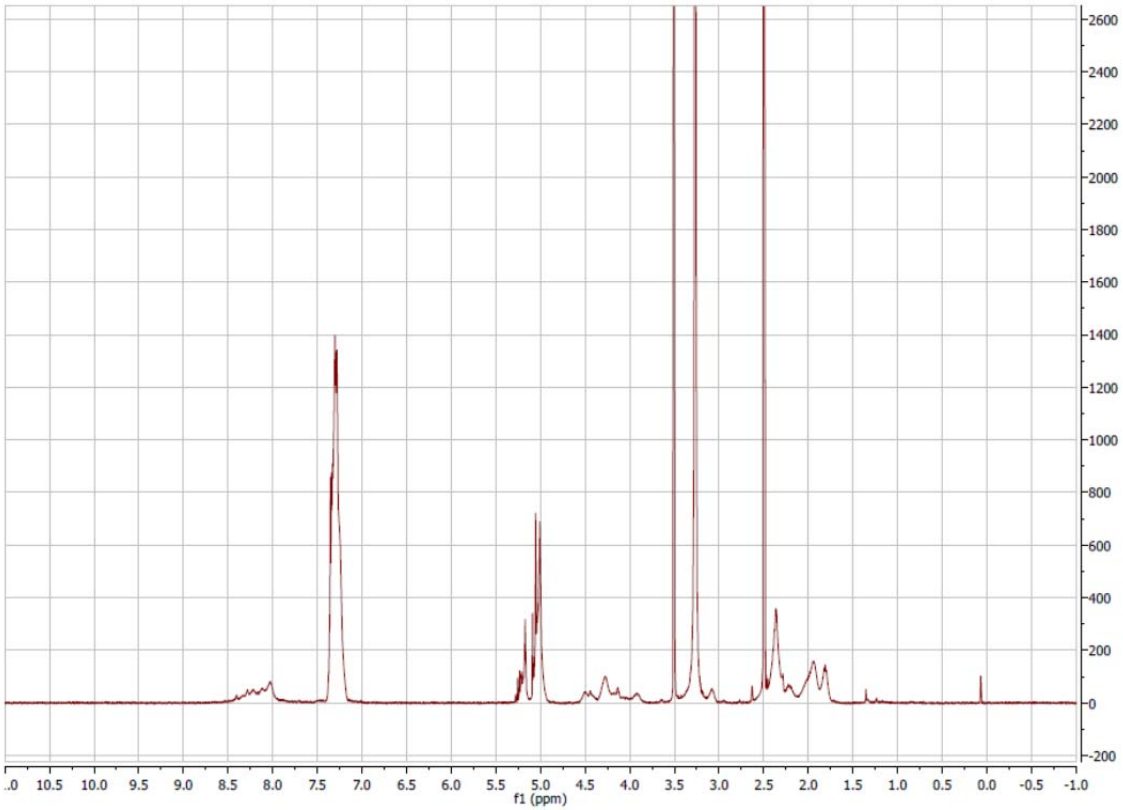

Figure B.31. ^{1}H NMR spectrum of mPEG-b-p(Glu-co-Cys) R=110

Parameters:

Frequency: 500 MHz

Experiment: ^{1}H

Temperature: 35°C

Solvent: D_6DMSO

Scans: 32

Relaxation Delay: 10 Seconds

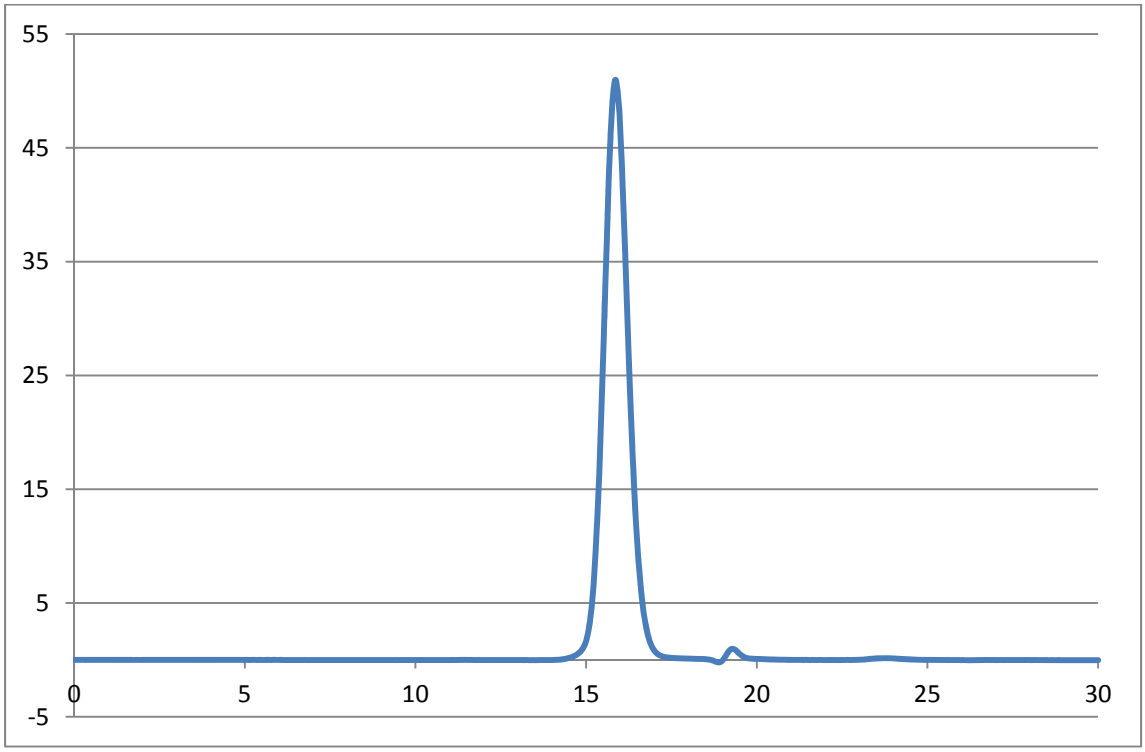

Figure B.32. GPC trace of mPEG-b-p(Glu-b-Cys) R=110

Parameters:

PDI: 1.13

M_w:

Experiment: GPC

Temperature: 50°C

Solvent: DMF

Flow Rate: 1.0 mL/min

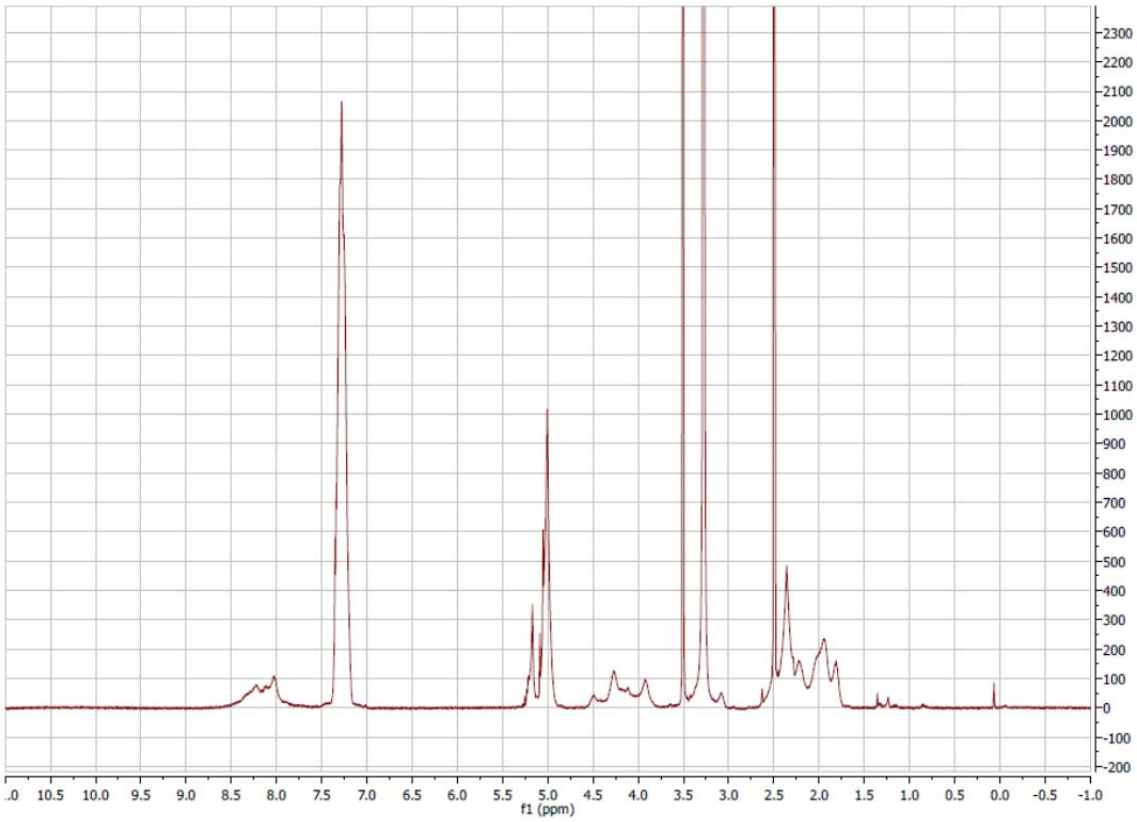

Figure B.33. ^{1}H NMR spectrum of mPEG-b-p(Glu-b-Cys) R=110

Parameters:

Frequency: 500 MHz

Experiment: ^{1}H

Temperature: 35°C

Solvent: D_6DMSO

Scans: 32

Relaxation Delay: 10 Seconds

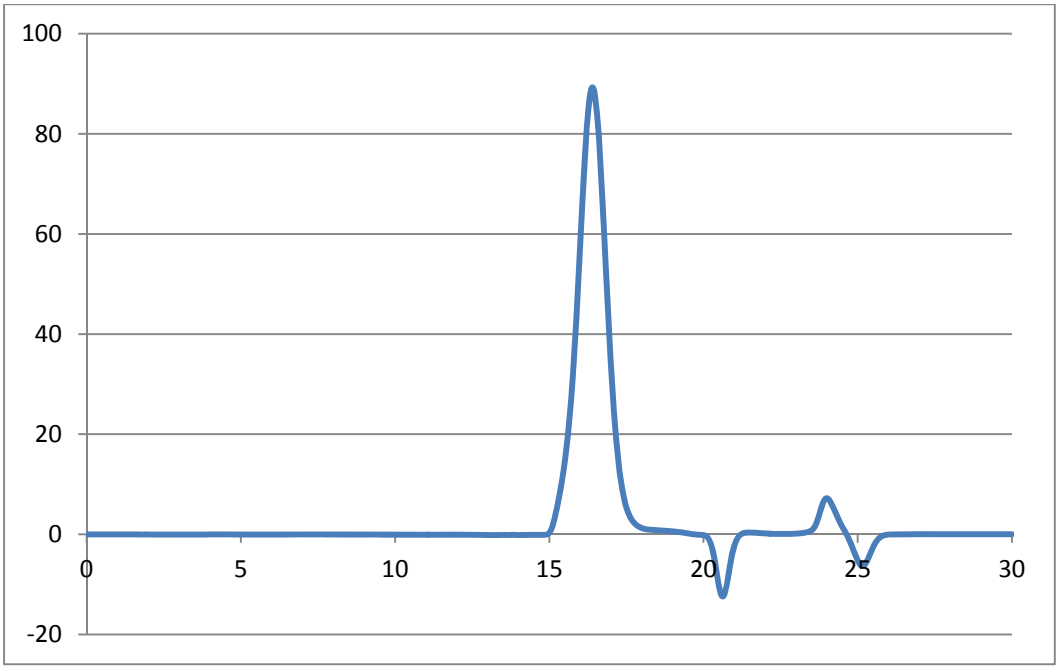

Figure B.34. GPC trace of mPEG-b-p(Glu-b-Cys) R=60

Parameters:

PDI: 1.19

M_w:

Experiment: GPC

Temperature: 50°C

Solvent: DMF

Flow Rate: 1.0 mL/min

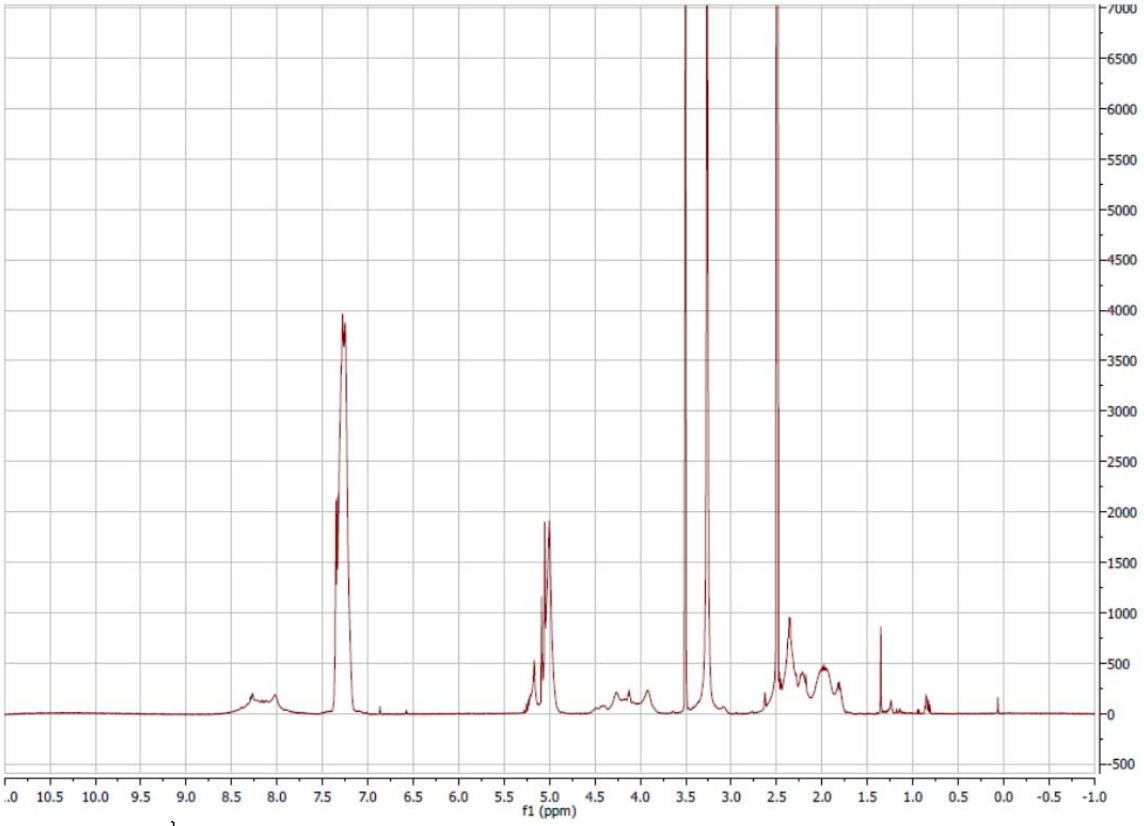

Figure B.35. ^{1}H NMR spectrum of mPEG-b-p(Glu-b-Cys) R=60

Parameters:

Frequency: 500 MHz

Experiment: ^{1}H

Temperature: 35°C

Solvent: D_6DMSO

Scans: 32

APPENDIX C

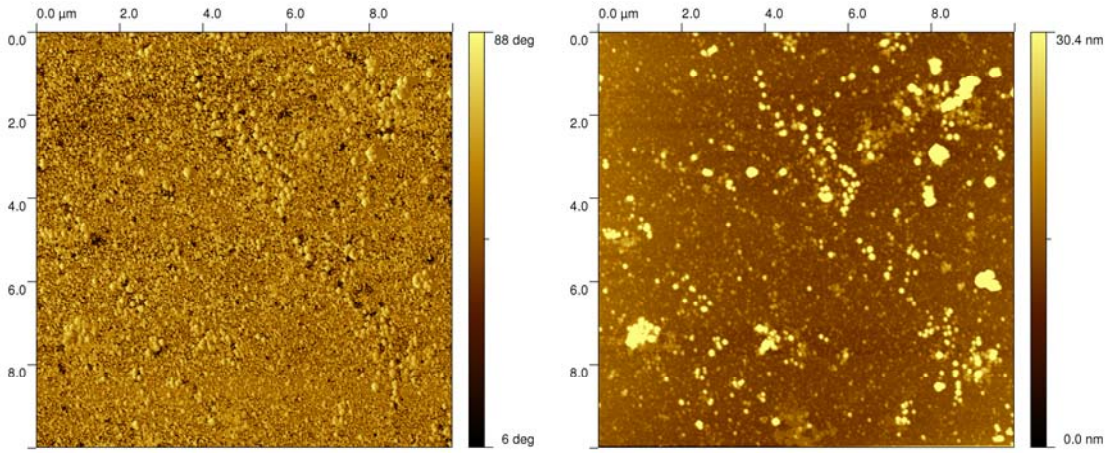

Figure C.1. AFM phase (right) and height (left) images of mPEG-b-p(Glu-b-Cys) R=60 that was dip coated on small (20 to 40 nm) nano particle gold on silicon surfaces.

Parameters:

Mode: Tapping

Cantilever: Silicon Arrow type

Frequency: 285 kHz

Force Constant: 42 N/m

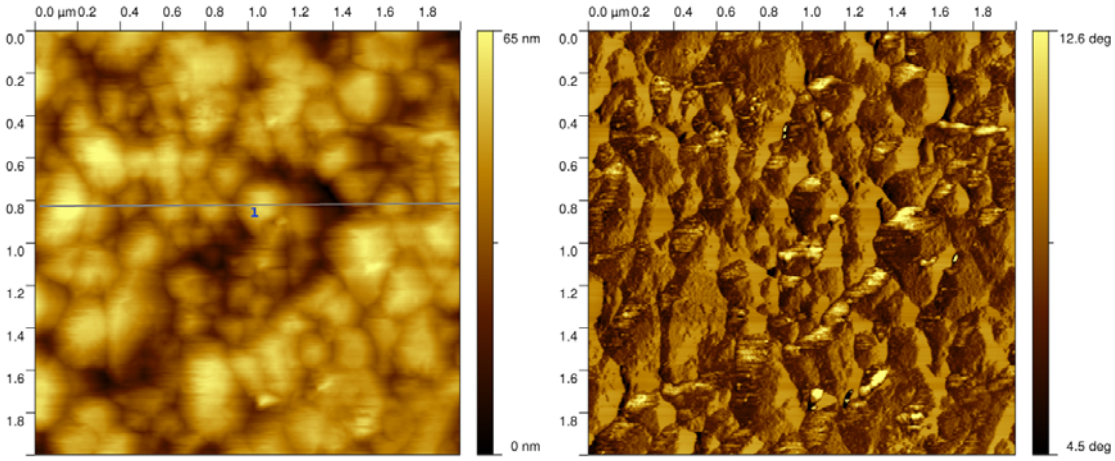

Figure C.2. AFM phase (right) and height (left) images of mPEG-b-p(Glu-b-Cys) R=120 that was dip coated onto gold on silicon surfaces.

Parameters:

Mode: Tapping

Cantilever: Silicon Arrow type

Frequency: 285 kHz

Force Constant: 42 N/m

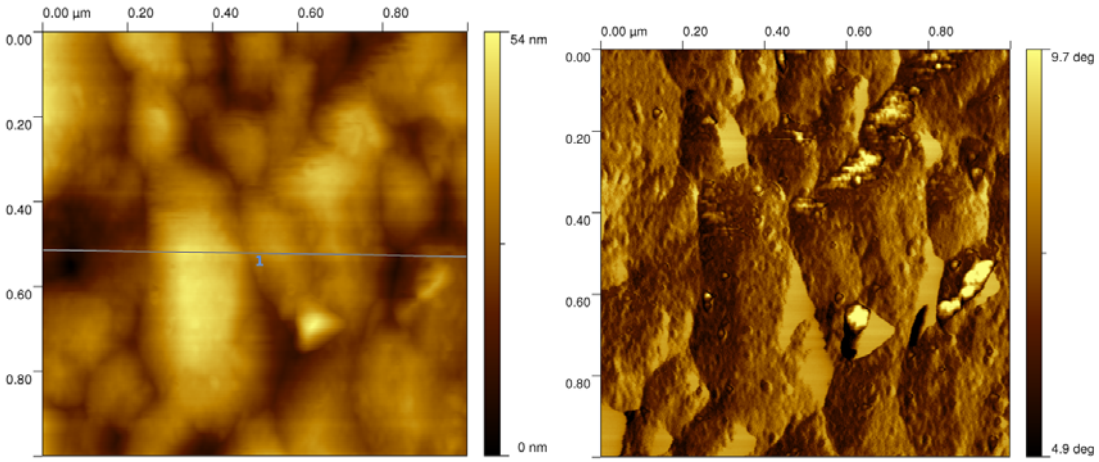

Figure C.3. AFM phase (right) and height (left) images of mPEG-b-p(Glu-b-Cys) R=120 that was dip coated onto gold on silicon surfaces.

Parameters:

Mode: Tapping

Cantilever: Silicon Arrow type

Frequency: 285 kHz

Force Constant: 42 N/m

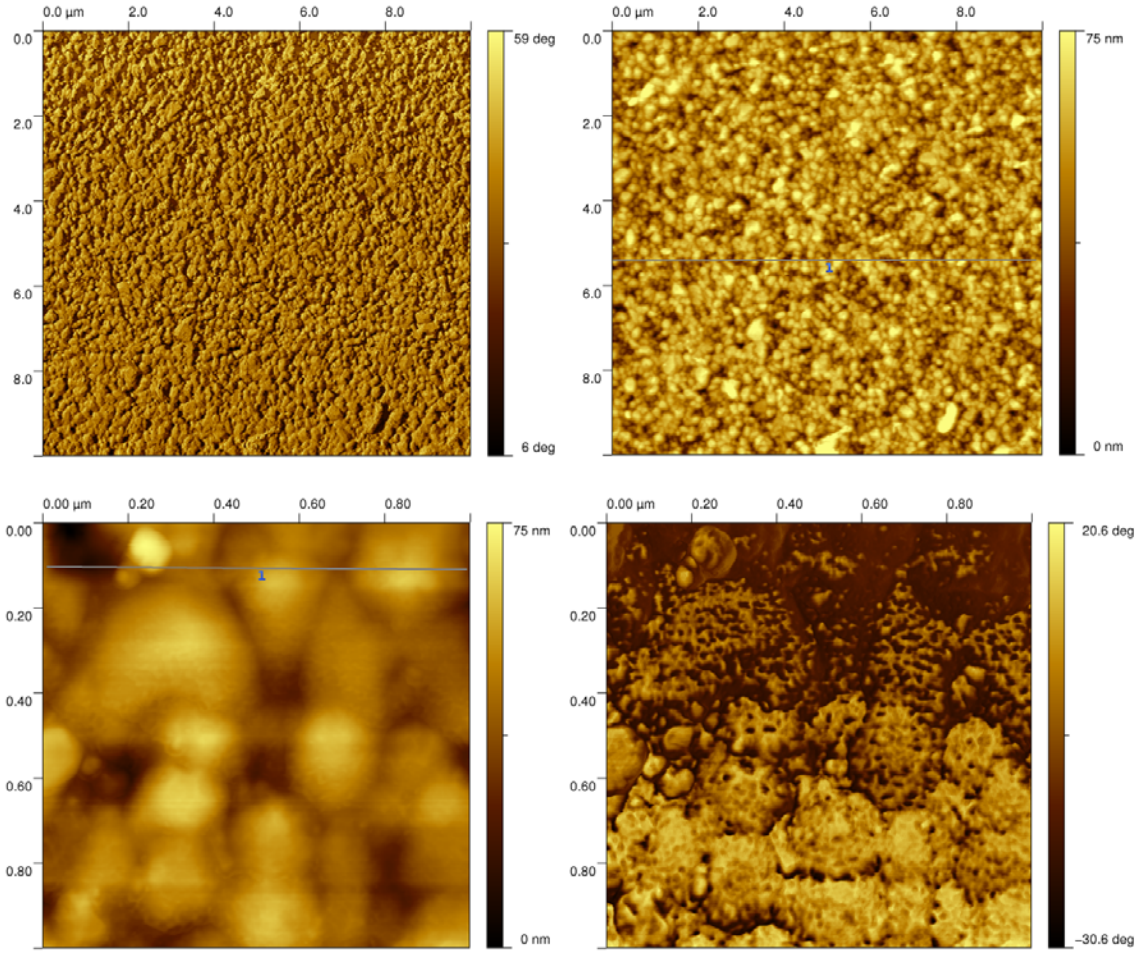

Figure C.4. AFM phase (right) and height (left) images of mPEG-b-p(Glu-b-Cys) R=120 that was dip coated onto gold on silicon surfaces.

Parameters:

Mode: Tapping

Cantilever: Silicon Arrow type

Frequency: 285 kHz

Force Constant: 42 N/m

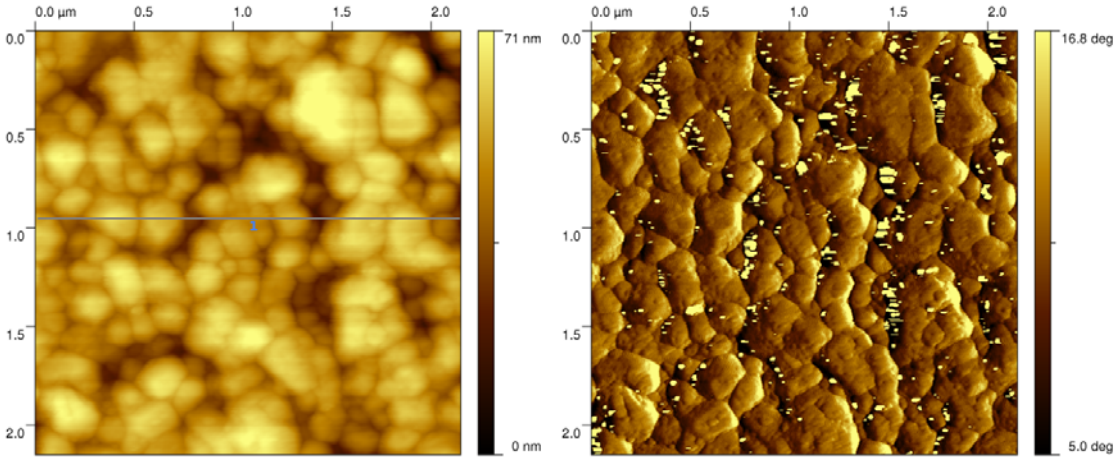

Figure C.5. AFM phase (right) and height (left) images of mPEG-b-p(Glu-co-Cys) R=60 that was dip coated onto gold on silicon surfaces.

Parameters:

Mode: Tapping

Cantilever: Silicon Arrow type

Frequency: 285 kHz

Force Constant: 42 N/m

REFERENCES

[1] W.-J. Yang, P. R. Griffiths, D. M. Byler, and H. Susi, "Protein Conformation by Infrared Spectroscopy: Resolution Enhancement by Fourier Self-Deconvolution," *Appl. Spectrosc.*, vol. 39, no. 2, pp. 282–287, Mar. 1985.

[2] C. Scholz, "Perspectives on: Materials Aspects for Retinal Prostheses," *Journal of Bioactive and Compatible Polymers*, vol. 22, no. 5, pp. 539 –568, 2007.

[3] F. Gekeler, A. Messias, M. Ottinger, K. U. Bartz-Schmidt, and E. Zrenner, "Phosphenes Electrically Evoked with DTL Electrodes: A Study in Patients with Retinitis Pigmentosa, Glaucoma, and Homonymous Visual Field Loss and Normal Subjects," *Investigative Ophthalmology & Visual Science*, vol. 47, no. 11, pp. 4966 –4974, Nov. 2006.

[4] A. M. Potts and J. Inoue, "The Electrically Evoked Response of the Visual System (EER)," *Investigative Ophthalmology & Visual Science*, vol. 9, no. 10, pp. 814 –819, Oct. 1970.

[5] J. M. Ong and L. da Cruz, "The bionic eye: a review," *Clinical & Experimental Ophthalmology*.

[6] D. T. Hartong, E. L. Berson, and T. P. Dryja, "Retinitis pigmentosa," *Lancet*, vol. 368, no. 9549, pp. 1795–1809, Nov. 2006.

[7] N. M. Bressler, S. B. Bressler, and S. L. Fine, "Age-related macular degeneration," *Survey of Ophthalmology*, vol. 32, no. 6, pp. 375–413.

[8] R. D. Jager, W. F. Mieler, and J. W. Miller, "Age-Related Macular Degeneration," *New England Journal of Medicine*, vol. 358, no. 24, pp. 2606–2617, 2008.

[9] T. J. Keen, C. F. Inglehearn, D. H. Lester, R. Bashir, M. Jay, A. C. Bird, B. Jay, and S. S. Bhattacharya, "Autosomal dominant retinitis pigmentosa: Four new mutations in rhodopsin, one of them in the retinal attachment site," *Genomics*, vol. 11, no. 1, pp. 199–205, Sep. 1991.

[10] C. H. Bunker, E. L. Berson, W. C. Bromley, R. P. Hayes, and T. H. Roderick, "Prevalence of retinitis pigmentosa in Maine," *Am. J. Ophthalmol*, vol. 97, no. 3, pp. 357–365, Mar. 1984.

[11] T. P. Dryja, T. L. McGee, E. Reichel, L. B. Hahn, G. S. Cowley, D. W. Yandell, M. A. Sandberg, and E. L. Berson, "A point mutation of the rhodopsin gene in one form of retinitis pigmentosa," *Nature*, vol. 343, no. 6256, pp. 364–366, Jan. 1990.

[12] G. J. Farrar, P. Kenna, S. A. Jordan, R. Kumar-Singh, M. M. Humphries, E. M. Sharp, D. M. Sheils, and P. Humphries, "A three-base-pair deletion in the peripherin-RDS gene in one form of retinitis pigmentosa," *Nature*, vol. 354, no. 6353, pp. 478–480, Dec. 1991.

[13] J. Grøndahl, "Estimation of prognosis and prevalence of retinitis pigmentosa and Usher syndrome in Norway," *Clinical Genetics*, vol. 31, no. 4, pp. 255–264, Apr. 1987.

[14] D. B. Shire, S. K. Kelly, Jinghua Chen, P. Doyle, M. D. Gingerich, S. F. Cogan, W. A. Drohan, O. Mendoza, L. Theogarajan, J. L. Wyatt, and J. F. Rizzo, "Development and Implantation of a Minimally Invasive Wireless Subretinal Neurostimulator," *Biomedical Engineering, IEEE Transactions on*, vol. 56, no. 10, pp. 2502–2511, 2009.

[15] S. R. Montezuma, J. Loewenstein, C. Scholz, and J. F. Rizzo, "Biocompatibility of Materials Implanted into the Subretinal Space of Yucatan Pigs," *Investigative Ophthalmology & Visual Science*, vol. 47, no. 8, pp. 3514 –3522, 2006.

[16] N. A. Alcantar, E. S. Aydil, and J. N. Israelachvili, "Polyethylene glycol-coated biocompatible surfaces," *J. Biomed. Mater. Res.*, vol. 51, no. 3, pp. 343–351, Sep. 2000.

[17] M. M. Villiers, P. Aramwit, and G. S. Kwon, Eds., *Nanotechnology in Drug Delivery*. New York, NY: Springer New York, 2009.

[18] N. V. Churaev, I. P. Sergeeva, and V. D. Sobolev, "Hydrodynamic Thickness and Deformation of Adsorbed Layers of Polyethylene Oxides," *Journal of Colloid and Interface Science*, vol. 169, no. 2, pp. 300–305, Feb. 1995.

[19] R. Sweitzer, C. Scholz, S. Montezuma, and J. F. Rizzo, "Evaluation of Subretinal Implants Coated with Amorphous Aluminum Oxide and Diamond-like Carbon," *Journal of Bioactive and Compatible Polymers*, vol. 21, no. 1, pp. 5 –22, Jan. 2006.
[20] K. Holmberg and K. Bergstrom, "Immobilization of proteins via PEG chains," *Poly (ethylene glycol) chemistry: biotechnical and biomedical applications*, p. 303, 1992.
[21] G. M. Bernacca, M. J. Gulbransen, R. Wilkinson, and D. J. Wheatley, "In vitro blood compatibility of surface-modified polyurethanes," *Biomaterials*, vol. 19, no. 13, pp. 1151–1165, Jun. 1998.
[22] J. D. Andrade, V. Hlady, and S. I. Jeon, "Polyethylene oxide and protein resistance: principles, problems, and possibilities," *Polymeric Materials: Science and Engineering*, pp. 60–61, 1993.
[23] S. I. Jeon, J. H. Lee, J. D. Andrade, and P. G. De Gennes, "Protein--surface interactions in the presence of polyethylene oxide:: I. Simplified theory," *Journal of colloid and interface science*, vol. 142, no. 1, pp. 149–158, 1991.
[24] S. Herman, G. Hooftman, and E. Schacht, "Poly (ethylene glycol) with reactive endgroups: I. Modification of proteins," *Journal of bioactive and compatible polymers*, vol. 10, no. 2, pp. 145–187, 1995.
[25] S. Zalipsky, "Functionalized Poly(ethylene glycols) for Preparation of Biologically Relevant Conjugates," *Bioconjugate Chemistry*, vol. 6, no. 2, pp. 150–165, Mar. 1995.
[26] R. F. Service, "Biotechnology: Designer Tissues Take Hold," *Science*, vol. 270, no. 5234, pp. 230 –232, Oct. 1995.
[27] T. J. Deming, "Living polymerization of α-amino acid-N-carboxyanhydrides," *J. Polym. Sci. A Polym. Chem.*, vol. 38, no. 17, pp. 3011–3018, 2000.
[28] H. R. Kricheldorf, "Polypeptides and 100 Years of Chemistry of α-Amino AcidN-Carboxyanhydrides," *Angew. Chem. Int. Ed.*, vol. 45, no. 35, pp. 5752–5784, Sep. 2006.
[29] C. Scholz and W. Vayaboury, "Synthesis of Poly(Amino Acids) and Poly(Amino Acid) Block Copolymers With Controlled Molecular Weights," *Poly Preprints*, vol. 49, no. 2, pp. 486–487, 2008.
[30] M. Szwarc, "Living polymers. Their discovery, characterization, and properties," *J. Polym. Sci. A Polym. Chem.*, vol. 36, no. 1, p. IX–XV, 1998.
[31] S. Penczek and H. R. Kricheldorf, *Models of biopolymers by ring-opening polymerization*. CRC Press, 1990.
[32] T. J. Deming, "Facile synthesis of block copolypeptides of defined architecture," *Nature*, vol. 390, no. 6658, pp. 386–389, Nov. 1997.
[33] W. Vayaboury, O. Giani, H. Cottet, A. Deratani, and F. Schué, "Living Polymerization of α-Amino AcidN-Carboxyanhydrides(NCA) upon Decreasing the Reaction Temperature," *Macromol. Rapid Commun.*, vol. 25, no. 13, pp. 1221–1224, Jul. 2004.
[34] M. Szwarc, "The kinetics and mechanism of N-carboxy-α-amino-acid anhydride (NCA) polymerisation to poly-amino acids," in *Fortschritte der Hochpolymeren-Forschung*, vol. 4/1, Berlin/Heidelberg: Springer-Verlag, 1965, pp. 1–65.
[35] T. J. Deming, "Transition Metal−Amine Initiators for Preparation of Well-Defined Poly(γ-benzyl l-glutamate)," *Journal of the American Chemical Society*, vol. 119, no. 11, pp. 2759–2760, Mar. 1997.
[36] T. Aliferis, H. Iatrou, and N. Hadjichristidis, "Living Polypeptides," *Biomacromolecules*, vol. 5, no. 5, pp. 1653–1656, 2004.
[37] N. M. B. Smeets, P. L. J. van der Weide, J. Meuldijk, J. A. J. M. Vekemans, and L. A. Hulshof, "A Scalable Synthesis of l-Leucine-N-carboxyanhydride," *Organic Process Research & Development*, vol. 9, no. 6, pp. 757–763, Nov. 2005.
[38] D. G. H. Ballard and C. H. Bamford, "212. The heterogeneous polymerization of□?-N-carboxyamino-acid anhydrides," *J. Chem. Soc.*, p. 1039, 1959.

[39] P. Dubois, O. Coulembier, and J.-M. Raquez, *Handbook of ring-opening polymerization*. Wiley-VCH, 2009.
[40] N. Hadjichristidis, H. Iatrou, S. Pispas, and M. Pitsikalis, "Anionic polymerization: High vacuum techniques," *Journal of Polymer Science Part A: Polymer Chemistry*, vol. 38, no. 18, pp. 3211–3234, Sep. 2000.
[41] M. Idelson and E. Blout, "Additions and Corrections: Polypeptides. XVIII. A Kinetic Study of the Polymerization of Amino Acid N-Carboxyanhydrides Initiated by Strong Bases.," *Journal of the American Chemical Society*, vol. 80, no. 24, p. 6701, Dec. 1958.
[42] H. Block, "α-aminoacid-N-carboxyanhydrides and related heterocycles: Syntheses, properties, peptide synthesis, polymerization H. R. Kricheldorf, Springer-Verlag, Berlin, 1987. pp.214,ISBN 3-540-17072-3," *Brit. Poly. J.*, vol. 21, no. 2, p. 182–182, 1989.
[43] M. Sela and E. Katchalski, "Spectrophotometric Titration of α-Amino Acid Copolymers Containing Tyrosine1," *Journal of the American Chemical Society*, vol. 78, no. 16, pp. 3986–3989, 1956.
[44] O. Lagrille, G. Danger, L. Boiteau, J.-C. Rossi, and J. Taillades, "Process improvement in amino acid N-carboxyanhydride synthesis by N-carbamoyl amino acid nitrosation," *Amino Acids*, vol. 36, no. 2, pp. 341–347, Apr. 2008.
[45] P. G. M. Wuts and T. W. Greene, *Greene's Protective Groups in Organic Synthesis*. Hoboken, NJ, USA: John Wiley & Sons, Inc., 2006.
[46] M. Bergman, "A Method For the Stepwise Degradation of Polypeptides." [Online]. Available: http://www.jbc.org/content/113/2/341.short. [Accessed: 08-Apr-2011].
[47] C. Scholz, W. Vayaboury, R. Sweitzer, D. B. Shire, and J. F. Rizzo, "Surface modification of Retinal Implants," *Poly Preprints*, vol. 47, no. 2, pp. 159–160, 2006.
[48] R. B. Woodward and C. H. Schramm, "Synthesis of Protein Analogs," *Journal of the American Chemical Society*, vol. 69, no. 6, pp. 1551–1552, Jun. 1947.
[49] F. Cardinaux, J. C. Howard, G. T. Taylor, and H. A. Scheraga, "Block copolymers of amino acids. I. Synthesis and structure of copolymers ofL-alanine orL-phenylalanine withD,L-lysine-d7 orD,L-lysine," *Biopolymers*, vol. 16, no. 9, pp. 2005–2028, Sep. 1977.
[50] W. B. Gratzer and P. Doty, "A Conformation Examination of Poly-L-alanine and Poly-D,L-alanine in Aqueous Solution," *Journal of the American Chemical Society*, vol. 85, no. 8, pp. 1193–1197, Apr. 1963.
[51] K. Inoue, H. Sakai, S. Ochi, T. Itaya, and T. Tanigaki, "Preparation and Conformation of Hexaarmed Star Poly(.beta.-benzyl-L-aspartates) Synthesized Utilizing Hexakis(4-aminophenoxy)cyclotriphosphazene," *Journal of the American Chemical Society*, vol. 116, no. 23, pp. 10783–10784, Nov. 1994.
[52] S. Kubota and G. D. Fasman, "The Beta conformation of polypeptides of valine, isoleucine, and threonine in solution and solid-state: Optical and infrared studies," *Biopolymers*, vol. 14, no. 3, pp. 605–631, Mar. 1975.
[53] H. Sekiguchi, "Mechanism of N-carboxy-α-amino acid anhydride (NCA) polymerization," *Pure Appl. Chem.*, vol. 53, no. 9, pp. 1689–1714, 1981.
[54] A. P. Nowak, V. Breedveld, L. Pakstis, B. Ozbas, D. J. Pine, D. Pochan, and T. J. Deming, "Rapidly recovering hydrogel scaffolds from self-assembling diblock copolypeptide amphiphiles," *Nature*, vol. 417, no. 6887, pp. 424–428, May 2002.
[55] T. J. Deming, "Polypeptide hydrogels via a unique assembly mechanism," *Soft Matter*, vol. 1, no. 1, p. 28, 2005.
[56] T. Kissel, Y. Li, and F. Unger, "ABA-triblock copolymers from biodegradable polyester A-blocks and hydrophilic poly(ethylene oxide) B-blocks as a candidate for in situ forming hydrogel delivery systems for proteins," *Adv. Drug Deliv. Rev*, vol. 54, no. 1, pp. 99–134, Jan. 2002.
[57] J. M. Harris, *Poly(ethylene glycol) chemistry: biotechnical and biomedical applications*. Springer, 1992.

[58] N. P. Desai, S. F. A. Hossainy, and J. A. Hubbell, “Surface-immobilized polyethylene oxide for bacterial repellence,” *Biomaterials*, vol. 13, no. 7, pp. 417–420, 1992.
[59] D. H. Atha and K. C. Ingham, “Mechanism of precipitation of proteins by polyethylene glycols. Analysis in terms of excluded volume.,” *Journal of Biological Chemistry*, vol. 256, no. 23, pp. 12108 –12117, Dec. 1981.
[60] K. J. Townsend, K. Busse, J. Kressler, and C. Scholz, “Contact Angle, WAXS, and SAXS Analysis of Poly(β-hydroxybutyrate) and Poly(ethylene glycol) Block Copolymers Obtained via Azotobacter vinelandii UWD,” *Biotechnology Progress*, vol. 21, no. 3, pp. 959–964, Jan. 2005.
[61] K. Uchida, Y. Hoshino, A. Tamura, K. Yoshimoto, S. Kojima, K. Yamashita, I. Yamanaka, H. Otsuka, K. Kataoka, and Y. Nagasaki, “Creation of a mixed poly(ethylene glycol) tethered-chain surface for preventing the nonspecific adsorption of proteins and peptides,” *Biointerphases*, vol. 2, no. 4, p. 126, 2007.
[62] B. Zhu, T. Eurell, R. Gunawan, and D. Leckband, “Chain-length dependence of the protein and cell resistance of oligo(ethylene glycol)-terminated self-assembled monolayers on gold,” *J. Biomed. Mater. Res*, vol. 56, no. 3, pp. 406–416, Sep. 2001.
[63] A. Halperin and D. E. Leckband, “From ship hulls to contact lenses: repression of protein adsorption and the puzzle of PEO,” *Comptes Rendus de l’Académie des Sciences - Series IV - Physics*, vol. 1, no. 9, pp. 1171–1178, Nov. 2000.
[64] V. B. Damodaran, C. J. Fee, and K. C. Popat, “Prediction of protein interaction behaviour with PEG-grafted matrices using X-ray photoelectron spectroscopy,” *Applied Surface Science*, vol. 256, no. 16, pp. 4894–4901, Jun. 2010.
[65] W. Vayaboury, O. Giani, H. Cottet, S. Bonaric, and F. Schué, “Mechanistic Study of Poly(Amino Acid) -Carboxyanhydride (NCA) Polymerization by Capillary electrophoresis,” *Macromol. Chem. Phys.*, vol. 209, no. 15, pp. 1628–1637, Aug. 2008.
[66] B. Lewin, *Genes VIII*, 1st ed. Benjamin Cummings, 2003.
[67] R. Giege, “Genetic code expansion,” *Nat Struct Mol Biol*, vol. 10, no. 6, pp. 414–416, Jun. 2003.
[68] A. Ambrogelly, S. Palioura, and D. Soll, “Natural expansion of the genetic code,” *Nat Chem Biol*, vol. 3, no. 1, pp. 29–35, Jan. 2007.
[69] C. Branden and J. Tooze, *Introduction to protein structure*. Garland Pub., 1991.
[70] J. L. T. Jeremy M Berg, “Biochemistry,” 2002. [Online]. Available: http://www.ncbi.nlm.nih.gov/books/NBK21154/. [Accessed: 15-Aug-2011].
[71] D. B. Bruce Alberts, “Molecular Biology of the Cell,” 1994. [Online]. Available: http://www.ncbi.nlm.nih.gov/books/NBK20684/. [Accessed: 15-Aug-2011].
[72] “Biochemistry - NCBI Bookshelf.” .
[73] C. B. Anfinsen, *Advances in Protein Chemistry*. Academic Press, 1958.
[74] “Advances in Protein Chemistry Vol 14 - Google Books.” .
[75] M. Nič, J. Jirát, B. Košata, A. Jenkins, and A. McNaught, Eds., “hydrogen bond,” in *IUPAC Compendium of Chemical Terminology*, 2.1.0 ed., Research Triagle Park, NC: IUPAC, 2009.
[76] M. Le Hellaye, N. Fortin, J. Guilloteau, A. Soum, S. Lecommandoux, and S. M. Guillaume, “Biodegradable Polycarbonate-b-polypeptide and Polyester-b-polypeptide Block Copolymers: Synthesis and Nanoparticle Formation Towards Biomaterials,” *Biomacromolecules*, vol. 9, no. 7, pp. 1924–1933, Jul. 2008.
[77] J. M. Anderson, D. F. Gibbons, R. L. Martin, A. Hiltner, and R. Woods, “The potential for poly-α-amino acids as biomaterials,” *Journal of Biomedical Materials Research*, vol. 8, no. 3, pp. 197–207, Jan. 1974.
[78] C.-M. Dong, K. M. Faucher, and E. L. Chaikof, “Synthesis and properties of biomimetic poly(L-glutamate)-b-poly(2-acryloyloxyethyllactoside)-b-poly(L-glutamate) triblock copolymers,” *J. Polym. Sci. A Polym. Chem.*, vol. 42, no. 22, pp. 5754–5765, 2004.

[79] R. Duncan, “The dawning era of polymer therapeutics,” *Nat Rev Drug Discov*, vol. 2, no. 5, pp. 347–360, May 2003.
[80] P. H. Maurer, “Antigenicity of Polypeptides (Poly Alpha Amino Acids),” *The Journal of Experimental Medicine*, vol. 121, no. 3, pp. 339 –349, Mar. 1965.
[81] Shih I..L., Van Y..T., and Shen M..H., “Biomedical Applications of Chemically and Microbiologically Synthesized Poly(Glutamic Acid) and Poly(Lysine),” *Mini Reviews in Medicinal Chemistry*, vol. 4, no. 2, pp. 179–188, 2004.
[82] M. Kunioka, “Biosynthesis and chemical reactions of poly(amino acid)s from microorganisms,” *Applied Microbiology and Biotechnology*, vol. 47, no. 5, pp. 469–475, May 1997.
[83] J. M. Buescher and A. Margaritis, “Microbial Biosynthesis of Polyglutamic Acid Biopolymer and Applications in the Biopharmaceutical, Biomedical and Food Industries,” *Critical Reviews in Biotechnology*, vol. 27, no. 1, pp. 1–19, Jan. 2007.
[84] L. H. Sperling, *Introduction to physical polymer science*. John Wiley and Sons, 2006.
[85] J. R. Fried, *Polymer science and technology*. Prentice Hall Professional Technical Reference, 2003.
[86] M. Nič, J. Jirát, B. Košata, A. Jenkins, and A. McNaught, Eds., *IUPAC Compendium of Chemical Terminology*, 2.1.0 ed. Research Triagle Park, NC: IUPAC, 2009.
[87] M. SZWARC, “/`Living/’ Polymers,” *Nature*, vol. 178, no. 4543, pp. 1168–1169, Nov. 1956.
[88] M. Sela and A. Berger, “The Terminal Groups of Poly-α-amino Acids,” *Journal of the American Chemical Society*, vol. 77, no. 7, pp. 1893–1898, Apr. 1955.
[89] K. Koga, A. Sudo, H. Nishida, and T. Endo, “Convenient and useful synthesis of N-carboxyanhydride monomers through selective cyclization of urethane derivatives of α-amino acids,” *Journal of Polymer Science Part A: Polymer Chemistry*, vol. 47, no. 15, pp. 3839–3844, Aug. 2009.
[90] G. J. M. Habraken, M. Peeters, C. H. J. T. Dietz, C. E. Koning, and A. Heise, “How controlled and versatile is N-carboxy anhydride (NCA) polymerization at 0 °C? Effect of temperature on homo-, block- and graft (co)polymerization,” *Polym. Chem.*, vol. 1, no. 4, p. 514, 2010.
[91] T. J. Deming, “Cobalt and Iron Initiators for the Controlled Polymerization of α-Amino Acid-N-Carboxyanhydrides,” *Macromolecules*, vol. 32, no. 13, pp. 4500–4502, Jun. 1999.
[92] D. L. Pickel, N. Politakos, A. Avgeropoulos, and J. M. Messman, “A Mechanistic Study of α-(Amino acid)-N-carboxyanhydride Polymerization: Comparing Initiation and Termination Events in High-Vacuum and Traditional Polymerization Techniques,” *Macromolecules*, vol. 42, no. 20, pp. 7781–7788, Oct. 2009.
[93] E. Katchalski and I. Z. Steinberg, “Proteins and Synthetic Polypeptides,” *Annu. Rev. Phys. Chem.*, vol. 12, no. 1, pp. 433–464, Oct. 1961.
[94] H. R. Kricheldorf, C. V. Lossow, N. Lomadze, and G. Schwarz, “Cyclic polypeptides by thermal polymerization of α-amino acid N-carboxyanhydrides,” *Journal of Polymer Science Part A: Polymer Chemistry*, vol. 46, no. 12, pp. 4012–4020, Jun. 2008.
[95] W. D. Fuller, M. S. Verlander, and M. Goodman, “A procedure for the facile synthesis of amino-acid N-carboxyanhydrides,” *Biopolymers*, vol. 15, no. 9, pp. 1869–1871, Sep. 1976.
[96] Y. Iwakura, K. Uno, and S. Kang, “The Synthesis and Reactions of 2-Isocyanatoacyl Chlorides,” *The Journal of Organic Chemistry*, vol. 30, no. 4, pp. 1158–1161, Apr. 1965.
[97] W. H. Daly and D. Poché, “The preparation of N-carboxyanhydrides of [alpha]-amino acids using bis(trichloromethyl)carbonate,” *Tetrahedron Letters*, vol. 29, no. 46, pp. 5859–5862, 1988.
[98] W. J. Mijs, *New methods for polymer synthesis*. Plenum Press, 1992.

[99] R. Wilder and S. Mobashery, "The use of triphosgene in preparation of N-carboxy .alpha.-amino acid anhydrides," *The Journal of Organic Chemistry*, vol. 57, no. 9, pp. 2755–2756, Apr. 1992.
[100] D. Poche, "An Unconventional Method for Purifying the N-carboxyanhydride Derivatives of γ-alkyl-L-glutamates," *Synthetic Comm.*, vol. 29, no. 5, pp. 843–854, Mar. 1999.
[101] S. Mobashery and M. Johnston, "A new approach to the preparation of N-carboxy .alpha.-amino acid anhydrides," *The Journal of Organic Chemistry*, vol. 50, no. 12, pp. 2200–2202, Jun. 1985.
[102] J. D. Copp and G. A. Tharp, "Optimization of the Penicillin Ring Expansion Reaction through the Use of an Alkene as an HCl Scavenger," *Organic Process Research & Development*, vol. 1, no. 1, pp. 92–94, Jan. 1997.
[103] P. D. Bartlett and I. Pöckel, "The Wagner—Meerwein Rearrangement. A Kinetic Reinvestigation of the Isomerization of Camphene Hydrochloride1," *J. Am. Chem. Soc.*, vol. 60, no. 7, pp. 1585–1590, 1938.
[104] E. R. Blout, C. de Lozé, S. M. Bloom, and G. D. Fasman, "The Dependence of the Conformations of Synthetic Polypeptides on Amino Acid Composition 1,2," *Journal of the American Chemical Society*, vol. 82, no. 14, pp. 3787–3789, Jul. 1960.
[105] T. Kōmoto, K. Y. Kim, M. Ōya, and T. Kawai, "Crystallization of polypeptides in the course of polymerization, 5. Effect of the steric hindrance on the crystal growth by the side chains," *Die Makromolekulare Chemie*, vol. 175, no. 1, pp. 283–299, Jan. 1974.
[106] P. Doty, J. H. Bradbury, and A. M. Holtzer, "Polypeptides. IV. The Molecular Weight, Configuration and Association of Poly-γ-benzyl-L-glutamate in Various Solvents," *Journal of the American Chemical Society*, vol. 78, no. 5, pp. 947–954, Mar. 1956.
[107] J. C. Mitchell, A. E. Woodward, and P. Doty, "Polypeptides. XVI. The Polydispersity and Configuration of Low Molecular Weight Poly-γ-benzyl-L-glutamates1," *Journal of the American Chemical Society*, vol. 79, no. 15, pp. 3955–3960, 1957.
[108] H. R. Kricheldorf and D. Muller, "Secondary structure of peptides," *Polymer Bulletin*, vol. 10, no. 11–12, pp. 513–520, 1983.
[109] H. R. Kricheldorf, D. Müller, and J. Stulz, "Secondary structure of peptides, 11. How to synthesize helical poly(L-phenylalanine)?," *Die Makromolekulare Chemie*, vol. 184, no. 7, pp. 1407–1421, Jul. 1983.
[110] B. J. Bennion and V. Daggett, "The molecular basis for the chemical denaturation of proteins by urea," *Proceedings of the National Academy of Sciences*, vol. 100, no. 9, pp. 5142 –5147, Apr. 2003.
[111] Q. Zou, S. M. Habermann-Rottinghaus, and K. P. Murphy, "Urea effects on protein stability: hydrogen bonding and the hydrophobic effect," *Proteins*, vol. 31, no. 2, pp. 107–115, May 1998.
[112] W. R. Gilkerson and K. K. Srivastava, "The Dipole Moment of Urea," *The Journal of Physical Chemistry*, vol. 64, no. 10, pp. 1485–1487, Oct. 1960.
[113] N. Sreerama and R. W. Woody, "Computation and Analysis of Protein Circular Dichroism Spectra," in *Numerical Computer Methods, Part D*, vol. Volume 383, Academic Press, 2004, pp. 318–351.
[114] N. Sreerama, S. Y. Venyaminov, and R. W. Woody, "Estimation of the number of alpha-helical and beta-strand segments in proteins using circular dichroism spectroscopy.," *Protein Sci*, vol. 8, no. 2, pp. 370–380, Feb. 1999.
[115] N. Sreerama and R. W. Woody, "Estimation of Protein Secondary Structure from Circular Dichroism Spectra: Comparison of CONTIN, SELCON, and CDSSTR Methods with an Expanded Reference Set," *Analytical Biochemistry*, vol. 287, no. 2, pp. 252–260, Dec. 2000.
[116] D. M. Byler and H. Susi, "Examination of the secondary structure of proteins by deconvolved FTIR spectra," *Biopolymers*, vol. 25, no. 3, pp. 469–487, Mar. 1986.

[117] H. Susi and D. M. Byler, “Fourier Deconvolution of the Amide I Raman Band of Proteins as Related to Conformation,” *Appl. Spectrosc.*, vol. 42, no. 5, pp. 819–826, Jul. 1988.
[118] T. J. Deming, “Polypeptide Materials: New synthetic methods and applications,” *Advanced Materials*, vol. 9, no. 4, pp. 299–311, Apr. 1997.
[119] G. Gaucher, M.-H. Dufresne, V. P. Sant, N. Kang, D. Maysinger, and J.-C. Leroux, “Block copolymer micelles: preparation, characterization and application in drug delivery,” *Journal of Controlled Release*, vol. 109, no. 1–3, pp. 169–188, Dec. 2005.
[120] M. R. Ghadiri, J. R. Granja, R. A. Milligan, D. E. McRee, and N. Khazanovich, “Self-assembling organic nanotubes based on a cyclic peptide architecture,” *Nature*, vol. 366, no. 6453, pp. 324–327, Dec. 1993.
[121] C. Noren, S. Anthony-Cahill, M. Griffith, and P. Schultz, “A general method for site-specific incorporation of unnatural amino acids into proteins,” *Science*, vol. 244, no. 4901, pp. 182 –188, Apr. 1989.
[122] U. L. R. Caroline Kohrer, “Proteins Carrying One or More Unnatural Amino Acids,” 2000. [Online]. Available: http://www.ncbi.nlm.nih.gov/books/NBK6136/. [Accessed: 18-Sep-2011].
[123] D. Mendel, J. Ellman, and P. G. Schultz, “Protein biosynthesis with conformationally restricted amino acids,” *Journal of the American Chemical Society*, vol. 115, no. 10, pp. 4359–4360, May 1993.
[124] G. Zubay, “In Vitro Synthesis of Protein in Microbial Systems,” *Annu. Rev. Genet.*, vol. 7, no. 1, pp. 267–287, Dec. 1973.
[125] J. E. Beecher and D. A. Tirrell, “Synthesis of protected derivatives of 3-pyrrolylalanine,” *Tetrahedron Letters*, vol. 39, no. 23, pp. 3927–3930, Jun. 1998.
[126] M. J. Wilson and D. L. Hatfield, “Incorporation of modified amino acids into proteins in vivo,” *Biochim. Biophys. Acta*, vol. 781, no. 3, pp. 205–215, Apr. 1984.
[127] W. M. Becker, L. J. Kleinsmith, and J. Hardin, *The world of the cell*. Benjamin Cummings, 2000.
[128] D. A. Tirrell, M. J. Fournier, and T. L. Mason, “Protein engineering for materials applications,” *Current Opinion in Structural Biology*, vol. 1, no. 4, pp. 638–641, Aug. 1991.
[129] R. B. Merrifield, “Solid Phase Peptide Synthesis. I. The Synthesis of a Tetrapeptide,” *Journal of the American Chemical Society*, vol. 85, no. 14, pp. 2149–2154, Jul. 1963.
[130] R. B. Merrifield, “Solid-Phase Peptide Synthesis. III. An Improved Synthesis of Bradykinin*,” *Biochemistry*, vol. 3, no. 9, pp. 1385–1390, 1964.
[131] A. R. Mitchell, S. B. H. Kent, M. Engelhard, and R. B. Merrifield, “A new synthetic route to tert-butyloxycarbonylaminoacyl-4-(oxymethyl)phenylacetamidomethyl-resin, an improved support for solid-phase peptide synthesis,” *The Journal of Organic Chemistry*, vol. 43, no. 14, pp. 2845–2852, Jul. 1978.
[132] J. R. Hernández and H. Klok, “Synthesis and ring-opening (co)polymerization of L-lysine N-carboxyanhydrides containing labile side-chain protective groups,” *Journal of Polymer Science Part A: Polymer Chemistry*, vol. 41, no. 9, pp. 1167–1187, May 2003.
[133] W. Siebourg, R. Lundberg, R. Lenz, and K. C. Frisch, “Gel Permeation Chromatographic Characterization of Sulfonated Polystyrenes,” *Macromolecules*, vol. 13, no. 4, pp. 1013–1016, Jul. 1980.
[134] A. Isidro-Llobet, M. Álvarez, and F. Albericio, “Amino Acid-Protecting Groups,” *Chemical Reviews*, vol. 109, no. 6, pp. 2455–2504, Jun. 2009.
[135] G. Barany and F. Albericio, “Three-dimensional orthogonal protection scheme for solid-phase peptide synthesis under mild conditions,” *Journal of the American Chemical Society*, vol. 107, no. 17, pp. 4936–4942, 1985.
[136] G. Barany and R. B. Merrifield, “A new amino protecting group removable by reduction. Chemistry of the dithiasuccinoyl (Dts) function,” *Journal of the American Chemical Society*, vol. 99, no. 22, pp. 7363–7365, Oct. 1977.

[137] J. Rizo, F. Albericio, E. Giralt, and E. Pedroso, “Reversible protection of lysine to facilitate the purification of protected peptide segments,” *Tetrahedron Letters*, vol. 33, no. 3, pp. 397–400, Jan. 1992.
[138] J. Rodríguez-Hernández, M. Gatti, and H.-A. Klok, “Highly Branched Poly(l-lysine),” *Biomacromolecules*, vol. 4, no. 2, pp. 249–258, Mar. 2003.
[139] P. J. Kocieński, *Protecting groups*. Thieme, 2005.
[140] S. A. Lawrence, *Amines: synthesis, properties and applications*. Cambridge University Press, 2004.
[141] K. Rurack and R. Martínez-Máñez, *The Supramolecular Chemistry of Organic-Inorganic Hybrid Materials*. John Wiley and Sons, 2010.
[142] A. S. Karakoti, S. Das, S. Thevuthasan, and S. Seal, “PEGylated Inorganic Nanoparticles,” *Angewandte Chemie International Edition*, vol. 50, no. 9, pp. 1980–1994, Feb. 2011.
[143] M. Packirisamy and S. Badilescu, *Biomems: Science and Engineering Perspectives*. Taylor & Francis US, 2011.
[144] T. McPherson, A. Kidane, I. Szleifer, and K. Park, “Prevention of Protein Adsorption by Tethered Poly(ethylene oxide) Layers: Experiments and Single-Chain Mean-Field Analysis,” *Langmuir*, vol. 14, no. 1, pp. 176–186, Sep. 2011.
[145] M. Oishi and Y. Nagasaki, “Synthesis, characterization, and biomedical applications of core–shell-type stimuli-responsive nanogels – Nanogel composed of poly[2-(N,N-diethylamino)ethyl methacrylate] core and PEG tethered chains,” *Reactive and Functional Polymers*, vol. 67, no. 11, pp. 1311–1329, Nov. 2007.
[146] H. Grönbeck, A. Curioni, and W. Andreoni, “Thiols and Disulfides on the Au(111) Surface: The Headgroup−Gold Interaction,” *Journal of the American Chemical Society*, vol. 122, no. 16, pp. 3839–3842, Apr. 2000.
[147] L. D. Unsworth, H. Sheardown, and J. L. Brash, “Protein Resistance of Surfaces Prepared by Sorption of End-Thiolated Poly(ethylene glycol) to Gold: Effect of Surface Chain Density,” *Langmuir*, vol. 21, no. 3, pp. 1036–1041, Feb. 2005.
[148] K. Bergström, E. Osterberg, K. Holmberg, A. S. Hoffman, T. P. Schuman, A. Kozlowski, and J. H. Harris, “Effects of branching and molecular weight of surface-bound poly(ethylene oxide) on protein rejection,” *J Biomater Sci Polym Ed*, vol. 6, no. 2, pp. 123–132, 1994.
[149] S. W. Shalaby and A. C. S. Meeting, *Polymers as biomaterials*. Plenum Press, 1984.
[150] H. Zhu, Z. Pan, E. W. Hagaman, C. Liang, S. H. Overbury, and S. Dai, “Facile one-pot synthesis of gold nanoparticles stabilized with bifunctional amino/siloxy ligands,” *Journal of Colloid and Interface Science*, vol. 287, no. 1, pp. 360–365, Jul. 2005.
[151] H. Zhu, C. Liang, W. Yan, S. H. Overbury, and S. Dai, “Preparation of highly active silica-supported Au catalysts for CO oxidation by a solution-based technique,” *J Phys Chem B*, vol. 110, no. 22, pp. 10842–10848, Jun. 2006.
[152] S. Hong, W. J. MacKnight, T. P. Russell, and S. P. Gido, “Structural Evolution of Multilayered, Crystalline−Amorphous Diblock Copolymer Thin Films,” *Macromolecules*, vol. 34, no. 9, pp. 2876–2883, 2001.
[153] J. F. Rusling, *Biomolecular films: design, function, and applications*. CRC Press, 2003.
[154] B. . Duggan and Y. . Tse, “Crystal growth in deformed metals by an impingement and spheroidisation process,” *Acta Materialia*, vol. 52, no. 2, pp. 387–393, Jan. 2004.
[155] D. Hull and D. J. Bacon, *Introduction to Dislocations*. Elsevier, 2011.